Improvement to the Stock Assessment of Witch Flounder in NAFO 3N+3O Division

by © Jiaying Chen

A Thesis submitted to the School of Graduate Studies in partial fulfillment of the requirements for the degree of Master of Science in Fisheries Science (Stock assessment)

Fisheries and Marine Institute

School of Fisheries

Memorial University of Newfoundland

June 15, 2022

St. John’s, Newfoundland and Labrador, Canada

Contents

Abstract

Traditional stock assessment models rely on statistical fitting to abundance indices, fishery catch and age-length-maturation data. Aging information is essential as it determines the growth function, maturity schedule and mortality. For many hard-to-age stocks, it is challenging in fisheries stock assessment to estimate cohort dynamics and fishing mortality at length from length-based data with existing approaches, e.g. age-based catch-at-length model (ACL). An age and length structured statistical catch-at-length model (ALSCL) has been developed for groundfish species that are hard to age. At the same time, abundance indices from scientific surveys as the core input for stock assessment can be standardized by various different ways. Therefore, it is essential to compare the efficiency of those approaches to find the best method to standardize the indices. In this study, I focus on improving the stock assessment of an important commercial stock of witch flounder in NAFO 3N+3O division. I first use a traditional design-based way and a spatiotemporal model to standardize length composition data from government surveys. Specifically, I compare the uncertainty between design-based and model-based indices for each length bins. I then apply ALSCL and ACL models to the length composition data standardized using the design-based and model-based estimators in the previous step to estimate the age-based population dynamics for NAFO Div. 3NO witch flounder.

Acknowledgments

I would like to express my sincere appreciation to my supervisor Dr. Jin Gao and co-supervisor Dr. Fan Zhang for their kindly help and guidance throughout the whole M.Sc. studies. Many thanks to the Fisheries and Marine Institute of the Memorial University of Newfoundland, Ocean Choice International, and Ocean Frontier Institute for providing funding for this research. I also thank the Fisheries and Ocean Canada staff who conducted the collection and processing of data that I used for stock assessment. Lastly, a huge thanks to my mom Lin and my boyfriend Haoran for their emotional support and encouragement.

List of Tables

.

List of Figures

Figure 3.53 The retrospective analyses for NAFO Div. 3NO witch flounder in ACL with model-based indices from 1995 to 2018 (except 2014).

Chapter 1 Introduction

1.1 Introduction

In this chapter, I provide an overview of the commercial witch flounder (*Glypocephalus cynoglossus*) fishery on the southern Grand Banks of Newfoundland in NAFO (Northwest Atlantic Fisheries Organization) Div. 3NO (Figure 1.1) including: witch flounder life history, witch flounder fishery history and management. I also describe the Canadian research vessel survey indices of NAFO Div. 3NO witch flounder stock.

1.2 Witch flounder life history

Witch flounder (*Glypocephalus cynoglossus*) is a small-mouthed, right-sided flatfish of the family Pleuronectidae found in deep and cold waters of the North Atlantic (Fairbairn, 1981; Burnett et al., 1992). In the western North Atlantic, the population is distributed from North Carolina (USA) to Labrador (Hamilton Bank)(Bowering, 1976). It is found in higher concentrations on the northeast Newfoundland shelf and is relatively high concentration along the southwest slope of the Grand Banks as well as the southern slope of the St. Pierre Bank (Bowering, 1976; Bowering & Brodie, 1991). In the Newfoundland region, witch flounder gathers on mud, clay, silt, or muddy sand substrates (Bowering, 1976; Faber & McAllister, 1979; Powles & Kohler, 1970). It is predominant at depths of 184 to 366 m (Bowering, 1976; Rabe, 1999). Witch flounders have been caught at temperatures ranging from 2 ℃ to 6 ℃ (Bowering, 1976), and the largest catches occurred on the eastern Newfoundland Shelf at the bottom temperature of 3.1-3.5℃ (Bowering, 1976).

As a long-lived flatfish, witch flounder can live to 25 years and grow to a size of 65-70 cm (Bowering, 1976; Rabe, 1999), and it is thought to grow slowly compared to other flatfish species (Burnett et al., 1992). The slowest and fastest-growing populations are found in the Gulf of St. Lawrence and on the northeast Newfoundland shelf respectively (Rabe, 1999). The witch flounder has a pelagic egg stage followed by a pelagic larval stage, a pelagic juvenile stage, a deep-demersal juvenile stage, and an adult phase (Powles & Kohler, 1970). The pelagic eggs of witch flounder range in diameter from 1.25 to 1.35 mm (Fahay, 1983). Hatching occurs 7-8 days after spawning at 7.8 to 9.4 °C (Cargnelli, 1999). The hatched larvae measure 3.5 to 5.6 mm in length and transformation (the left eye moves over to the right side of its head) to the pelagic juvenile stage generally occurs at 22-35 mm body length (Fahay, 1983). At the pelagic juvenile stage, they may persist in the water column for up to one year (Powles & Kohler, 1970). The deep-demersal phase occurs in very deep water when metamorphosis is complete at 4-12 months of age and juveniles settle on the bottom (Powles & Kohler, 1970). They are in the adult phase when the body length is over 30 cm (Powles & Kohler, 1970).

Males and females reach sexual maturity at the age range of 4-6 years and 6-8 years respectively (Bowering, 1976). Age and length at 50% maturity ranged from 4.2 to 6.2 years and 25 to 30 cm for males, 8.42 to 10.21 years and 40 to 50 cm for females in an early study (Bowering, 1976). However, the data from surveys in the 2000s suggest that maturation is now at a smaller size than in the 1970s, length at 50% maturity decreases 6 cm for males and 9 cm for females in the Gulf of St. Lawrence (Swain et al., 2012). The fecundity of females varies with size, ranging from 48800 eggs for a 31cm fish to 508300 eggs for a 60 cm fish (Burnett et al., 1992).

The spawning of witch flounder occurs mostly during April-September but varies from one area to another (Bowering, 1990). Spawning occurs mainly during March-June on the Grand Bank, January-February in southwest Newfoundland and the northern Gulf of St. Lawrence (Bowering, 1990). The combined influence of both depth and temperature may be significant in determining spawning time (Bowering, 1990).

The main food items consumed by adult witch flounders are polychaete worms while small crustaceans, sea cucumbers, molluscs and echinoderms are occasionally consumed (Bowman & Michaels, 1984; Cargnelli, 1999). Witch flounders are preyed upon by several species such as thorny skates and smooth skates, spiny dogfish, monkfish (Goosefish), white hake, Atlantic halibut, and harp seal (Collette & Klein-MacPhee, 2002).

1.3 Div. 3NO witch flounder fishery catch history

Witch flounder fishery began in the late 1940s with the establishment of otter-trawling fleets in Newfoundland (Bowering, 1976). From the 1970s to the 1990s, it became a significant component of commercial species in the northwest Atlantic (Fairbairn, 1981; Bowering, 1990). Landings are mostly taken by bottom otter trawls complemented by Danish seines (Rabe, 1999). In NAFO Divisions 3NO, witch flounder fishery began in the 1960s (Brodie et al., 2011). The catch history of the Div. 3NO witch flounder fishery from 1960 to 2018 is shown in Figure 1.2. Catches in the 1960s reached the peak at 11000-12000 tons in 1967-68 and during the next several years, catches remained relatively high (Maddock Parsons et al., 2020). In 1971, the catch was 15000 tons, reaching the peak in the time series (Lee et al., 2014). Then, catch subsequently declined over the next decade, reaching a low level of about 2400 tons in 1980 and 1981 (BOWERING, 1995). With a substantial increase in fishing effort in the NAFO Regulation Area, catches rose rapidly to levels of 8800 and 9100 tons in 1985 and 1986 respectively and remained relatively high in 1987 and 1988 at 7600 and 7300 tons respectively (BOWERING, 1995; Rogers & Morgan, 2019). During 1990-93 estimated catches were in the range of 4200-5000 tons (Rogers & Morgan, 2019). The estimated catch for 1994 was about 1100 tons despite there being no direct fishing on this stock (Rogers & Morgan, 2019). The Div. 3NO witch flounder stocks have been under a complete moratorium by the Fisheries Commission for directed fishing from 1995 to 2014 (Maddock Parsons et al., 2020).

The witch flounder fishery was essentially a by-product of the haddock fishery in the early 1960s until its collapse at which time the witch flounder became a by-catch of Atlantic cod and American plaice on the Grand Bank (Bowering, 1976; Templeman, 1966). In 1995, witch flounder became a bycatch of Greenland halibut fishery and the catch dropped to 300 tones after the moratorium was introduced in NAFO Div. 3NO (Rogers & Morgan, 2019). Bycatch increased steadily and reached 763 tons in 1999 (Rogers & Morgan, 2019). It continually declined again in the next several years and reached an estimated 450 tons in 2002 (Rogers & Morgan, 2019). Catches were estimated to be 1544 tons in 2003 which declined to 222 tons in 2007, increased steadily to 421 tons in 2010, then declined slightly to 335 tons in 2014 (Rogers & Morgan, 2019). After the moratorium period, catches were consistent with the bycatch range (300-400 tons) in 2015, jumped to 1062 tons in 2016 and declined again to 641 tons and 862 tons in 2018 and 2019 respectively (Maddock Parsons et al., 2020).

1.4 Div. 3NO witch flounder fishery management

All witch flounder stocks that are subject to management measures in the Northwest Atlantic are identified by geographic divisions or combinations of divisions of NAFO (Bowering & Brodie, 1991). Witch flounder is managed as four independent units or stock areas in the Newfoundland region under the regulation of NAFO since 1974 (Bowering, 1976; Fairbairn, 1981). They are 1) northeast Newfoundland and northern Grand Bank (NAFO Division 2J, 3K, and 3L), 2) southwest Grand Bank (NAFO Div. 3N and 3O), 3) St. Pierre Bank (NAFO Div. 3Ps), and 4) northern Gulf of St. Lawrence (NAFO Div. 4RS) (Bowering, 1976, 1990). However, after investigating the genetic variability, six stocks have been identified in the Newfoundland region (Fairbairn, 1981). In my thesis, we focus on southwest Grand Bank stock (Div. 3NO).

The Div. 3NO stock has been under TAC (total allowable catch) regulation by NAFO since 1974 (Rogers & Morgan, 2019). In general, from 1974 to 1993, TACs were set based on average historical catches; from 1994 to 2014, TACs were set based on the poor state of this stock; since 2015, TACs were set based on advice developed from the surplus production model in a Bayesian framework (Maddock Parsons et al., 2020). Specifically, TAC for Div. 3NO witch flounder was set as 10000 tons in 1974 and remained in effect until 1978 based on average historical catches (Rogers & Morgan, 2019). Due to the decline in commercial catches, TAC was reduced to 7000 tons in 1979 and remained at that level until 1980 (Rogers & Morgan, 2019). It further dropped to 5000 tons in 1981 and remained in effect until 1993 (Rogers & Morgan, 2019). To ensure the resource sustainability of this stock, NAFO Fisheries Commission implemented a TAC of 3000 tons in 1994 and introduced a complete moratorium for directed fishing in 1995, which was continued through 2014 (Rogers & Morgan, 2019). After the moratorium period, the harvest control rules that biomass shouldn't be below *Blim* (biomass limit reference point) and fishing mortality should not exceed *Flim* (fishing mortality limit reference point) have been used to determine TAC. A TAC of 1000 tons was adopted in 2015, and a TAC increased to 2172 tons and 2225 tons in 2016 and 2017 respectively, but a TAC dropped to 1116 tons in 2018 (Maddock Parsons et al., 2020). In the 2019 assessment of this stock, NAFO Scientific Council recommended no directed fishing on witch flounder in 2019-2021 based on the probability of the stock being below *Blim* (biomass limit reference point) is 14% (Maddock Parsons et al., 2020). However, NAFO Fisheries Commission adopted a TAC of 1175 for 2019 to 2021 (Maddock Parsons et al., 2020).

Div.3NO witch flounder is assessed yearly in the June NAFO Scientific Council Meeting (Maddock Parsons et al., 2020). The last official meeting report available online was 2020 (Maddock Parsons et al., 2020). There is no available analytical model applied on witch flounder stock before 2006, the status of this stock was assessed based on catch and survey results (Maddock Parsons et al., 2020). From 2006 to 2013, a non-equilibrium surplus production model incorporating covariates (ASPIC) was adopted to assess this stock by applying catch and survey biomass data (Maddock Parsons et al., 2020). There were concerns that the poor model suitability including unreasonably high B (biomass)/*Bmsy* (biomass at maximum sustainable yield) ratio, poor observed to estimated CPUE relationship, and strong residual patterns, this production model was rejected, and the application of a surplus production model in a Bayesian framework was first explored in 2014 (Maddock Parsons et al., 2020; Morgan et al., 2015). In 2015-2020, a surplus production model in a Bayesian framework was used to evaluate Div. 3NO witch flounder and as the basis for the advice for this stock (Joanne Morgan & Lee, 2018; Maddock Parsons et al., 2020). As for 2020, the stock was 44% of *Bmsy* (59880 tons) with a 14% risk of the stock being below *Blim* (30% *Bmsy*) and a 4% risk of F (fishing mortality) greater than *Fmsy* (maximum rate of fishing mortality at maximum sustainable yield) (Maddock Parsons et al., 2020).

1.5 Research vessel surveys

Bottom trawl surveys are designed to sample fish by towing a large trawl of specified width across the bottom for a standard unit of time or distance (Cadigan, 2011; Kimura & Somerton, 2006). The catch rate of several trawls over a specified time is taken as reflecting the fish density in the area swept (R. Francis, 1984; Kimura & Somerton, 2006). These bottom trawl surveys provide critical fisheries independent information (e.g. stock distribution, abundance and species composition) for assessment and management of many stocks in the Northwest Atlantic (Fogarty et al., 1986; Smith, 1997). Stratified-random sampling with the proportional allocation of sampling units (i.e. strata) is the most widely used survey design for demersal fisheries to estimate abundance indices for stock assessment models (Cadigan, 2011; Smith, 1997).

1.5.1 Stratified random sampling

Stratified random sampling is a flexible and efficient sampling design commonly used in fishery-independent surveys (Cochran, 1977). Stratified random sampling, usually divides a target survey area into different homogeneous subgroups known as strata and conducts simple random sampling within each stratum (Xu et al., 2015). The samples are drawn independently in different strata that are spatially contiguous, and the strata boundaries are set primarily based on depth (Cadigan, 2011; Cochran, 1977). The populations in strata are non-overlapping, and they comprise the entire population in the target survey area (Cochran, 1977). When the strata have been determined, at least two survey sets are sampled from every stratum for the purpose of computing variance estimates, and these survey sets are standardized catches at the randomly selected sampling sites within stratum (Cochran, 1977).

Stratified random sampling has several advantages over survey designs such as complete survey or pure random sampling in the fisheries field. First, the fish population size for a management unit is too large to sample all of them. Random sampling can provide an unbiased estimate of the whole population size, which is the benefit to improve efficiency (Cochran, 1977; Thompson, 2012b). Second, in pure random sampling, samples may themselves be aggregated, which can result in over or under-estimate of the entire population even though each possible sample is equally likely to occur (Kimura & Somerton, 2006; Lenarz & Adams, 1980). Compared with that, stratified random sampling ensures a high degree of representativeness of all the strata, which can improve the precision of the entire population estimate by combining the stratum-level estimates (Cochran, 1977; Grosslein, 1969). For these reasons, stratified random sampling is applied in research vessel surveys for NAFO Div. 3NO witch flounder. The strata map for NAFO Div. 3NO witch flounder stock area is shown in Figure 1.3.

1.5.2 Spring and Fall surveys

Stratified-random research vessel surveys have been conducted on the Grand Banks in NAFO Div. 3NO during spring since 1971; Fall surveys have been conducted since 1990 (Rogers & Morgan, 2019). Due to operational difficulties, there were an incomplete spring survey in 2006 and no fall survey in 2014 (Maddock Parsons et al., 2020). Beginning with the fall survey in 1995, NAFO changed its survey gear from an *Engel 145* groundfish trawl with bobbin gear to a *Campelen 1800* shrimp trawl using rockhopper gear (Rogers & Morgan, 2019), and the *Campelen* has been found that catches a greater size range of most commercial species than the *Engel 145* trawl because of the smaller mesh size (McCallum & Walsh, 1996; Walsh & McCallum, 1997). Catch in weight in different strata for each NAFO division of the stock area (Div. 3NO) from Canadian RV spring and fall surveys is shown in Figure 1.4-1.5. In NAFO Div. 3NO, spring and fall surveys were completed for most strata in all years from 1991 to 2018 with coverage of depth ranging from 93 to 731m (Maddock Parsons et al., 2020).

For spring surveys in NAFO Div. 3NO, the stock indices trends are mainly dominated by NAFO Div.3O estimated biomass and abundance indices (Rogers & Morgan, 2019). The biomass and abundance indices increased gradually from 1996 to 1997, and increased with fluctuations from 1997 to 2003, followed by a decrease from 2003 to 2005 (Figure 1.6). The values fluctuated from 2007 to 2010, increased substantially from 2007 to 2013, and reached their highest peak in the time series in 2013, with biomass at 24395 (tons), abundance at 68.347 (millions)) (Figure 1.6). These indices declined sharply from 2013 to 2015, followed by a sightly increase from 2015 to 2018 (Figure 1.6).

For fall surveys in NAFO Div. 3NO, biomass and abundance declined from 1995 to 1997, followed by a sightly increase from 1997 to 1999 (Figure 1.7). The values fluctuated from 1999 to 2004 but showed a generally increasing trend (Figure 1.7). The indices declined from 2004 to 2007 but followed by a sharp increase from 2007 to 2009 and reached their peak in the time series in 2009 (biomass at 37707 t, abundance at 84.859 millions). The peak is followed by a significantly overall downward trend from 2009 to 2016 (Figure 1.7). Fall survey indices remained stable from 2017 to 2018 (Figure 1.7).

The geographic distribution of witch flounder catch in weight in Canadian spring and fall RV surveys (1984-2018) in NAFO Div. 3NO is shown in Figure 1.8-1.9. The NAFO Div. 3NO witch flounder stock is mainly distributed along the southwestern slope of the Grand Bank but with a higher concentration in NAFO Div. 3O.

Canadian spring and fall RV survey length-frequency data from 1995 to 2018 in NAFO Div. 3NO are presented in Figures 1.10-1.11 as abundance at length. In spring and fall RV surveys, witch flounder with a body length of 30 cm to 50 cm have the most frequency, and the length of more than 55 cm or less than 5 cm are rarely seen. After 2004, compared with the fall survey, the distribution of length-frequency between 30cm and 50cm in the spring survey was flatter and increased less (Maddock Parsons et al., 2020). From 2015 to 2019, fish in length 30 cm to 50 cm were not as prominent as they were from 2012 to 2014 in the spring survey or from 2008 to 2013 in the fall survey. In the fall survey, juveniles with a length less than 21cm showed a few obvious peaks in the time series that may appear in consecutive years (e.g. peak at 9 cm in 1997, peak at 11 cm in 1998, peak at 18 cm in 1999). This cohort tracking may indicate the recruitment of year classes (Maddock Parsons et al., 2020).

Due to witch flounder are more widely and evenly distributed on the Grand bank in fall than in spring (Maddock Parsons et al., 2020; Rogers & Morgan, 2019), I only use the fall survey to compute the indices for the assessment model.

Figures

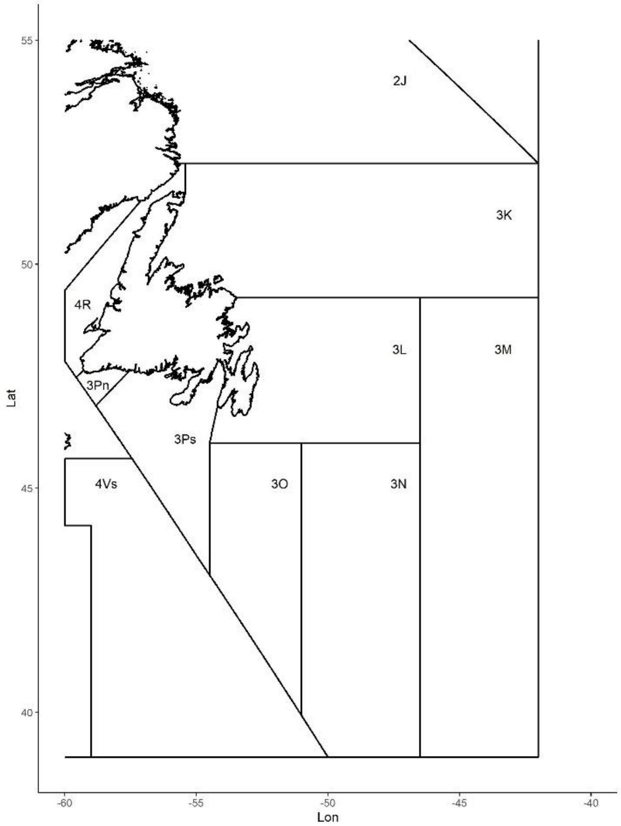

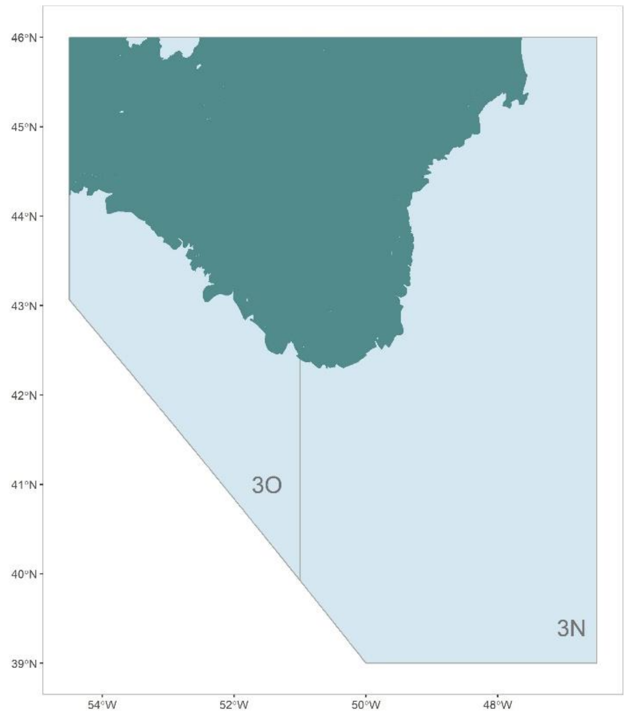

Figure 1.1 Map of eastern Canada showing NAFO Divisions (left) and map of NAFO Div. 3NO in the Northwest Atlantic (right). The dark green color shows the Grand Banks.

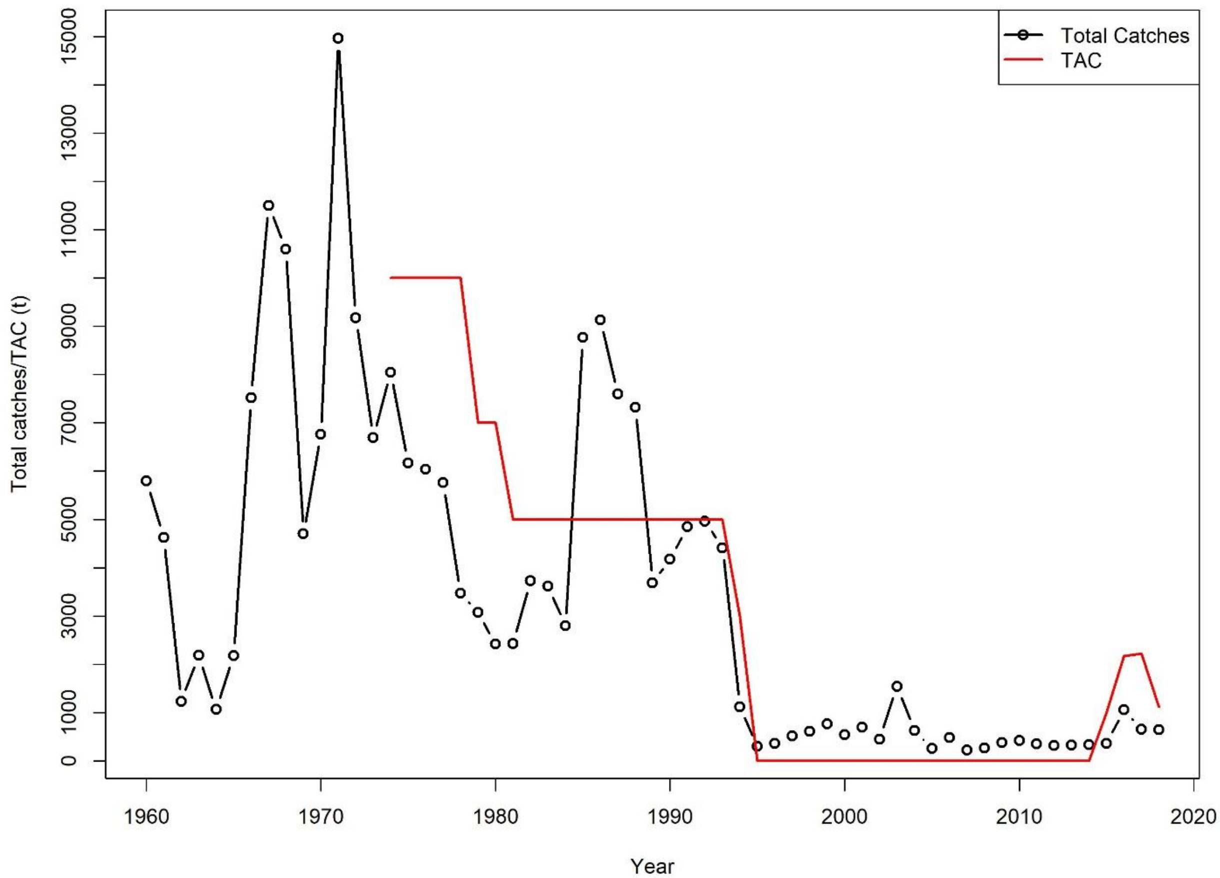

Figure 1.2 Commercial catch and total allowable catch (TACs) of witch flounder in NAFO Div. 3NO from 1960-2018. From 1960 to 1973, there was no TAC. From 1995 to 2014, witch flounder fishery under a complete moratorium.

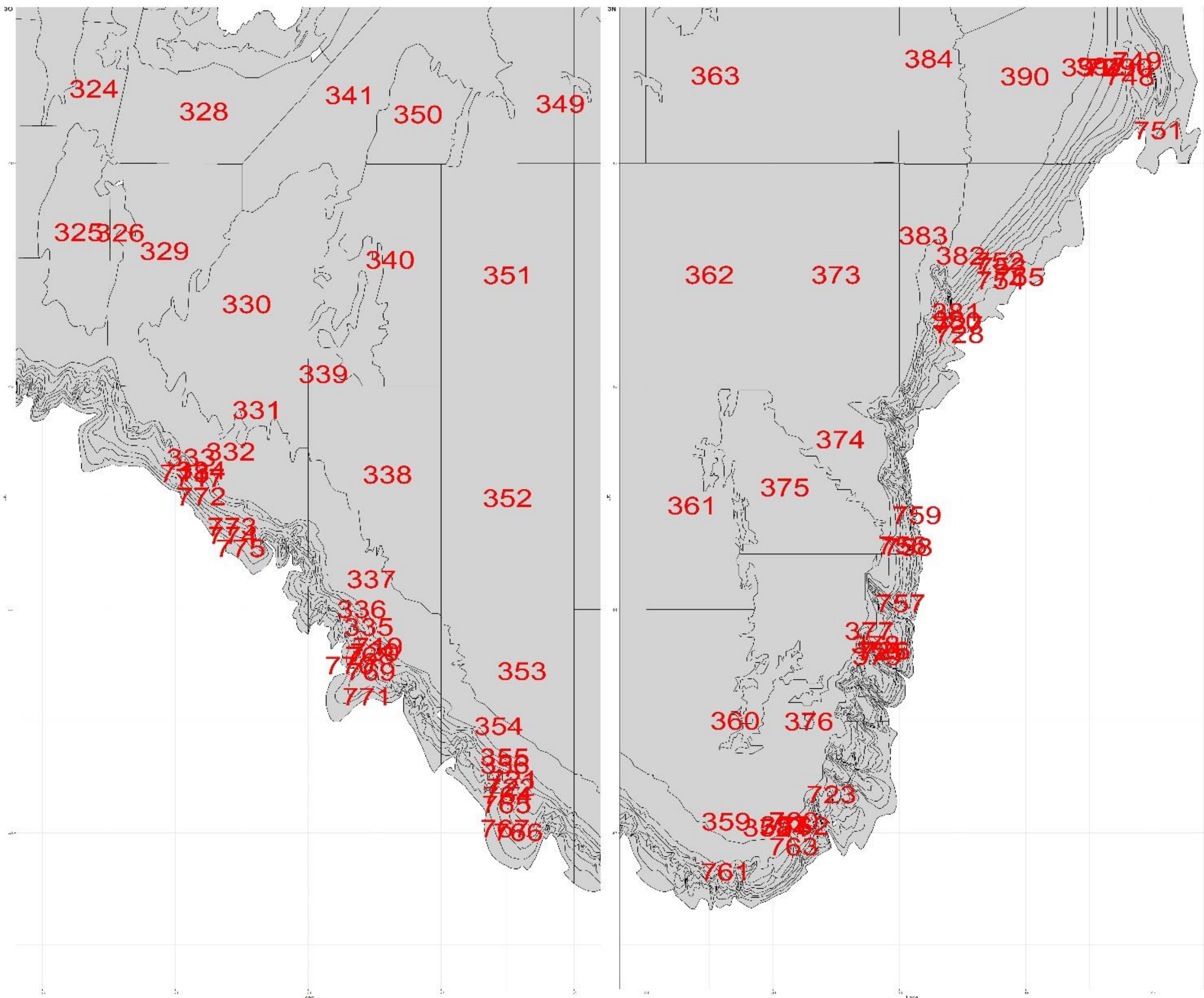

Figure 1.3 Strata map of NAFO Div. 3N and 3O. Strata numbers are marked in red in the figure.

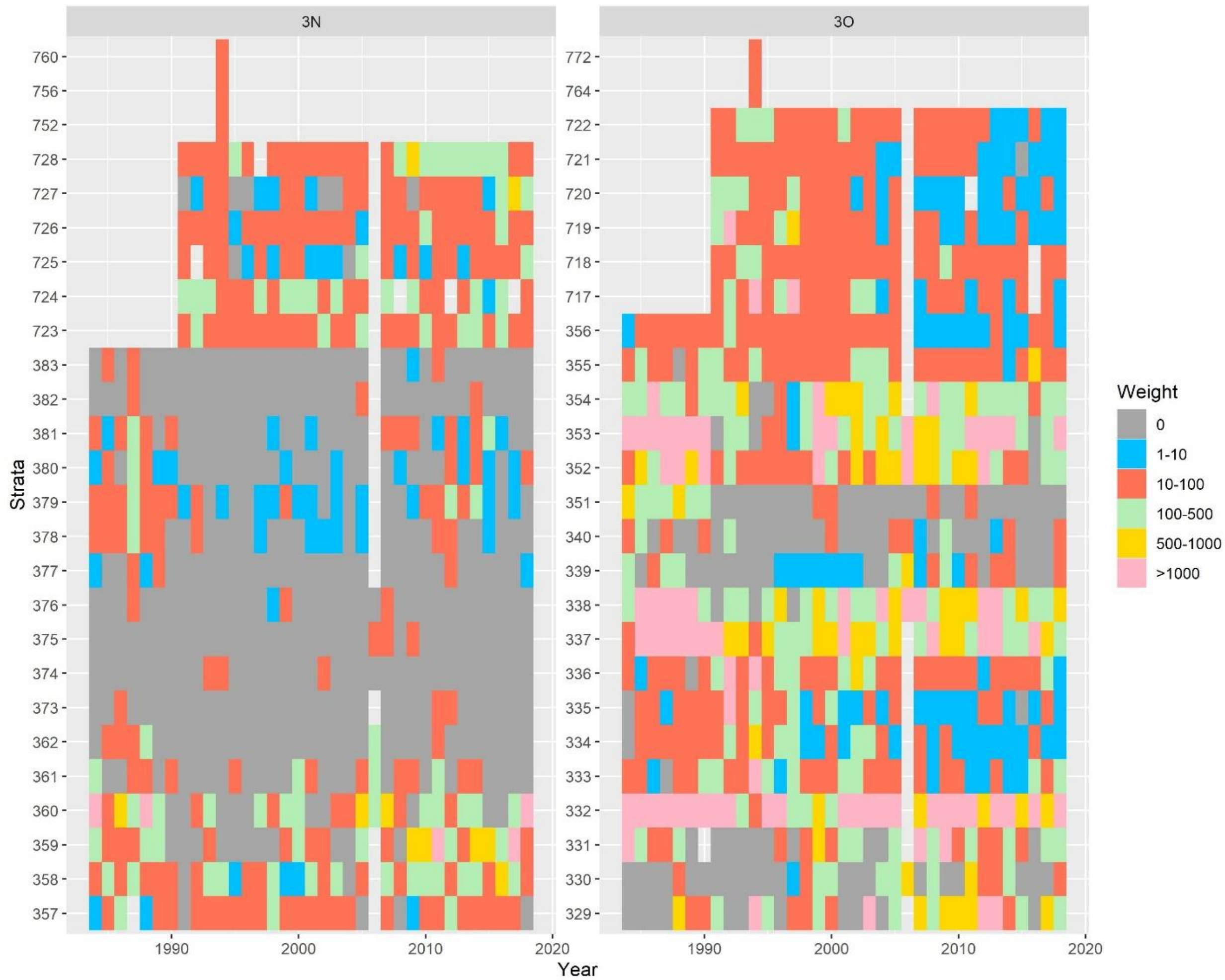

Figure 1.4 The catch of witch flounder in weight from the annual spring Canadian RV survey in NAFO Div. 3NO. Each grid color represents the range value of catch weight in the corresponding stratum and year based on the color bar.

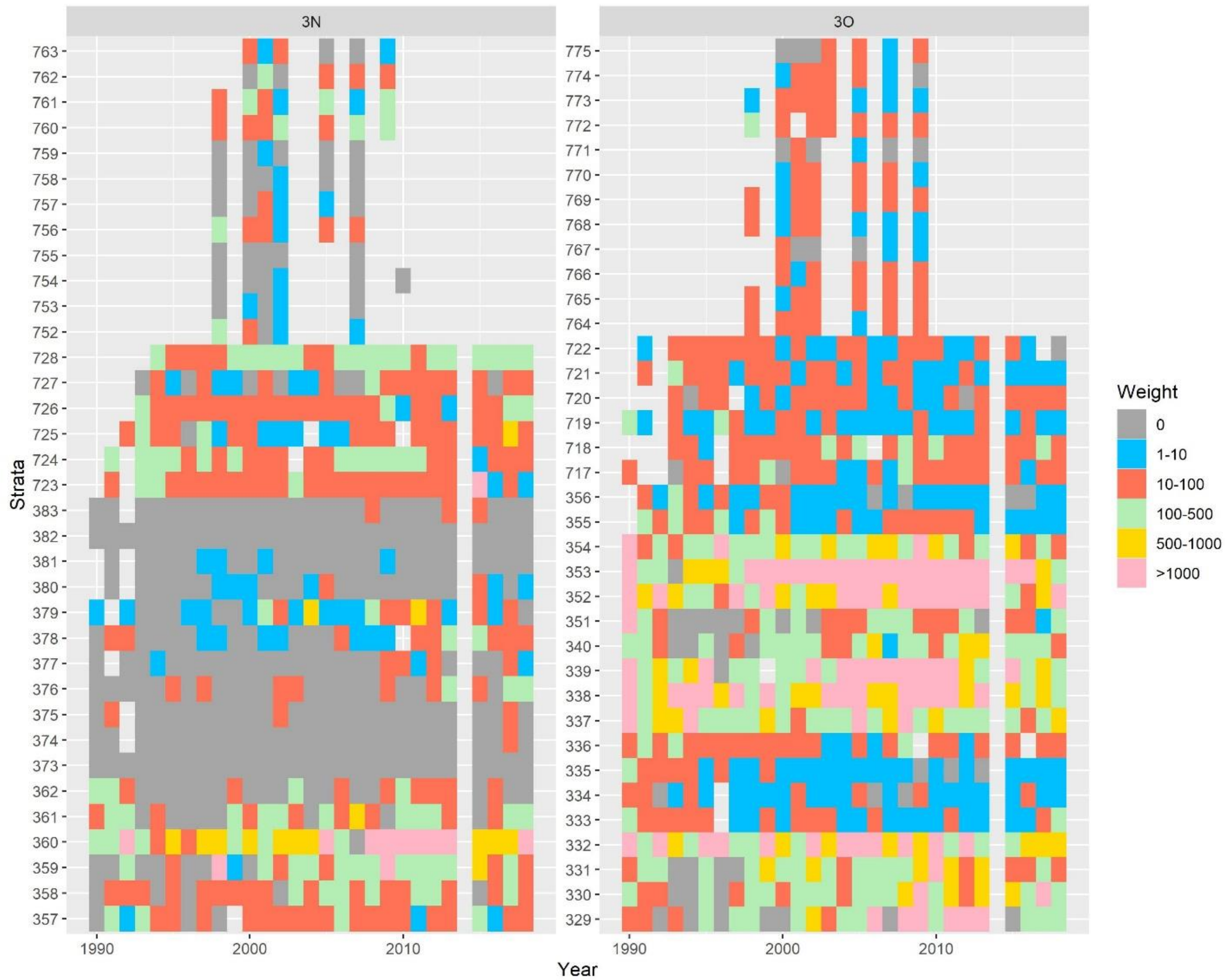

Figure 1.5 The catch of witch flounder in weight from the annual fall Canadian RV survey in NAFO Div. 3NO. Each grid color represents the range value of catch weight in the corresponding stratum and year based on the color bar.

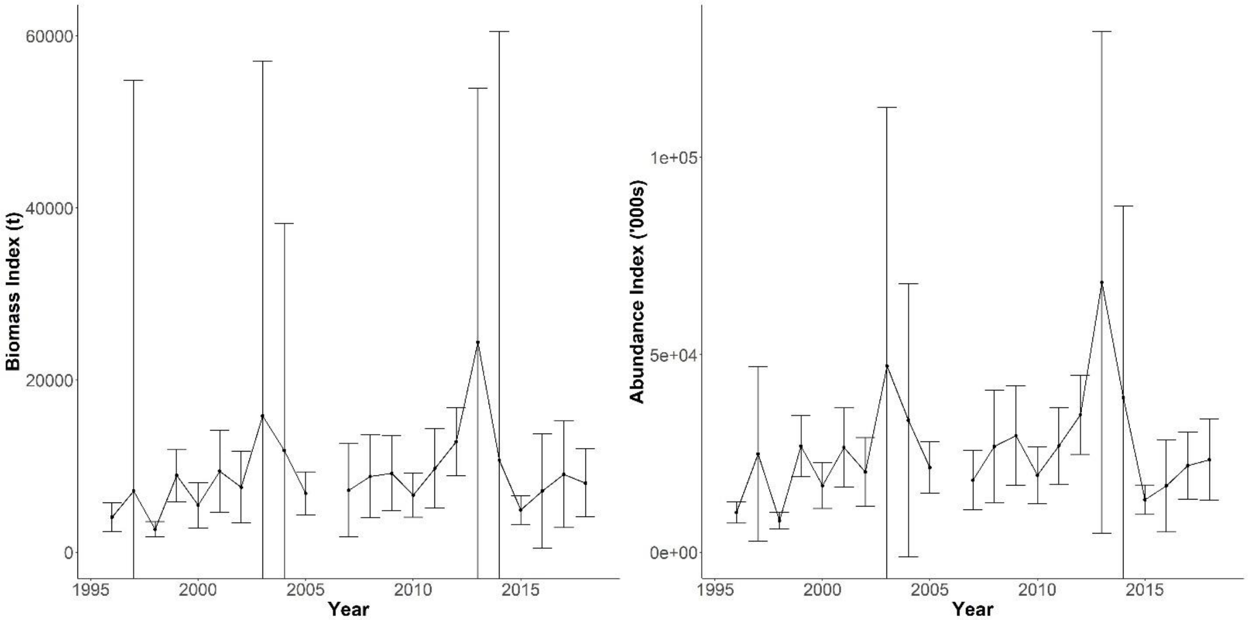

Figure 1.6 Biomass (t) and abundance ('000s), with associated 95% confidence intervals, for witch flounder from Canadian spring RV survey in NAFO Div. 3NO during 1996-2018. There was no data in 2006 due to incomplete coverage of the survey.

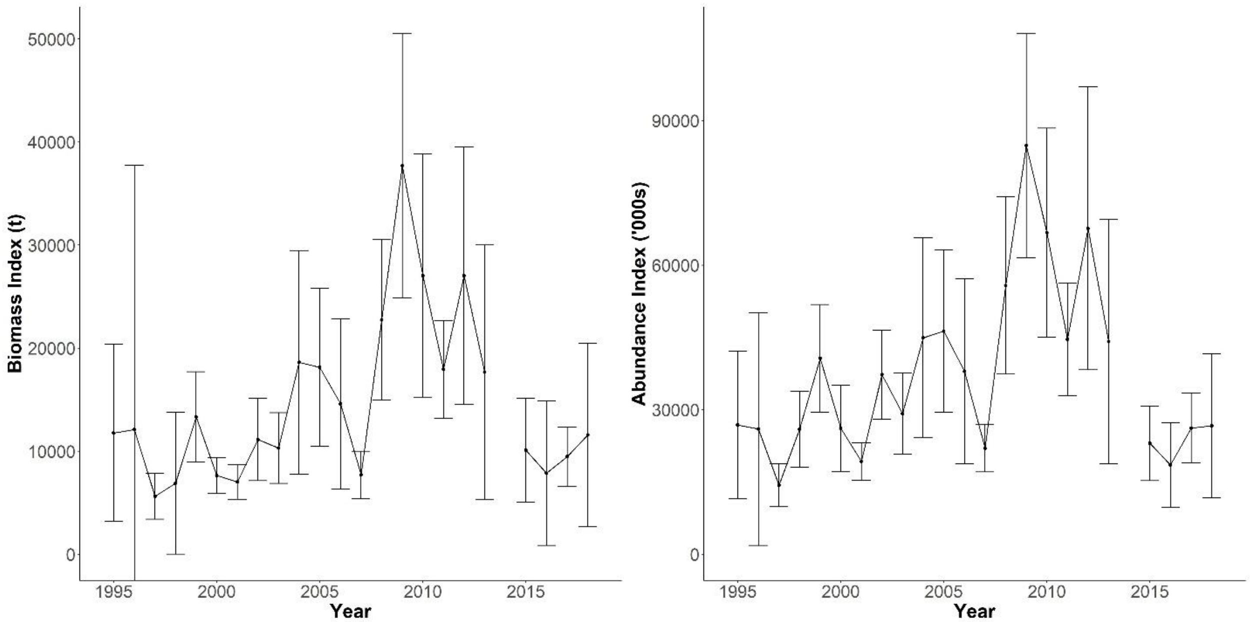

Figure 1.7 Biomass (t) and abundance (‘000s), with associated 95% confidence intervals, for witch flounder from Canadian fall RV survey in NAFO Div. 3NO during 1995-2018. There was no data in 2014 due to operational difficulties.

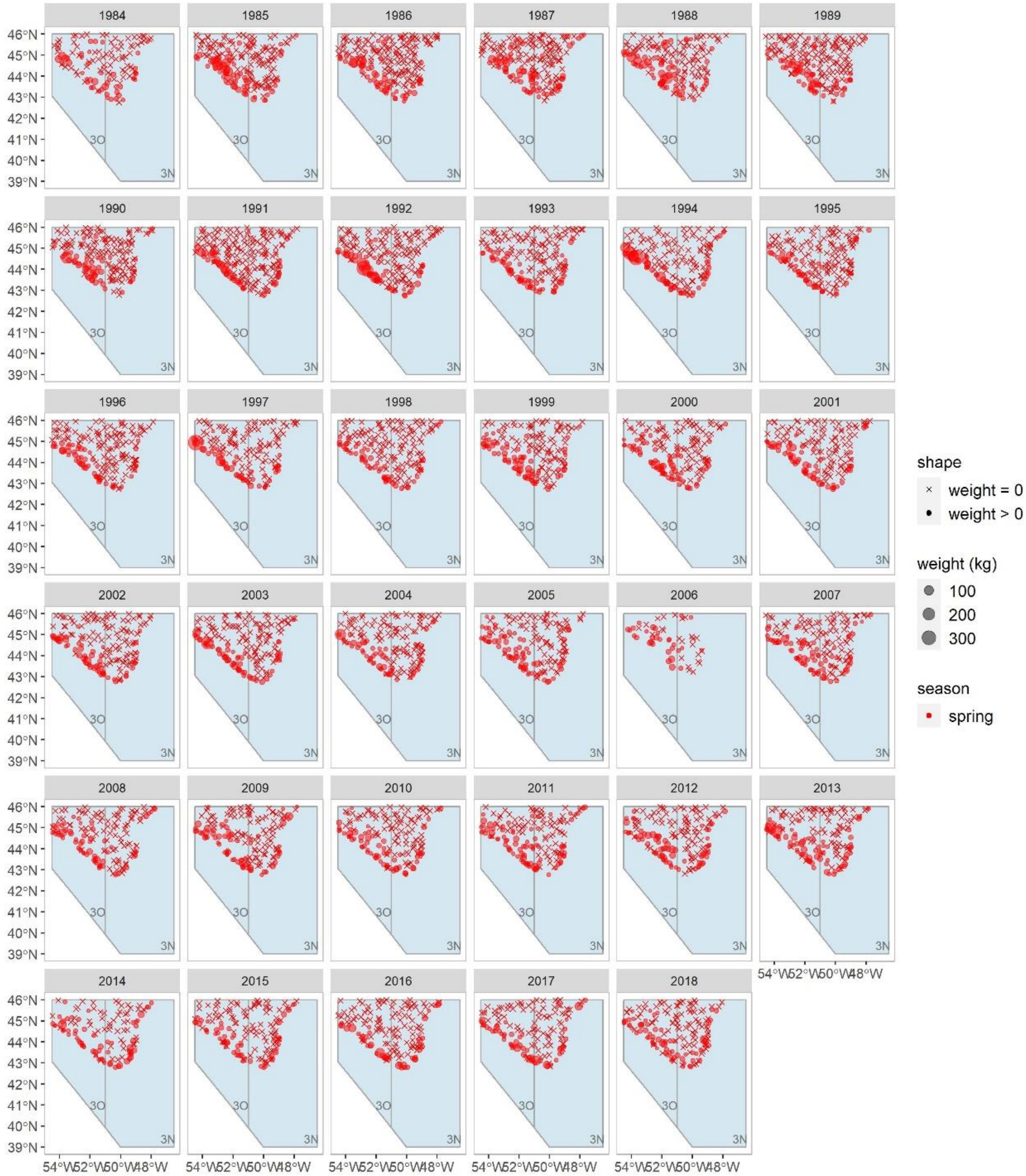

Figure 1.8 Distribution of NAFO Div. 3N and 3O witch flounder catch in weight (kg) from Canadian spring RV surveys during 1984 to 2018.

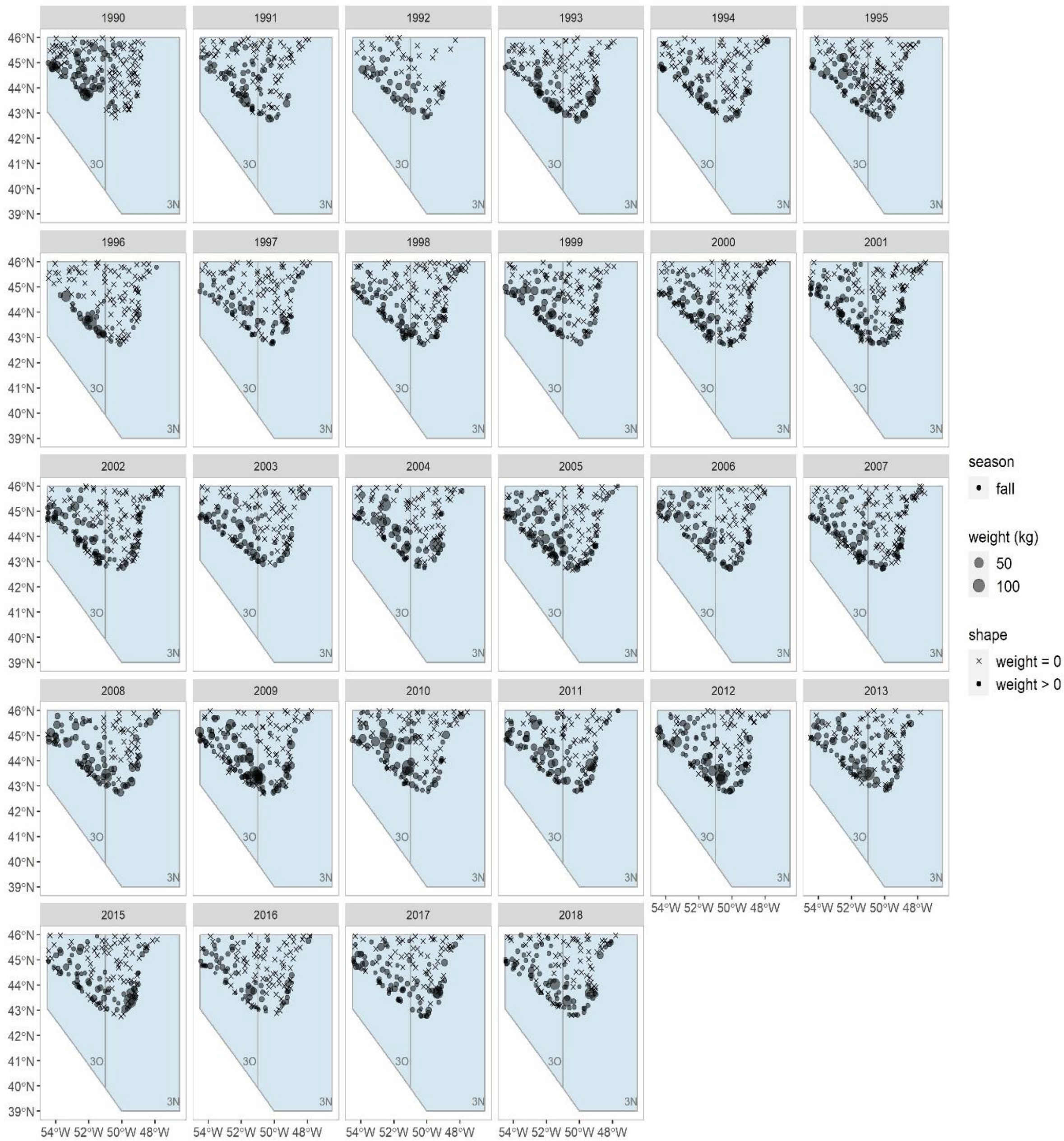

Figure 1.9 Distribution of NAFO Div. 3N and 3O witch flounder catch in weight (kg) from Canadian fall RV surveys during 1984 to 2018.

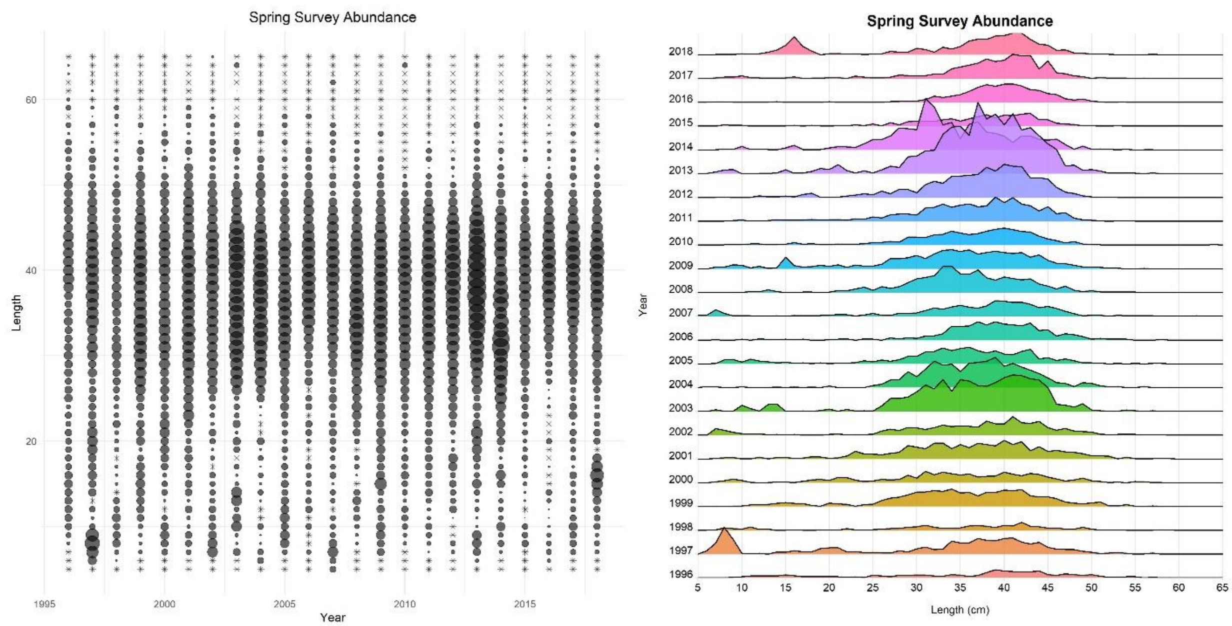

Figure 1.10 Length bubble and ridge plots of witch flounder from Canadian spring RV surveys (1996-2018) in NAFO Div. 3NO.

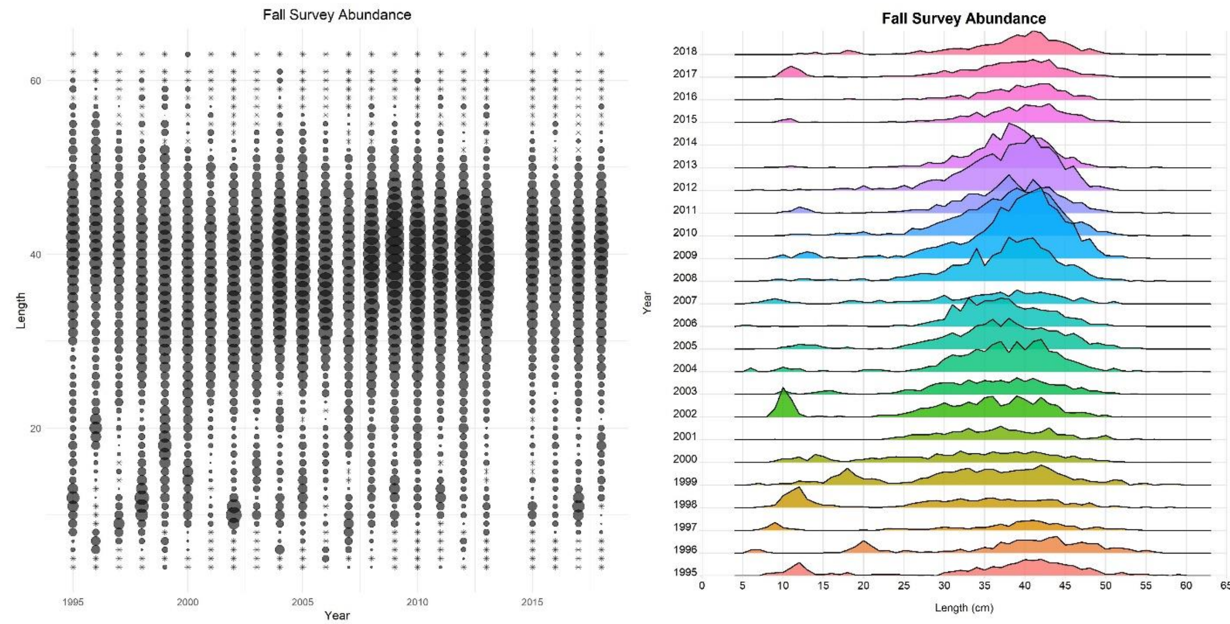

Figure 1.11 Length bubble and ridge plots of witch flounder from Canadian fall RV surveys (1995-2018) in NAFO Div. 3NO.

1.6 Bibliography

BOWERING, W. (1995). Assessment of witch flounder in NAFO Divisions 3NO. *NAFO SCR Doc*, *63*.

Bowering, W. R. (1976). Distribution, Age and Growth, and Sexual Maturity of Witch Flounder (Glyptocephalus cynoglossus) in Newfoundland Waters. *Journal of the Fisheries Research Board of Canada*, *33*(7), 1574–1584. https://doi.org/10.1139/f76-198

Bowering, W. R. (1990). Spawning of witch flounder (Glyptocephalus cynoglossus L.) in the Newfoundland-Labrador area of the northwest Atlantic as a function of depth and water temperature. *Fisheries Research*, *9*(1), 23–39.

Bowering, W. R., & Brodie, W. B. (1991). Distribution of commercial flatfishes in the Newfoundland-Labrador region of the Canadian Northwest Atlantic and changes in certain biological parameters since exploitation. *Netherlands Journal of Sea Research*, *27*(3–4), 407–422.

Bowman, R. E., & Michaels, W. L. (1984). *Food of seventeen species of northwest Atlantic fish*.

Brodie, W., Parsons, D., Murphy, E., & Dwyer, K. (2011). An assessment of the witch flounder resource in NAFO Divisions 3NO. *NAFO SCR Doc*, *11*, 029.

Burnett, J., Ross, M. R., & Clark, S. H. (1992). Several biological aspects of the witch flounder (Glyptocephalus cynoglossus (L.)) in the Gulf of Maine-Georges Bank region. *J. Northw. Atl. Fish. Sci*, *12*, 15–25.

Cadigan, N. G. (2011). Confidence intervals for trawlable abundance from stratified-random bottom trawl surveys. *Canadian Journal of Fisheries and Aquatic Sciences*, *68*(5), 781–794.

Cargnelli, L. M. (1999). *Essential fish habitat source document. Witch flounder, Glyptocephalus cynoglossus, life history and habitat characteristics*.

Cochran, W. G. (1977). *Sampling Techniques: 3d Ed*. Wiley.

Collette, B. B., & Klein-MacPhee, G. (2002). *Bigelow and Schroeder's Fishes of the Gulf of Maine*. Smithsonian Institution.

Faber, D. J., & McAllister, D. E. (1979). Development of Fishes of the Mid-Atlantic Bight. An Atlas of egg, larval and juvenile stages. *Journal of the Fisheries Board of Canada*, *36*(6), 706–707.

Fahay, M. P. (1983). Guide to the early stages of marine fishes occurring in the western North Atlantic Ocean, Cape Hatteras to the southern Scotian Shelf. *Journal of Northwest Atlantic Fishery Science*, *4*.

Fairbairn, D. J. (1981). Which witch is which? A study of the stock structure of witch flounder (Glyptocephalus cynoglossus) in the Newfoundland region. *Canadian Journal of Fisheries and Aquatic Sciences*, *38*(7), 782–794.

Fogarty, M. J., Idoine, J. S., Almeida, F. P., & Pennington, M. (1986). Modelling trends in abundance based on research vessel surveys. *ICES CM*.

Francis, R. (1984). An adaptive strategy for stratified random trawl surveys. *New Zealand Journal of Marine and Freshwater Research*, *18*(1), 59–71.

Grosslein, M. D. (1969). *Groundfish survey methods*. Bureau of Commercial Fisheries, Biological Laboratory.

Joanne Morgan, M., & Lee, E. (2018). Surplus production models in a Bayesian framework applied to witch flounder in NAFO Div. 3NO. *NAFO SCR Doc*, *18*, 053.

Kimura, D. K., & Somerton, D. A. (2006). Review of statistical aspects of survey sampling for marine fisheries. *Reviews in Fisheries Science*, *14*(3), 245–283.

Lee, E., Regular, P., Brodie, B., Rideout, R. M., Dwyer, K., Ings, D., & Morgan, J. (2014). An assessment of the witch flounder resource in NAFO Divisions 3NO. *NAFO SCR Doc*, *14*, 029.

Lenarz, W. H., & Adams, P. B. (1980). Some statistical considerations of the design of trawl surveys for rockfish (Scorpaenidae). *Fishery Bulletin*, *78*(3–4), 659.

Maddock Parsons, D., Rogers, B., & Rideout, R. (2020). An assessment of the witch flounder resource in NAFO Divisions 3NO. *NAFO SCR Doc*, *20*, 046.

McCallum, B. R., & Walsh, S. J. (1996). Groundfish survey trawls used at the Northwest Atlantic Fisheries Centre, 1971-present. *NAFO SCR Doc*, *96*(50), 18.

Morgan, M. J., Hvingel, C., & Koen-Alonso, M. (2015). Surplus production models in a Bayesian framework applied to witch flounder in NAFO Div. 3NO. *NAFO SCR*, *15*, 37.

Powles, P. M., & Kohler, A. C. (1970). Depth distributions of various stages of witch flounder (Glyptocephalus cynoglossus) off Nova Scotia and in the Gulf of St. Lawrence. *Journal of the Fisheries Board of Canada*, *27*(11), 2053–2062.

Rabe, J. (1999). *The behaviour, growth, and survival of witch flounder and yellowtail flounder larvae in relation to prey availability*. Memorial University of Newfoundland.

Rogers, B., & Morgan, J. (2019). An assessment of the witch flounder resource in NAFO Divisions 3NO. *NAFO SCR Doc*, *19*, 034.

Smith, S. J. (1997). Analysis of data from bottom trawl surveys. *Oceanographic Literature Review*, *44*(7), 747–748.

Swain, D. P., Savoie, L., Aubry, É., & du Golfe, R. (2012). *Assessment of witch flounder (Glyptocephalus cynoglossus) in the Gulf of St. Lawrence (NAFO Divisions 4RST), February 2012*.

Templeman, W. (1966). *Marine resources of Newfoundland*.

Thompson, S. K. (2012). Simple random sampling. *Sampling*, 9–37.

Walsh, S. J., & McCallum, B. R. (1997). Performance of the Campelen 1800 shrimp trawl during the 1995 Northwest Atlantic Fisheries Centre autumn groundfish survey. *NAFO Sci. Coun. Studies*, *29*, 105–116.

Xu, B., Ren, Y., Chen, Y., Xue, Y., Zhang, C., & Wan, R. (2015). Optimization of stratification scheme for a fishery-independent survey with multiple objectives. *Acta Oceanologica Sinica*, *34*(12), 154–169.

Chapter 2 Standardizing fall survey indices

2.1 Introduction

Standardized fishery-independent survey data are the most important information for fisheries stock assessment and management (Smith, 1990; Thorson et al., 2015). The main types of fishery-independent survey data include abundance index (the number of sampled fish caught for each year) and compositional data (the sampled population grouped by age, length, sex, etc. for each year) (Fisch et al., 2021; Maunder et al., 2020). There are also two forms of compositional data, counts (e.g. age- or length-specific abundance index) and proportions (e.g. the proportion of the number of fish at length or age). The total abundance and compositional data (proportions), or only compositional data (counts), historically have been used as input data within age- or size-structured assessment models in North America (Fisch et al., (Thorson & Haltuch, 2019). By fitting these data, the estimated stock cohort dynamics (track the number of fish in age or size classes over time), mortality, and growth of fish are provided, which are critical information to the fisheries management (Fisch et al., 2021; Punt, 2017). Thus, it is essential to ensure that the compositional data is as accurate and precise as possible (Maunder et al., 2020).

However, the compositional data derived from survey sampling only represent sample data from localized sample sites, which implies that these indices must be standardized precisely to represent the total stock (Thorson, 2014). There are two main approaches to standardizing these data, which are the design-based approach and the model-based approach respectively.

The design-based approach infers the finite fish population according to the randomness induced by the stratified random sampling design (Rogers & Morgan, 2019; Smith, 1990), which calculates the average catch in number of each category within each stratum, then generates the abundance indices of each category in each stratum weighted by area (Smith, 1990). Fisheries and Oceans Canada (DFO) and Northeast Fisheries Science Centers of the U.S. National Marine Fisheries Service (NMFS) primarily utilize a design-based approach to estimate indices of abundance for each category (Cadigan, 2011; Thorson et al., 2015). In this approach, the catches (response variable) in the survey are treated as observed without error at sample sites, and the inferences of this approach are based only on randomly selected sample sites in the survey (Cadigan, 2011; J. Chen et al., 2004; Smith, 1990).

In design-based theory, the value of the sample mean with any given sample may be larger or smaller than the true population mean. But, when accounting for all possible samples, the expected value of the sample mean equals the population mean (Thompson, 2012a). Thus, an obvious advantage of the design-based approach is that it can provide an unbiased estimator for the population mean, and the unbiased estimator does not depend on any assumptions about the population itself (e.g. escape rate from the net, distribution, and natural mortality) (Thompson, 2012a). This advantage is particularly evident in situations where we know very little about natural populations (Thompson, 2012a). And, the design-based approach also has been used in the recent stock assessment reports to indicate the stock status of NAFO Div. 3 NO witch flounder (Maddock Parsons et al., 2020; Rogers & Morgan, 2019).

The inferences of the design-based approach assume that the sampling sites in each stratum represent all locations in each stratum. However, poor sampling of the catch or occasional big tows may occur at randomly selected sample sites (Maunder et al., 2020). Although the design-based approach can obtain a relatively representative or balanced sample with a high probability by avoiding personal biases in selection (Thompson, 2012a), a serious disadvantage of this approach is that the estimated indices are less accurate for large spatial strata (Maunder et al., 2020), which results in imprecise information for abundance estimator (Thorson, 2014). Moreover, this approach uses area weighting to calculate the total statistical weight for each stratum, which may increase the uncertainty of estimated total abundance (Maunder et al., 2020). For example, large spatial strata with small sample sizes may have a higher weight compared to small spatial strata with large sample sizes and may have a similar weight as large spatial strata with large sample sizes, which results in the large variance may be introduced in abundance estimates from large strata with small sample sizes (Maunder et al., 2020). In addition, this approach also cannot account for the uncertain measurement of the stock in each sample site (e.g. different areas swept by a trawl and different fish catch rates) (Cadigan, 2011; Smith, 1990).

The model-based approach analyzes the survey compositional data conditional on a statistical model to predict composition index over a gird across the region of interest (Peel et al., 2013; Thorson et al., 2015) and makes inference according to an assumed probability function for the response variable (Cao et al., 2017; J. Chen et al., 2004). The main difference between the design-based approach and the model-based approach is the values of the variables of interest in the population (the CPUE from each sample unit) are assumed as random variables rather than fixed variables, and these random variables follow a parametric probability distribution (J. Chen et al., 2004; Thompson, 2012a). In this approach, stock composition indices are defined and estimated by estimating model parameters (J. Chen et al., 2004). Same as the design-based approach, the data that is input to the model for estimating are the size compositional data derived from fishery-independent survey observations.

The advantages of using the model-based approach are as follows. a) The model-based approach may have more precise and accurate estimated composition data than the design-based because such methods can handle missing survey data and other non-sampling errors (Thompson, 2012a). b) The model-based approach can derive estimators that make the most efficient use of the sample data, also it can assess estimators under different assumptions about the stock population (Thompson, 2012a). c) The model-based approach can account for covariates (e.g. different survey time and locations, multiple fishing gears and sampling vessels (Thorson et al., 2015)) and make good use of auxiliary information (e.g. bottom temperature, depth and bottom substrate type), which can avoid confounding systematic trends with variability and lead more precise estimates of composition index (Cao et al., 2017; Thompson, 2012a; Thorson et al., 2015). However, the model-based estimates can potentially be biased compared to the design-based approach, due to model-based estimates of the survey population mean are not based on the sample mean (Smith, 1990). Therefore, a thorough comparison needs to be conducted before inputting the survey indices into the stock assessment model.

As mentioned above, the design-based approach may have large variance in abundance estimates (Thompson, 2012a). The spatial distribution of fish stock can vary greatly over time due to fishing and natural mortality, migration, and recruitment (J. Chen et al., 2004). If the fish density within each stratum is roughly assumed to be constant, then any systematic trend within a stratum would be interpreted as random variability, which may result in inflating the coefficient of variation (Peel et al., 2013). Based on the above considerations, a model-based approach has been used to standardize RV survey compositional data of witch flounder.

In this chapter, I first describe two methods (i.e. design-based approach and model-based approach) of standardizing fall RV survey size compositional data for NAFO Div. 3NO witch flounder. I then estimate the abundance-at-length indices and the proportion-at-length indices through two methods and compare the performance of the two approaches.

2.2 Methods

2.2.1 Data input

I used annual fall size-compositional data (using length subsampling of each sample from stratified random bottom trawl surveys) conducted by DFO from 1995 to 2018 for NAFO Div. 3NO witch flounder. Considering different fishing gear was used in pre-1995 and no conversion factors available to adjust the catch, only post 1995 survey data are analyzed in this thesis. Since catches of fish less than 10 cm in length and greater than 52 cm are low enough in most years (mostly zero catches) (Figure 1.9), I have eliminated these length categories for ease of calculation. So the size-compositional data is structured into 21 length categories with a bin size of 2 cm, where the starting length is 10 cm, and the ending length is 52 cm.

2.2.2 Estimating design-based indices

Survey design-based abundance index is an estimate of the catch at all sample sites in the survey region (Thompson, 2012a). The total catch for length category *c* in stratum h in year *t* is

$$\tau_{ch}(t) = \sum_{a=1}^{N_h(t)} y_{cha}\,(t) \tag{2.1}$$

where $N_h(t)$ is the number of sampling units in stratum h in year *t*, $y_{cha}(t)$ is the observed value in ath unit for length category *c* in stratum h in year *t*. An unbiased estimator of τ_{ch} is

$$\hat{\tau}_{ch}(t) = N_h(t)\bar{y}_{ch}(t) \tag{2.2}$$

where $\bar{y}_{ch}(t)$ is the sample mean for length category c in stratum h in year t, as calculated from

$$\bar{y}_{ch}(t) = \frac{1}{n_h(t)} \sum_{i=1}^{n_h(t)} y_{cha}\,(t) \tag{2.3}$$

where n_h is the number of units sampled in stratum h in year t. We treat the abundance of the uncovered stratum or strata as missing. An unbiased estimator for the total population and the population mean (mean catch number per trawl unit) for length category c in year t are equations (2.4) and (2.5) respectively, in which $H(t)$ presents the number of strata in year t and $N(t)$ represents the number of all sampling units in year t.

$$\hat{\tau}_c(t) = \sum_{h=1}^{H(t)} \hat{\tau}_{ch}\,(t) \tag{2.4}$$

$$\hat{y}_c(t) = \frac{1}{N(t)} \sum_{h=1}^{H(t)} \hat{\tau}_{ch}(t) \tag{2.5}$$

I then use $\hat{\tau}_c(t)$ to calculate total abundance across all length categories in year t

$$\hat{\tau}(t) = \sum_{c=1}^{n_c} \hat{\tau}_c(t) \tag{2.6}$$

where n_c is number of total length categories. The proportion of abundance for each length category c in year t is

$$\hat{P}_c(t) = \frac{\hat{\tau}_c(t)}{\hat{\tau}(t)} \tag{2.7}$$

The finite-population variance for length category c in stratum h in year t is given by equation (2.8).

$$\sigma_{ch}^2(t) = \frac{1}{N_h(t) - 1} \sum_{i=1}^{N_h(t)} (y_{chi}(t) - \mu_{ch}(t))^2 \tag{2.8}$$

Where $\mu_{ch}(t) = \frac{\tau_{ch}(t)}{N_h(t)}$ is the population mean for length category c in stratum h in year t. The variance of the total population for length category c in year t is

$$var(\hat{\tau}_c(t)) = \sum_{h=1}^{H(t)} N_h(t)\,(N_h(t) - n_h(t))\,\frac{\sigma_{ch}^2(t)}{n_h(t)} \tag{2.9}$$

An unbiased estimator of the variance of the total population $var(\hat{\tau}_c(t))$ for length category c is given in equation (2.10).

$$\widehat{var}(\hat{\tau}_c(t)) = \sum_{h=1}^{H(t)} N_h(t)(N_h(t) - n_h(t))\,\frac{s_{ch}^2(t)}{n_h(t)} \tag{2.10}$$

where s_{ch}^2 is the sample variance for length category c in stratum h in year t.

$$s_{ch}^2(t) = \frac{1}{n_h(t) - 1} \sum_{i=1}^{n_h(t)} (y_{cha}(t) - \bar{y}_{ch}(t))^2 \tag{2.11}$$

The variance of the population mean for length category c in year t is given by

$$var(\hat{y}_c(t)) = \sum_{h=1}^{H(t)} \left(\frac{N_h(t)}{N(t)}\right)^2 (1 - f_h(t)) \frac{\sigma_{ch}^2(t)}{n_h(t)} \tag{2.12}$$

where $f_h(t) = \frac{n_h(t)}{N_h(t)}$ is the sampling fraction in year t. An unbiased estimator for the variance of the population mean $var(\hat{y}_c(t))$ for length category c is

$$\widehat{var}(\hat{y}_c(t)) = \sum_{h=1}^{H(t)} \left(\frac{N_h(t)}{N(t)}\right)^2 (1 - f_h(t)) \frac{s_{ch}^2(t)}{n_h(t)} \tag{2.13}$$

The estimation variance for proportion $\hat{P}_c(t)$ is

$$SE[\hat{P}_c(t)]^2 \approx \frac{\hat{\tau}_c(t)^2}{\widehat{\tau(t)}^2}\{\frac{\widehat{var}(\hat{y}_c(t))}{\hat{\tau}_c(t)^2} - 2\frac{\widehat{var}(\hat{y}_c(t))}{\hat{\tau}_c(t)\hat{\tau}(t)} + \frac{\sum_{c=1}^{n_c} \widehat{var}(\hat{y}_c(t))}{\widehat{\tau(t)}^2}\} \tag{2.14}$$

2.2.3 Estimating model-based indices

The vector autoregressive spatiotemporal (VAST) model is an R package developed by (Thorson & Barnett, 2017) to estimate abundance indices and/or compositional data for a target species in the time series by simultaneously estimating spatiotemporal variation in density using spatially referenced data (Thorson, 2019). VAST builds upon spatiotemporal delta-generalized linear mixed model analysis (Thorson et al., 2015). I implement VAST package (ver. 3.6.1 available online) in the R statistical environment to estimate abundance-at-length and the proportion-at-length for NAFO Div. 3NO witch flounder.

The delta model is commonly used by scientists to analyze sampling data from fishery surveys. Delta model that included in VAST consists of two separately generalized linear mixed effect models (GLMMs) that models encounter probability (the probability of at least one individual capture for tows at a given location and time) and the positive catch rates (the probability distribution for sample abundance when encountered) (Thorson, 2018, 2019). The resulting predictions from these two GLMMs provide estimates of local density and total abundance of given species (Thorson, 2018; Thorson et al., 2015). Spatio-temporal variations are estimated using Gaussian Markov random fields (Lindgren et al., 2011; Thorson et al., 2015). I use gamma distribution for positive catch rates. Specifically, the probability distribution function for survey sampling data is

$$\Pr(\mathrm{n}_c(i) = B) = \begin{cases} 1 - p_c(i) & \text{if } B = 0 \\ p_c(i) \times \mathrm{Gamma}\{\mathrm{B}|r_c(i), {\sigma_m}^2(c)\} & \text{if } B > 0 \end{cases} \tag{3.1}$$

where $\mathrm{n}_c(i)$ is abundance-at-length for sample i, $p_c(i)$ is the predicted encounter probability $r_c(i)$ is the predicted abundance density for positive catch rates, and ${\sigma_m}^2(c)$ is the dispersion parameter for probability density function ($\mathrm{Gamma}\{B|r_c(i), {\sigma_m}^2(c)\}$) for positive catch rates.

In the conventional delta model, the encounter probability is modelled via the logit-link function (Thorson, 2018).

$$p_c(i) = logit^{-1}(a_1(i)) \tag{3.2}$$

$$r_c(i) = \alpha_i \times log^{-1}(a_2(i))$$

where α_i is the area-swept for sample i and we treat α_i as an offset for expected number of individuals encountered, $a_1(i)$ is the linear predictor for encounter probability, $a_2(i)$ is the linear predictor for positive catch rates. The equations of two linear predictors $a_1(i)$ and $a_2(i)$ that are involved in two separate GLMMs of the conventional delta model are

$$a_1(i) = \beta_1(c, t_i) + \sigma_{\omega 1}(c)\omega_1(c, s_i) + \sigma_{\varepsilon 1}(c)\varepsilon_1(c, s_i, t_i) \quad (3.3)$$

$$a_2(i) = \beta_2(c, t_i) + \sigma_{\omega 2}(c)\omega_2(c, s_i) + \sigma_{\varepsilon 2}(c)\varepsilon_2(c, s_i, t_i)$$

where $\beta_1(c, t_i)$ and $\beta_2(c, t_i)$ are intercepts for encounter probability and positive catch rates respectively for each length category c and time t. $\omega_1(c, s_i)$ and $\omega_2(c, s_i)$ are random effects representing spatial variation at location s_i of each sample i, $\sigma_{\omega 1}(c)$ and $\sigma_{\omega 2}(c)$ represent standard deviation for spatial variation in the two linear predictors respectively, $\varepsilon_1(c, s_i, t_i)$ and $\varepsilon_2(c, s_i, t_i)$ are random effects representing spatiotemporal variation among location s_i and time t_i of each sample i, $\sigma_{\varepsilon 1}(c)$ and $\sigma_{\varepsilon 2}(c)$ represent standard deviation for spatiotemporal variation in two linear predictors respectively (Thorson, 2019; Thorson & Haltuch, 2019). I assume an independent intercept for each size and year, which is designed to minimize the estimation covariance for size composition between sizes and years.

I specify 200 locations ('knots') distributed over the entire spatial grid to approximate all spatial and spatiotemporal variation terms. A k-means algorithm that included in VAST was used to define the location of 200 knots to minimize the total distance between the sampling data location to their nearest knot (Thorson, 2019). I varied the number of knots to make sure that the results are qualitatively similar to results from more knots while still having manageable computational time. The distribution of knots is shown in (Figure 2.1). The spatial variables at the sampled location are assumed equal to their value at the nearest knot. I specify spatial and spatiotemporal random effects that follow a multivariate normal distribution:

$$\omega_1(c) \sim MVN(\mathbf{0}, \mathbf{R_1}) \qquad (3.4)$$
$$\omega_2(c) \sim MVN(\mathbf{0}, \mathbf{R_2})$$
$$\varepsilon_1(c,t) \sim MVN(\mathbf{0}, \mathbf{R_1})$$
$$\varepsilon_2(c,t) \sim MVN(\mathbf{0}, \mathbf{R_2})$$

where $\mathbf{R_1}$ and $\mathbf{R_2}$ are correlation matrices for $p_c(i)$ and $r_c(i)$ respectively, and approximated as following a Matern function (Lindgren et al., 2011):

$$\mathbf{R_1}(s, s+h) = \frac{1}{2^{\nu-1}\,\Gamma(\nu)} \times (\kappa_1|h\mathbf{H}|)^{\nu} \times K_{\nu}(\kappa_1|h\mathbf{H}|) \qquad (3.5)$$
$$\mathbf{R_2}(s, s+h) = \frac{1}{2^{\nu-1}\,\Gamma(\nu)} \times (\kappa_2|h\mathbf{H}|)^{\nu} \times K_{\nu}(\kappa_2|h\mathbf{H}|)$$

where H is a two-dimensional linear transformation representing geometric anisotropy, ν is the Matern smoothness (fixed at 1.0), κ_1 and κ_2 govern the decorrelation distance for the first linear predictor and the second linear predictor respectively (Thorson et al., 2015; Thorson & Haltuch, 2019).

The estimation of VAST model parameters is performed in R using Template model builder (TMB) package. TMB is an open source R package developed by (Kristensen et al., 2015) at the Danish Technical University, which is inspired by the Automatic Differentiation Model Builder package (ADMB) and formulated in C++ (D. A. Fournier et al., 2012; Kristensen et al., 2015). TMB is designed for large, and complex hierarchical models (e.g. delta-generalized linear mixed model) and used to fit non-linear statistical latent variable (random effects) models to data (Kristensen et al., 2015). The users can define the joint likelihood for the data and the random effects as a C++ template function, and conduct pre- and post-processing of data in R (Kristensen et al., 2015). The TMB package allows users to estimate and maximize the Laplace approximation of the marginal likelihood where the random effects have been automatically integrated out, as well as obtain the first and second derivatives of the marginal likelihood by using automatic differentiation (AD) (Kristensen et al., 2015)

I use TMB package to estimate model parameters by implementing Laplace approximation to the marginal likelihood of fixed effects ($\beta_1(c, t_i), \sigma_{\omega 1}, \sigma_{\varepsilon 1}(c)$, $\beta_2(c, t_i)$, $\sigma_{\omega 2}(c)$, $\sigma_{\varepsilon 2}(c)$, and ${\sigma_m}^2(c)$), and using a gradient-based nonlinear optimizer to identify the maximum likelihood estimate of fixed effects. I use the stochastic partial differential equation (SPDE) to approximate the probability of the spatial and spatiotemporal random effects ($\omega_1(c, s_i)$, $\varepsilon_1(c, s_i, t_i)$, $\omega_2(c, s_i)$, $\varepsilon_2(c, s_i, t_i)$) (Lindgren et al., 2011; Thorson, 2019). I also apply the epsilon bias-correction estimator in TMB, which accounts for bias caused by the nonlinear transformation of random effects (Thorson, 2019). I use two Newton-step to tighten convergence and confirm the model converges (maximum gradient of the marginal likelihood of fixed effects is $< 10^{-6}$). The model estimated parameters are used to predict abundance density in length category c at each location s among year t. The equation of the predict abundance density is

$$d_c(s,t) = p_c(s,t) \times r_c(s,t) \tag{3.6}$$

The predicted abundance in length category c for the entire spatial domain is

$$I_c(t) = \sum_{s=1}^{n_s} a(s) \times d_c(s,t) \tag{3.7}$$

where $a(s)$ is the trawable unit area associated with the knot s, $d_c(s,t)$ is predict abundance density for length category c at every location s among year t. The predicted total abundance across all length categories for the entire spatial domain is

$$I(t) = \sum_{c=1}^{n_c} I_c(t) \tag{3.8}$$

the proportion for each length category is

$$P_c(t) = \frac{I_c(t)}{I(t)} \tag{3.9}$$

And the estimate of proportion variance is

$$SE[P_c(t)]^2 \approx \frac{I_c(t)^2}{I(t)^2}\{\frac{SE[I_c(t)]^2}{I_c(t)^2} - 2\frac{SE[I_c(t)]^2}{I_c(t)I(t)} + \frac{\sum_{c=1}^{n_c} SE[I_c(t)]^2}{I(t)^2}\} \tag{3.10}$$

where $SE[I_c(t)]$ is standard error of predicted population abundance for length category c.

2.3 Results

I apply both design-based estimator and model-based estimator to length compositional data for NAFO Div. 3NO witch flounder. The plots of predicted abundance in density for 21 length categories in the model-based estimator from 1995 to 2018 (except 2014) are shown in (Figures 2.2-2.22). This indicates that witch flounder is mainly concentrated along the western edges of the Grand Bank in the deep water (Figures 2.2-2.22). The high-density area of the juvenile witch flounder with a body length of 10 to 14 cm shifted from the northwest to the southwest of NAFO Div. 3NO from 1996 to 1998 (Figures 2.2-2.3). The juvenile witch flounder with a body length of 22 to 36 cm was relatively evenly distributed in NAFO Div. 3NO, with no obvious change, from 1995 to 2018 (Figures 2.8-2.14). The adults greater than 40 cm in length was distributed in shallower waters compared to younger fish (Figures 2.17-2.22).

The comparison of the predicted abundance-at-length from the two approaches is shown in (Figure 2.23). The indices estimated from the model-based approach are smoother and show smaller CI than that from design-based approach (Figures 2.23 - 2.24). The estimated indices for 32 to 40 length categories from design-based estimator are obviously larger than that from model-based estimator. The comparison of the predicted proportion at length is shown in (Figure 2.24). Both design-based estimator and model-based estimator generate relatively similar estimates of the proportion of abundance-at-length, and similar trends in cohort dynamics are also shown in these estimates. For example, strong cohorts at the length of 36-40 cm first appear in 2004, which can be continually identified until 2018.

2.4 Discussion

Standardizing survey indices typically takes into account the following: a) spatial and temporal differences in sampling intensity; b) non-independent samples in survey data; c) the effect of covariates (e.g. vessel effects, habitat covariates and catchability covariates) (Thorson, 2014). My study focuses on standardizing size-compositional abundance data using design-based approach and model-based approach and comparing the results. The results demonstrate the model-based estimator substantially improves precision compared to the design-based estimator, by providing smaller confidence intervals and smaller coefficient of variation (Figure 2.23-2.25). Allowing information to be shared among areas that help resolve problems associated with highly weighted but poorly sampled large spatial strata (Maunder et al., 2020). For example, when sampling intensity varies among areas, the model-based estimator can get smaller variance estimates than the design-based estimator. The model-based estimator can potentially further increase estimation precision by including habitat covariates in future research. In the model-based estimator, the spatial variation can be estimated and spatially-correlated habitat variability can be controlled (Shelton et al., 2014). But in the design-based estimator, the spatially-correlated variables cannot be explicitly included, which results in residual variance among samples within each stratum (Cao et al., 2017; Thorson et al., 2021). When using the design-based estimator, this residual variance results in an increase in the variance of the estimated compositional data, which also results in increased standard errors (Thorson et al., 2021).

In both approaches, compositional data may include statistical non-independent samples (Thorson, 2014). For example, fish caught in one tow might have similar size, and, consequently, repeated samples from individual tows may not reflect independent samples from the whole stock (Thorson, 2014). So the effective sample sizes may be smaller than the actual sample sizes (the total number of fish counted)(R. C. Francis, 2011; Thorson, 2014). The data types that are integrated into the stock assessment model in the US West Coast are usually abundance index and compositional data (proportions) (Thorson & Haltuch, 2019). Inputting the compositional data (proportions) that includes statistical non-independent samples in the stock assessment model may result in imprecision for estimated indices (Thorson & Haltuch, 2019). Thus, it is particularly important to estimate the effective sample size, which can contribute to determining the data weighting to ensure compositional data (proportions) aren't more influential on estimated abundance trends than abundance index (R. C. Francis, 2011; Thorson, 2014). The estimated effective sample size can be calculated in both approaches based on the variance for estimated compositional data (proportions) using the following formula respectively (Thorson, 2014).

$$S_{design-based}(t) = Median_c \left\{ \frac{\hat{P}_c(t)(1-\hat{P}_c(t))}{SE[\hat{P}_c(t)]^2} \right\} \tag{3.11}$$

$$S_{model-based}(t) = Median_c \left\{ \frac{P_c(t)(1-P_c(t))}{SE[P_c(t)]^2} \right\} \tag{3.12}$$

The comparison of estimated effective sample size between two approaches are shown in (Figure 2.26), which indicates the estimated effective sample sizes in the model-based approach is greater than the design-based approach. This result implies that the model-based estimator utilizes more sample sizes from survey than design-based estimator, thus making the estimation more accurate.

I find general agreement in trends between design-based and model-based indices. However, from 2004 to 2013 (except 2007), design-based indices are considerably higher in 32 to 40 cm (Figure 2.23). This could be due to potential biases introduced by model-based approach. Thorson and Haltuch (2019) demonstrated that VAST and design-based indices agree very well in a simulated dataset from bottom trawl surveys in the Eastern Bering Sea. Although VAST minimizes the estimated imprecision for size composition between sizes and years. I use "epsilon bias-correction estimator” to correct for retransformation bias (Thorson, 2019) and in VAST, bias in the spatial and spatiotemporal variations can still be present for this particular DFO survey configuration. Further research using simulation studies is needed to quantify this potential bias.

Tables

Table 2.1: List of symbols for a stratified random sampling design (design-based estimator)

Symbol	Name
τ_{ch}	Total catch for length category *c* in stratum *h*
$\hat{\tau}_{ch}$	Unbiased estimator of τ_{ch}
$\hat{\tau}_{c}$	Total catch for length category *c* in all strata
$\hat{\tau}$	Total abundance across all length categories
n_c	Number of total length categories
n_h	Number of units sampled in stratum *h*
N_h	Number of sampling units in stratum *h* ($N_h = \frac{Stratum\ area}{Swept\ area}$)
N	Number of all sampling units
y_{cha}	Observed value in ath unit for length category *c* in stratum *h*
$\bar{y}_{ch}$	Sample mean for length category *c* in stratum *h*
$\hat{y}_{c}$	Population mean for length category *c* in all strata
H	Number of strata
$\hat{P}_{c}$	Proportion of abundance in each length category *c*
μ_{ch}	Population mean for length category *c* in stratum *h*
s_{ch}^2	Sample variance for length category *c* in stratum *h*
f_h	Sampling fraction

Table 2.2 List of names and symbols describing the VAST models

Symbol	Name	Type
$\mathrm{n}_c(i)$	observed abundance-at-length for sample i	Data
α_i	area-swept for sample i	Data
I	Sample index	Index
t	Time index	Index
s	Site index	Index
c	Length category	Index
$a_1(i)$	The first linear predictor of encounter probability	
$a_2(i)$	The second linear predictor of positive catch rates	
$\beta_1(c, t_i)\ and\ \beta_2(c, t_i)$	Temporal Intercept	Fixed effect
$\sigma_{\omega 1}(c)$ and $\sigma_{\omega 2}(c)$	Standard deviation for spatial variation	Fixed effect
$\sigma_{\varepsilon 1}(c)$ and $\sigma_{\varepsilon 2}(c)$	Standard deviation for spatiotemporal variation	Fixed effect
${\sigma_m}^2(c)$	Dispersion parameter for probability density function	Fixed effect
$\omega_1(c, s_i)$ and $\omega_2(c, s_i)$	Spatial variation at location s_i of each sample i	Random effect
$\varepsilon_1(c, s_i, t_i)$ and $\varepsilon_2(c, s_i, t_i)$	Spatiotemporal variation among location s_i and time t_i of each sample i	Random effect
$p_c(i)$	Predicted encounter probability for sample i	Derived quantity
$r_c(i)$	Predicted abundance density for positive catch rates for sample i	Derived quantity
$d_c(s, t)$	Predict abundance density	Derived quantity
$a(s)$	Area associated with the knot *s*	Derived quantity
$I_c(t)$	Predicted abundance in length category *c* for the entire spatial domain	Derived quantity
$I(t)$	Predicted total abundance across all length categories for the entire spatial domain	Derived quantity

Figures

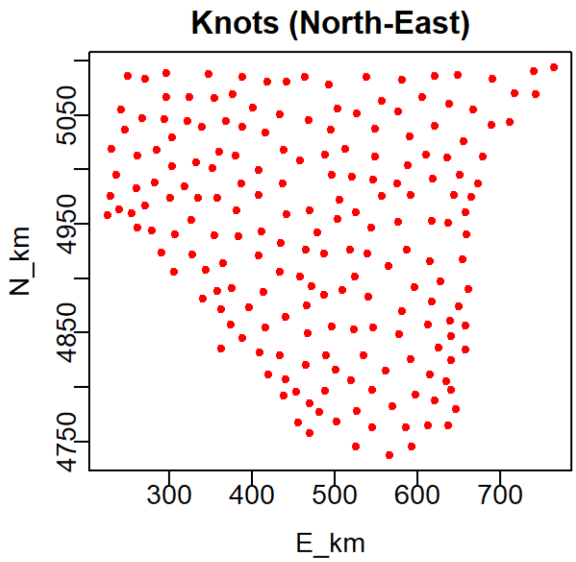

Figure 2.1 Map of distribution of in NAFO Div. 3NO. E_km and N_km are distances converted from latitude and longitude.

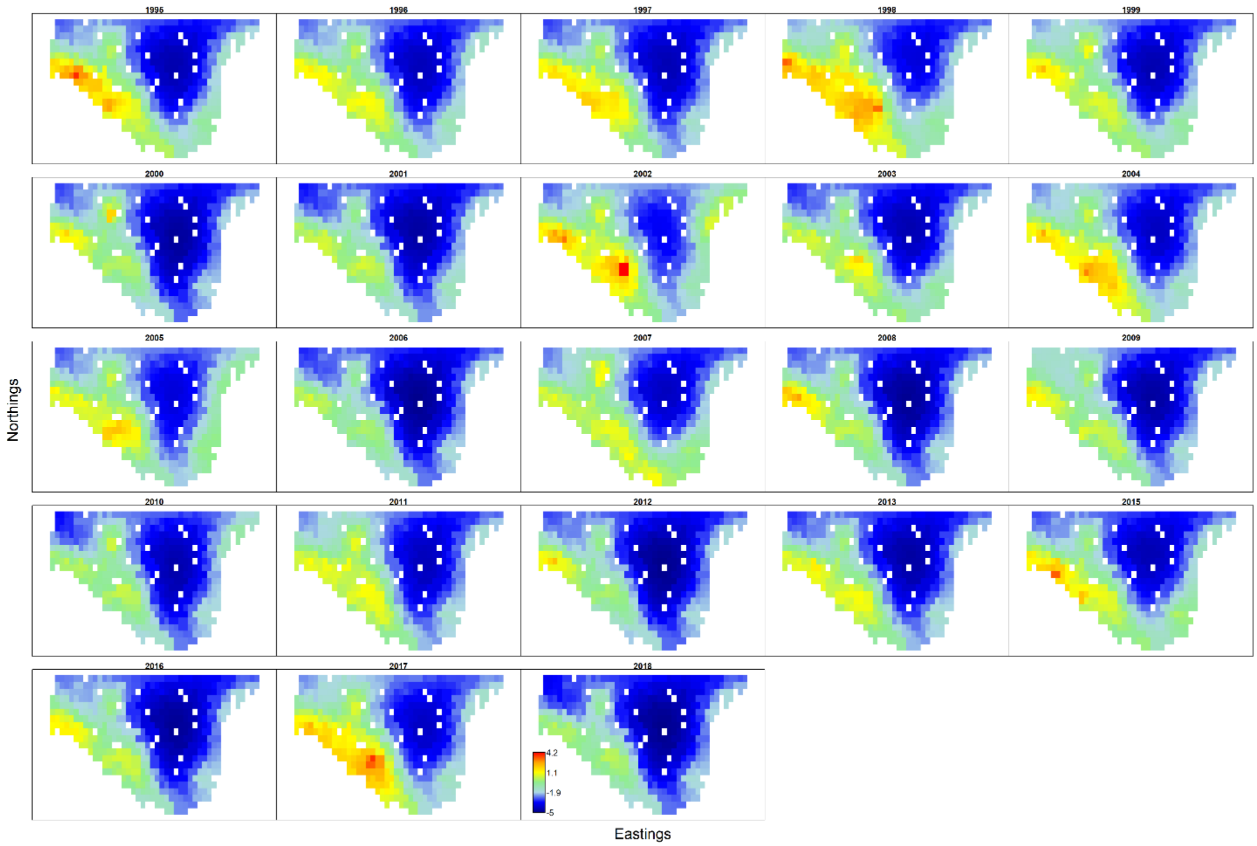

Figure 2.2 Distribution plot of predicted abundance in density for lengths 10-12 cm of witch flounder in NAFO Div. 3NO from 1995 to 2018 (except 2014).

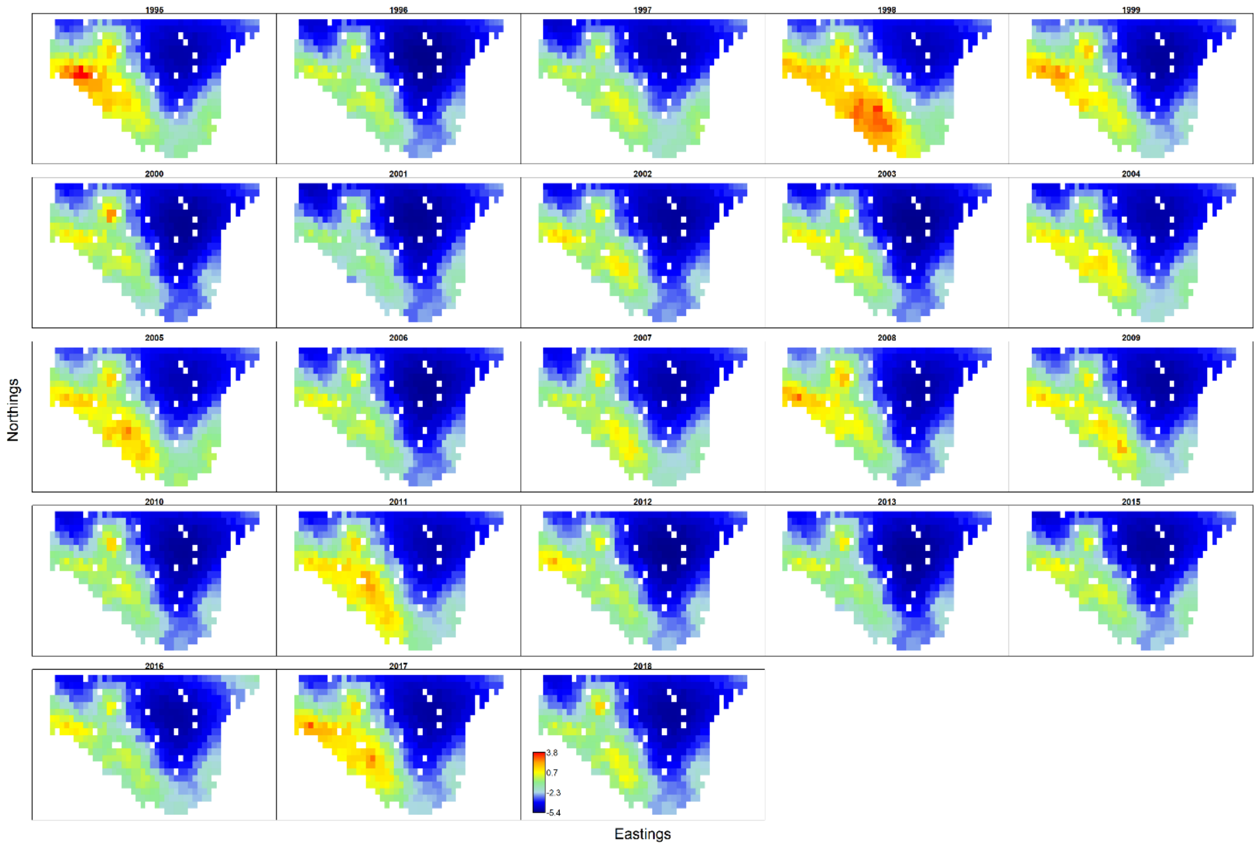

Figure 2.3 Distribution plot of predicted abundance in density for lengths 12-14 cm of witch flounder in NAFO Div. 3NO from 1995 to 2018 (except 2014).

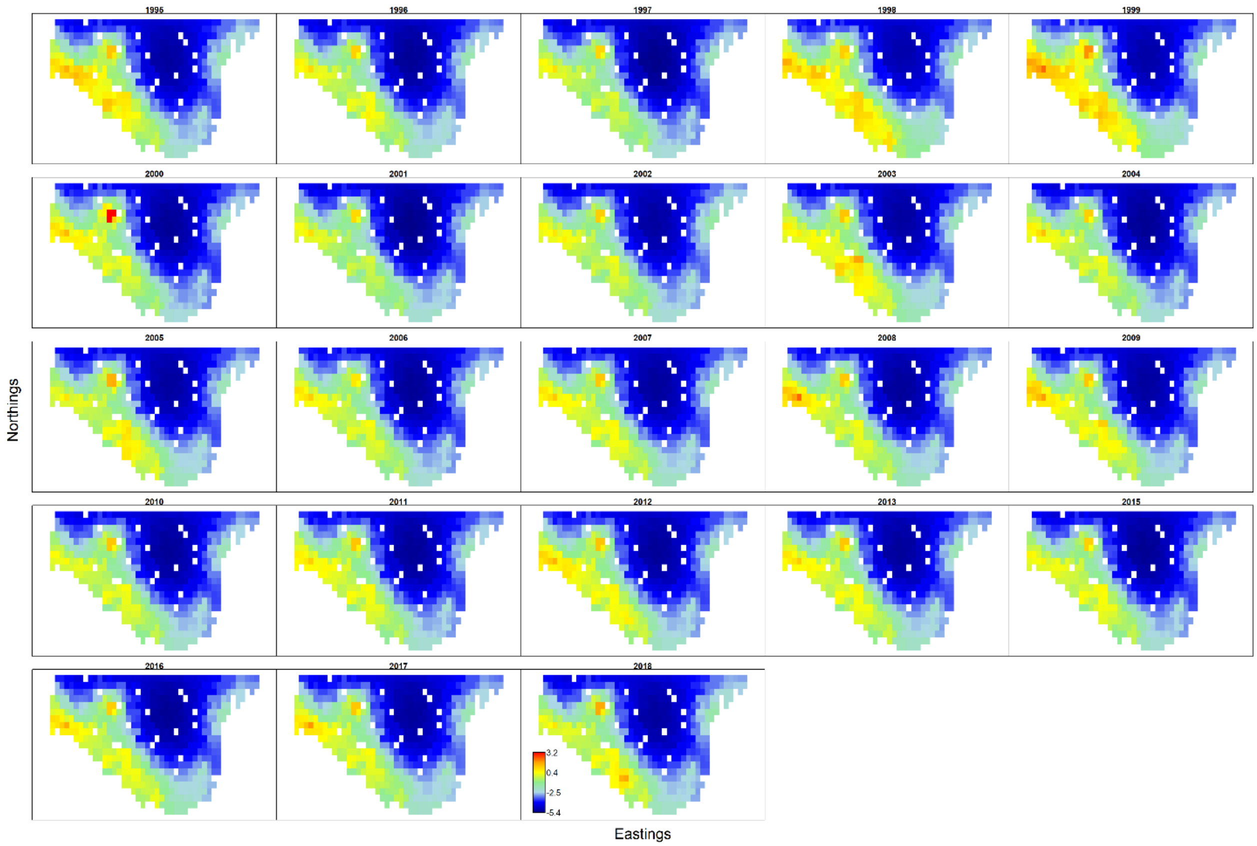

Figure 2.4 Distribution plot of predicted abundance in density for lengths 14-16 cm of witch flounder in NAFO Div. 3NO from 1995 to 2018 (except 2014).

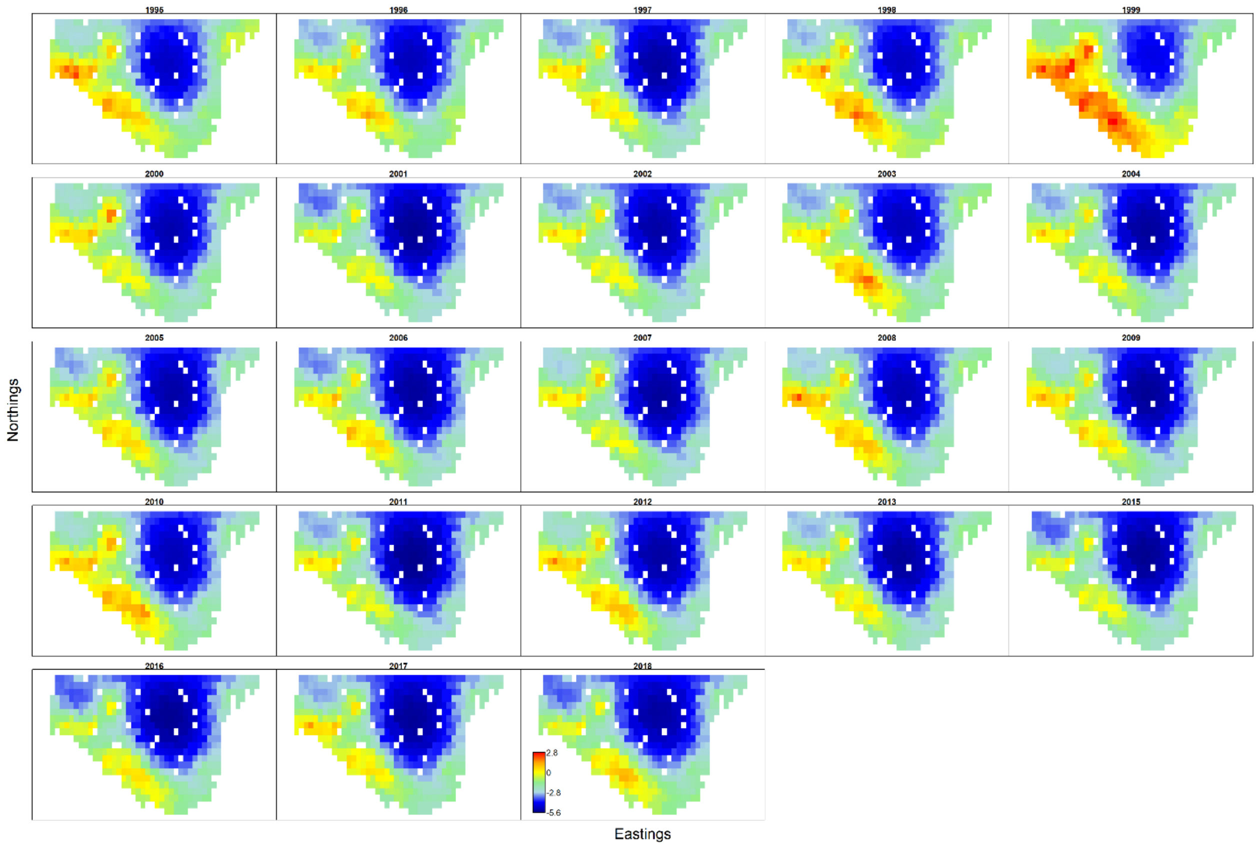

Figure 2.5 Distribution plot of predicted abundance in density for lengths 16-18 cm of witch flounder in NAFO Div. 3NO from 1995 to 2018 (except 2014).

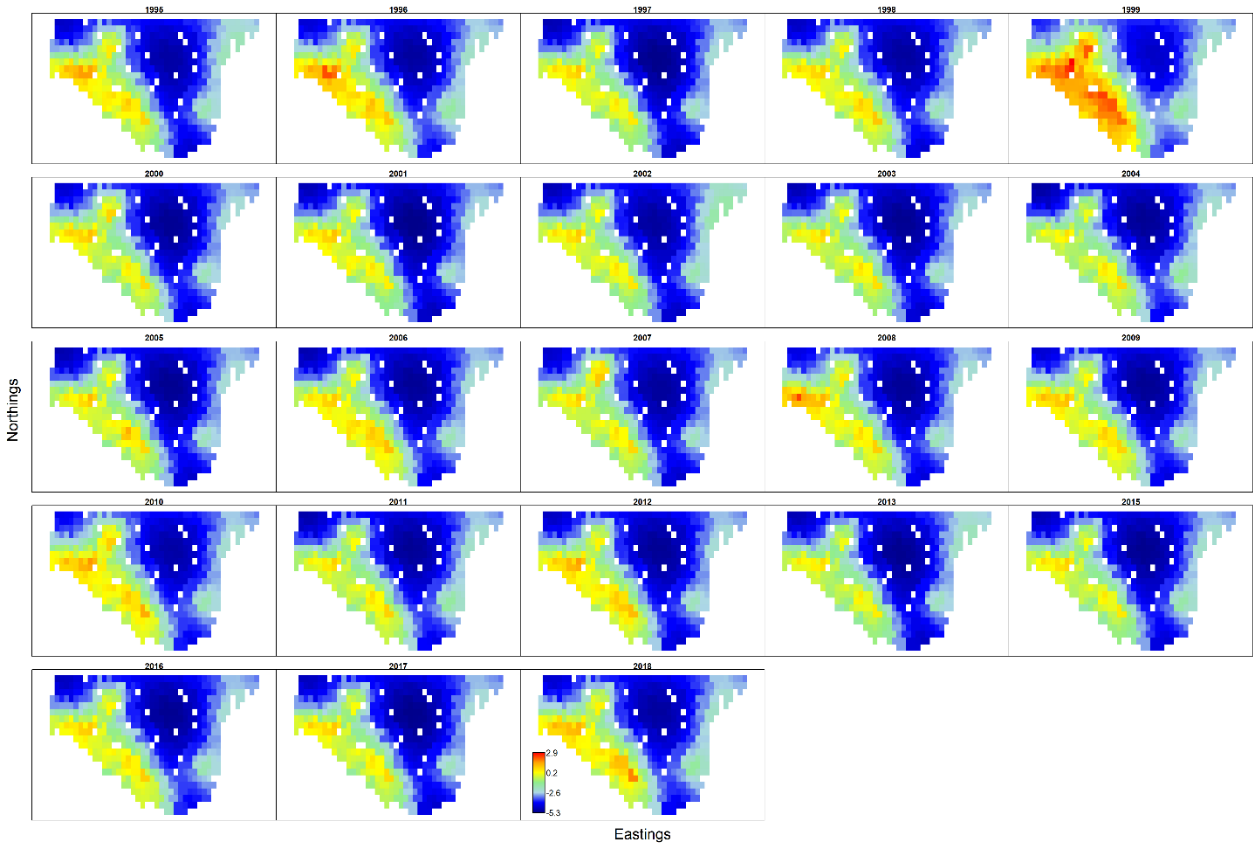

Figure 2.6 Distribution plot of predicted abundance in density for lengths 18-20 cm of witch flounder in NAFO Div. 3NO from 1995 to 2018 (except 2014).

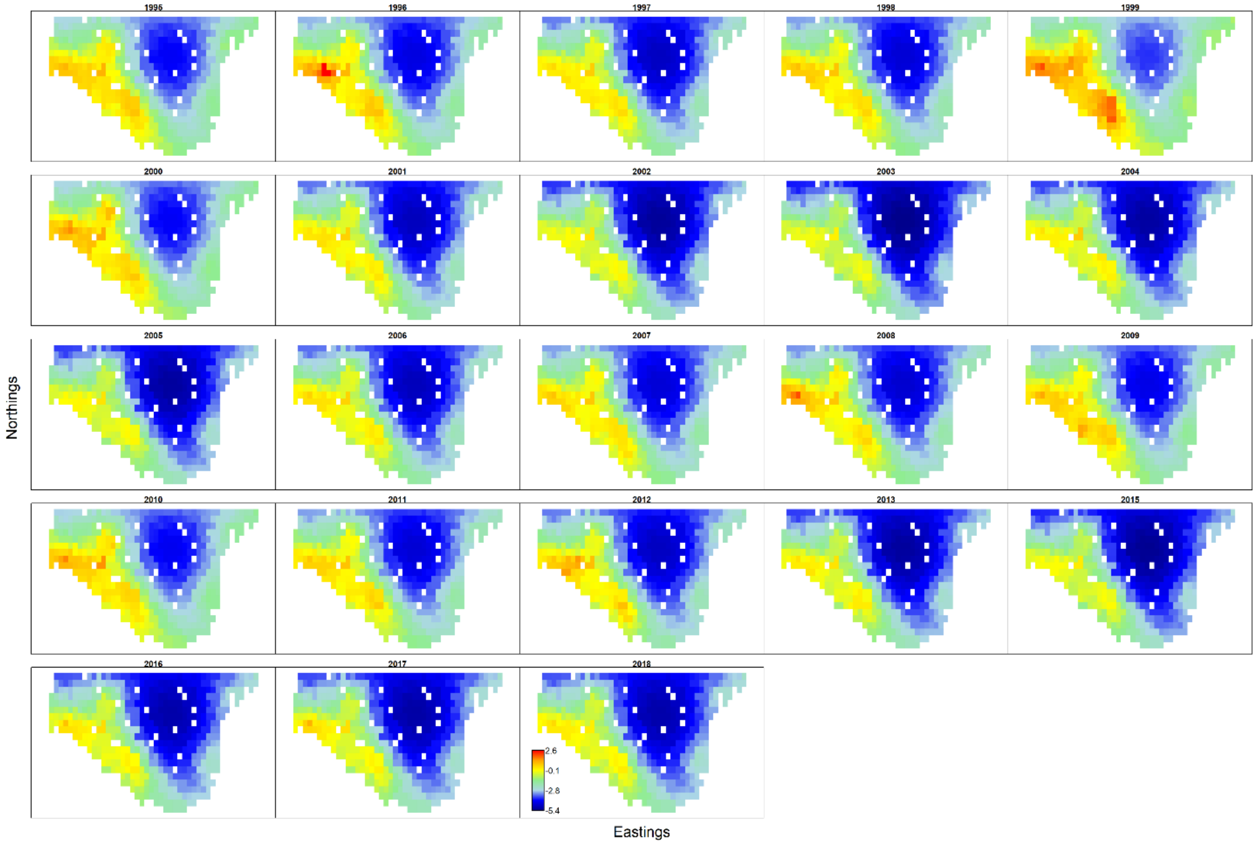

Figure 2.7 Distribution plot of predicted abundance in density for lengths 20-22 cm of witch flounder in NAFO Div. 3NO from 1995 to 2018 (except 2014).

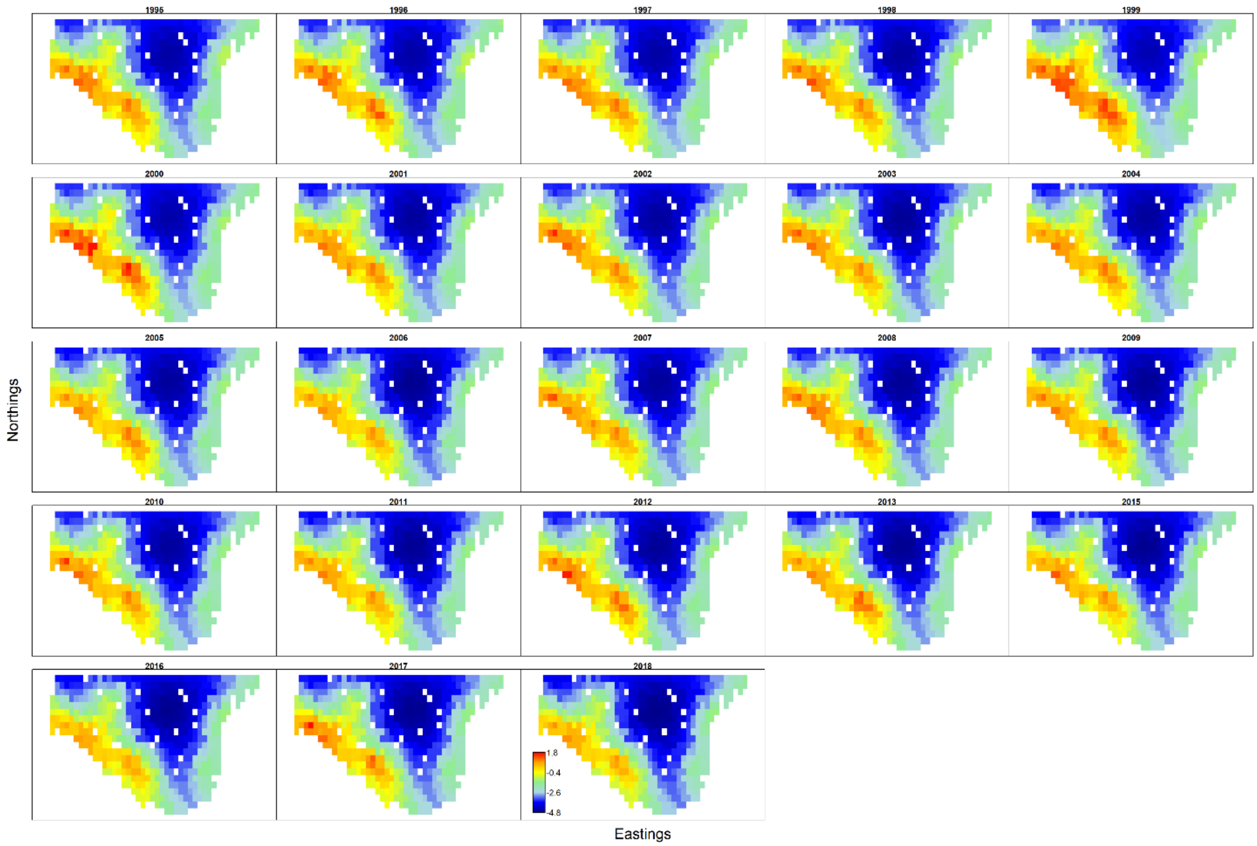

Figure 2.8 Distribution plot of predicted abundance in density for lengths 22-24 cm of witch flounder in NAFO Div. 3NO from 1995 to 2018 (except 2014).

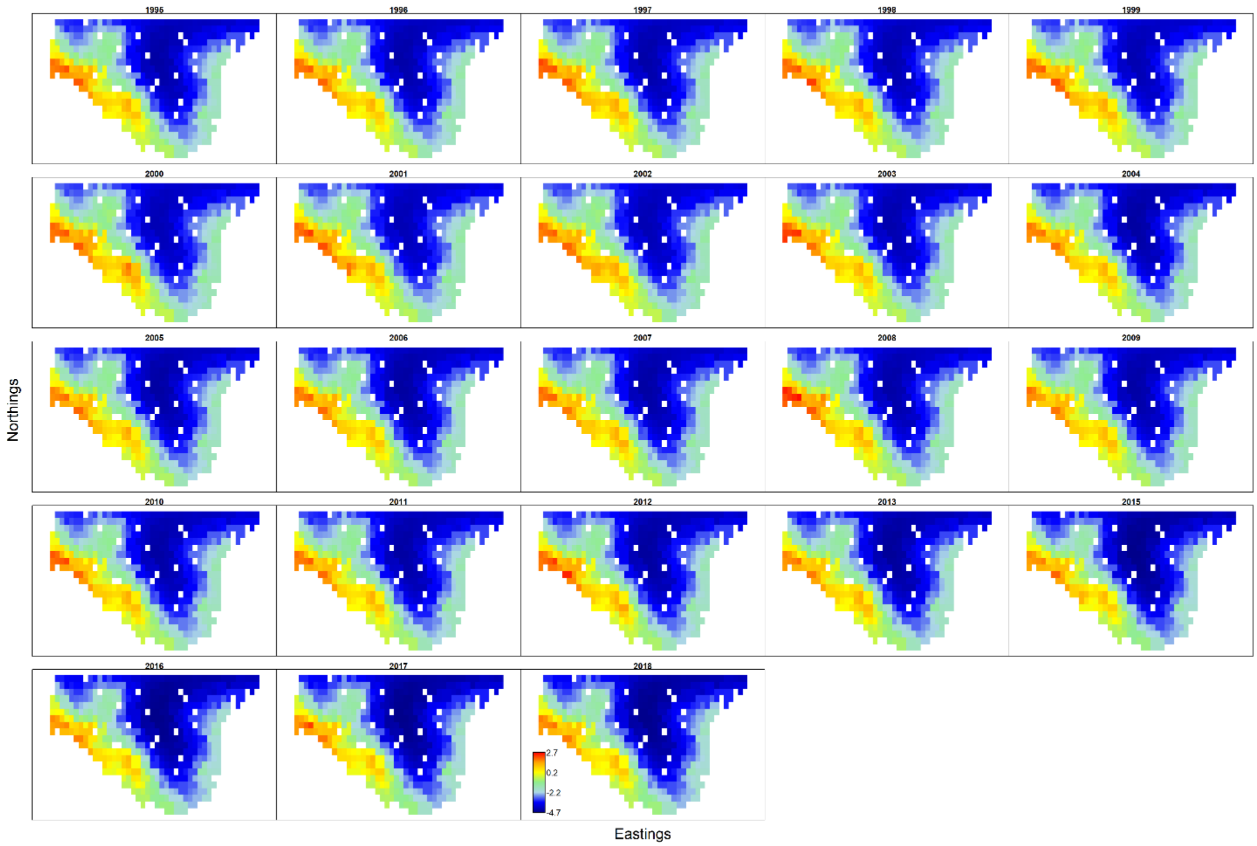

Figure 2.9 Distribution plot of predicted abundance in density for lengths 24-26 cm of witch flounder in NAFO Div. 3NO from 1995 to 2018 (except 2014).

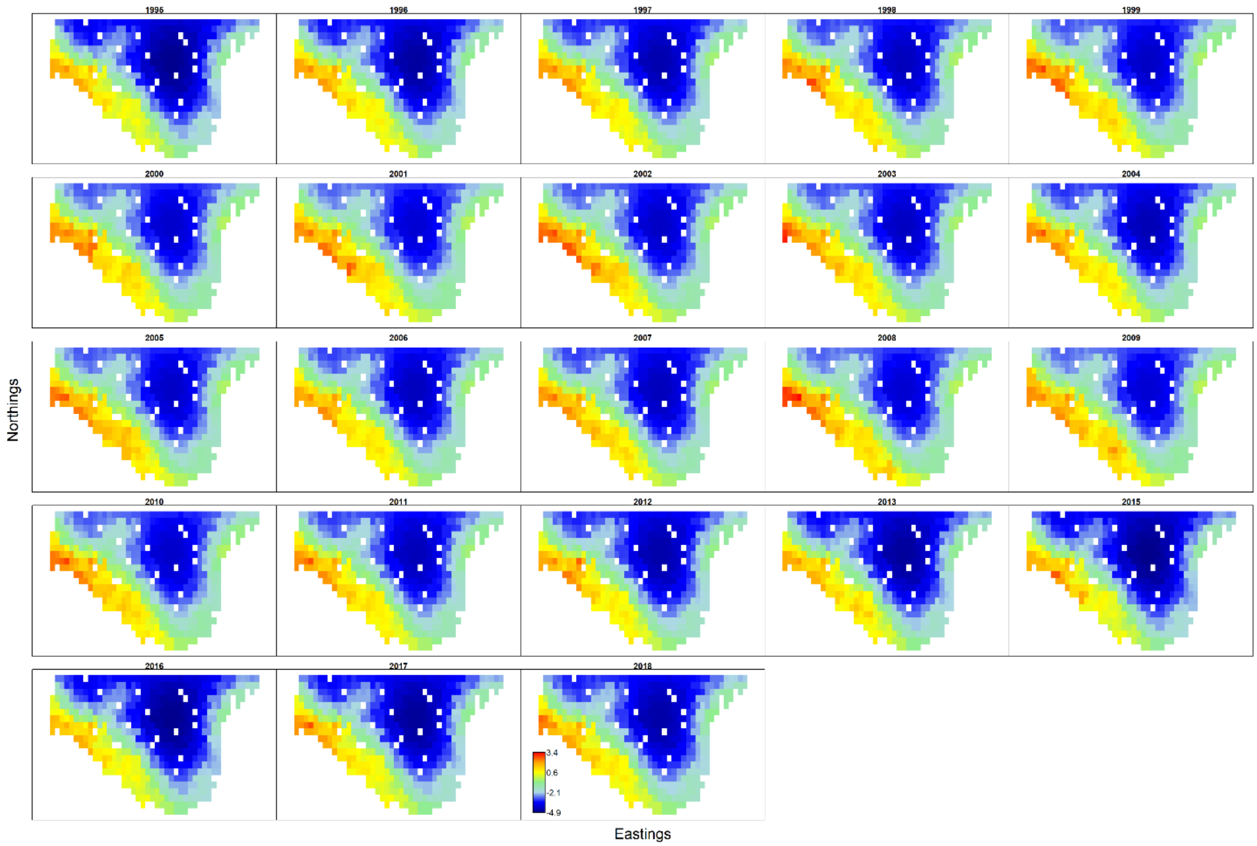

Figure 2.10 Distribution plot of predicted abundance in density for lengths 26-28 cm of witch flounder in NAFO Div. 3NO from 1995 to 2018 (except 2014).

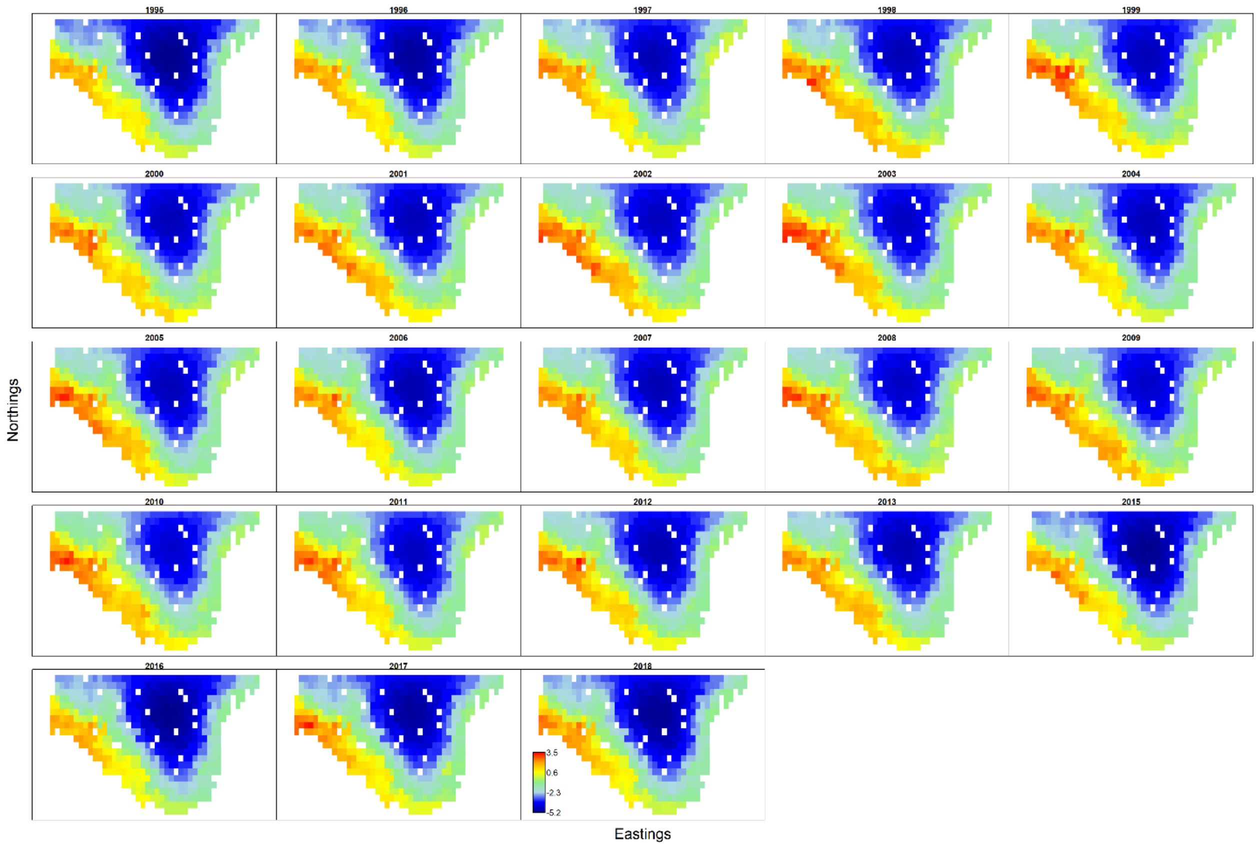

Figure 2.11 Distribution plot of predicted abundance in density for lengths 28-30 cm of witch flounder in NAFO Div. 3NO from 1995 to 2018 (except 2014).

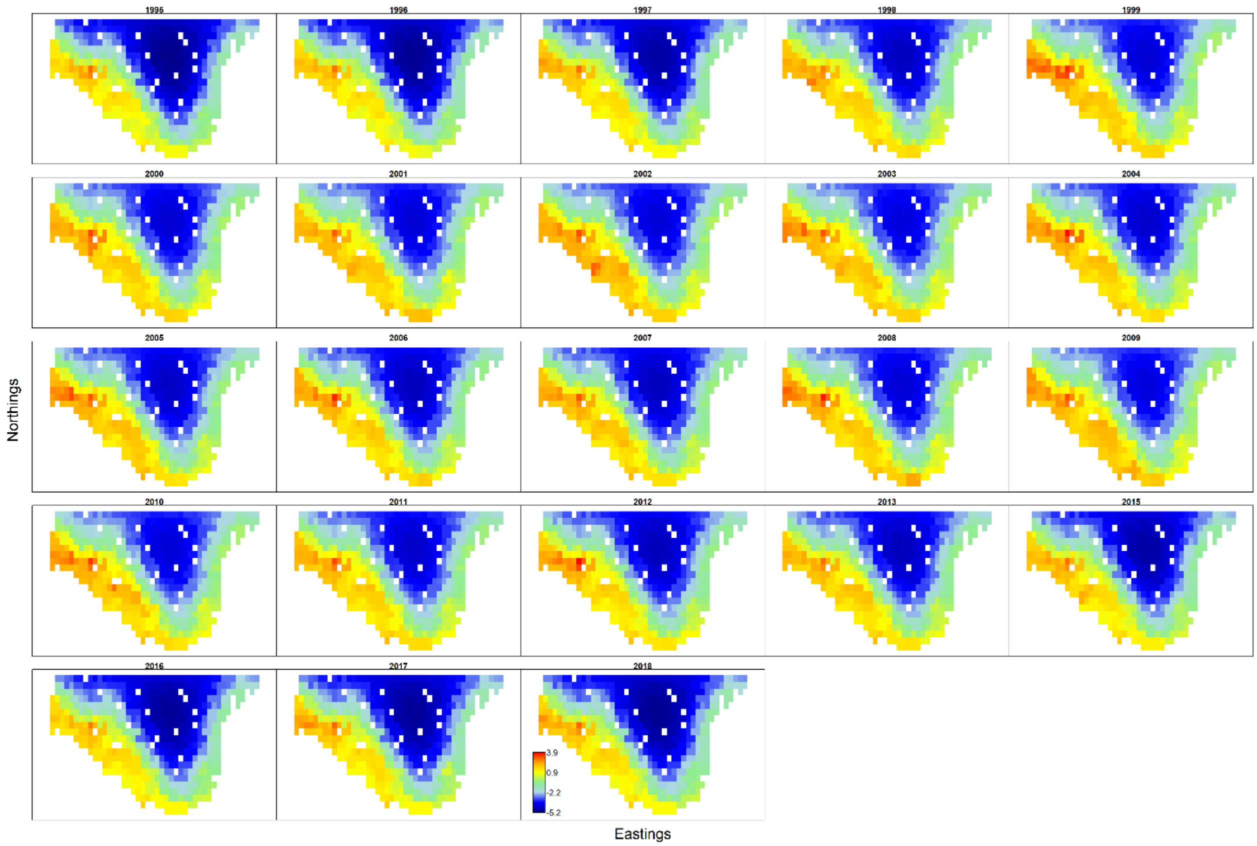

Figure 2.12 Distribution plot of predicted abundance in density for lengths 30-32 cm of witch flounder in NAFO Div. 3NO from 1995 to 2018 (except 2014).

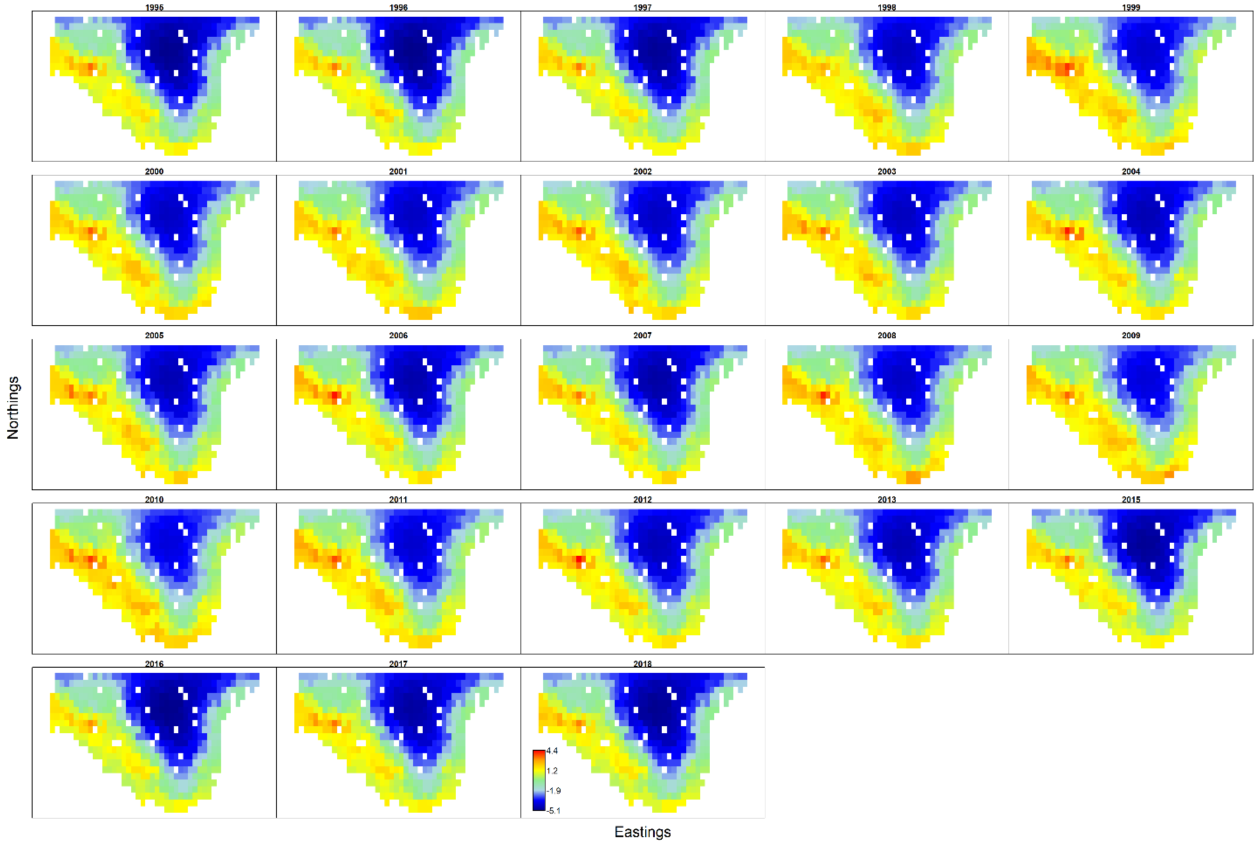

Figure 2.13 Distribution plot of predicted abundance in density for lengths 32-34 cm of witch flounder in NAFO Div. 3NO from 1995 to 2018 (except 2014).

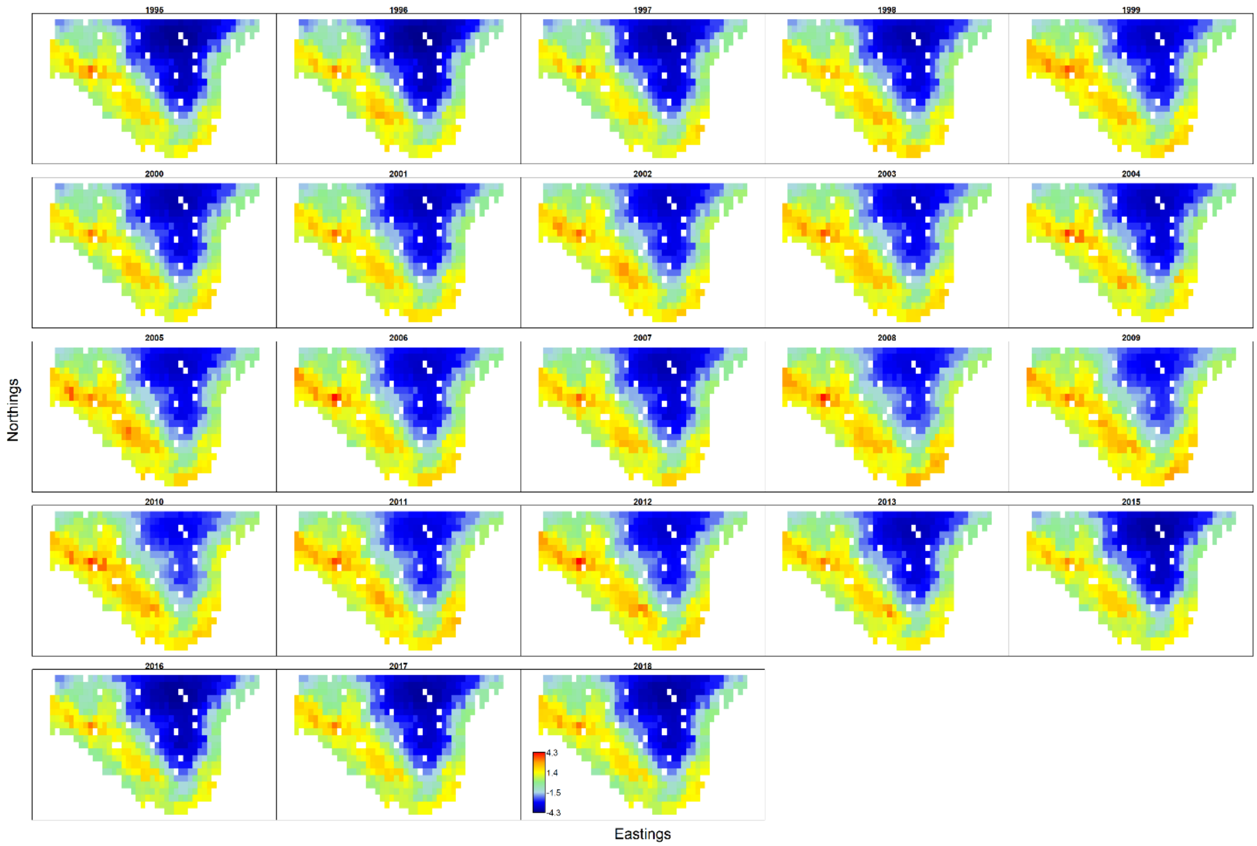

Figure 2.14 Distribution plot of predicted abundance in density for lengths 34-36 cm of witch flounder in NAFO Div. 3NO from 1995 to 2018 (except 2014).

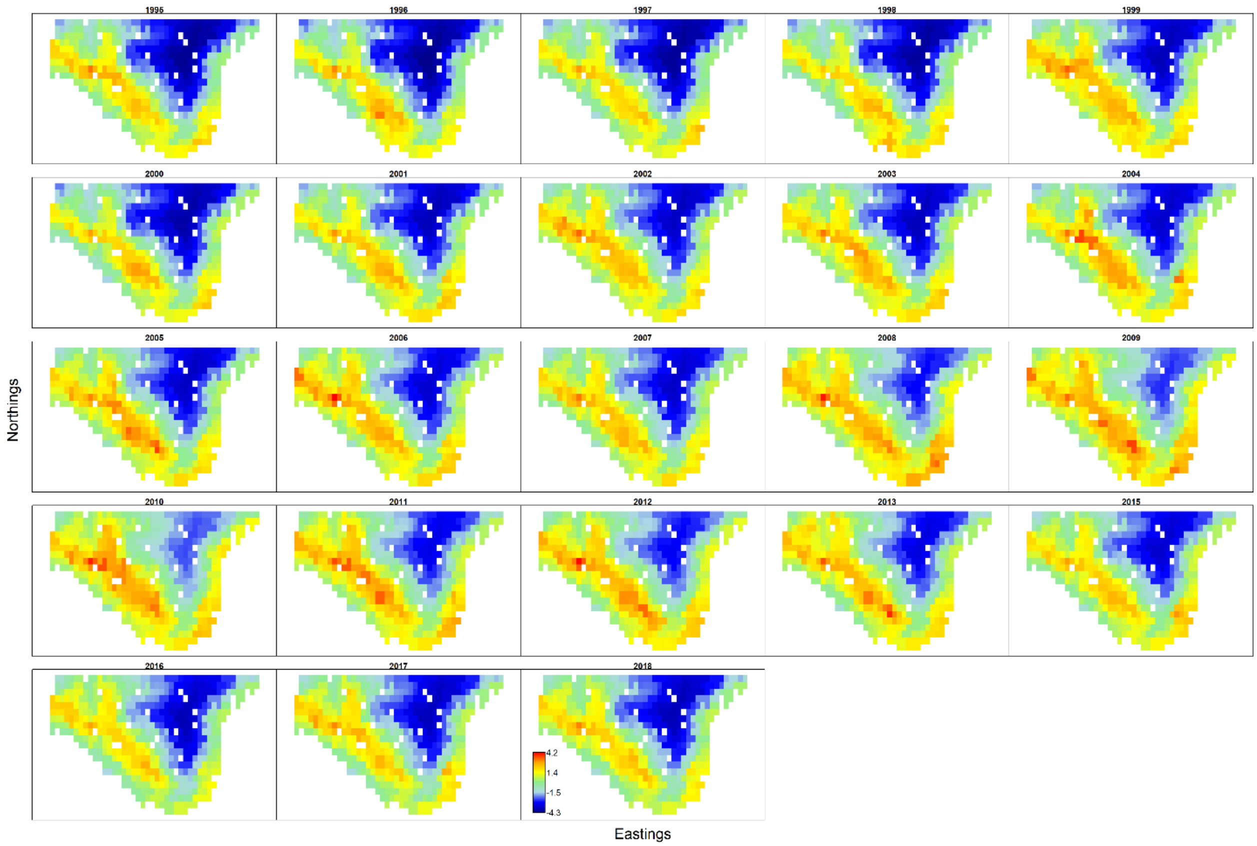

Figure 2.15 Distribution plot of predicted abundance in density for lengths 36-38 cm of witch flounder in NAFO Div. 3NO from 1995 to 2018 (except 2014).

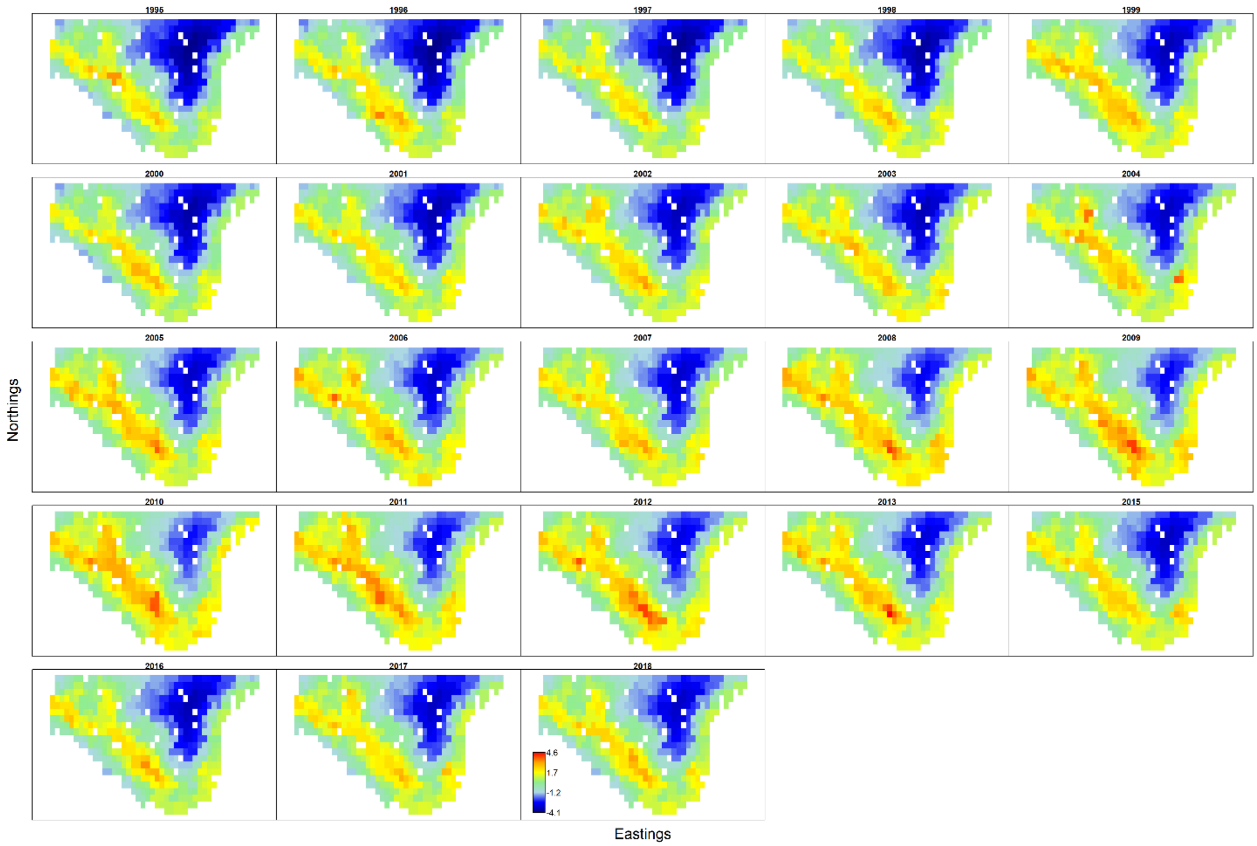

Figure 2.16 Distribution plot of predicted abundance in density for lengths 38-40 cm of witch flounder in NAFO Div. 3NO from 1995 to 2018 (except 2014).

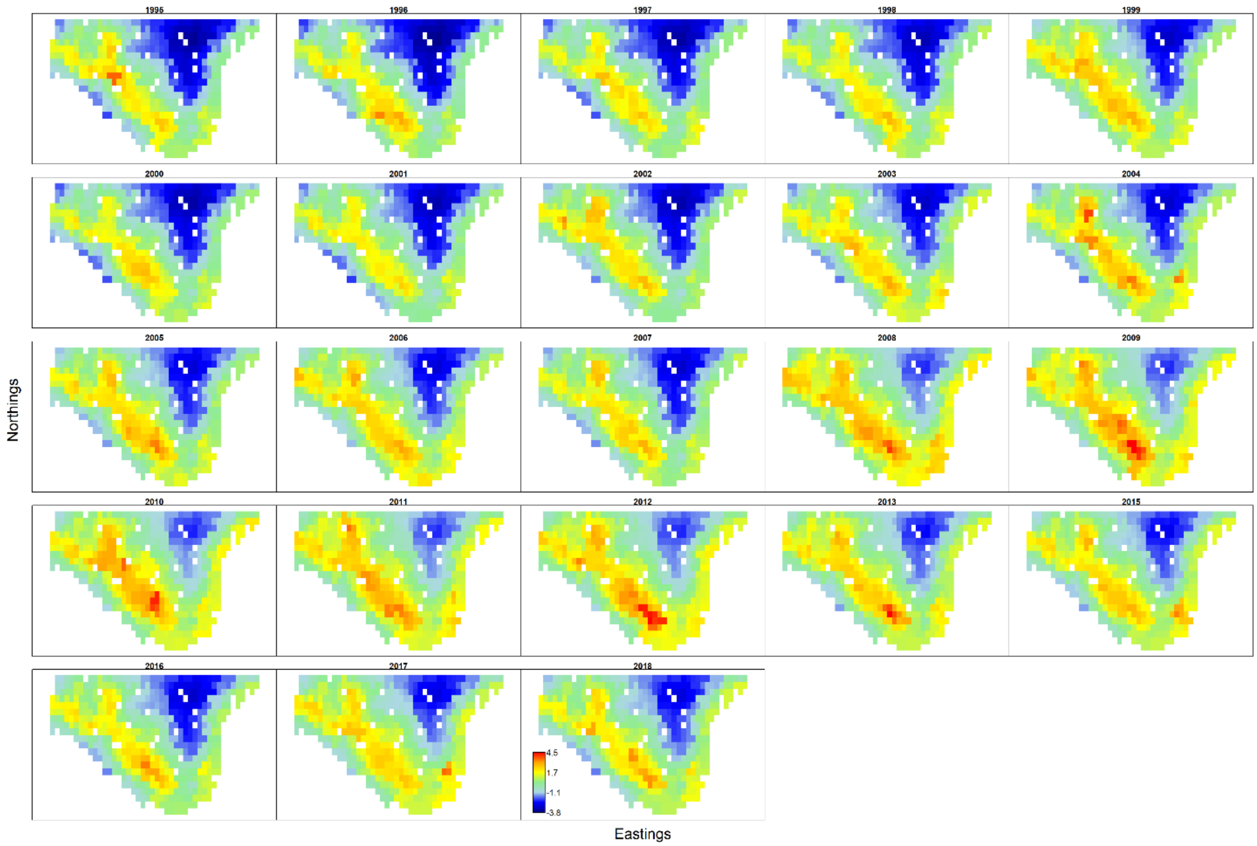

Figure 2.17 Distribution plot of predicted abundance in density for lengths 40-42 cm of witch flounder in NAFO Div. 3NO from 1995 to 2018 (except 2014).

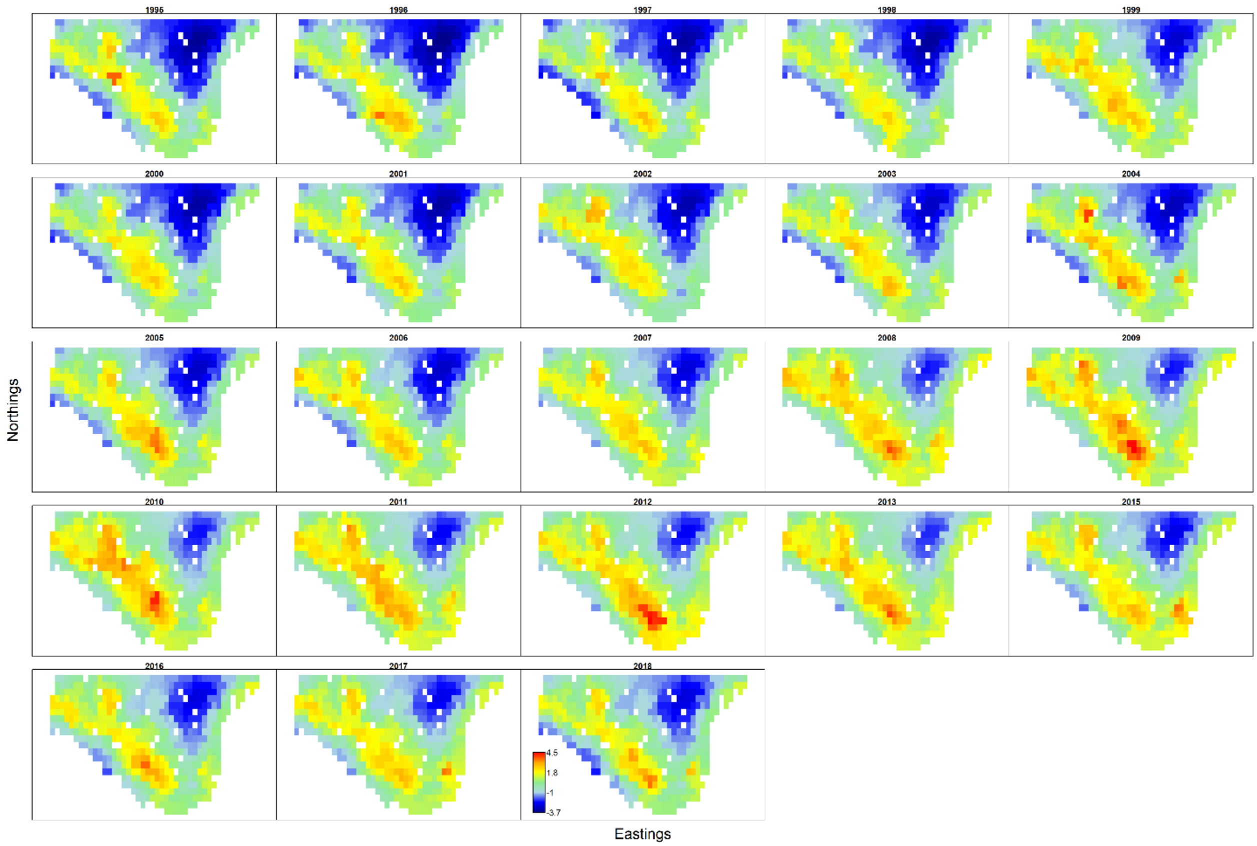

Figure 2.18 Distribution plot of predicted abundance in density for lengths 42-44 cm of witch flounder in NAFO Div. 3NO from 1995 to 2018 (except 2014).

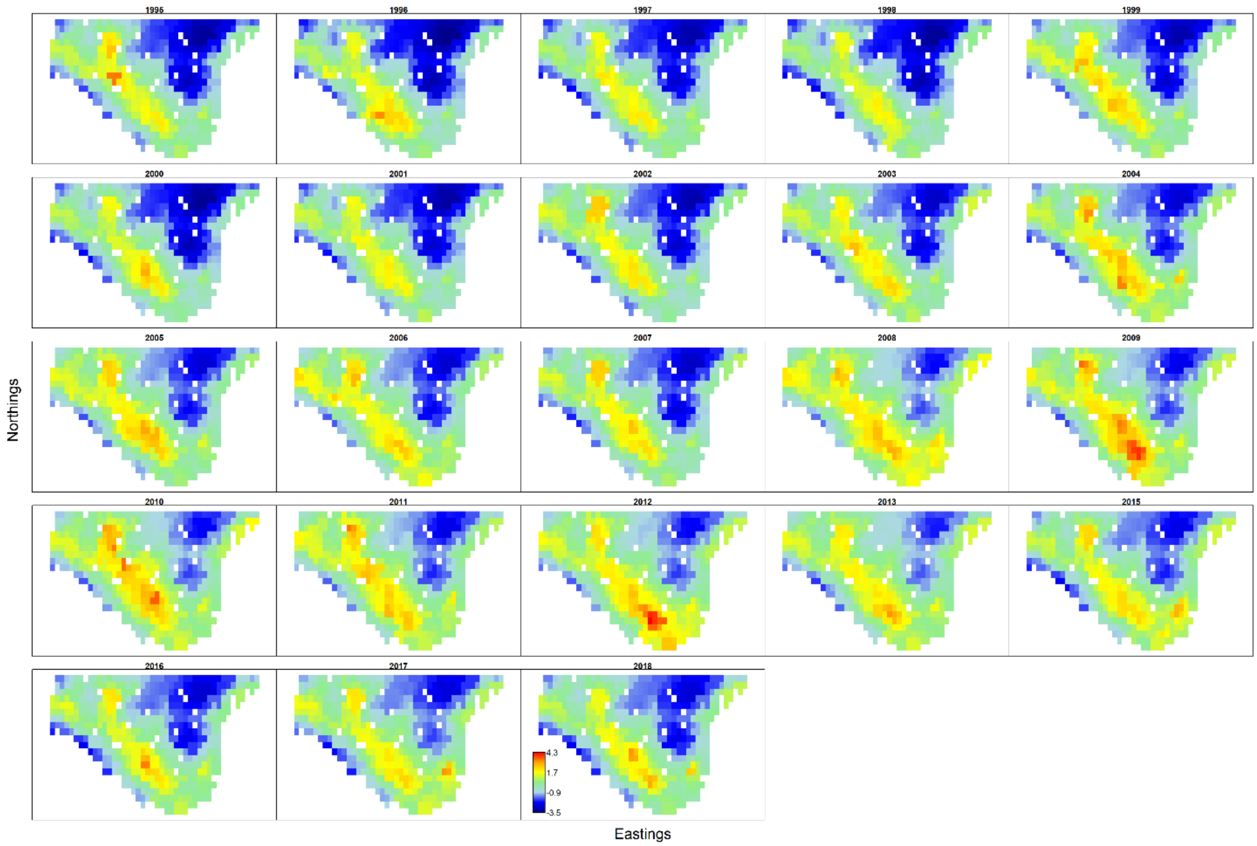

Figure 2.19 Distribution plot of predicted abundance in density for lengths 44-46 cm of witch flounder in NAFO Div. 3NO from 1995 to 2018 (except 2014).

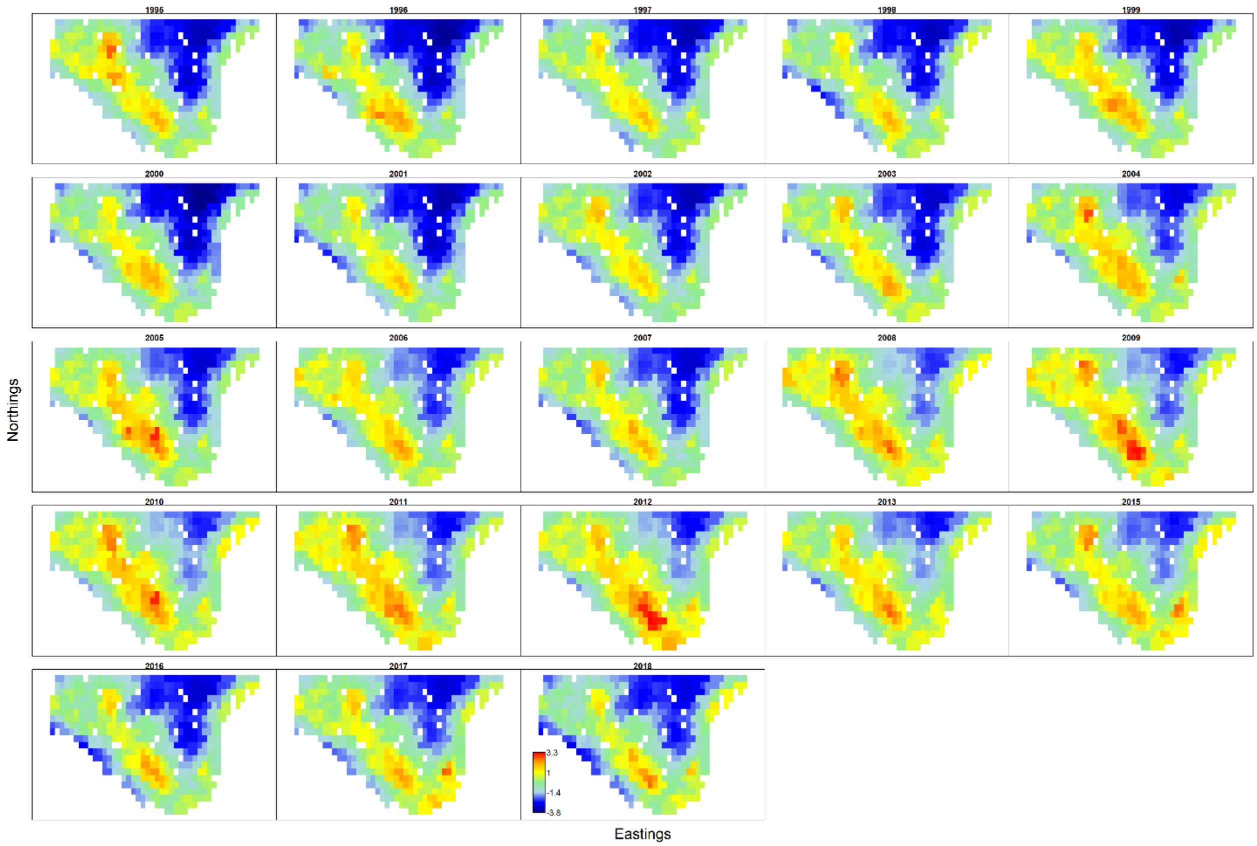

Figure 2.20 Distribution plot of predicted abundance in density for lengths 46-48 cm of witch flounder in NAFO Div. 3NO from 1995 to 2018 (except 2014).

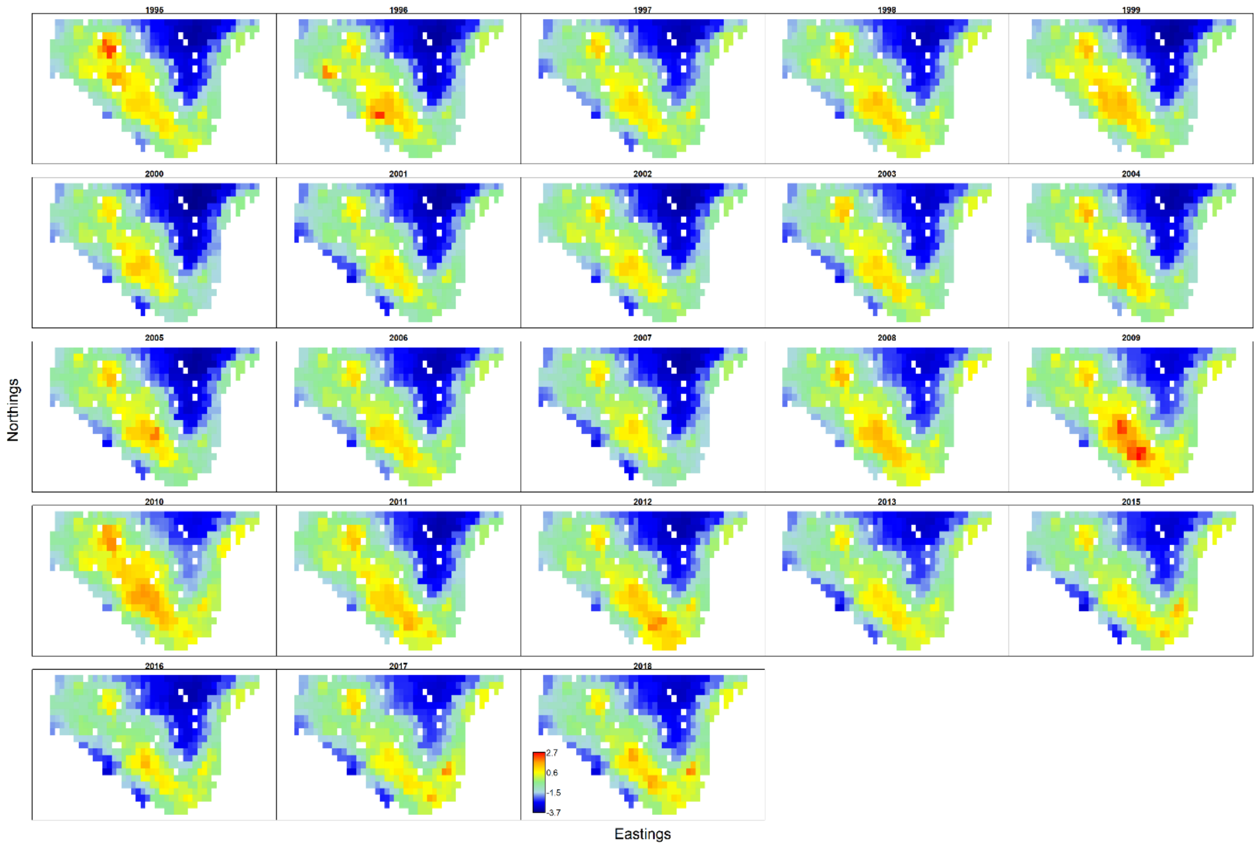

Figure 2.21 Distribution plot of predicted abundance in density for lengths 48-50 cm of witch flounder in NAFO Div. 3NO from 1995 to 2018 (except 2014).

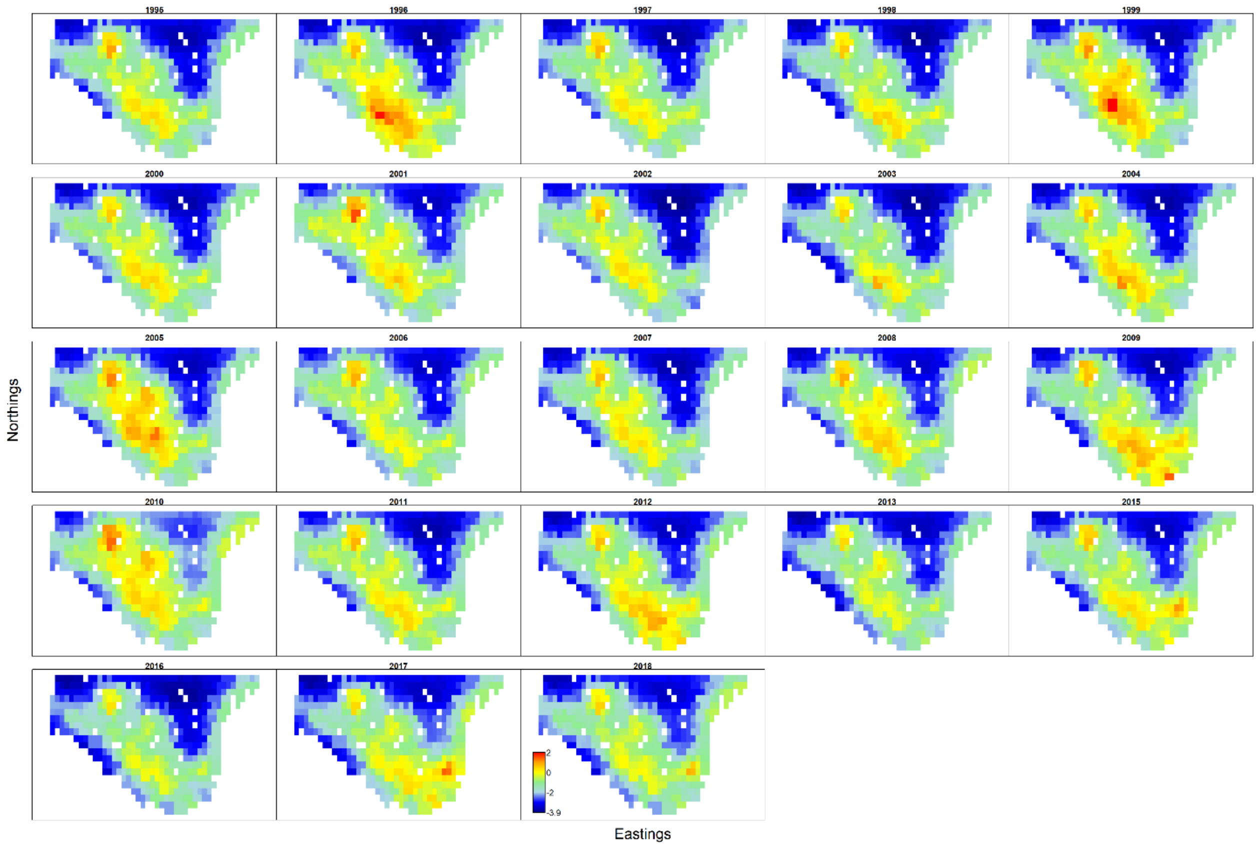

Figure 2.22 Distribution plot of predicted abundance in density for lengths 50-52 cm of witch flounder in NAFO Div. 3NO from 1995 to 2018 (except 2014).

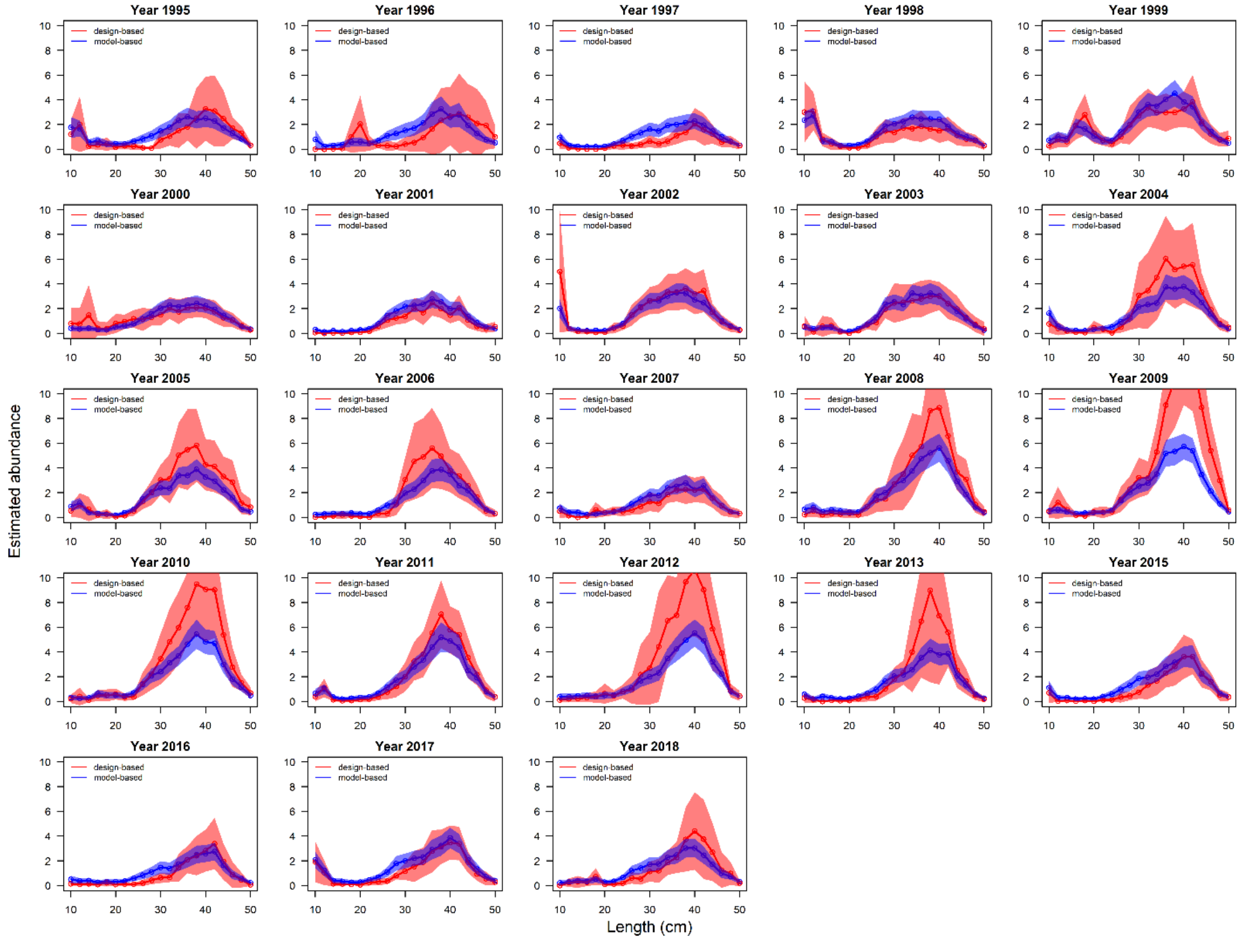

Figure 2.23 Comparison of estimated abundance-at-length (millions) for 21 length categories of witch flounder in NAFO Div. 3NO from 1995 to 2018 (except 2014) by using the design-based estimator (blue) and model-based estimator (red).

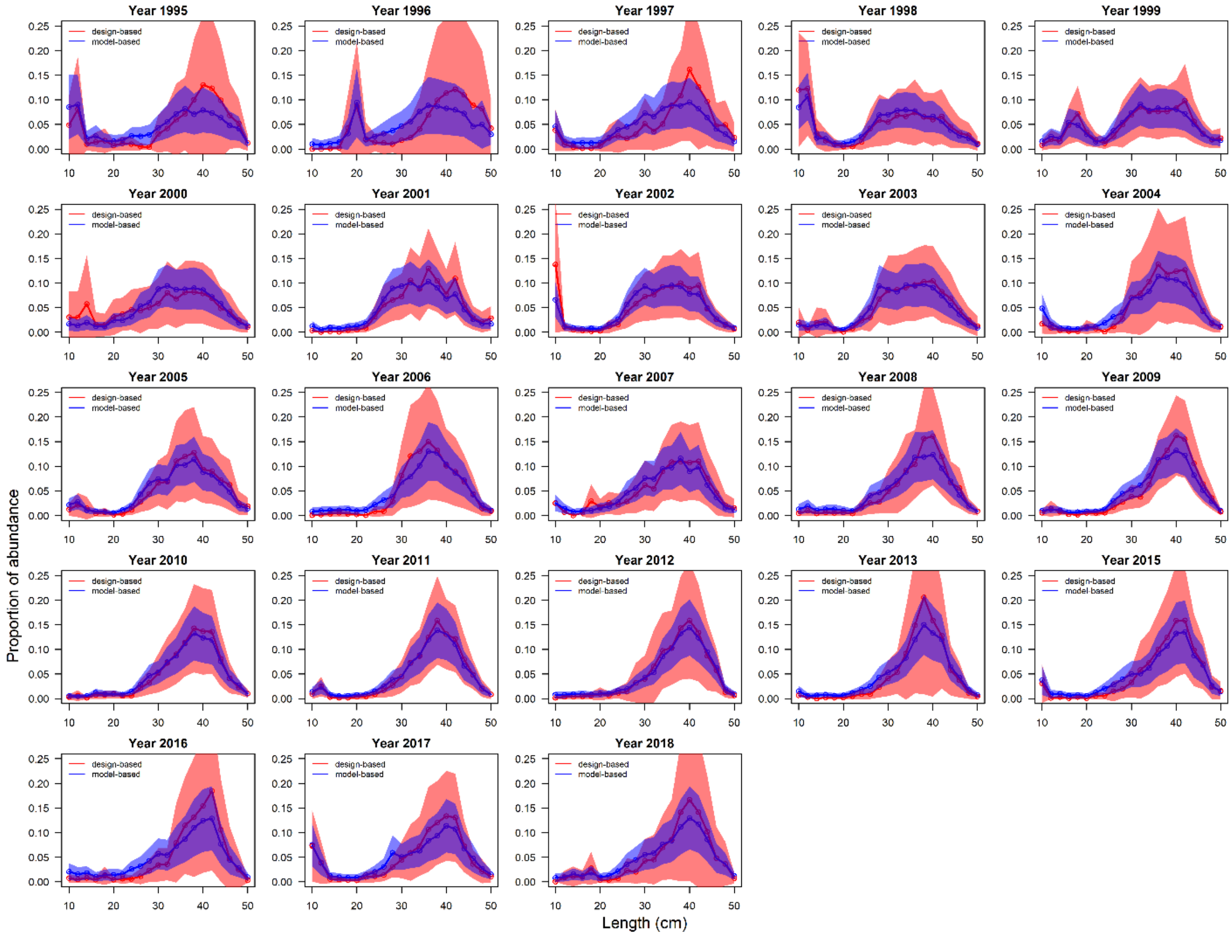

Figure 2.24 Comparison of predicted proportion of abundance-at-length for 21 length categories of witch flounder in NAFO Div. 3NO from 1995 to 2018 (except 2014) by using the design-based estimator (blue) and model-based estimator (red). The shaded area is the 95% confidence intervals.

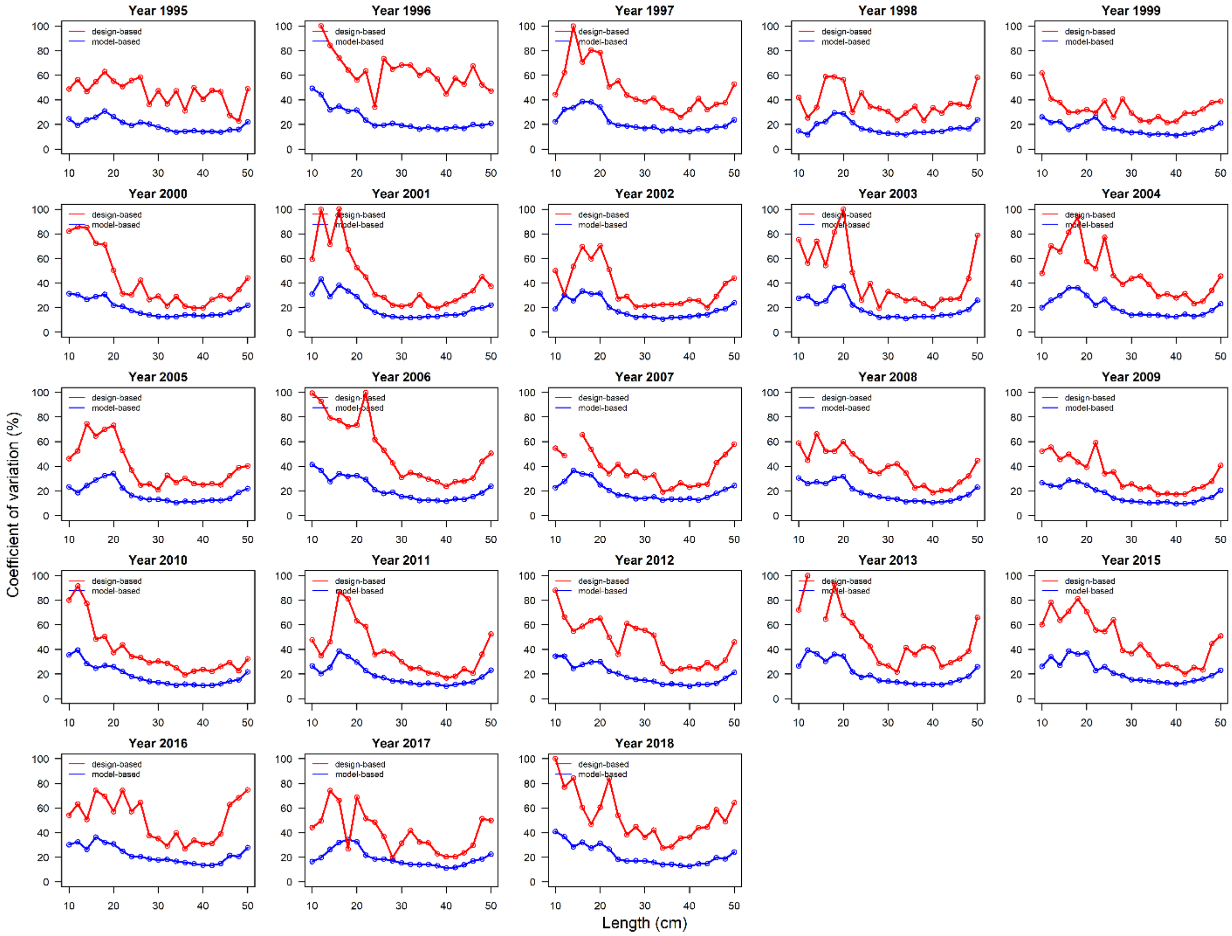

Figure 2.25 Comparison of coefficient of variation for 21 length categories of witch flounder in NAFO Div. 3NO from 1995 to 2018 (except 2014) by using the design-based estimator (blue) and model-based estimator (red).

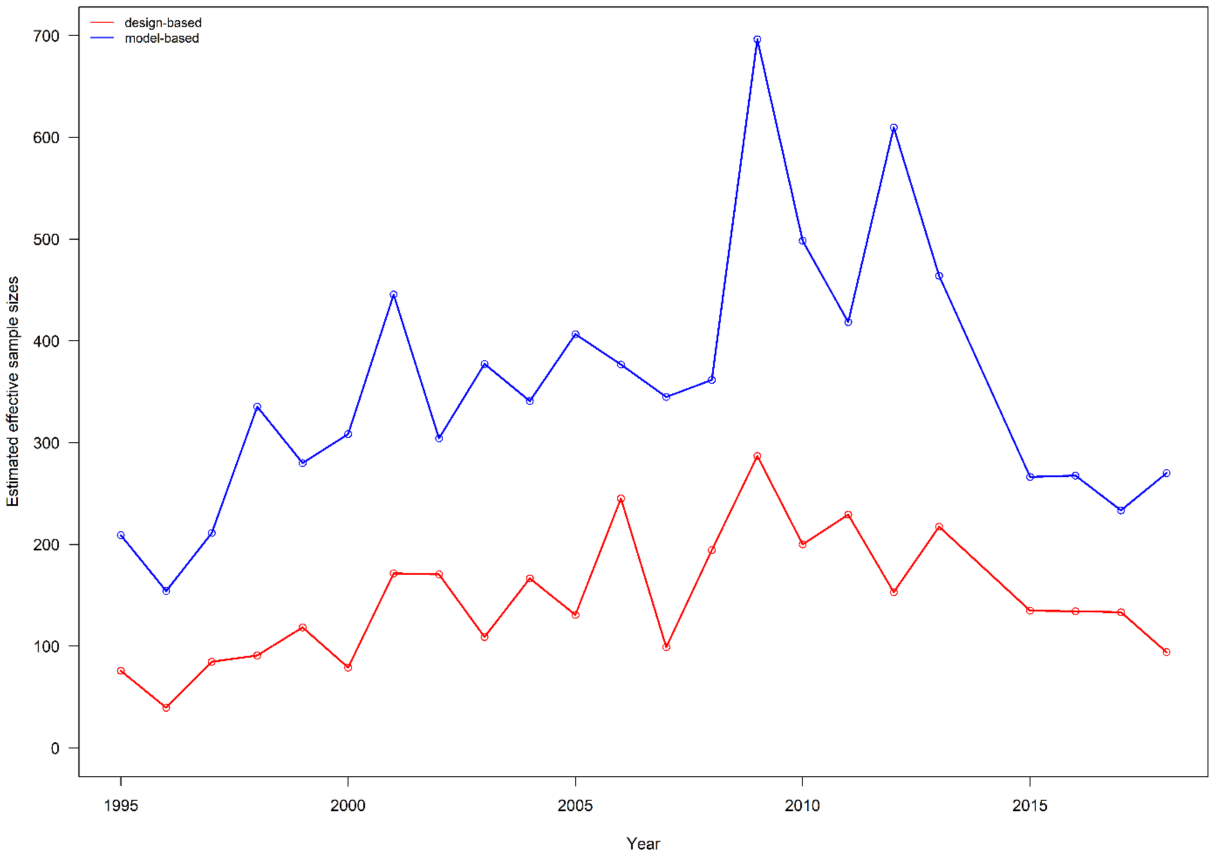

Figure 2.26 The estimated effective sample sizes for the design-based approach (red) and the model-based approach (blue) from 1995 to 2018 (except 2014).

2.5 Bibliography

Cadigan, N. G. (2011). Confidence intervals for trawlable abundance from stratified-random bottom trawl surveys. Canadian Journal of Fisheries and Aquatic Sciences, 68(5), 781–794.

Cao, J., Thorson, J. T., Richards, R. A., & Chen, Y. (2017). Spatiotemporal index standardization improves the stock assessment of northern shrimp in the Gulf of Maine. Canadian Journal of Fisheries and Aquatic Sciences, 74(11), 1781–1793.

Chen, J., Thompson, M. E., & Wu, C. (2004). Estimation of fish abundance indices based on scientific research trawl surveys. Biometrics, 60(1), 116–123.

Fisch, N., Camp, E., Shertzer, K., & Ahrens, R. (2021). Assessing likelihoods for fitting composition data within stock assessments, with emphasis on different degrees of process and observation error. Fisheries Research, 243, 106069.

Fournier, D. A., Skaug, H. J., Ancheta, J., Ianelli, J., Magnusson, A., Maunder, M. N., Nielsen, A., & Sibert, J. (2012). AD Model Builder: Using automatic differentiation for statistical inference of highly parameterized complex nonlinear models. Optimization Methods and Software, 27(2), 233–249.

Francis, R. C. (2011). Data weighting in statistical fisheries stock assessment models. Canadian Journal of Fisheries and Aquatic Sciences, 68(6), 1124–1138.

Kristensen, K., Nielsen, A., Berg, C. W., Skaug, H., & Bell, B. (2015). TMB: automatic differentiation and Laplace approximation. ArXiv Preprint ArXiv:1509.00660.

Lindgren, F., Rue, H., & Lindström, J. (2011). An explicit link between Gaussian fields and Gaussian Markov random fields: The stochastic partial differential equation approach. Journal of the Royal Statistical Society: Series B (Statistical Methodology), 73(4), 423–498.

Maddock Parsons, D., Rogers, B., & Rideout, R. (2020). An assessment of the witch flounder resource in NAFO Divisions 3NO. NAFO SCR Doc, 20, 046.

Maunder, M. N., Thorson, J. T., Xu, H., Oliveros-Ramos, R., Hoyle, S. D., Tremblay-Boyer, L., Lee, H. H., Kai, M., Chang, S.-K., & Kitakado, T. (2020). The need for spatio-temporal modeling to determine catch-per-unit effort based indices of abundance and associated composition data for inclusion in stock assessment models. Fisheries Research, 229, 105594.

Peel, D., Bravington, M. V., Kelly, N., Wood, S. N., & Knuckey, I. (2013). A model-based approach to designing a fishery-independent survey. Journal of Agricultural, Biological, and Environmental Statistics, 18(1), 1–21.

Punt, A. E. (2017). Some insights into data weighting in integrated stock assessments. Fisheries Research, 192, 52–65.

Rogers, B., & Morgan, J. (2019). An assessment of the witch flounder resource in NAFO Divisions 3NO. NAFO SCR Doc, 19, 034.

Shelton, A. O., Thorson, J. T., Ward, E. J., & Feist, B. E. (2014). Spatial semiparametric models improve estimates of species abundance and distribution. Canadian Journal of Fisheries and Aquatic Sciences, 71(11), 1655–1666.

Smith, S. J. (1990). Use of statistical models for the estimation of abundance from groundfish trawl survey data. Canadian Journal of Fisheries and Aquatic Sciences, 47(5), 894–903.

Thompson, S. K. (2012). Sampling (Vol. 755). John Wiley & Sons.

Thorson, J. T. (2014). Standardizing compositional data for stock assessment. ICES Journal of Marine Science, 71(5), 1117–1128.

Thorson, J. T. (2018). Three problems with the conventional delta-model for biomass sampling data, and a computationally efficient alternative. Canadian Journal of Fisheries and Aquatic Sciences, 75(9), 1369–1382.

Thorson, J. T. (2019). Guidance for decisions using the Vector Autoregressive Spatio-Temporal (VAST) package in stock, ecosystem, habitat and climate assessments. Fisheries Research, 210, 143–161.

Thorson, J. T., & Barnett, L. A. (2017). Comparing estimates of abundance trends and distribution shifts using single-and multispecies models of fishes and biogenic habitat. ICES Journal of Marine Science, 74(5), 1311–1321.

Thorson, J. T., Cunningham, C. J., Jorgensen, E., Havron, A., Hulson, P.-J. F., Monnahan, C. C., & von Szalay, P. (2021). The surprising sensitivity of index scale to delta-model assumptions: Recommendations for model-based index standardization. Fisheries Research, 233, 105745.

Thorson, J. T., & Haltuch, M. A. (2019). Spatiotemporal analysis of compositional data: Increased precision and improved workflow using model-based inputs to stock assessment. Canadian Journal of Fisheries and Aquatic Sciences, 76(3), 401–414.

Thorson, J. T., Shelton, A. O., Ward, E. J., & Skaug, H. J. (2015). Geostatistical delta-generalized linear mixed models improve precision for estimated abundance indices for West Coast groundfishes. ICES Journal of Marine Science, 72(5), 1297–1310.

Chapter 3 Stock assessment models for NAFO Div. 3NO witch flounder

3.1 Introduction

Single-species stock assessment models are demographic analyses designed to estimate historical and current abundance and biomass, determine the population dynamic, evaluate the stock status relative to the reference point and the consequences of current harvest policies, and form the basis for forecasts to evaluate the implication under different harvest rules (Methot Jr & Wetzel, 2013; Punt et al., 2013). Depending on the model structure and data utilized, single-species stock assessment models can largely be assorted into the following three categories: a) surplus production models, b) age-structured models, and c) size- (or length-/stage-) structured models (Punt et al., 2013).

Surplus production models are age- and size-aggregated models that approximate changes in biomass based on the biomass of the previous year, the surplus production in biomass, and the catches by the fishery (Winker et al., 2020). A surplus production model in a Bayesian framework developed by NAFO Scientific Council was accepted and has been applied to assess NAFO Div. 3NO witch flounder stock since 2015 (Morgan et al., 2015; Rogers & Morgan, 2019). The input data were fishery-dependent catch data and fishery-independent Canadian spring and autumn survey series data (Rogers & Morgan, 2019). This surplus production model provides estimates of biomass and fishing mortality and evaluates the status of the stock relative to precautionary reference points (Morgan & Lee, 2018). However, model results indicated that the change in population size from 2014 to 2015 was very large and abrupt, which cannot be explained in the process being modelled and this change was subsequently for by increasing the process error (Morgan & Lee, 2018). In addition, the size and structure dynamics of the witch flounder stock are almost totally unknown in this model.

Age-structured models are the more preferred method and widely used in many fisheries stock assessments (D. A. Fournier et al., 1998). The models range from simple deterministic methods such as virtual population (or cohort) analysis to more complex statistical models that incorporate variability in data and various population dynamics (D. A. Fournier et al., 1998; Quinn, 2003). These age-structured models use multiple sources of data such as catch, age/size composition data, length-or weight-at-age information, and maturity information to clarify the population dynamics by estimating model parameters and deriving outputs (Ono et al., 2015). The advantage of these models is that by taking into account information such as fish life-history traits, fishery characteristics. Changes in population structure, natural mortality, and recruitment over time can be determined, which can reduce the uncertainty in stock assessment (Y. Chen et al., 2003; Magnusson & Hilborn, 2007). Therefore, age-structured models are considered more reliable to reconstruct the “true” population dynamics than surplus production models (Hilborn & Walters, 2013). However, age-based data (e.g. catch-at-age) are usually expensive and time-consuming to measure and therefore not obtained for many stocks. Moreover, the aging of many fisheries stocks may be hard or inaccurate (Campana & Thorrold, 2001; D. Fournier & Archibald, 1982). Aging accuracy often decreases with age for long-lived species (e.g. witch flounder), meaning older fish are given poor age estimates (Marriott & Mapstone, 2006). To address these problems, size-structured models have been developed.

While the majority of assessments conducted for fish stocks are based on surplus production models or age-structured models, size-structured models are increasingly being performed for hard-to-age species stocks (Akselrud et al., 2017; Punt et al., 2013). Size- (or length-/stage-) structured models are usually applied to estimate population dynamics when catch-at-length data is easier and cheaper to acquire and more accurate than catch-at-age data (Andersen, 2020; Cronin-Fine & Punt, 2020). However, size-structured models cannot provide age-based biological reference points for fishery management, due to the inability to estimate cohort dynamics creating a challenge in stock management.

An approach to address this challenge is the age-based statistical catch-at-length (ACL) model (D. A. Fournier et al., 1998). Age-length transition matrix used in ACL to convert number-at-age to number-at-length. When age data are unavailable or not reliable for fisheries, ACL can estimate age-based cohort dynamics by fitting length-based data. However, the major issue of ACL is that it only accounts for age-dependent population processes and ignores the length-dependent mortality within age, which may lead to bias in population dynamics estimation (Punt et al., 2013).

An age and length structured statistical catch-at-length model (ALSCL) developed by (Zhang & Cadigan, n.d.) is another approach to address this problem and has been applied to yellowtail flounder in NAFO Div. 3LNO. Specifically, ALSCL uses a full stochastic growth transition matrix to estimate age-based population dynamics from length-based data, and tracks the dynamics of age- and size-structure over time simultaneously by integrating length-based and age-based fishing mortality, which keeps the advantages of both age-structured models and size-structured models (Zhang & Cadigan, n.d.).

In Chapter 2, I standardized survey catch-at-length indices using design-based approach and model-based approach, but the consequences on stock assessment are not clear.
It's possible that the more precise model-based estimates result in more precise estimates of cohort dynamics when utilized in a size-structured assessment model. In addition, the impact of input data choice (design- or model-based data) has not been assessed and the performance of ALSCL model and ACL model for NAFO Div. 3NO witch flounder assessment has never been compared. Thus, I generate four combinations for NAFO Div. 3NO witch flounder assessment: (1) design-based indices and ALSCL model. (2) model-based indices and ALSCL model. (3) design-based indices and ACL model. (4) model-based indices and ACL model. In this chapter, I first describe the data input and structures of ALSCL and ACL, then apply four combinations to estimate the population dynamics for NAFO Div. 3NO witch flounder, and finally compare the assessment results for four combinations to see whether the results are sensitive to indices and model choices.

3.2 Methods

3.2.1 Data input

I use the standardized NAFO Div. 3NO witch flounder fishery RV survey design-based indices and model-based indices from 1995 to 2018 in Chapter 2 as the input abundance-at-length indices in both ALSCL and ACL models. I define 21 length bins with 2cm bin widths: {10-12, 12-14, 14-16, … 48-50, 50-52}. The input weight-at-length data for four combinations is formulated by

$$W_{l,t} = a_t l^{b_t}, l = 1, \dots, L \; and \; t = 1, \dots, T \tag{3.1}$$

where a and b are constants ($a = 0.001464, b = 3.40980$) across all years that are derived from (Durán & Paz, 2000). Due to the lack of maturity information for NAFO Div. 3NO witch flounder, I used maturity data from Gulf of Maine and Gulf of St. Lawrence as empirical data to generate the maturity-at-length data for witch flounder. The length at 50% and 95% maturity is 29 cm and 51 cm respectively.

3.2.2 ALSCL model

The core of ALSCL is the three-dimensional population dynamics, which are modelled by length-based survival and growth transition matrix within each cohort, across length bins *(l=1,…,L)*, ages *(a=1,…,A)* and years *(t=1,…,T)*. In this model, I specify 21 length bins with a width of 2 cm. I set the maximum age (A) at 25, which is equal to the maximum reported age for witch flounder (Bowering, 1978). I use years from 1995 to 2018 (except for 2014).

The equation of three-dimensional population dynamics is given in

$$\boldsymbol{n}_{l|a,t} = \boldsymbol{G} * (\boldsymbol{n}_{l|a-1,t-1} \circ e^{-\boldsymbol{z}_{l|t-1}}) \tag{3.2}$$

where $\boldsymbol{n}_{l|a,t}$ is length-specific number for individuals at age *a* in year *t*, $\boldsymbol{z}_{l|t-1}$ is length-specific total mortality rates for individuals in year *t*-1, $\boldsymbol{G}$ is the growth transition matrix. Refer to (Zhang & Cadigan, n.d.) for details of this model.

$$\boldsymbol{G} = \begin{bmatrix} p_{11} & \cdots & p_{1L} \\ \vdots & \ddots & \vdots \\ p_{L1} & \cdots & p_{LL} \end{bmatrix} \tag{3.3}$$

where the elements in each column of $\boldsymbol{G}$ sums to one, and p_{ij} represents the probability of moving from length bin *j* to length bin *i* after one year. The equation of p_{ij} is

$$p_{ij} = \int_{l_i - 1}^{l_i} f_{\Delta}(y - \bar{l}_j \mid \bar{l}_j, \boldsymbol{\theta})\, dy \tag{3.4}$$

where $\bar{l}_j$ is the starting mean value of initial length, $\boldsymbol{\theta}$ are parameters to be estimated (detail in below), $f_{\Delta}()$ is the probability density function (pdf) of the growth increment $y - \bar{l}_j$, which is assumed to follow a normal distribution, $f_{\Delta}(x) \sim N(\mu_x, \sigma_x)$. The mean growth increment is formulated as

$$\mu_x = E\,(y - \bar{l}_j \mid \bar{l}_j, \boldsymbol{\theta}) = \frac{\Delta_{max}}{1+e^{-log(19)*\frac{x-l_{50}}{l_{95}-l_{50}}}} \tag{3.5}$$

where parameters $\boldsymbol{\theta}$ =($\Delta_{max}, l_{50}, l_{95}$), Δ_{max}= $(1 - e^{-k}) * L_{\infty}$ that is derived from Von Bertalanffy (VonB) equation and k and L_{∞} are VonB model parameters that to be estimated, l_{50} *and* l_{95} are lengths where growth increments are 50% and 95% of Δ_{max}, respectively, and the value of μ_x decreases with increasing values of x.

The total mortality rate for each length bin *l* in year *t* is the sum of the length-specific fishing mortality rate and the natural mortality rate.

$$Z_{l,t} = F_{l,t} + M_{l,t} \tag{3.6}$$

$Z_{l,t}$ is assumed to be correlated across length and years, log ($Z_{l,t}$) is assumed to follow a multivariate normal (MVN) distribution, log ($Z_{l,t}$) ~ $MVN(\mu_z, \Sigma_z)$, where μ_z is assumed to be the same mean for all *l* and *t*, Σ_z is a separable covariance matrix.

$$\Sigma_z = Cov\left[\Sigma_{z,l,t}, \Sigma_{z,l-1,t-1}\right] = \frac{{\sigma_z}^2 {\phi_L}^{|i|} {\phi_T}^{|j|}}{(1 - {\phi_L}^2)(1 - {\phi_T}^2)}, l = 1, \dots, L \text{ and } t = 1, \dots, T \tag{3.7}$$

where ${\sigma_z}^2$ is the variance, ϕ_L and ϕ_T are the length and year autocorrelation coefficients respectively. ALSCL predicts $Z_{l,t}$ by estimating μ_z, ${\sigma_z}^2, \phi_L$ and ϕ_T. I also assume $M_{l,t}$ for witch flounder to be constant for all length bin *l* in year t ($M_{l,t}$ =0.2), so that $F_{l,t}$ can be derived from the estimated $Z_{l,t}$.

The recruitment is predicted to follow AR1 variation over time,

$$r_t = \bar{r}e^{\varepsilon_t}, t = 1, \dots, T \tag{3.8}$$

$$r_{l|t} = r_t * \boldsymbol{p}_{l|r,t} \tag{3.9}$$

where $\bar{r}$ is the mean recruitment and ε_t is the recruitment deviation that is assumed to follow MVN distribution with mean 0 and AR(1) covariance with correlation and stationary variance, $\varepsilon_t \sim MVN(0, \frac{{\sigma_r}^2 \phi_r}{(1-{\phi_r}^2)})$ and the length distribution of recruitment is assumed to be normal, $\boldsymbol{p}_{l|r,t}$ is the probabilities that recruitment is in each length bin, $r_{l|t}$ is recruitment-at-length in year *t*.

The length-specific abundance at age *a* in the first model year is calculated by

$$n_{l|a,1} = n_{a,1} * \boldsymbol{p}_{l|a,1} \tag{3.10}$$

$$n_{a,1} = r_1 e^{-Z_{init}(a-1)} e^{\varepsilon_a}, a = 1, \dots, A \tag{3.11}$$

where $n_{a,1}$ is stock number-at-age in the first model year, $\boldsymbol{p}_{l|a,1}$ is the probabilities that abundance-at-age is in each length bin in the first model year, r_1 is the recruitment in the first model year, Z_{init} is the initial total natural mortality for age group in the first model year, ε_a are independent random variables that follow normal distribution.

The equations of biomass $b_{l,a,t}$ and spawning stock biomass $ssb_{l,a,t}$ are

$$b_{l,a,t} = n_{l,a,t} wt_{l,t} \tag{3.12}$$

$$ssb_{l,a,t} = b_{l,a,t} mat_{l,t} \tag{3.13}$$

where $wt_{l,t}$ and $mat_{l,t}$ are the weight-at-length and maturity-at-length in year *t* respectively. And the total biomass b_t and spawning stock biomass ssb_t are

$$b_t = \Sigma_l b_{l,t} \tag{3.14}$$

$$b_{l,t} = \Sigma_a b_{l,a,t} \tag{3.15}$$

$$ssb_t = \Sigma_l ssb_{l,t} \tag{3.16}$$

$$ssb_{l,t} = \Sigma_a ssb_{l,a,t} \tag{3.17}$$

The time-series length-based survey indices $I_{l,t}$ is formulated by

$$log(I_{l,t}) = log(q_l) + log(n_{l,t}) + \varepsilon_{l,t} \tag{3.18}$$

where q_l is the catchability at length *l* that is assumed to be constant across year *t*, $\varepsilon_{l,t}$ are assumed to be independent and identically distributed lognormal survey measurement errors of survey number at length, $\varepsilon_{l,t} \overset{iid}{\sim} N(0, \sigma_I)$, where σ_I is the survey index standard deviation. Due to the lack of catchability at length information for NAFO Div. 3NO witch flounder, I set the maximum of the q_l is equal to one and designate the length pattern using a logistic function parameterized according to lengths at 50% and 95% survey catchability (L_{50}, L_{95}) which are 27 cm and 32 cm respectively (Figure 3.9). The Population scale will be sensitive to this q assumption and, consequently, population estimations such as abundance and biomass are considered to be relative.

The total mortality at age a in year t is calculated by

$$Z_{a,t} = log(n_{a,t}) - log(n_{a-1,t-1}) \tag{3.19}$$

where $n_{a,t}$ is stock number-at-age in year t, , $Z_{a,t}$ are derived from age-based population dynamics, and $F_{a,t} = Z_{a,t} - M_{a,t}$ *where* $M_{a,t}$ *is assumed to be* 0.2

3.2.3 ACL model

The ACL model consists of two main parts: a) the stochastic Von Bertalanffy growth model and age-length transition. b) the age-based catch-at-length model.

a. Description of the Von Bertalanffy growth model and the age-length transition

To convert the number-at-age to the number-at-length, ACL starts from the Von Bertalanffy growth model:

$$L_a = L_\infty(1 - e^{-k(a-a_0)}) \tag{3.20}$$

The length information was measured for the bin size of 2 cm. It is assumed that there is a mid-point of the length bins, L ∈ (l - 1 cm, l + 1 cm). It is also assumed that length at age is normally distributed with a mean L_a and a standard deviation τL_a, L at age a~ $N(L_a, \tau L_a)$. ACL applies the formula of cumulative distribution function (CDF) for the normal distribution, the probability was calculated as follows:

$$\boldsymbol{P} = Pr\{\, L(a) \in l\} = \phi\left\{\frac{l - L_a\ + 1}{\tau L_a}\right\} - \phi\left\{\frac{l - L_a\ - 1}{\tau L_a}\right\} \tag{3.21}$$

Where $P_{l,a}$ is the probability that a fish is in length-bin *l* with a given age a, $\phi \sim N\{mean = 0, standard\ deviation = 1\}$.

b. Description of the age-based catch-at-length model

$$n_{a+1,t+1} = n_{a,t}e^{-Z_{a,t}} \tag{3.22}$$

$$Z_{a,t} = F_{a,t} + M_{a,t} \tag{3.23}$$

Where $n_{a,t}$ is the number of fish at age *a* in year *t*, $n_{a+1,t+1}$ is the predicted population in the next year. $Z_{a,t}$ is the total mortality, which equal the sum of fishing mortality rate *F* and natural mortality rate *M*. $M_{a,t}$ is assumed to be constant and is equal to 0.2. $Z_{a,t}$ is assumed to be correlated across length and years, log ($Z_{a,t}$) is assumed to follow a multivariate normal (MVN) distribution, log ($Z_{a,t}$) ~ $MVN(\mu_z, \Sigma_z)$, where μ_z is assumed to be the same mean for all *a* and *t*, Σ_z is a separable covariance matrix.

$$Cov\left(\Sigma_{Z,a,t}, \Sigma_{Z,a-i,t-j)}\right) = \frac{\sigma_Z^2 \phi_A^{|i|} \phi_T^{|j|}}{(1 - \phi_A^2)(1 - \phi_A^2)}, a = 1, \dots, A\ and\ t = 1, \dots, T. \tag{3.24}$$

where ${\sigma_z}^2$ is the variance, ϕ_A and ϕ_T are the age and year autocorrelation coefficients separately. ACL predicts $Z_{a,t}$ by estimating $\mu_z,\ {\sigma_z}^2, \phi_L$ and ϕ_T.

Recruitment is predicted to follow AR1 variation over time,

$$r_t = \bar{r}e^{\varepsilon_t}, t = 1, \ldots, T \tag{3.25}$$

where $\bar{r}$ is the mean recruitment and ε_t is the recruitment deviation that is assumed to follow MVN distribution in stationary process, $\varepsilon_t \sim MVN(0, \frac{{\sigma_r}^2\phi_r}{(1-{\phi_r}^2)})$ and the length distribution of recruitment is assumed to be normal.

The first model year number-at-age is calculated by

$$n_{a,1} = r_1 e^{-Z_{init}(a-1)} e^{\varepsilon_a}, a = 1, \ldots, A \tag{3.26}$$

where r_1 is the recruitment in the first model year, Z_{init} is the initial total natural mortality for age group in the first model year, and ε_a are independent random variables that follow normal distribution, ε_a ~ N(0, σ_{init}), where σ_{init} is assumed to be constant across ages.

Using the age-length transition matrix $\boldsymbol{P}$ to convert number-at-age to number-at-length.

$$\boldsymbol{n}_{l|t} = \boldsymbol{P} * \boldsymbol{n}_{a|t} \tag{3.27}$$

The biomass and spawning stock biomass at length bin l in year t is calculated by

$$b_{l,t} = n_{l,t} wt_{l,t} \tag{3.28}$$

$$ssb_{l,t} = b_{l,t} mat_{l,t} \tag{3.29}$$

Where $wt_{l,t}$ and $mat_{l,t}$ are the weight-at-length and maturity-at-length in year *t* respectively. And the total biomass and spawning stock biomass are

$$b_t = \Sigma_l b_{l,t} \tag{3.30}$$

$$ssb_t = \Sigma_l ssb_{l,t} \tag{3.31}$$

The time-series survey catch-at-length indices $I_{l,t}$ is formulated by

$$log(I_{l,t}) = log(q_l) + log(n_{l,t}) + \varepsilon_{l,t} \tag{3.32}$$

where q_l is the catchability at length *l* that is assumed to be constant across year *t*, $\varepsilon_{l,t}$ are assumed to be independent and identically distributed lognormal survey measurement errors of survey number at length, $\varepsilon_{l,t} \overset{iid}{\sim} N\,(0, \sigma_I)$, where σ_I is the survey index standard deviation. Due to the lack of catchability at length information for NAFO Div. 3NO witch flounder, I set the maximum of the q_l is equal to one and designate the length pattern using a logical function parameterized according to lengths at 50% and 95% fishing selection (L_{50}, L_{95}) which are assumed to be 27 cm and 32 cm respectively (Figure 3.9).

3.3 Results

I fit standardized fall survey abundance-at-length, weight-at-length, and maturity-at-length data of NAFO Div. 3NO witch flounder in four combinations to estimate their relative abundance, recruitment, biomass and stock spawning biomass.

3.3.1 Models diagnostics

Four combinations all successfully converged, and the fits for ALSCL and ACL with model-based indices are fairly good, but the fits for ALSCL and ACL with design-based indices are bad, via inspection for patterns in the residuals (Figures 3.1-3.8). ALSCL and ACL with model-based indices underestimated the survey abundance indices for length groups of 10 to 14 cm in the early model years and length groups of 26 cm to 30 cm in the recent model years, and slightly overestimated the indices for length groups of 32 to 34 cm among model years (Figures 3.3 & 3.7). ALSCL and ACL with design-based indices underestimated the survey abundance indices for length groups of 12 to 14 cm among model years and length groups of 34 cm to 52 cm in the recent model years (Figures 3.1 & 3.5). The residual plots for four combinations are shown in (Figures 3.2 & 3.4 & 3.6 &3.8). The residuals in ALSCL and ACL with model-based indices are much smaller and show fewer trends than that in ALSCL and ACL with design-based indices.

3.3.2 Population estimation

For ALSCL model with design-based indices, the results show an overall fluctuating trend in the estimated relative total abundance and recruitment from 1995 to 2018 (Figure 3.10). The total abundance decreased from 1995 to 1996, increased from 1996 to 1999, and reached the peak in 1999, and fluctuated from 2000 to 2011, then followed a decreasing trend from 2011 to 2018 (Figure 3.10). Recruitment has the same trend as abundance (Figure 3.10). The relative total stock biomass and spawning stock biomass both show a trend of first falling, then rising and falling again from 1995 to 2018 (Figure 3.10). The VonB growth curve indicates the VonB model parameters k and L_∞ estimated at 0.22 and 53.98 cm respectively, it also showed witch flounder approaches L_∞ at age 15 (Figure 3.11).

For ALSCL model with model-based indices, the results indicate a long-term decreased trend in the relative total abundance and recruitment (Figure 3.10). The relative total abundance dropped sharply from 1995 to 1997, increased rapidly from 1997 to 1998, and reached the peak in 1998, and decreased sharply again between 1998 and 2001, then fluctuated from 2001 to 2018 (Figure 3.10). Recruitment has the same trend as abundance (Figure 3.10). The relative total stock biomass shows a first increased and then decreased trend between 1995 to 2018, with a peak in 2010 (Figure 3.10). Similarly, the relative spawning stock biomass (SSB) follows this trend over time (Figure 3.10). The VonB growth curve indicates the VonB model parameters k and L_∞ estimated at 0.28 and 46.46 cm respectively, it also showed witch flounder approaches L_∞ at age 12 (Figure 3.11).

The results of ALSCL model with design-based indices have larger confidence intervals of estimated relative population indices than ALSCL model with model-based indices (Figure 3.10). The results indicate the estimated relative abundance and recruitment in ALSCL model with model-based indices from 1995 to 2018 are larger than those in ALSCL model with design-based indices, especially in 1998, and the estimated relative biomass and SSB from 1995 to 2018 are not significantly different in these two ALSCL combinations (Figure 3.10). The results also indicate no clear stock-recruitment relationship in these two ALSCL combinations (Figure 3.10). The trend of relative total abundance and relative total biomass is different in the time series in these two ALSCL combinations, which indicates that may have a strong variation in age structure over time. Based on the estimates of relative abundance-at-age, there are substantial differences in the patterns of temporal variation between age groups. For example, for ALSCL model with design-based indices, while abundance in age 4-6 groups decreased over time, abundance in age 9-10 groups increased; for ALSCL model with model-based indices, while abundance in age 1 group decreased over time, abundance in age 2-4 groups increased (Figure 3.12). Similarly, the estimates of relative abundance-at-length also indicate obviously different temporal variation patterns among younger and older length groups, that is, in both combinations, while abundance in younger length groups (10-12 cm) decreased over time, abundance increased in older length groups (40-46 cm) over time (Figure 3.13).

For ACL model with design-based indices, the results show an overall fluctuating trend in the estimated relative total abundance and recruitment from 1995 to 2018 (Figure 3.14). The estimated relative abundance and recruitment decreased from 1995 to 1996, increased rapidly from 1996 to 1998, and fluctuated and overall decreased from 1998 to 2016, and show a trend of rising first and then falling from 2017 to 2018 (Figure 3.14). Both relative abundance and recruitment reached a peak in 1999 (Figure 3.14). The total relative stock biomass and spawning stock biomass both show a trend of first falling, then rising and falling again from 1995 to 2018 (Figure 3.14). The VonB growth curve indicates the VonB model parameters k and L_∞ are 0.27 and 44.59 cm respectively, it also showed witch flounder approaches L_∞ at age 13 (Figure 3.15).

For ACL model with model-based indices, the results indicate a long-term decreased trend in the total abundance and recruitment (Figure 3.14). The estimated relative abundance fluctuated from 1995 to 1999, and sharply decreased from 1999 to 2000, then show an overall upward trend from 2000 to 2017, then followed a sharp downward trend from 2017 to 2018 (Figure 3.14). The estimated relative recruitment increased from 1995 to 1996, and sharply decreased from 1996 to 1999, then fluctuated from 2000 to 2011, then followed an overall upward trend from 2011 to 2018 (Figure 3.14). The estimated relative abundance and recruitment reached a peak in 1995 and 1996 respectively (Figure 3.14). The estimated relative total stock biomass and spawning stock biomass show a first increased and then decreased trend between 1995 to 2018 (Figure 3.14). The VonB growth curve indicates the VonB model parameters k and L_∞ are 0.12 and 46.24 cm respectively, it also showed witch flounder approaches L_∞ at age 25 (Figure 3.15).

The results of ACL model with design-based indices have larger confidence intervals of estimated relative population indices than ACL model with model-based indices (Figure 3.14). The results indicate the estimated relative abundance and recruitment in ACL model with model-based indices from 1995 to 1999 and 2015 to 2017 are almost twice those in ACL model with design-based indices, and the estimated relative biomass and SSB from 1995 to 2018 are not significantly different in these two combinations (Figure 3.14). The results also indicate that recruitment was relatively constant over a wide range of SSB levels, with no clear stock-recruitment relationship in these two ACL combinations (Figure 3.14). Based on the estimates of relative abundance-at-age and abundance-at-length, there are substantial differences in the patterns of temporal variation between age or length groups in these two ACL combinations (Figure 3.16-3.17).

3.3.3 length-based survey indices estimation

The ALSCL and ACL models with design-based indices predicted length-based survey indices show completely different trends from the observed indices among years, especially from 2000 to 2018 (Figures 3.18 & 3.20).

The ALSCL and ACL models with model-based indices predicted length-based survey indices reflect the same trends as observed indices (Figures 3.19 & 3.21). The lengths corresponding to the peaks in the estimations are slightly greater than that in observations across most years (Figures 3.19 & 3.21). Noticeably, in some years (e.g. 1998 and 2011), small peaks in the observed survey indices for catch with length less than 20cm are not shown in the prediction indices (Figures 3.19 & 3.21).

3.3.4 Fishing mortality estimation

For ALSCL model with design-based indices, fishing mortality at age or length is very stable from 1995 to 2018 with very little change, and fishing mortality less than 0.1 for all age or length groups (Figure 3.22). For ALSCL model with model-based indices, fishing mortality at age shows a trend of first rising, then falling, and then fluctuating between 0 and 0.5 among all age groups, except for age 1 and age 2 groups (Figure 3.22). For age greater than 3 groups, fishing mortality shows a substantially same trend over time, with a peak value in 1998 (Figure 3.22). The estimates of fishing mortality at length indicate that fishing mortality is equal to 0 for length groups of 10 to 24 cm, with an overall decreasing trend for length groups of 24 to 52 cm (Figure 3.23).

For ACL model with design-based indices and model-based indices, fishing mortality is equal to 0 for all age groups due to the estimated total mortality is smaller than assumed natural mortality (0.2). And fishing mortality at length cannot be produced in these two combinations (Figure 3.24).

3.3.5 Sensitivity analyses

I found that the assessment results are sensitive to the indices choices. In both ALSCL and ACL models, the abundance estimated by model-based indices is much larger than the abundance estimated by design-based indices, from 1995 to 2018, especially in the early and recently model years (Figures 3.10 & 3.14); the abundance-at-age estimated by model-based indices is larger than that estimated by design-based indices for age 1-3 and 13-25 groups, and the abundance-at-age estimated by model-based indices is smaller than that estimated by design-based indices for age 5-10 groups (Figures 3.12 & 3.16); the abundance-at-length estimated by model-based indices is much larger than that estimated by design-based indices for length at 10-18 cm groups, and the abundance-at-length estimated by model-based indices is smaller than that estimated by design-based indices for length at 18-40 cm groups (Figures 3.13 & 3.17); the survey indices residuals estimated by model-based indices is much smaller than that estimated by design-based indices, especially in young age groups or small length groups (Figures 3.25-3.28).

I found the assessment results to be less sensitive to model choices compared to indices choices. For ALSCL and ACL models with design-based indices, the results show that the estimated abundance, recruitment, biomass and spawning stock biomass in the time series have similar values and trends (Figure 3.29). The estimated abundance among age or length groups in these two combinations also has a similar trend but estimates in ACL are basically larger than in ALSCL (Figures 3.30-3.31). The estimated fishing mortality in both ALSCL and ACL is below 0.1 and doesn't have obvious changes among age groups (Figure 3.32). For ALSCL and ACL models with model-based indices, the estimated abundance in ACL is higher than in ALSCL, especially in 1996, estimated abundance in ACL was about double that in ALSCL (Figure 3.34); the estimated recruitment in ACL and ALSCL fluctuates within the relatively same range, but not in the same trend, and the estimated biomass and spawning biomass in these two combinations are very close and have relatively the same trends (Figure

3.34); the estimated abundance-at-age in ACL is much higher than in ALSCL since age 7 group (Figure 3.35); the estimated abundance-at-length in ACL have similar values and trends as in ALSCL (Figure 3.36). Compare to ALSCL, ACL only can provide the estimation of fishing mortality at age and cannot produce the estimated fishing mortality at length (Figure 3.37). Regardless design-based or model-based indices are fitted in ACL, the estimated total mortality in ACL is smaller than assumed natural mortality (0.2), so the estimated fishing mortality is equal to 0, which is unrealistic (Figure 3.36). The estimated growth of witch flounder's body length in ALSCL is faster than in ACL (Figures 3.33 & 3.38).

I found that ALSCL and ACL models are sensitive to the survey catchability q_l. I conducted the sensitivity analyses for both models based on the two different length-dependent survey catchabilities calculated by using a logistic function and assumed lengths at 50% and 95% selection. Due to the lack of accurate survey catchability values for 3NO witch flounder, I use the estimated survey catchability of groundfish that is close to the witch flounder's biology (i.e. American plaice) in the NAFO Div. 3NO region as a reference for estimation. The estimated L_{50} and L_{95} for American plaice are 17.8 cm and 26 cm respectively (Kumar et al., 2020). So I run ALSCL with nine different assumed survey catchabilities, L_{50} = {18, 21, 23, 25, 27, 31, 27, 27, 27, L_{95} = {23, 26, 28, 30, 32, 36, 31, 33, 29}, I also run ACL with L_{50} = {18, 21, 23, 25, 27, 31, 27, 27, 27, L_{95} = {23, 26, 28, 30, 32, 36, 31, 30, 29}. The corresponding AICs for ALSCL and ACL models with nine different survey catchabilities are listed in Table 3.3. I found ACL model is more sensitive to the survey catchability than ALSCL model, due to ACL model failing to converge in the first four runs. When L_{50} is 27 cm and L_{95} is 32 cm, the AIC of ALSCL model is the smallest and the fit performs the best;

when L_{50} is 27 cm and L_{95} is 30 cm, the AIC of ACL model is the smallest and the best fit is achieved.

I also compared the stock assessment results in ALSCL and ACL models based on two different catchabilities (q1: L_{50} is 27 cm, L_{95} is 29 cm; q2: L_{50} is 27 cm, L_{95} is 32 cm) by fitting model-based indices. The estimation results under different catchabilities are significantly different in both ALSCL and ACL models, and the models under lower q values produce extremely high estimated abundance and biomass. In ALSCL model, the estimated abundance under q1 is almost 10 times the estimated abundance under q2 (Figure 3.39), and the estimated biomass under q1 is more than 1.5 times the estimated biomass under q2 (Figure 3.40); the estimated abundance at age or length under q1 is much higher than the estimated abundance at age or length under q2 in the young age (age 1-2) and small length (10-26 cm) (Figures 3.41-3.42); the estimated fishing mortality at age or length under q1 is basically larger than the estimated fishing mortality at age or length under q2 (Figures 3.43-3.44); the estimated growth rate under q2 is greater than that under q1 before age 9 (Figure 3.45). In ACL model, the estimated abundance under q1 is almost 30 times the estimated abundance under q2 in the first and second model years (Figure 3.46); the estimated biomass under q1 is more than 2 times the estimated biomass under q2 (Figure 3.47); the estimated abundance at age or length under q1 is much higher than the estimated abundance at age or length under q2 in the young age (age 1-6) and small length (10-26 cm) (Figures 3.48-3.49); the estimated fishing mortality at age is equal to 0 under q1 and q2 (Figure 3.50); the estimated growth curve under q1 is similar to that under q2 (Figure 3.51).

3.3.6 Retrospective analyses for ALSCL and ACL models with model-based indices

I performed eight-year retrospective analyses on total abundance, recruitment, total biomass, and spawning stock biomass for ALSCL model. The results for ALSCL model are shown in Figure 3.52, which indicate that there are almost no retrospective patterns (that are systematic changes in historic estimates of population size with the inclusion or exclusion data for an additional year (Hurtado-Ferro et al., 2015)). Thus, I consider the retrospective patterns for ALSCL model to be good.

I only performed three-year retrospective analyses on total abundance, recruitment, total biomass, and spawning stock biomass for ACL model due to ACL model failing to converge in retrospective analyses from 2013 to 2009. The results for ACL model are shown in Figure 3.53, which indicates that there are a few retrospective patterns. For the 2016 assessment year, the estimates of abundance, recruitment, biomass and spawning stock biomass were low but revised at a high level for the 2017 and 2018 assessment years (Figure 3.53).

I also calculated Mohn’s rho to quantify the severity of retrospective pattern for both ALSCL and ACL models (Mohn, 1999). The absolute value of Mohn's rho in ACL was greater than the absolute value of Mohn's rho in ALSCL in retrospective analyses of abundance, recruitment, biomass and spawning stock biomass, which indicates ALSCL model is more robust than ACL model in retrospective analyses (Figure 3.52-3.53).

3.4 Discussion

By comparing the results of the four combinations, it is found that the assessment results of NAFO Div. 3NO witch flounder are very sensitive to the choice of indices, and also sensitive to the choice of model based on the results in sensitivity and retrospective analyses. In ALSCL and ACL models, results estimated with design-based indices have large residuals compared to observations and have larger confidence intervals than those estimated with model-based indices, which indicates that standardization of survey indices using VAST may effectively improve the accuracy of assessment. If only focus on the results from fitting model-based indices for both models, ALSCL can take account into length-dependent fishing mortality but ACL cannot, ALSCL has more wide applicability for different catchabilities than ACL, and ALSCL has fewer retrospective patterns than ACL. The trend of ALSCL estimated recruitment by fitting model-based indices (Figure 3.10) is consistent with the trend of recruitment index derived from NAFO Div. 3NO fall Canadian RV survey, and the trend of biomass dynamic predicted by the two models with model-based indices (Figure 3.10) is basically the same, showing a trend of first rising and then falling (Rogers & Morgan, 2019). ALSCL and ACL models suggest there is a strong variation of age structure over time, which cannot be identified by the current surplus production assessment model. In addition, ALSCL and ACL models also can provide the growth curve of witch flounder by estimating the VonB parameters. The male and female combined estimation of L_∞ in ALSCL and ACL models by fitting model-based indices are 46.46 cm and 46.24 cm respectively (Figure 3.38), which are smaller than the values estimated by (Bowering, 1976) (L_∞ are almost 56 cm and 62 cm for 3NO male and female witch flounder respectively). This may be a result of the miniaturization of mature fish due to overfishing in the 1970s and 1980s (Rogers & Morgan, 2019).

The three-dimensional structure of ALSCL provides the estimate of population dynamics incorporating both age- and length-dependent fishing mortality. Compared with the current surplus production model in a Bayesian framework that was used for the assessment of this stock in NAFO Div. 3NO (Rogers & Morgan, 2019), ALSCL is able to produce the estimations of age-based population dynamics, including abundance, recruitment, biomass, spawning stock biomass and age-dependent and length-dependent fishing mortality, but due to lack of landings information, all estimates are relative, the current assessment model used by DFO is only able to estimate biomass dynamics and overall fishing mortality(Rogers & Morgan, 2019). The ACL estimates the age-based cohort dynamics only via the estimated age-dependent fishing mortality. It is criticized for its lack of accounting for length-dependent mortality within the same age group (Punt et al., 2013). In general, fishing gears have different selectivity for different lengths, and fish of the same age may have different body lengths, and the body length will not increase after a certain age, and the length-dependent fishing mortality is associated with the length-dependent fishing selectivity. Therefore, the assumptions that constant fishing mortality within the same age and ignoring length-dependent mortality within age are used in ACL may result in inaccurate estimation of cohort dynamics.

Since no sex ratio of NAFO Div. 3NO witch flounder was provided in the Fall survey data, I simply assumed a sex ratio of 1:1 in ALSCL and ACL models. However, the maturity of males and females at the same body length is different, and the maximum body length that can be achieved is also different. For example, the lengths at 50 % maturity of males and females witch flounder are 26.6 cm and 29.2 cm respectively (Swain et al., 2012). Assuming males and females have the same maturity can lead to bias in the estimated spawning stock biomass.

A major challenge for ALSCL and ACL models is obtaining accurate survey catchability. Assessment results for NAFO Div. 3NO witch flounder are very sensitive to survey catchability. It is difficult to address this problem if survey fishing is unavailable.

Another challenge for ALSCL and ACL models is estimating natural mortality. In both models, I estimated the total mortality, and fishing mortality that is derived from the total mortality and fixed natural mortality. I cannot estimate the fishing mortality and natural mortality separately with only survey length-based data. A natural mortality value of 0.2 has traditionally been used for all ages and for both males and females in the most stock assessment (Maunder & Wong, 2011). But this value may smaller or larger for witch flounder, which can result in inaccurate estimation of cohort dynamics. Lorenzen M can be used in the future to make the natural mortality more realistic (Lorenzen, 2011), but the stochastic M could potentially be confounded with deviations in catchabilities.

The current stock assessment for NAFO Div. 3NO witch flounder only uses the survey indices data and the total commercial catch data (Maddock Parsons et al., 2020; Rogers & Morgan, 2019). In ALSCL and ACL models, I only use the survey catch-at-length data, so the absolute estimates of stock size cannot be provided. If the commercial catch-at-length data is available, ALSCL and ACL is very flexible to integrate that data and enables to provide the absolute estimates of stock size, which can improve the accuracy of stock assessment and give more precise reference points.

Tables

Table 3.1 The list of fixed effects and random effects of ALSCL

Parameter	Description
Fixed effect	
$\log(\bar{r})$	Log of mean recruitment
$\log(\sigma_r)$	Log of standard deviation of log recruitment
$\log(\phi_r)$	Log of autocorrelation of recruitment
$\log(Z_{init})$	Log of initial total mortality in the first model year
$\log(\sigma_{init})$	Log of standard deviation of log number-at-age in the first model year
$\log(cv_{init})$	Log of coefficient of variance of initial size of each cohort in the first model year
$\log(cv_{inc})$	Log of coefficient of variation of growth increment
$\log(L_\infty)$	Log of L_∞ in the Von Bertalanffy growth model
$\log(k)$	Log of k in the Von Bertalanffy growth model
$\log(L_0)$	Log of initial length of witch flounder (i.e., mean length at the age of 0), fixed to be 0.04.
$\log(\mu_z)$	Log of mean of total mortality for all lengths and years.
$\log(\sigma_z)$	Log of standard deviation of log total mortality
$\log(\phi_T)$	Log of autocorrelation of total mortality among years
$\log(\phi_L)$	Log of autocorrelation of total mortality among length classes
$\log(\sigma_I)$	Log of survey index standard deviation
Random effects	
ε_t	Recruitment deviation
ε_z	Deviation of total mortality across lengths and years
ε_a	Deviation of number-at-age in the first model year

Table 3.2 The list of fixed effects and random effects of ACL

Parameter	**Description**
	Fixed effect
$\log(\bar{r})$	Log of mean recruitment
$\log(\sigma_r)$	Log of standard deviation of log recruitment
$\log(\phi_r)$	Log of autocorrelation of recruitment
$\log(Z_{init})$	Log of initial total mortality in the first model year
$\log(\sigma_{init})$	Log of standard deviation of log number-at-age in the first model year
$\log(cv_{init})$	Log of coefficient of variance of initial size of each cohort in the first model year
$\log(L_\infty)$	Log of L_∞ in the Von Bertalanffy growth model
$\log(k)$	Log of k in the Von Bertalanffy growth model
$\log(a_0)$	Log of the theoretical age of witch flounder when size is zero
$\log(\mu_z)$	Log of mean of total mortality for all lengths and years.
$\log(\sigma_z)$	Log of standard deviation of log total mortality
$\log(\phi_T)$	Log of autocorrelation of total mortality among years
$\log(\phi_A)$	Log of autocorrelation of total mortality among age classes
$\log(\sigma_I)$	Log of survey index standard deviation
	Random effects
ε_t	Recruitment deviation
ε_z	Deviation of total mortality across lengths and years
ε_a	Deviation of number-at-age in the first model year

Table 3.3 The L_{50}, L_{95} and corresponding AICs for ALSCLs and ACLs resulting from inputting nine different survey catchabilities in sensitivity analyses.

ALSCL	L_{50}	L_{95}	AIC
q1	18	23	675.4820
q2	21	26	378.5578
q3	23	28	292.2846
q4	25	30	247.4288
q5	27	32	240.5592
q6	31	36	250.8287
q7	27	31	272.6340
q8	27	33	272.8006
q9	27	29	429.0152
ACL	L_{50}	L_{95}	**AIC**
q1	18	23	false converge
q2	21	26	false converge
q3	23	28	false converge
q4	25	30	false converge
q5	27	32	230.9924
q6	31	36	243.5120
q7	27	31	212.9385
q8	27	30	209.4273
q9	27	29	240.0318

Figures

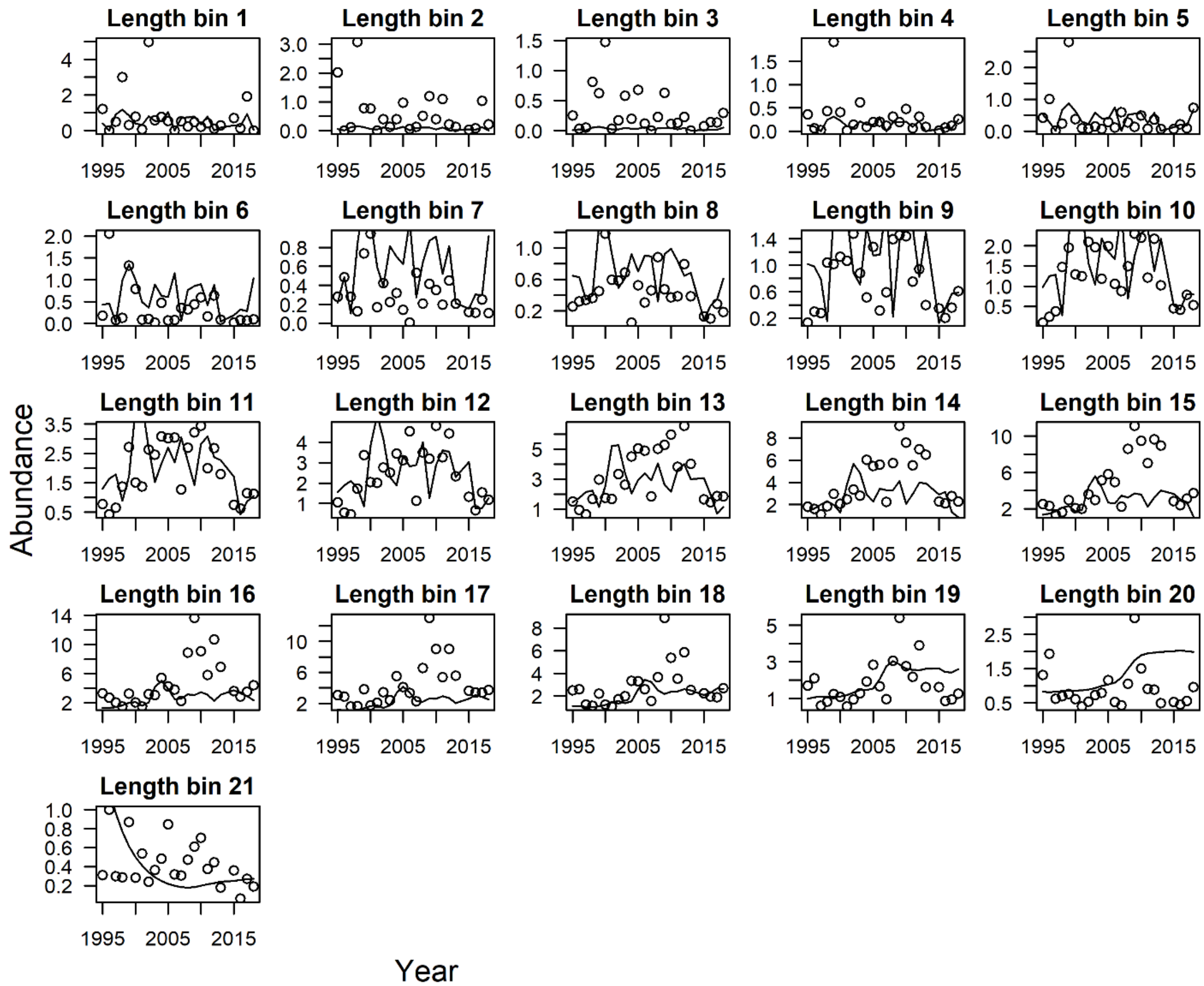

Figure 3.1 Observed and predicted survey catch-at-length (millions) by ALSCL with design-based indices for NAFO Div. 3NO witch flounder from 1995 to 2018 (except 2014).

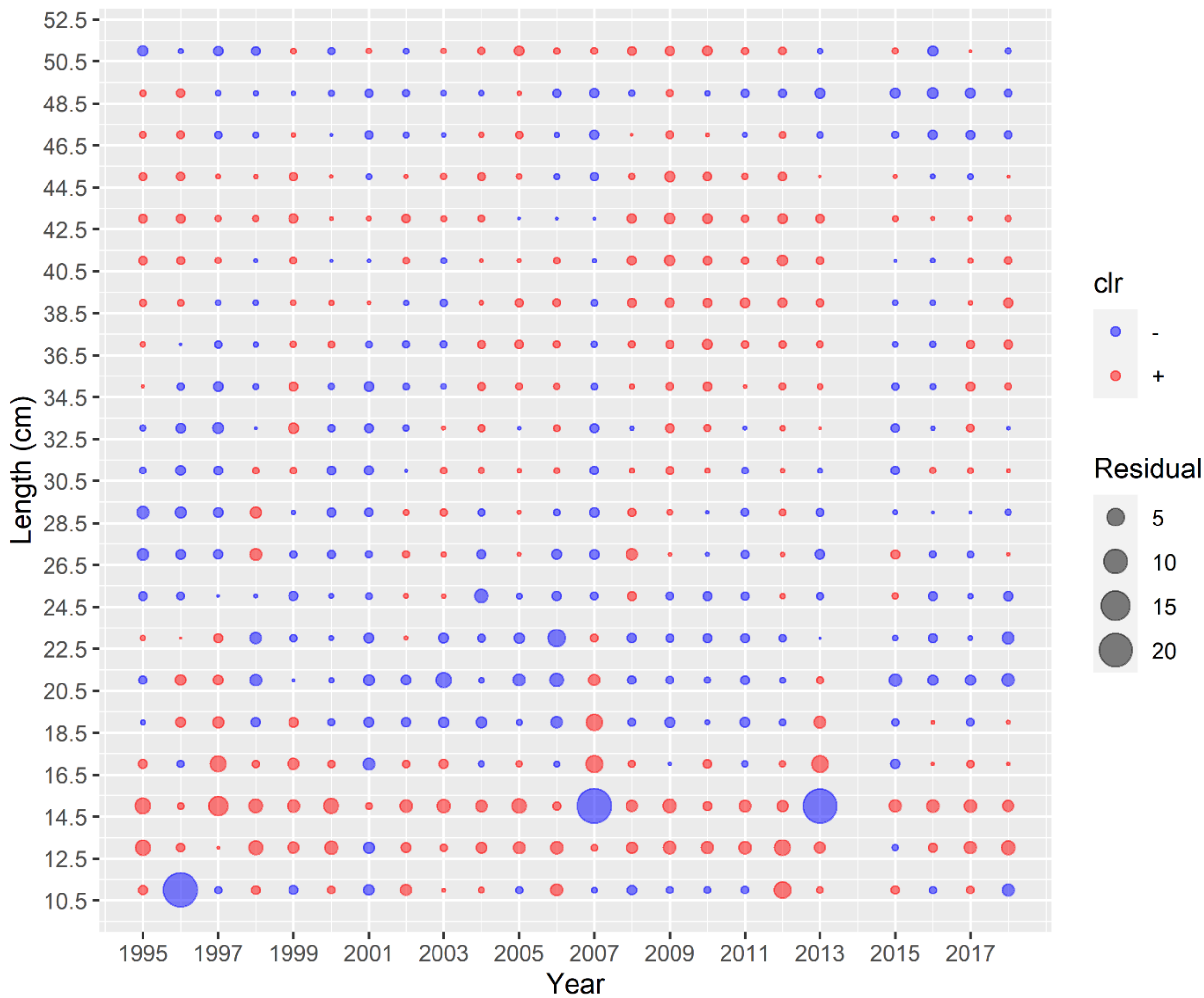

Figure 3.2 The residual plot of the predicted survey log-catch at length by ALSCL with design-based indices for NAFO Div. 3NO witch flounder from 1995 to 2018 (except 2014). Red bubbles are positive residuals while bule bubbles are negative residuals.

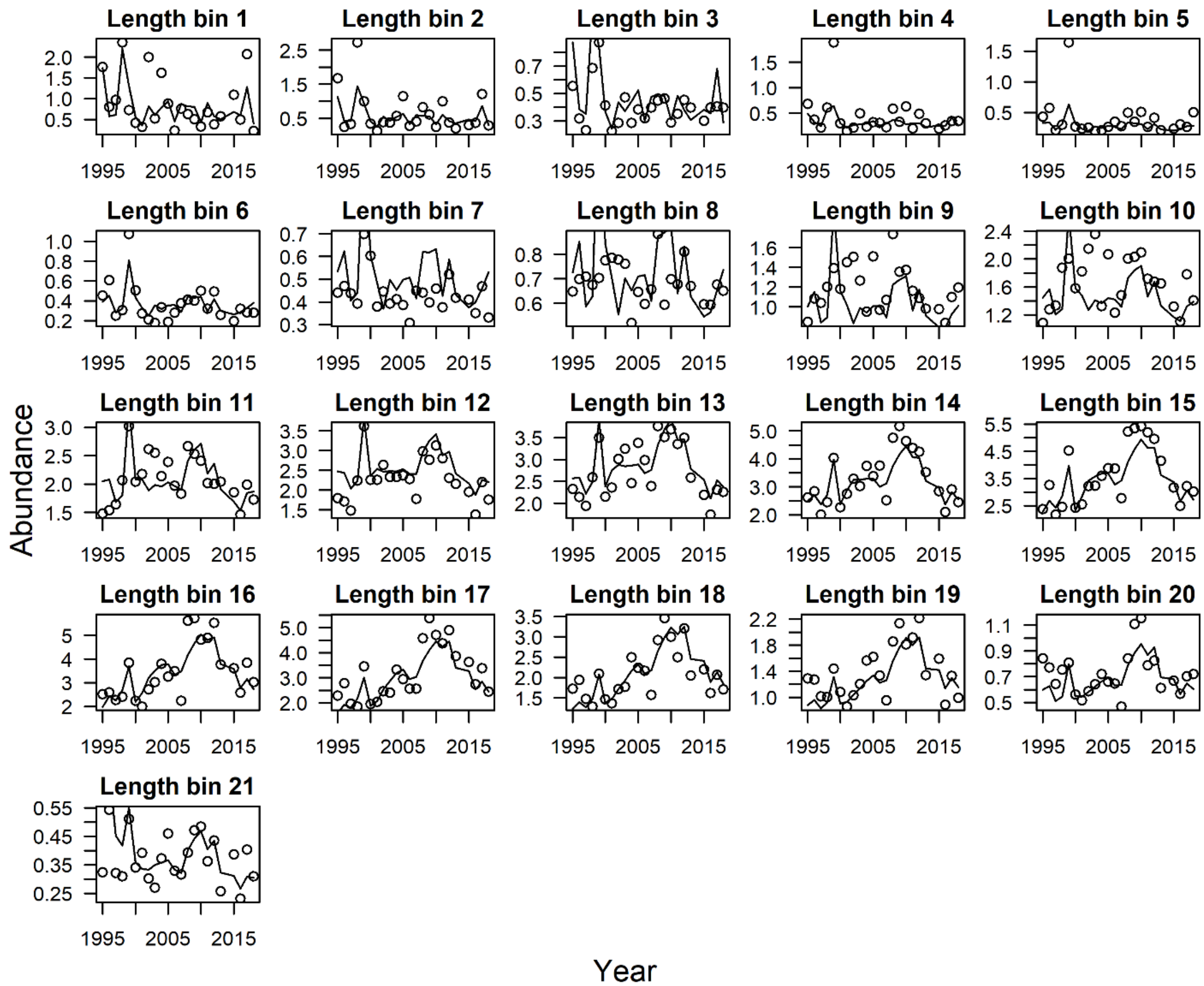

Figure 3.3 Observed and predicted survey catch-at-length (millions) by ALSCL with model-based indices for NAFO Div. 3NO witch flounder from 1995 to 2018 (except 2014).

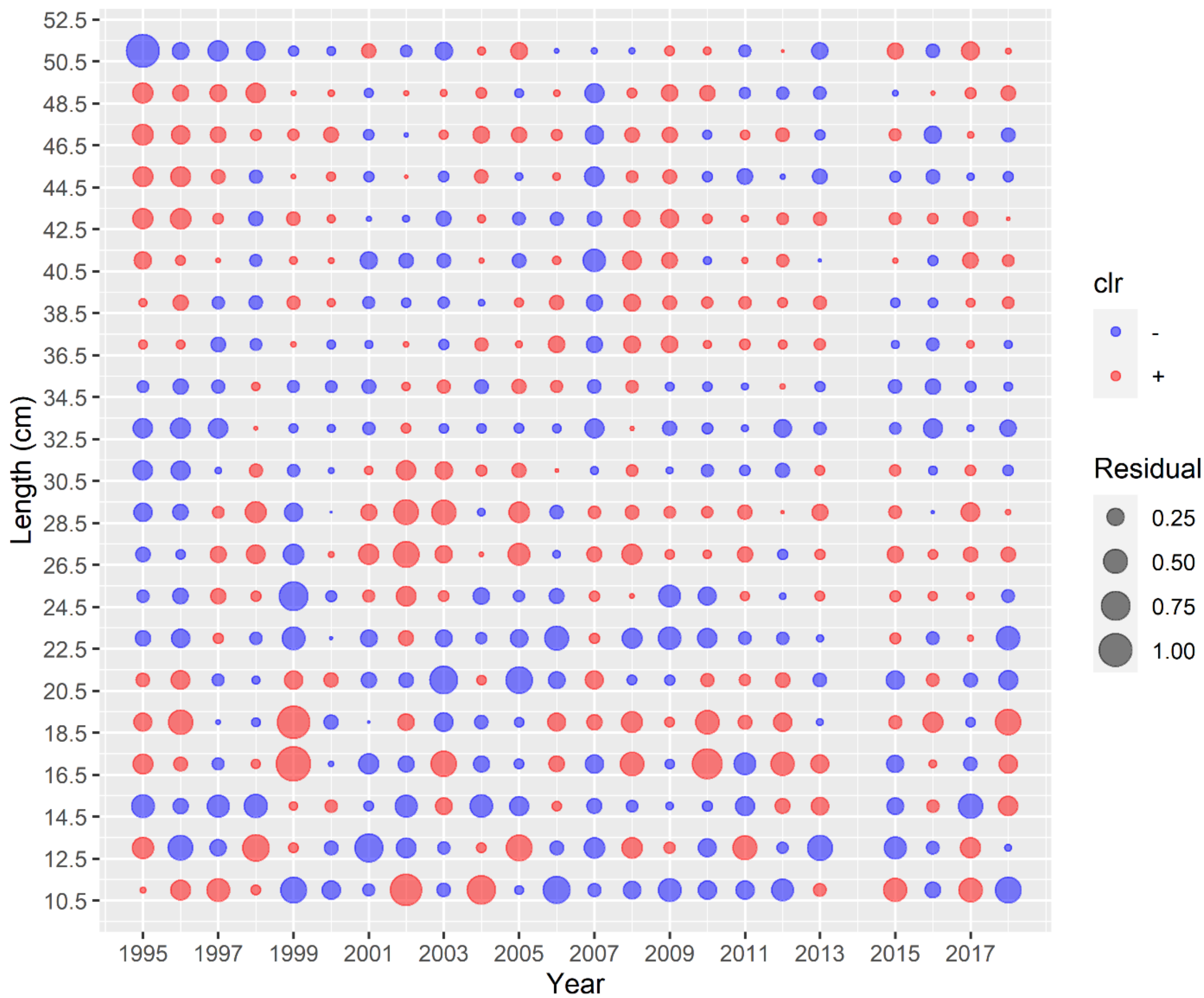

Figure 3.4 The residual plot of the predicted survey log-catch at length by ALSCL with model-based indices for NAFO Div. 3NO witch flounder from 1995 to 2018 (except 2014). Red bubbles are positive residuals while bule bubbles are negative residuals.

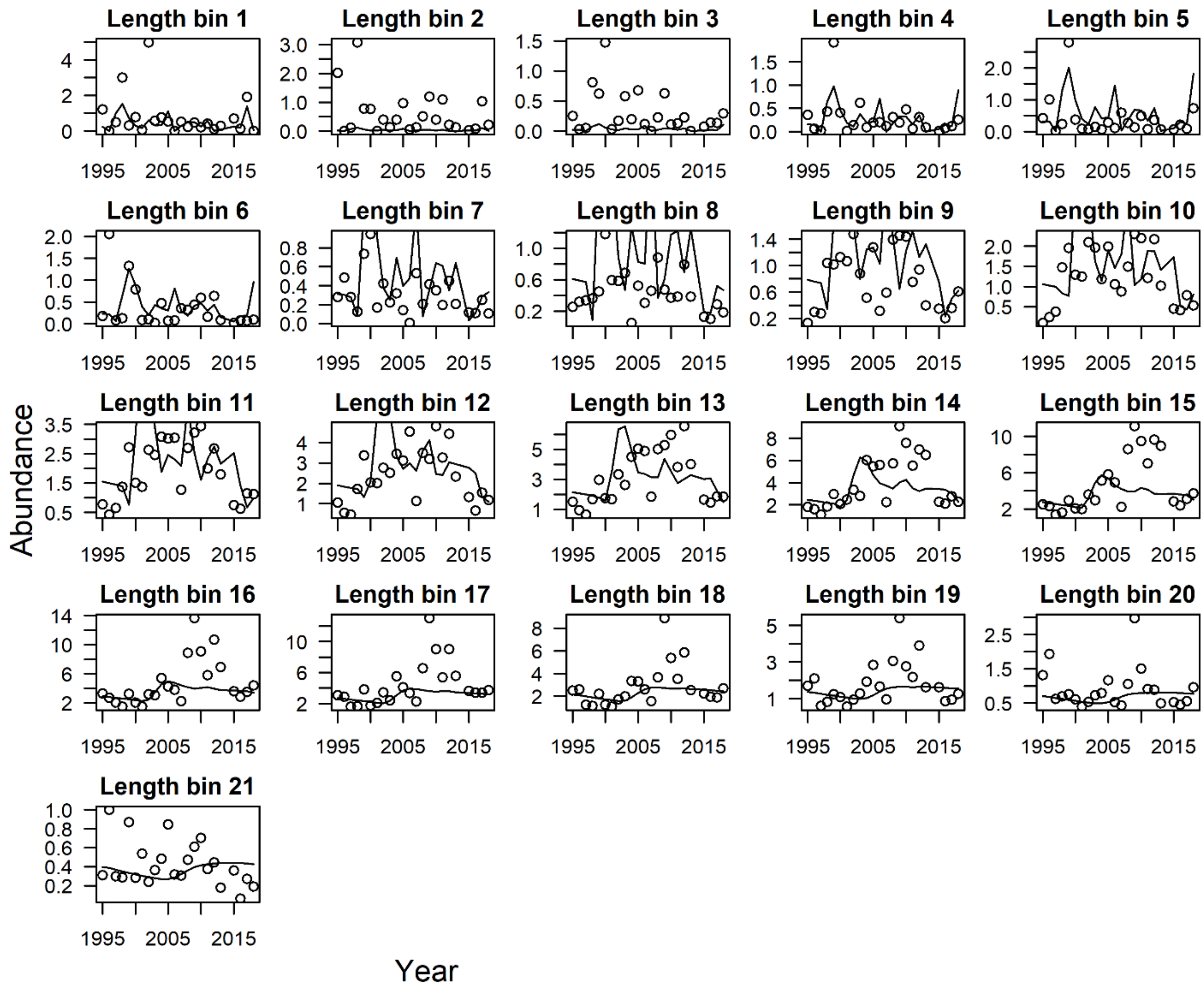

Figure 3.5 Observed and predicted survey catch-at-length (millions) by ACL with design-based indices for NAFO Div. 3NO witch flounder from 1995 to 2018 (except 2014).

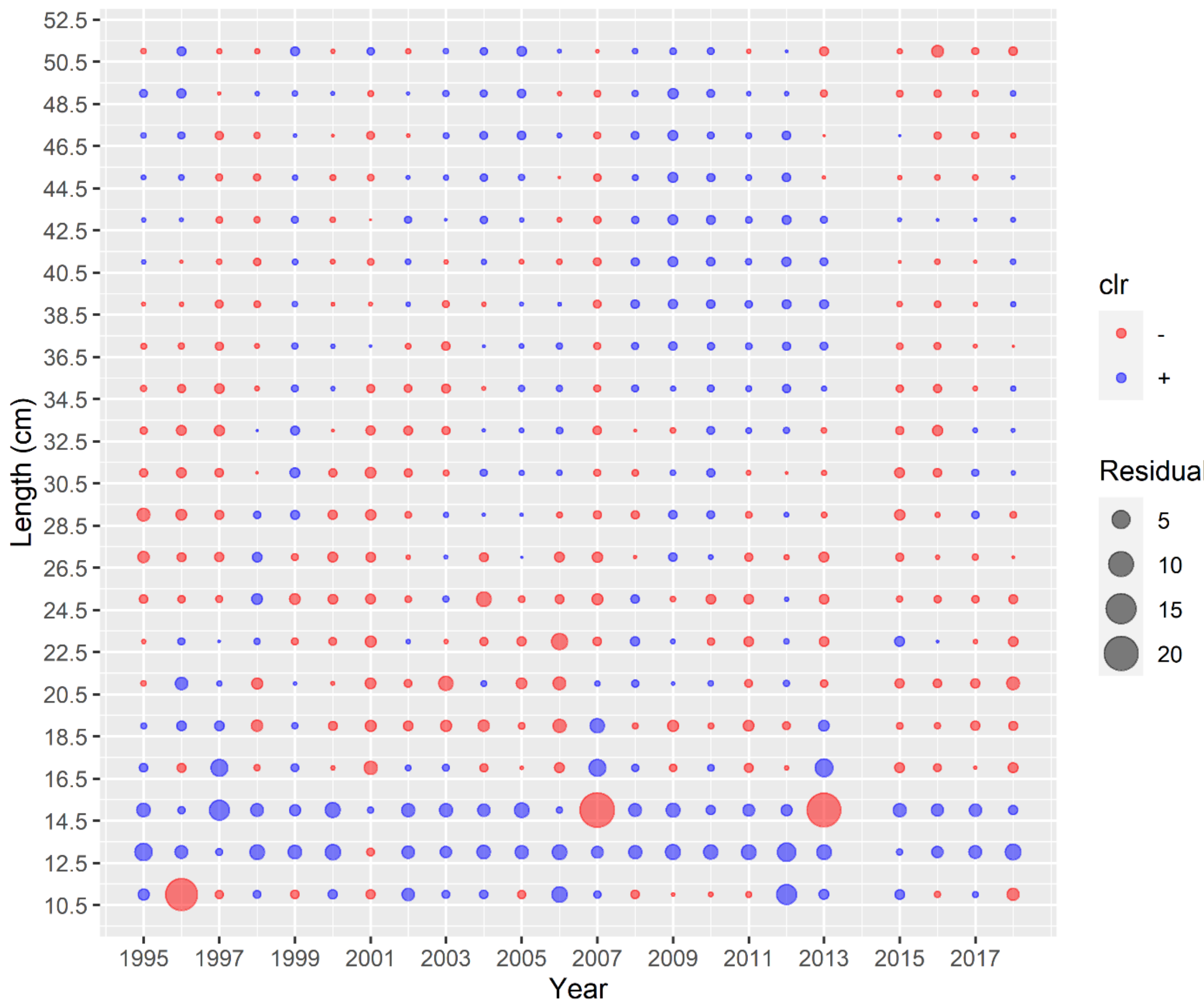

Figure 3.6 The residual plot of the predicted survey log-catch at length by ACL with design-based indices for NAFO Div. 3NO witch flounder from 1995 to 2018 (except 2014). Red bubbles are positive residuals while bule bubbles are negative residuals.

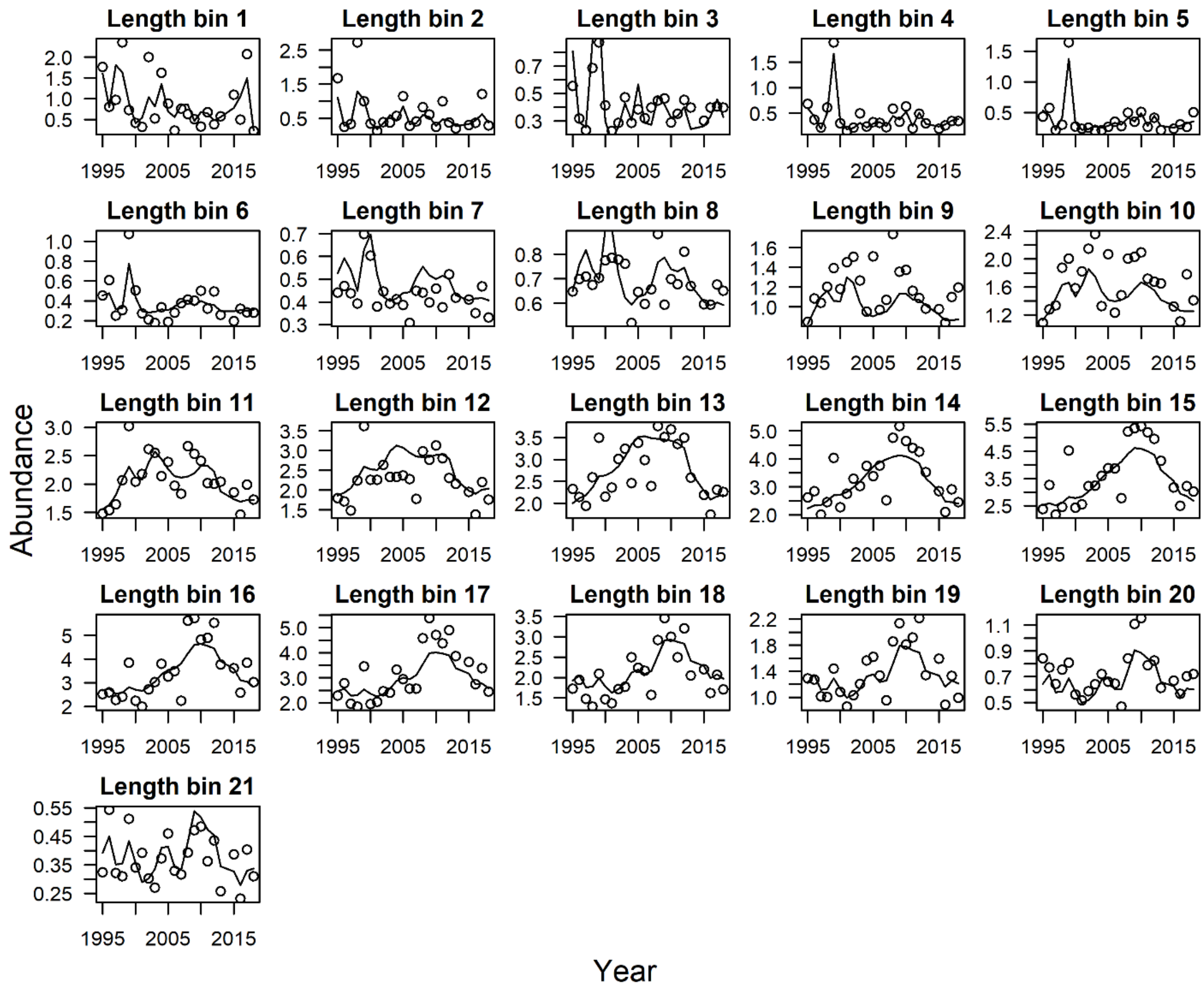

Figure 3.7 Observed and predicted survey catch-at-length (millions) by ACL with model-based indices for NAFO Div. 3NO witch flounder from 1995 to 2018 (except 2014).

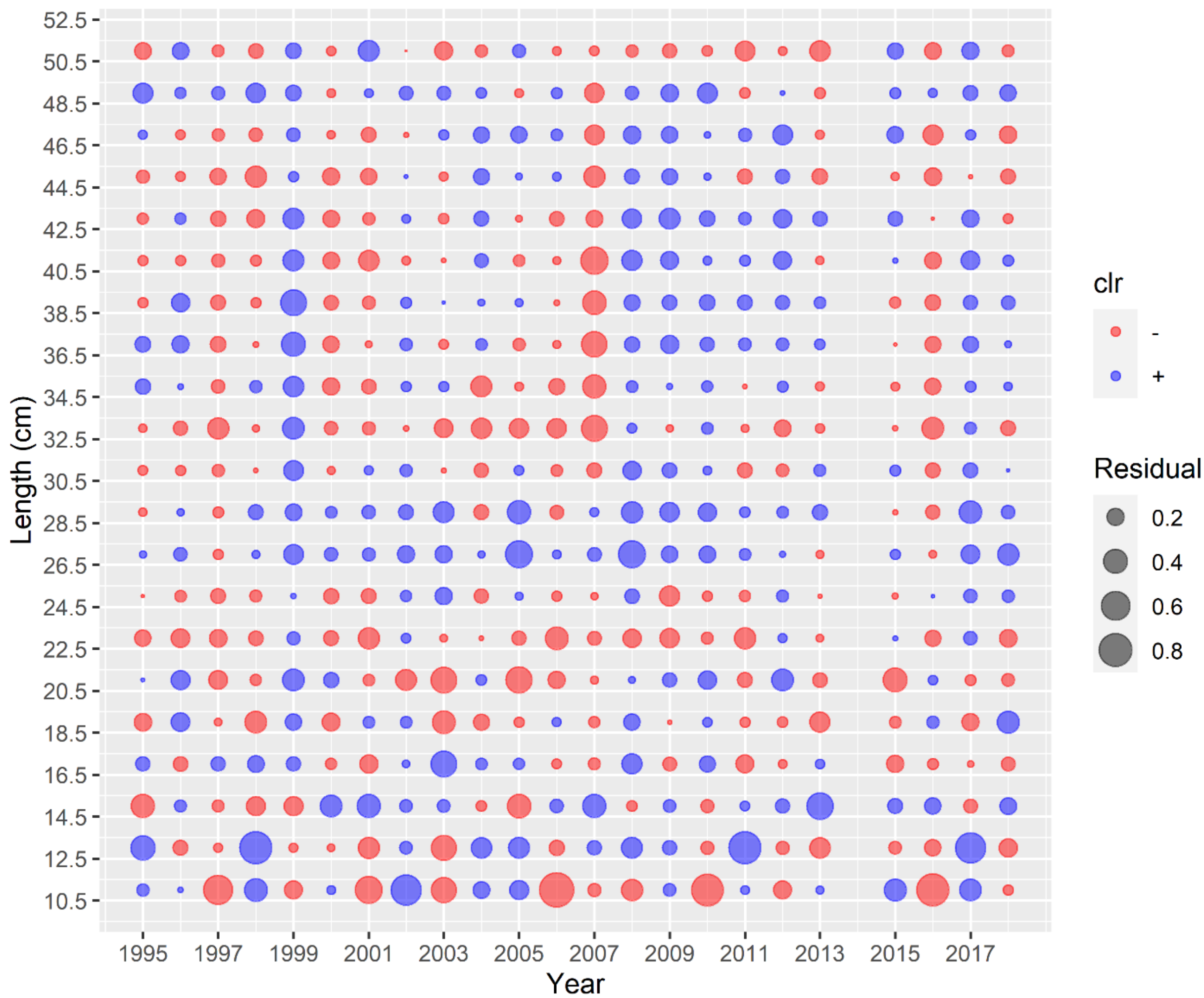

Figure 3.8 The residual plot of the predicted survey log-catch at length by ACL with model-based indices for NAFO Div. 3NO witch flounder from 1995 to 2018 (except 2014). Red bubbles are positive residuals while bule bubbles are negative residuals.

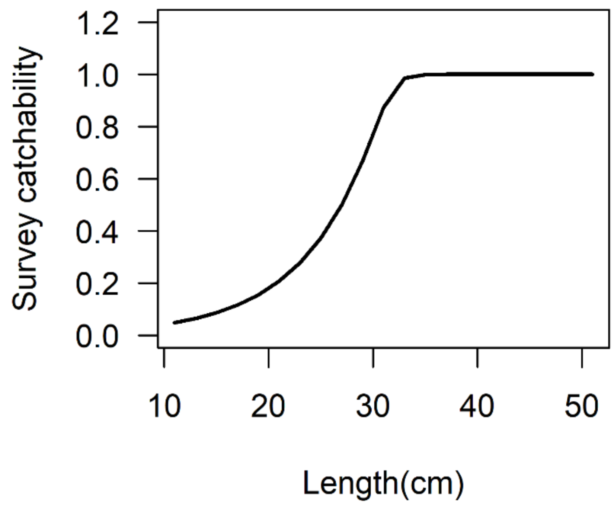

Figure 3.9 The assumed survey catchability at length for NAFO Div. 3NO witch flounder.

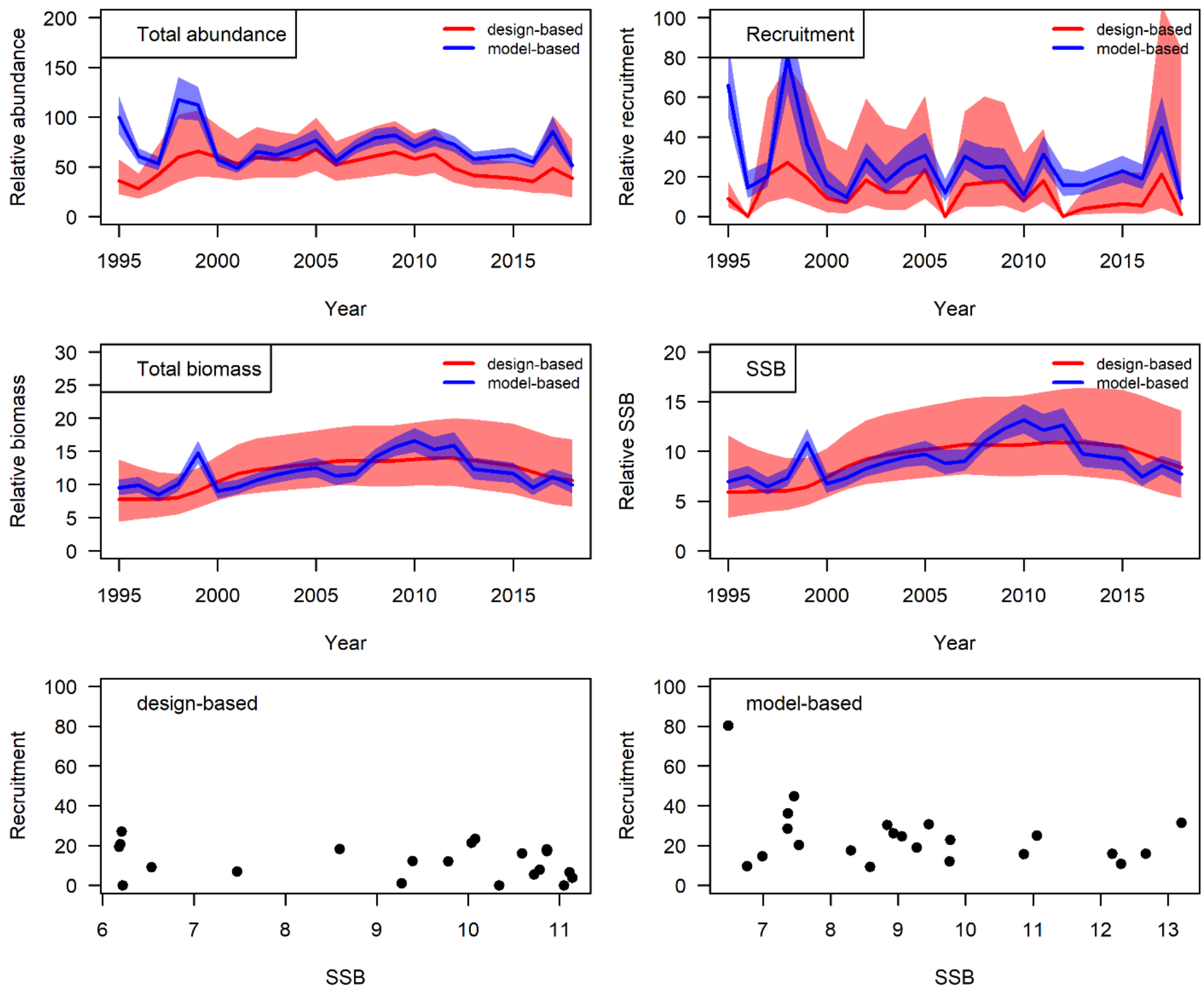

Figure 3.10 From top to bottom are the estimated total abundance and recruitment (millions), the estimated total biomass and spawning stock biomass (Kt), and the estimated stock-recruitment relationship for NAFO Div. 3NO witch flounder in ALSCL with design-based and model-based indices. Red line is the estimates with design-based indices and blue line is the estimates with model-based indices. The covered areas by red and blue are 95% confidence intervals.

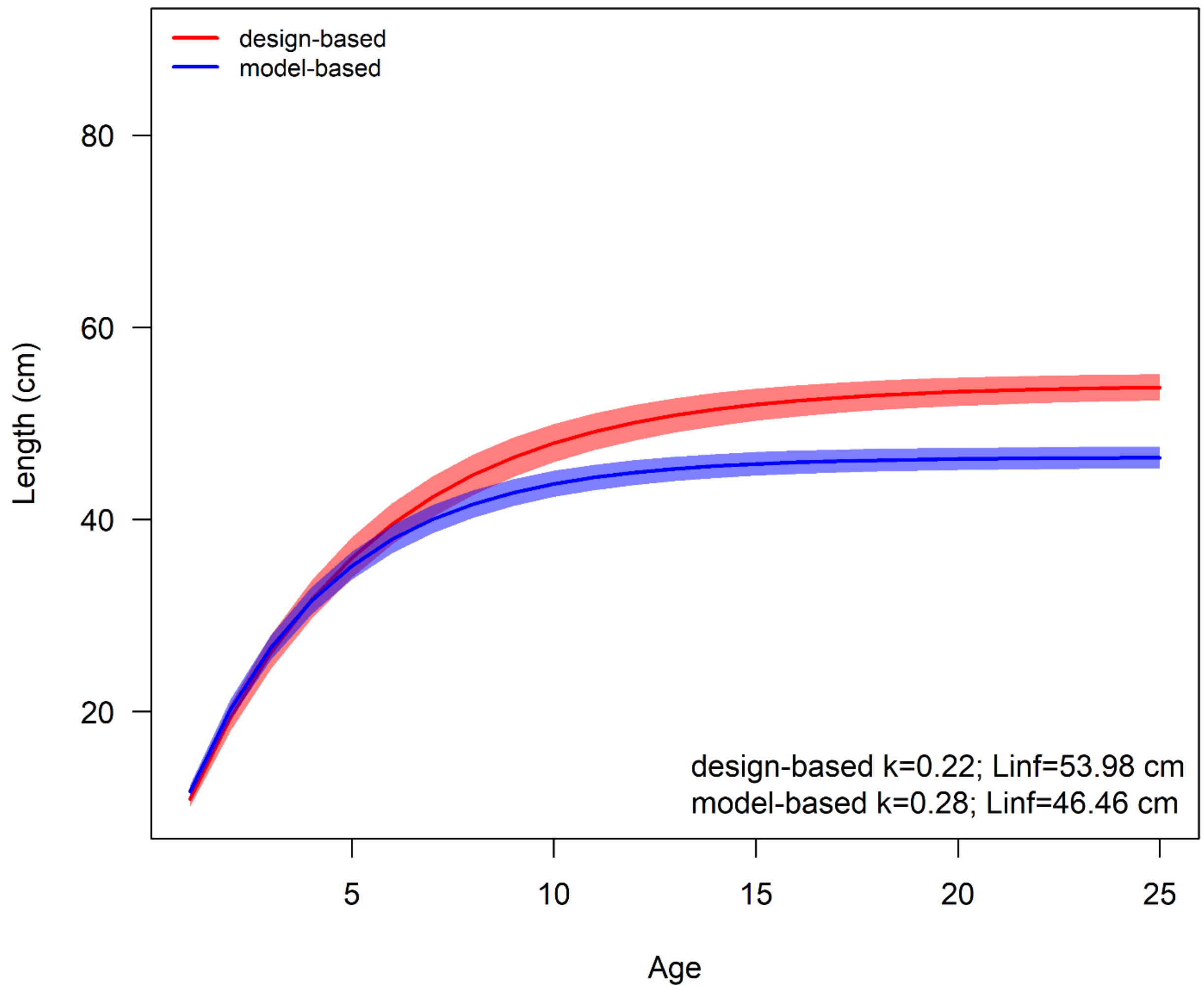

Figure 3.11 The estimated VonB growth curve of NAFO Div. 3NO witch flounder in ALSCL model with design-based indices and model-based indices. Red line is the estimates with design-based indices and blue line is the estimates with model-based indices. The covered areas by red and blue are 95% confidence intervals.

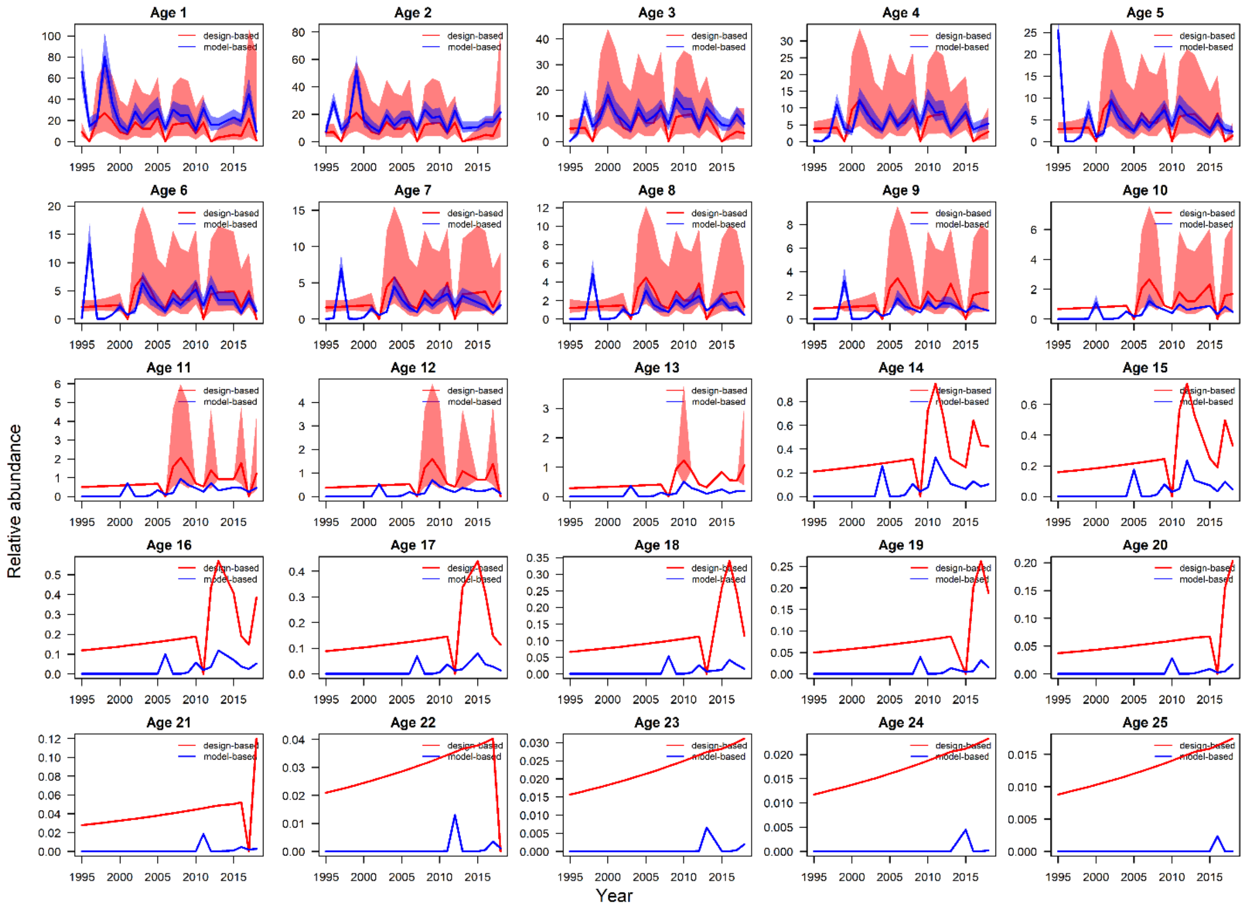

Figure 3.12 The estimated abundance-at-age (millions) for NAFO Div. 3NO witch flounder in ALSCL model with design-based indices and model-based indices from 1995 to 2018 (except 2014). Red line is the estimates with design-based indices and blue line is the estimates with model-based indices. The covered areas by red and blue are 95% confidence intervals.

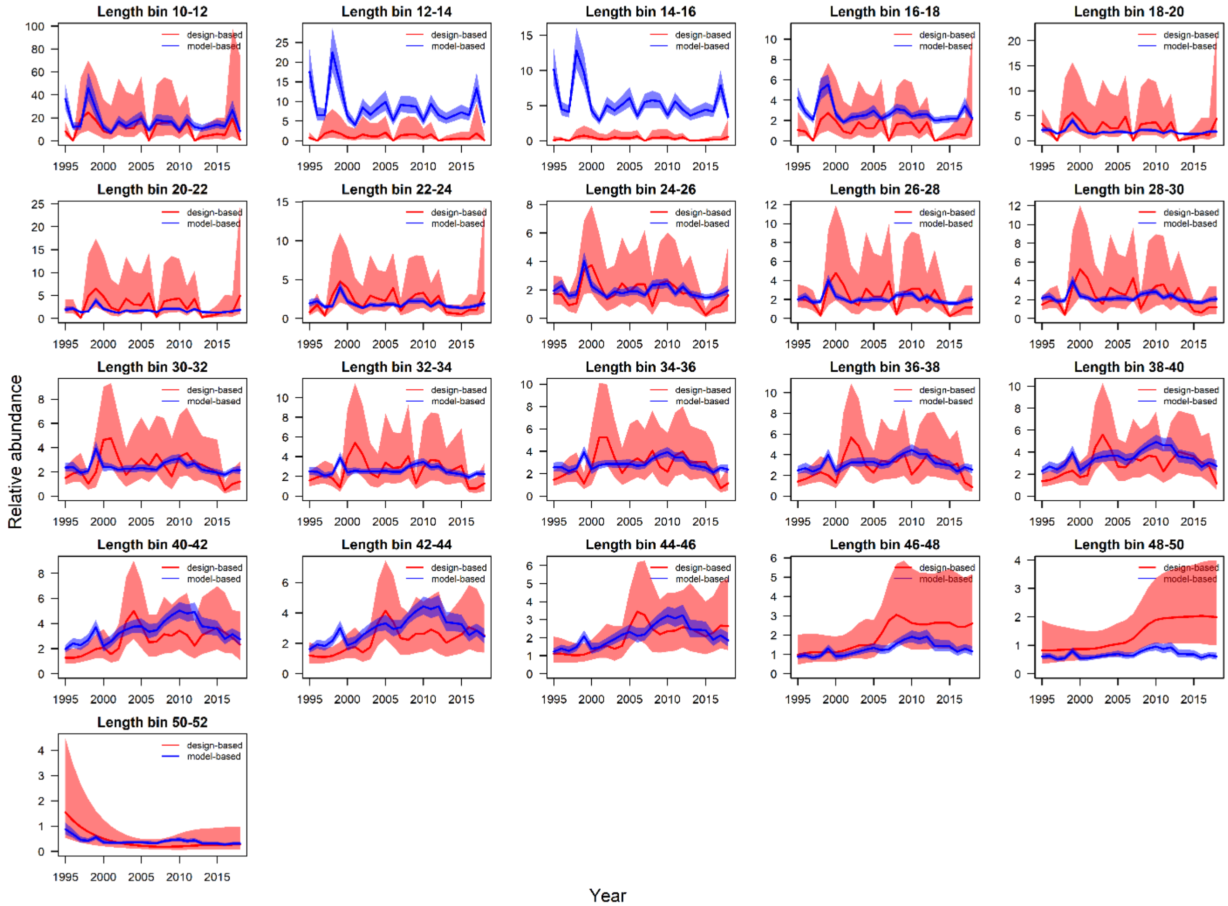

Figure 3.13 The estimated abundance-at-length (millions) for NAFO Div. 3NO witch flounder in ALSCL model with design-based indices and model-based indices from 1995 to 2018 (except 2014). Red line is the estimates with design-based indices and blue line is the estimates with model-based indices. The covered areas by red and blue are 95% confidence intervals.

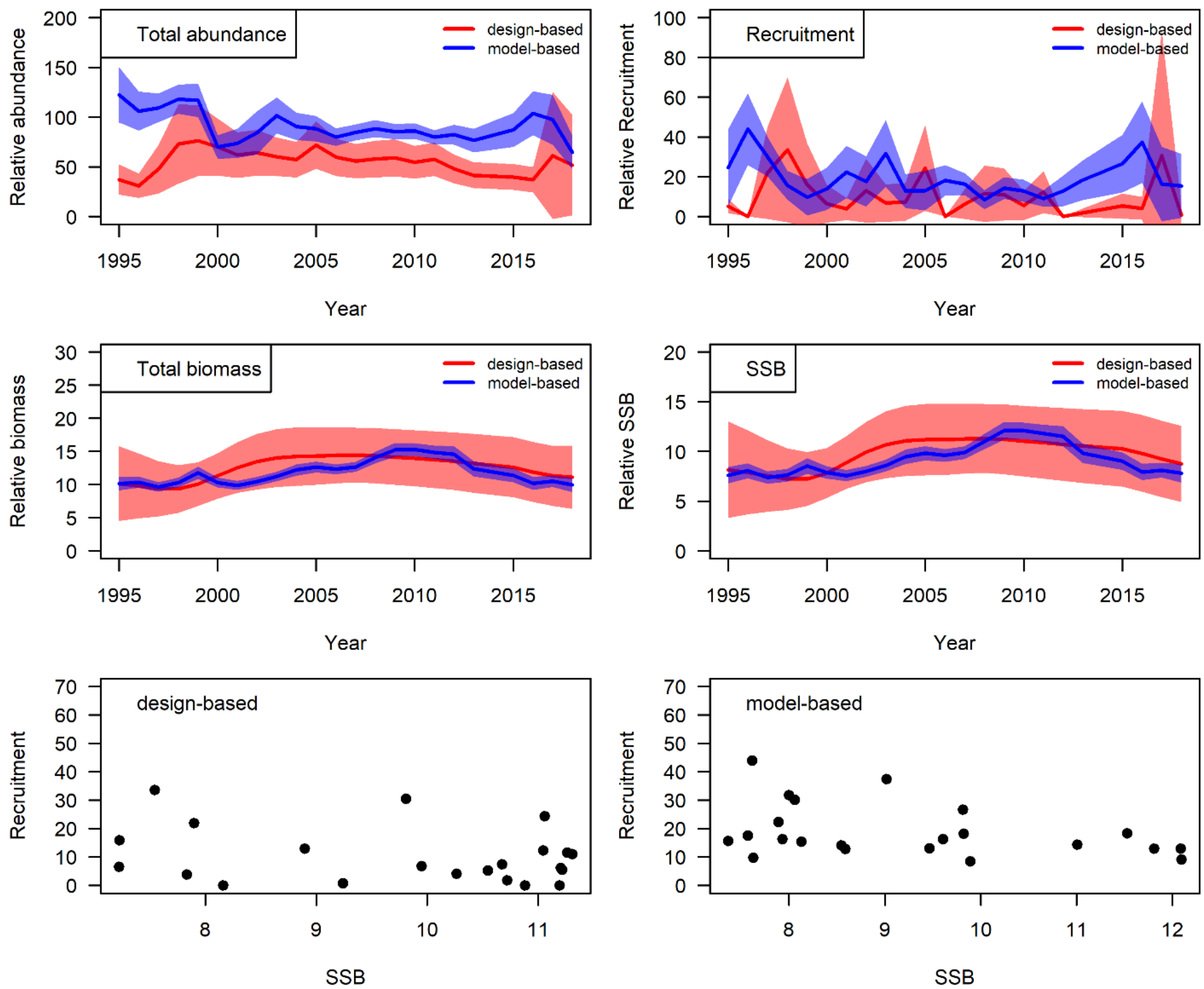

Figure 3.14 From top to bottom are the estimated total abundance and recruitment (millions), the estimated total biomass and spawning stock biomass (Kt), and the estimated stock-recruitment relationship for NAFO Div. 3NO witch flounder in ACL with design-based and model-based indices. Red line is the estimates with design-based indices and blue line is the estimates with model-based indices. The covered areas by red and blue are 95% confidence intervals.

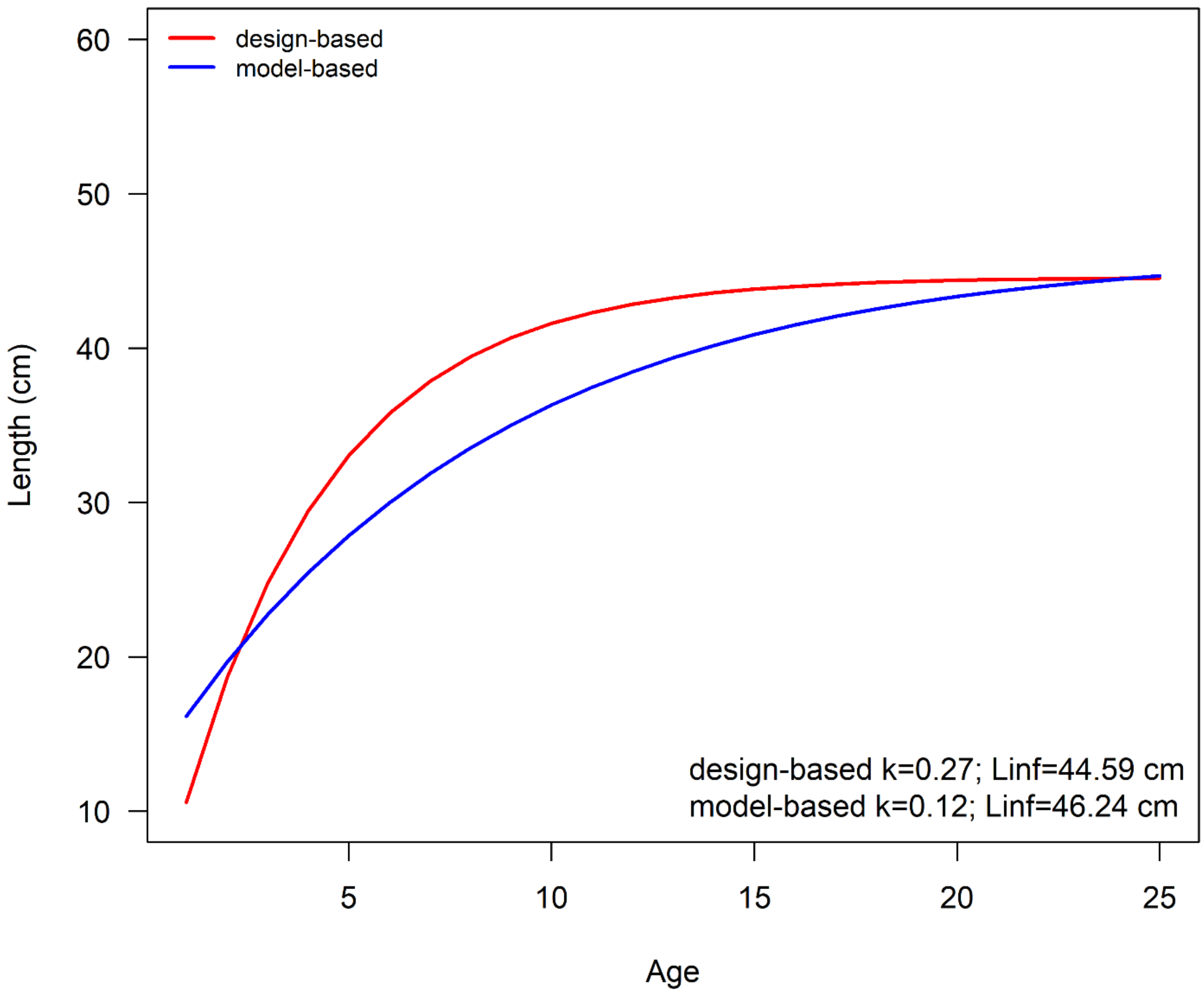

Figure 3.15 The estimated VonB growth curve of NAFO Div. 3NO witch flounder in ACL model with design-based indices and model-based indices. Red line is the estimates with design-based indices and blue line is the estimates with model-based indices. The covered areas by red and blue are 95% confidence intervals.

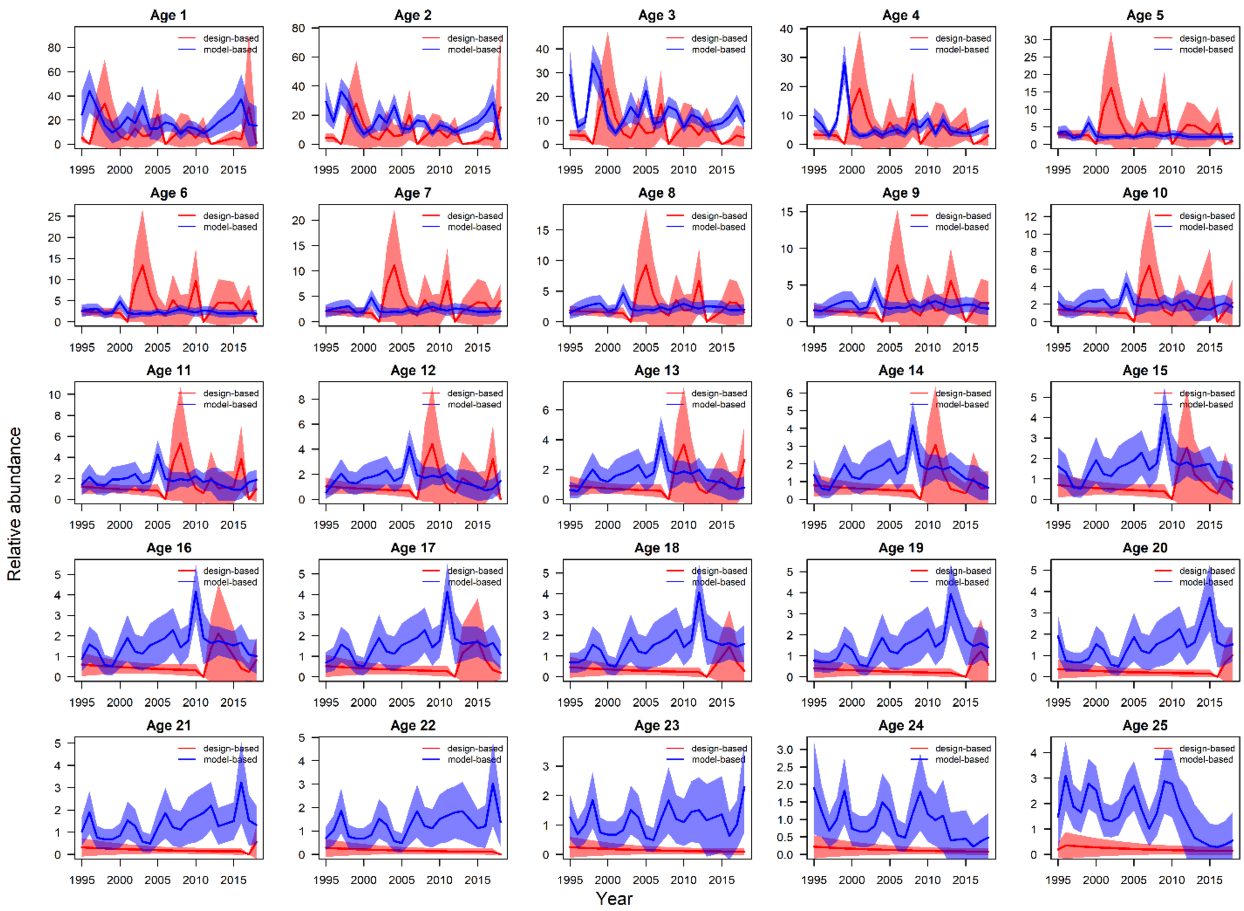

Figure 3.16 The estimated abundance-at-age (millions) for NAFO Div. 3NO witch flounder in ACL model with design-based indices and model-based indices from 1995 to 2018 (except 2014). Red line is the estimates with design-based indices and blue line is the estimates with model-based indices. The covered areas by red and blue are 95% confidence intervals.

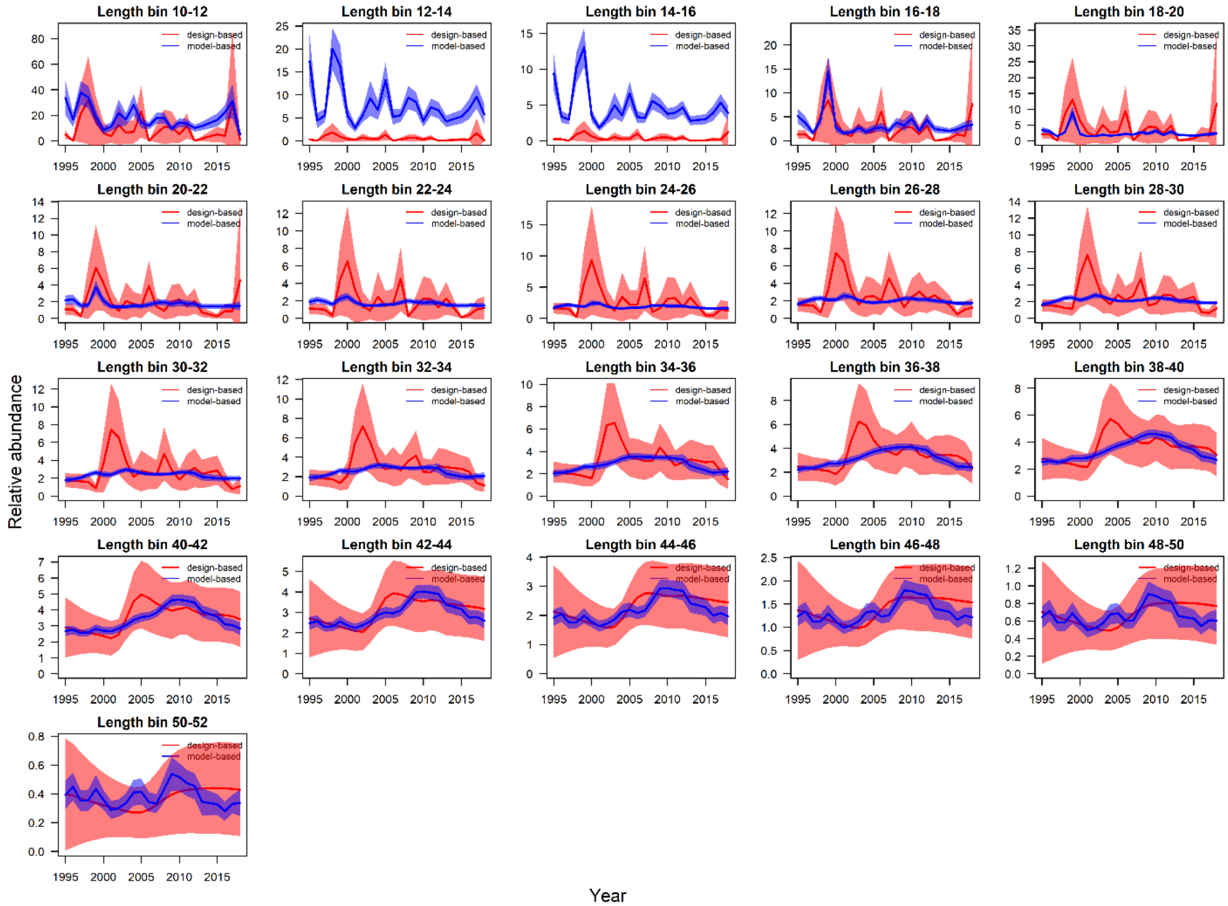

Figure 3.17 The estimated abundance-at-length (millions) for NAFO Div. 3NO witch flounder in ACL model with design-based indices and model-based indices from 1995 to 2018 (except 2014). Red line is the estimates with design-based indices and blue line is the estimates with model-based indices. The covered areas by red and blue are 95% confidence intervals.

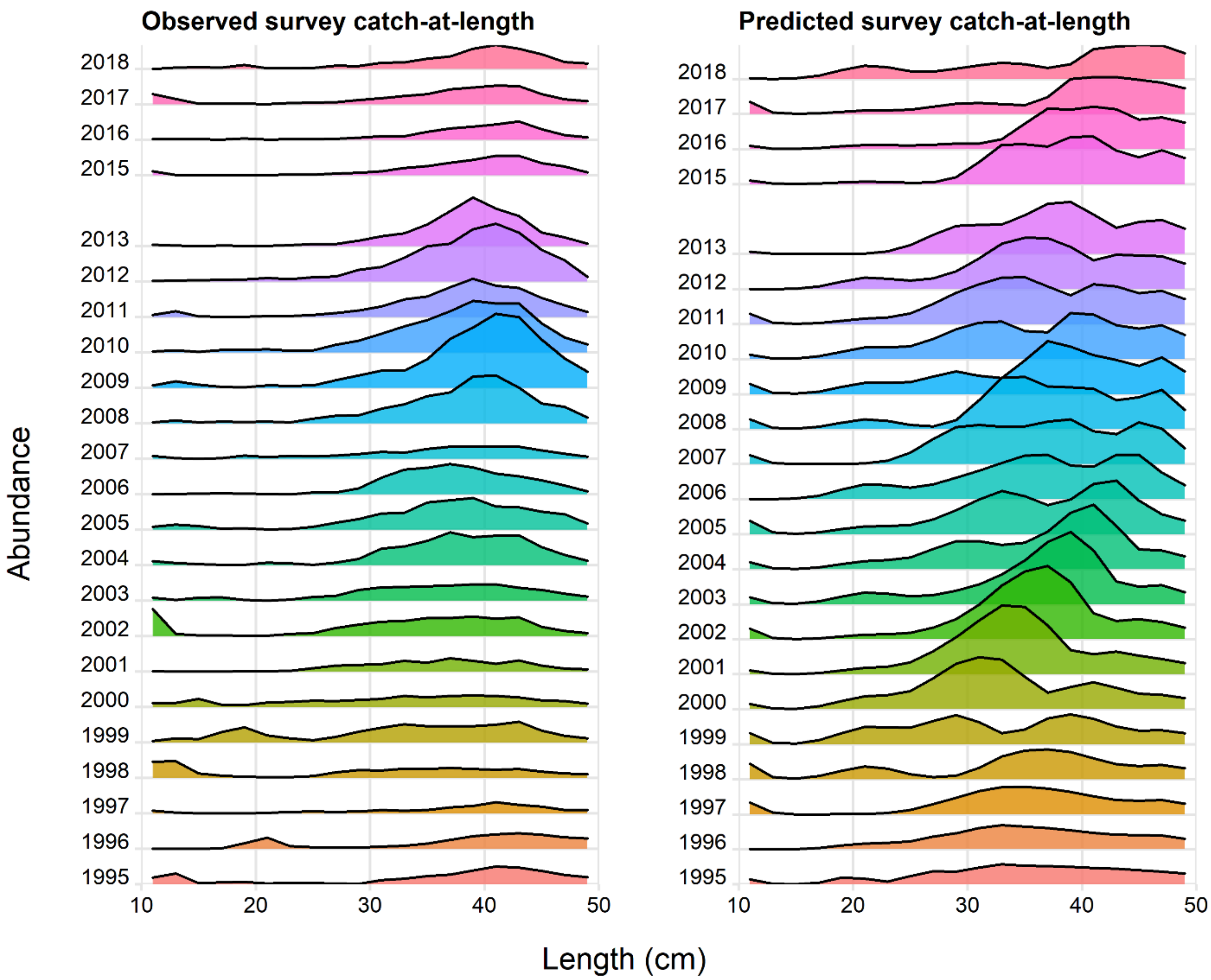

Figure 3.18 The observed survey catch-at-length and the model estimated catch-at-length indices for NAFO Div. 3NO witch flounder in ALSCL with design-based indices from 1995 to 2018 (except 2014).

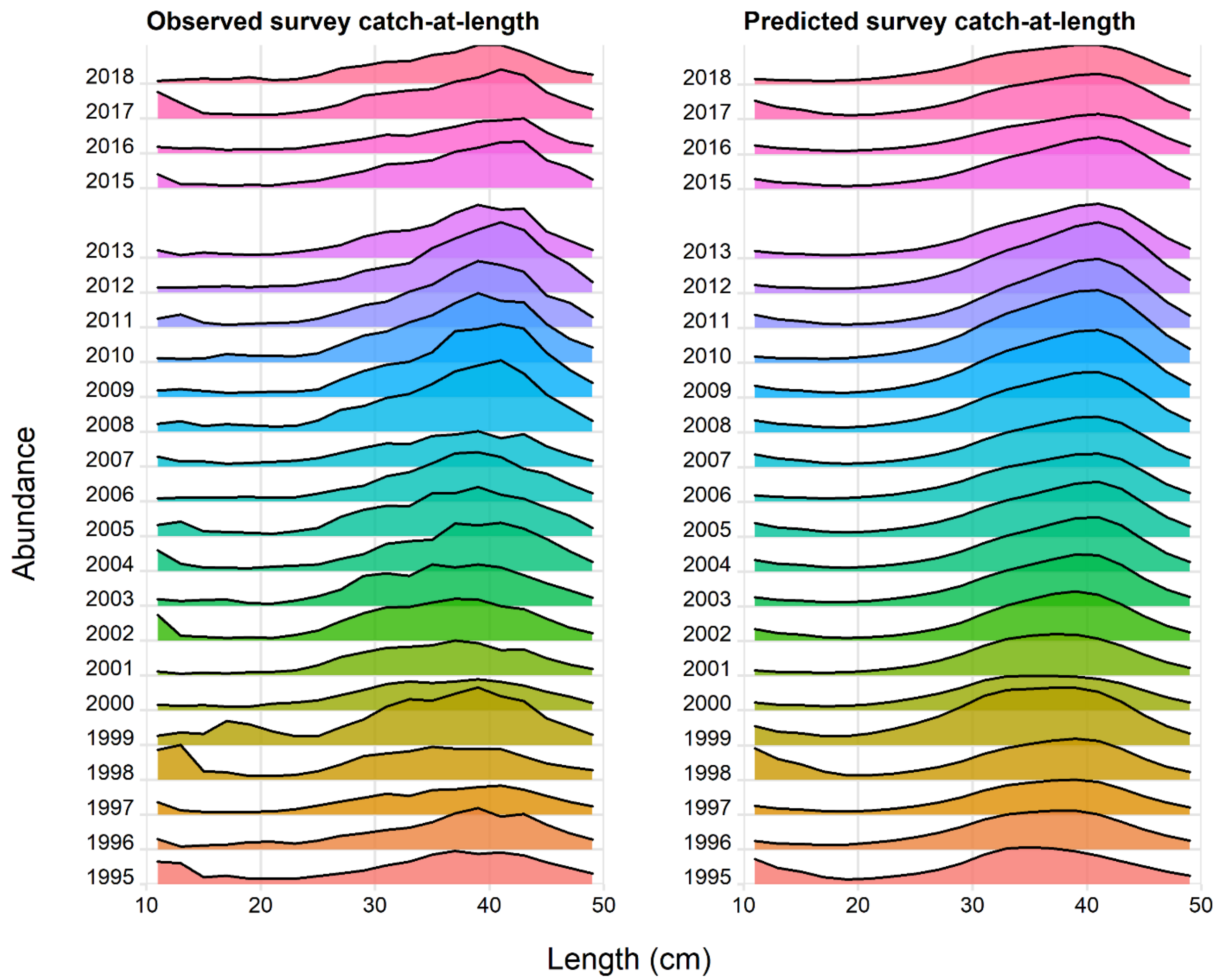

Figure 3.19 The observed survey catch-at-length and the model estimated catch-at-length indices for NAFO Div. 3NO witch flounder in ALSCL with model-based indices from 1995 to 2018 (except 2014).

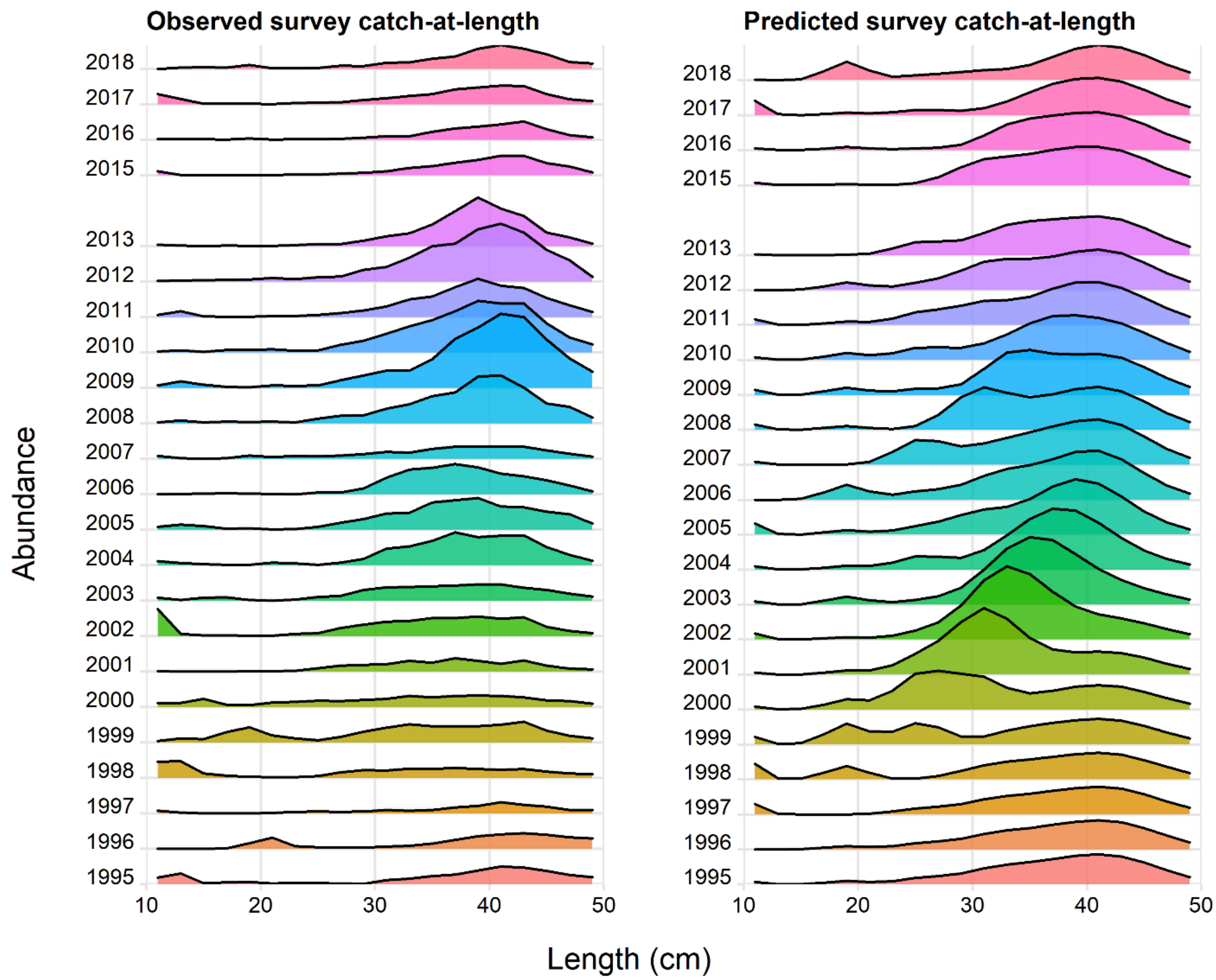

Figure 3.20 The observed survey catch-at-length and the model estimated catch-at-length indices for NAFO Div. 3NO witch flounder in ACL with design-based indices from 1995 to 2018 (except 2014).

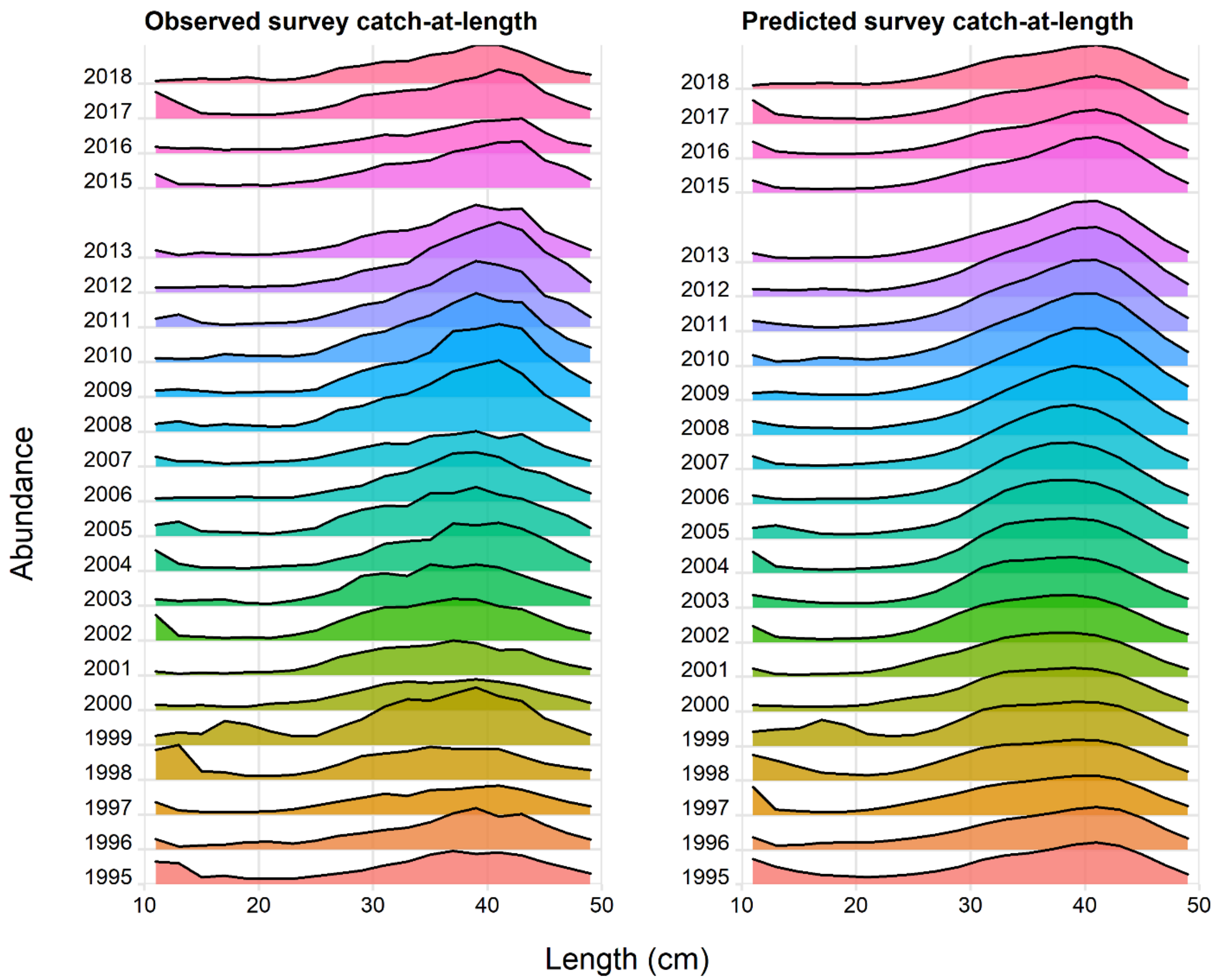

Figure 3.21 The observed survey catch-at-length and the model estimated catch-at-length indices for NAFO Div. 3NO witch flounder in ACL with model-based indices from 1995 to 2018 (except 2014).

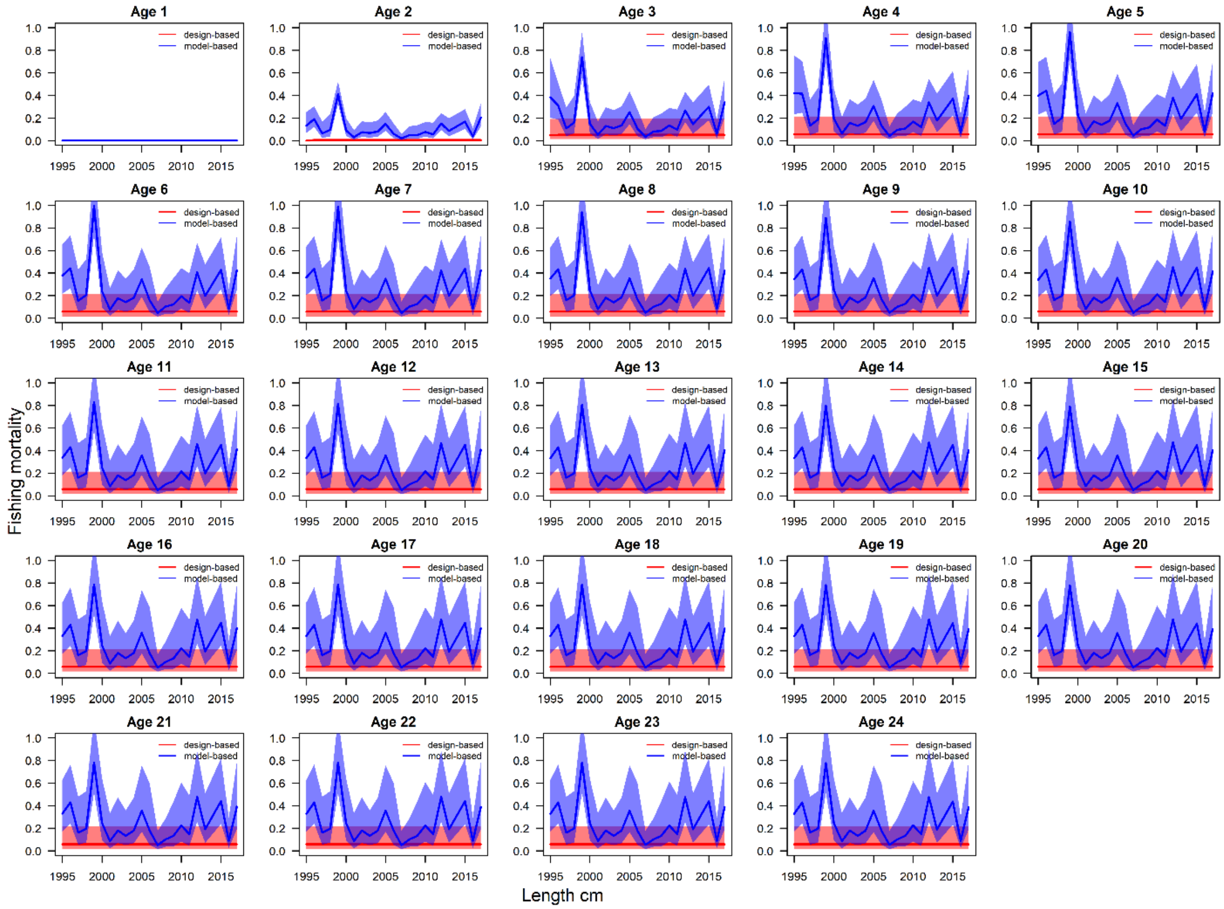

Figure 3.22 The estimated fishing mortality at age for NAFO Div. 3NO witch flounder in ALSCL with design-based and model-based indices from 1995 to 2018 (except 2014). Red line is the estimates with design-based indices and blue line is the estimates with model-based indices. The covered areas by red and blue are 95% confidence intervals.

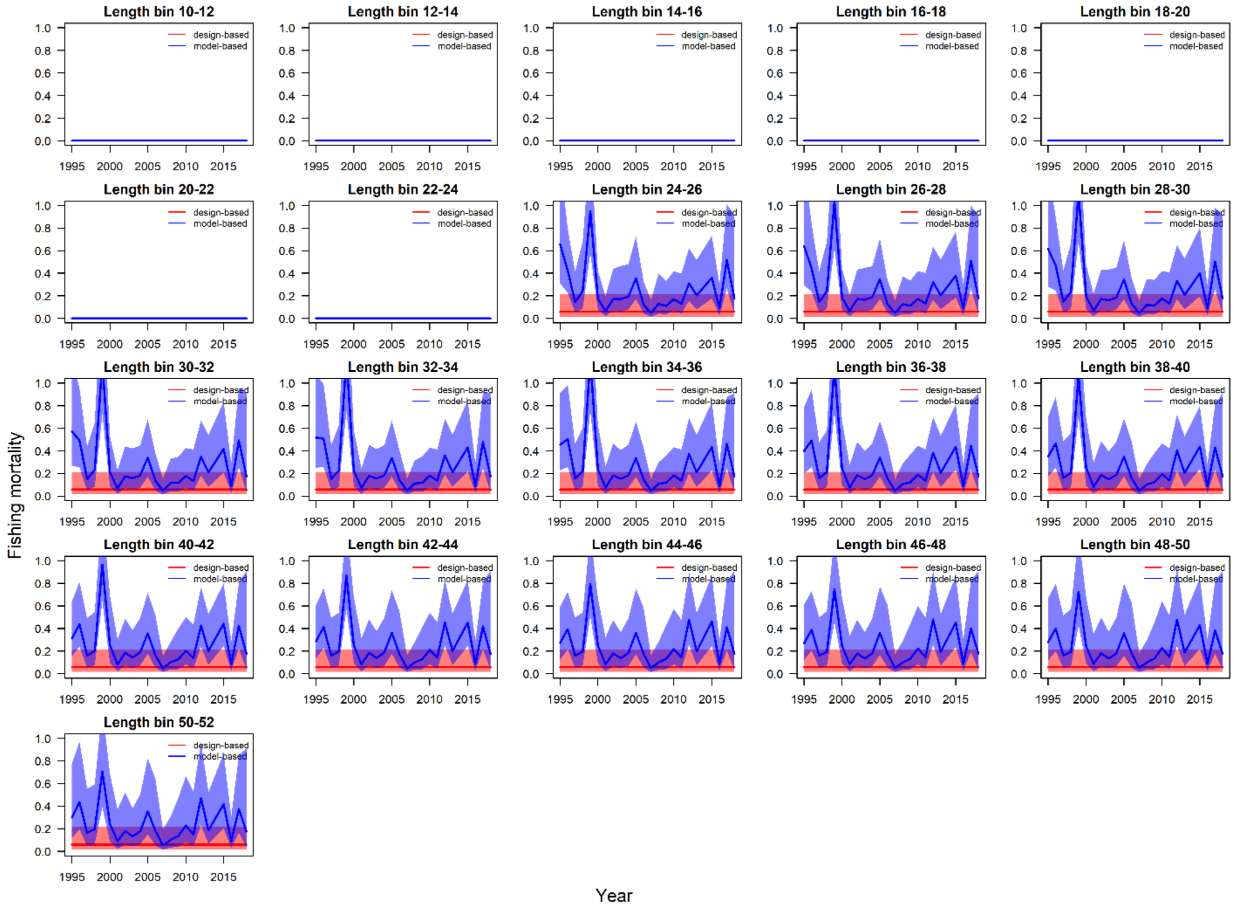

Figure 3.23 The estimated fishing mortality at length for NAFO Div. 3NO witch flounder in ALSCL with design-based and model-based indices from 1995 to 2018 (except 2014). Red line is the estimates with design-based indices and blue line is the estimates with model-based indices. The covered areas by red and blue are 95% confidence intervals.

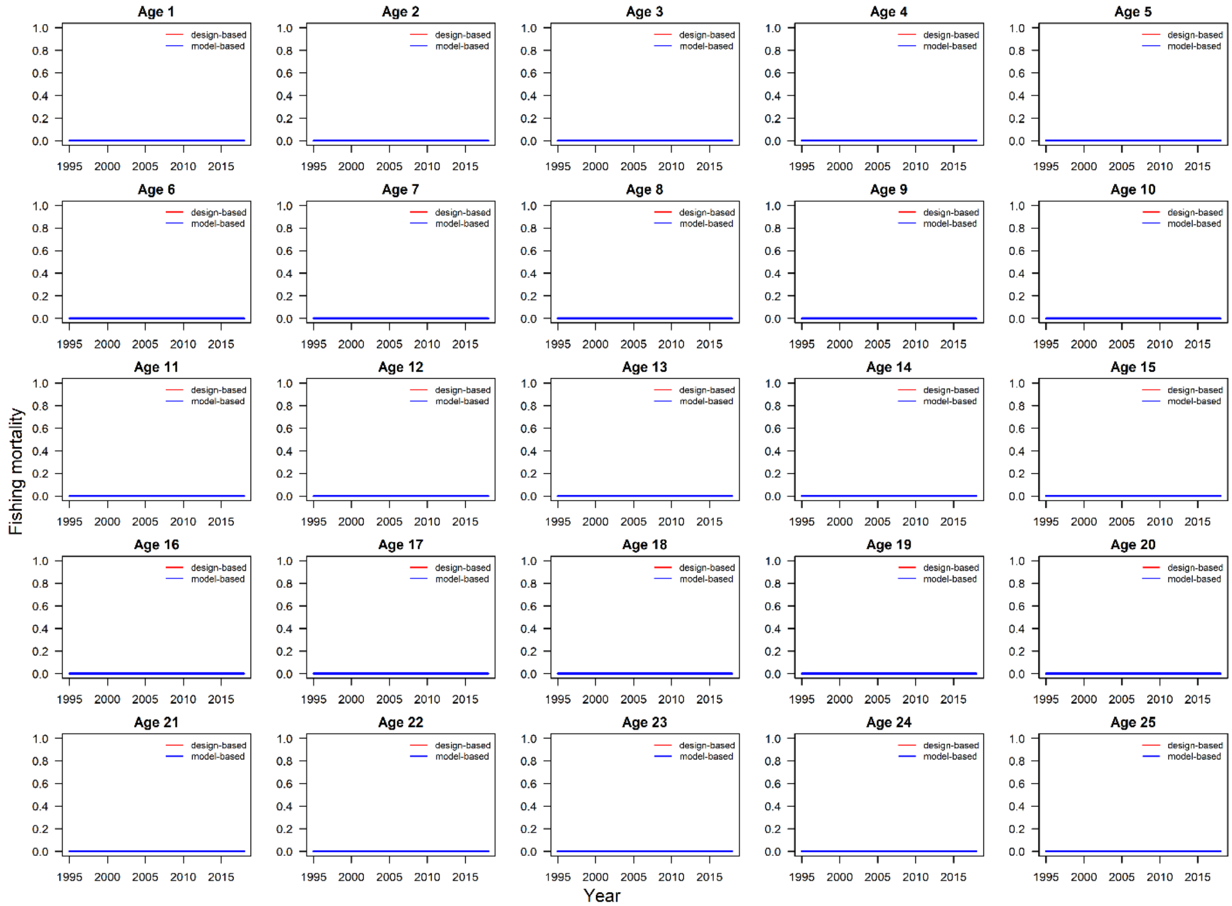

Figure 3.24 The estimated fishing mortality at age for NAFO Div. 3NO witch flounder in ACL with design-based and model-based indices from 1995 to 2018 (except 2014). Red line is the estimates with design-based indices and blue line is the estimates with model-based indices. The covered areas by red and blue are 95% confidence intervals.

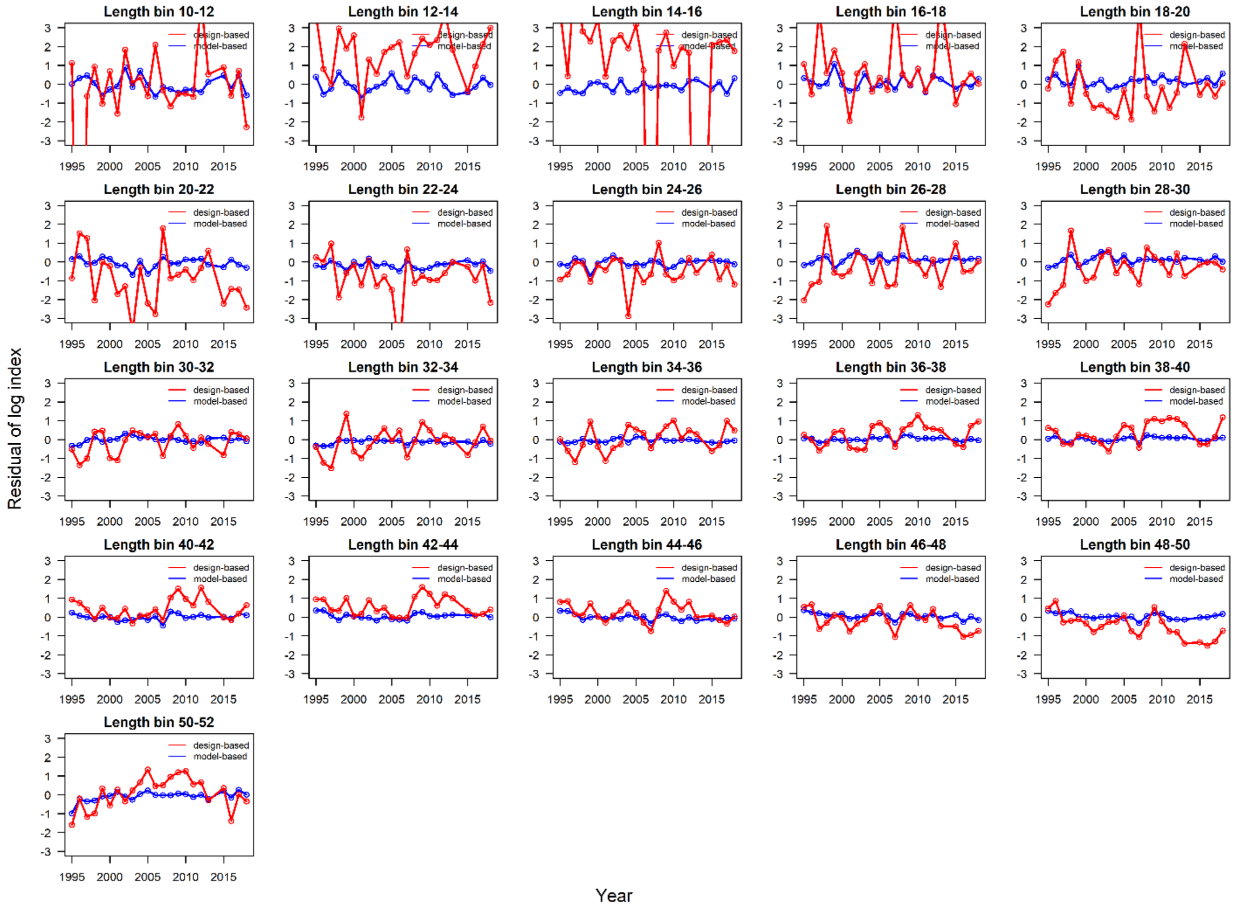

Figure 3.25 The estimated residual of log indices (by length) for NAFO Div. 3NO witch flounder in ALSCL with design-based and model-based indices from 1995 to 2018 (except 2014). Red line is the estimates with design-based indices and blue line is the estimates with model-based indices.

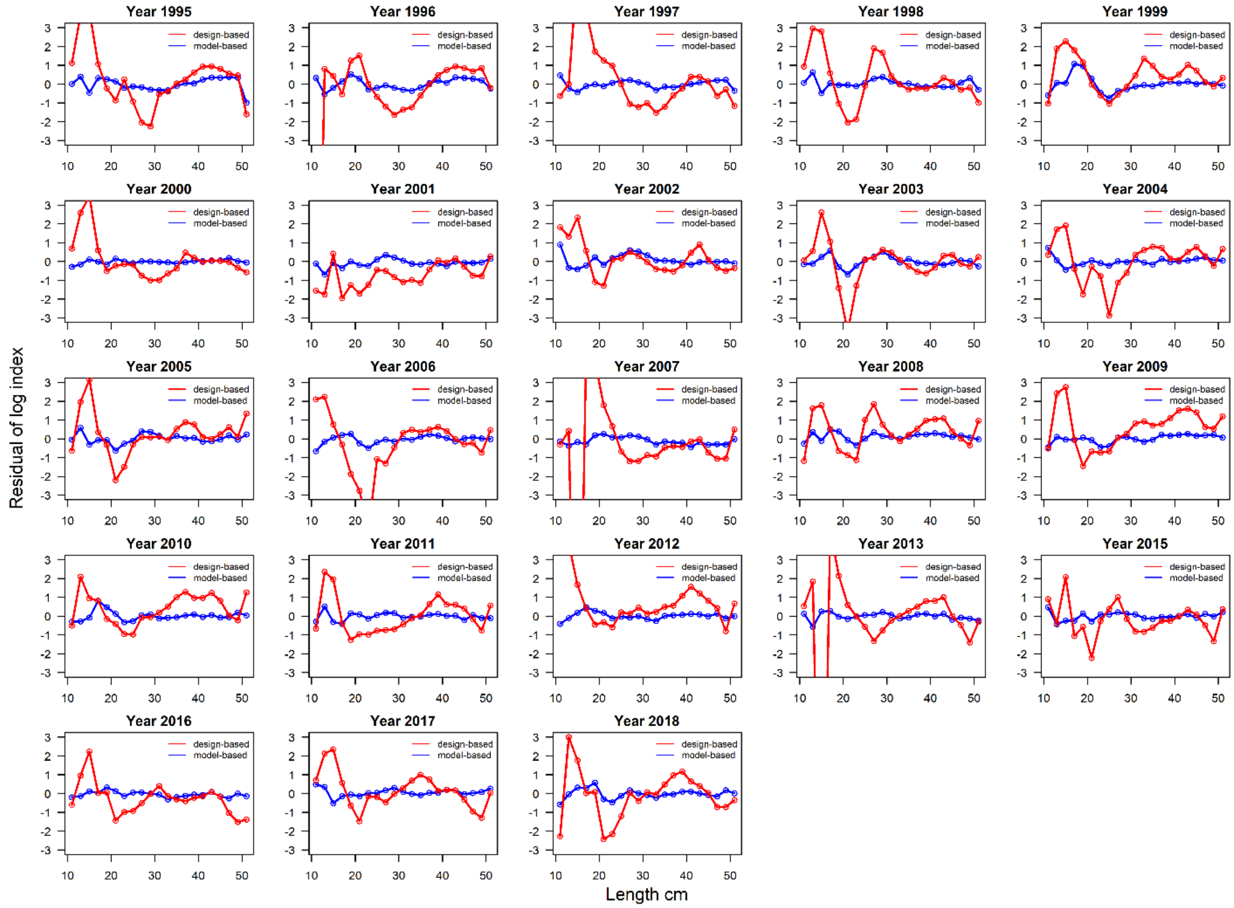

Figure 3.26 The estimated residual of log indices (by year) for NAFO Div. 3NO witch flounder in ALSCL with design-based and model-based indices from 1995 to 2018 (except 2014). Red line is the estimates with design-based indices and blue line is the estimates with model-based indices.

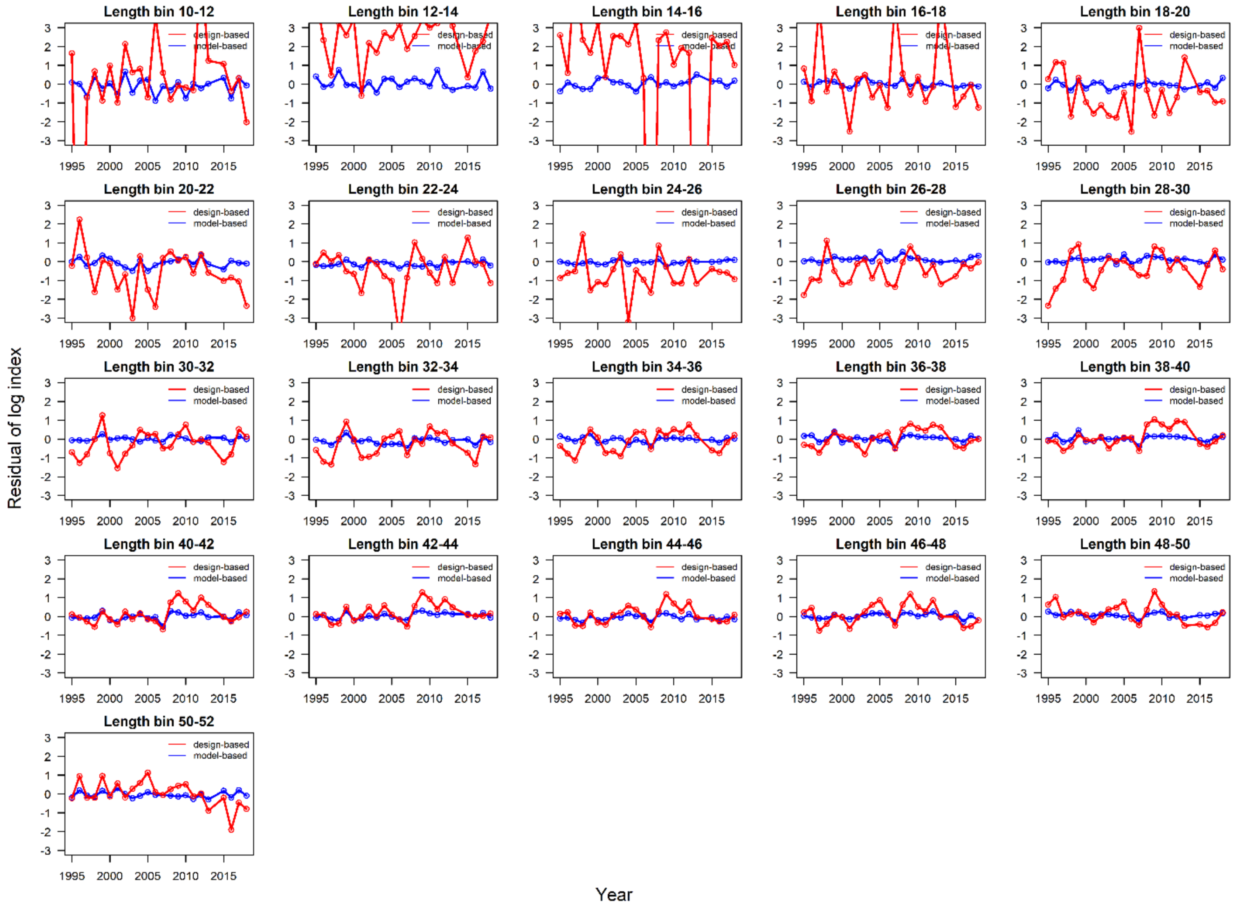

Figure 3.27 The estimated residual of log indices (by length) for NAFO Div. 3NO witch flounder in ACL with design-based and model-based indices from 1995 to 2018 (except 2014). Red line is the estimates with design-based indices and blue line is the estimates with model-based indices.

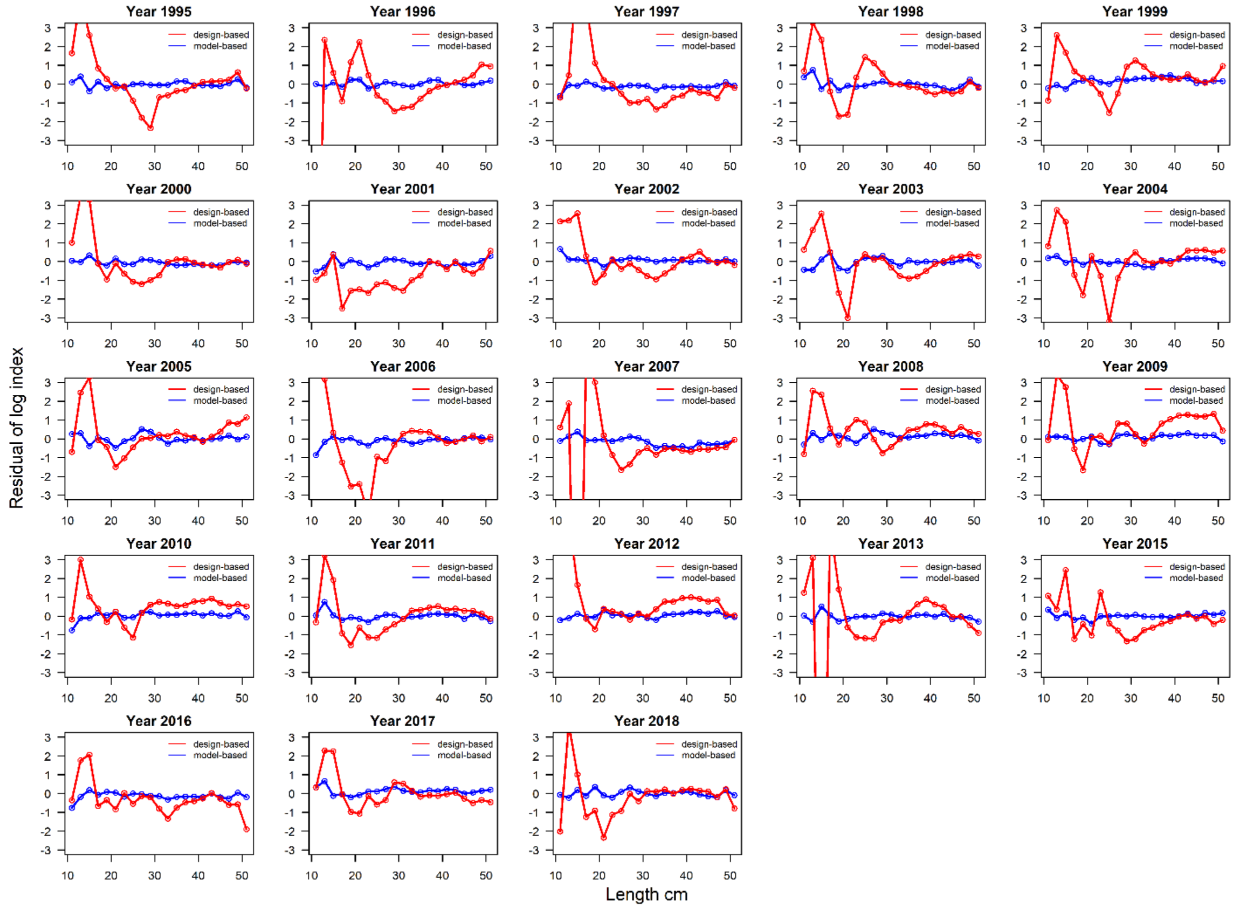

Figure 3.28 The estimated residual of log indices (by year) for NAFO Div. 3NO witch flounder in ACL with design-based and model-based indices from 1995 to 2018 (except 2014). Red line is the estimates with design-based indices and blue line is the estimates with model-based indices.

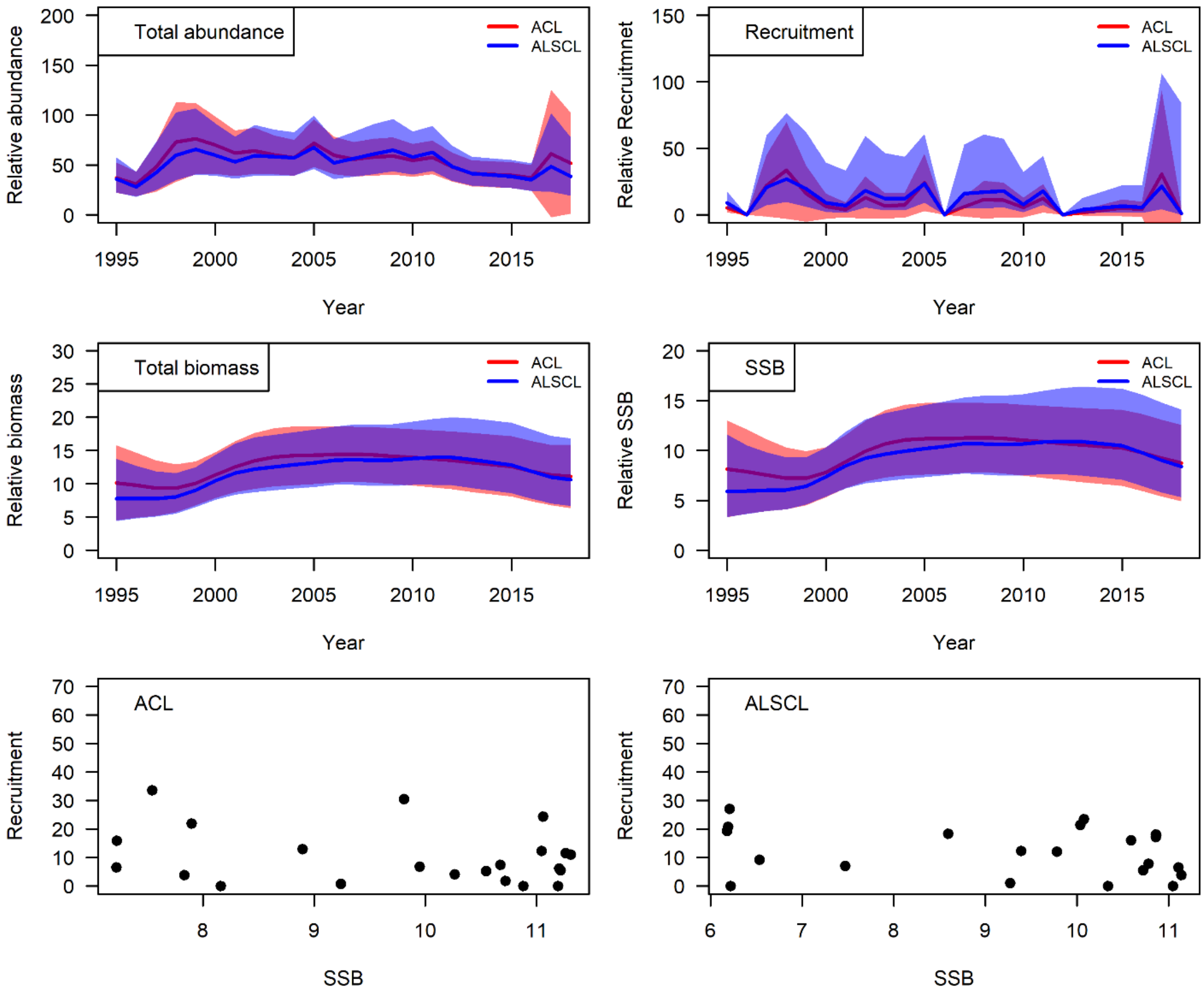

Figure 3.29 From top to bottom are the estimated total abundance and recruitment (millions), the estimated total biomass and spawning stock biomass (Kt), and the estimated stock-recruitment relationship for NAFO Div. 3NO witch flounder in ACL and ALSCL models with design-based indices. Red line is the estimates in ACL model and blue line is the estimates in ALSCL model. The covered areas by red and blue are 95% confidence intervals.

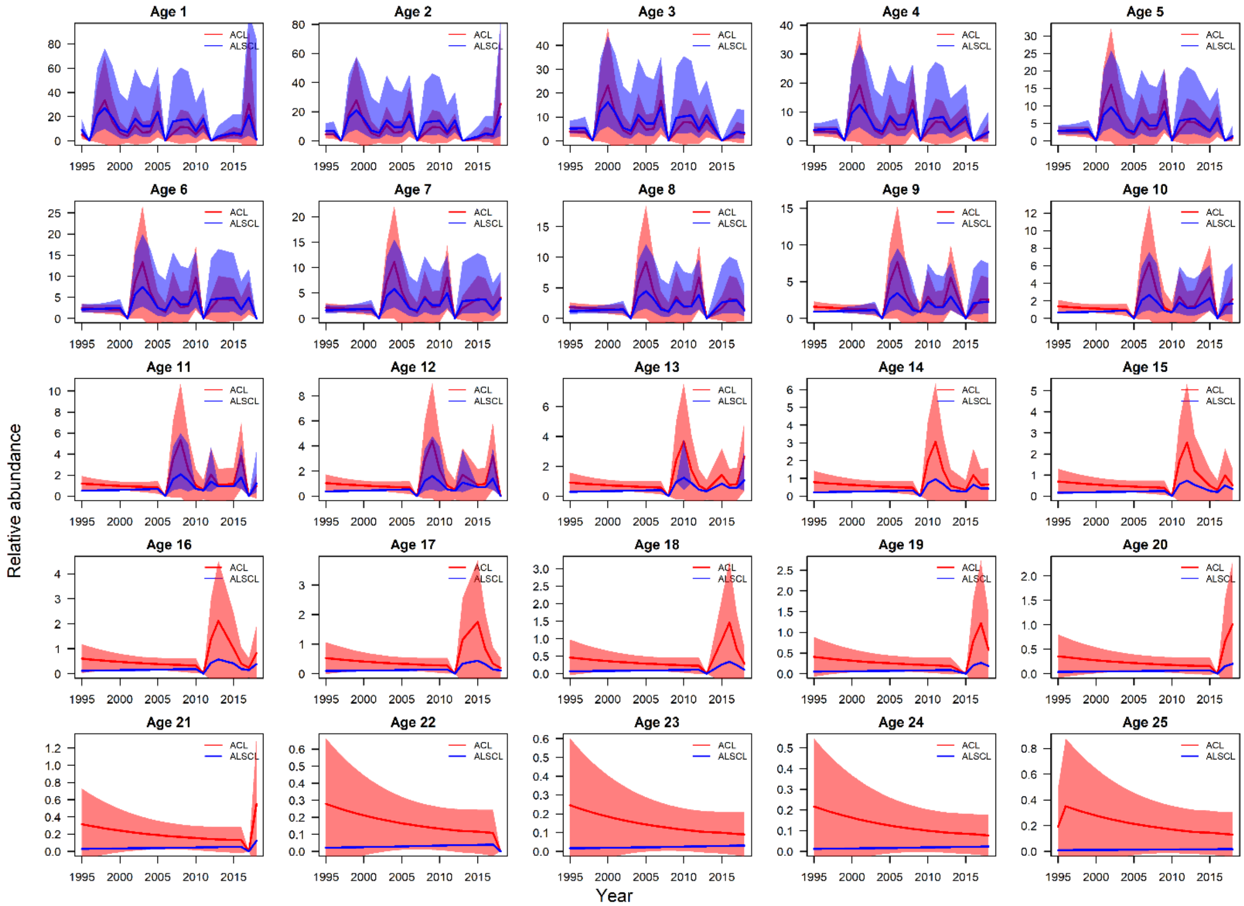

Figure 3.30 The estimated abundance-at-age (millions) for NAFO Div. 3NO witch flounder in ACL and ALSCL models with design-based indices. Red line is the estimates in ACL model and blue line is the estimates in ALSCL model. The covered areas by red and blue are 95% confidence intervals.

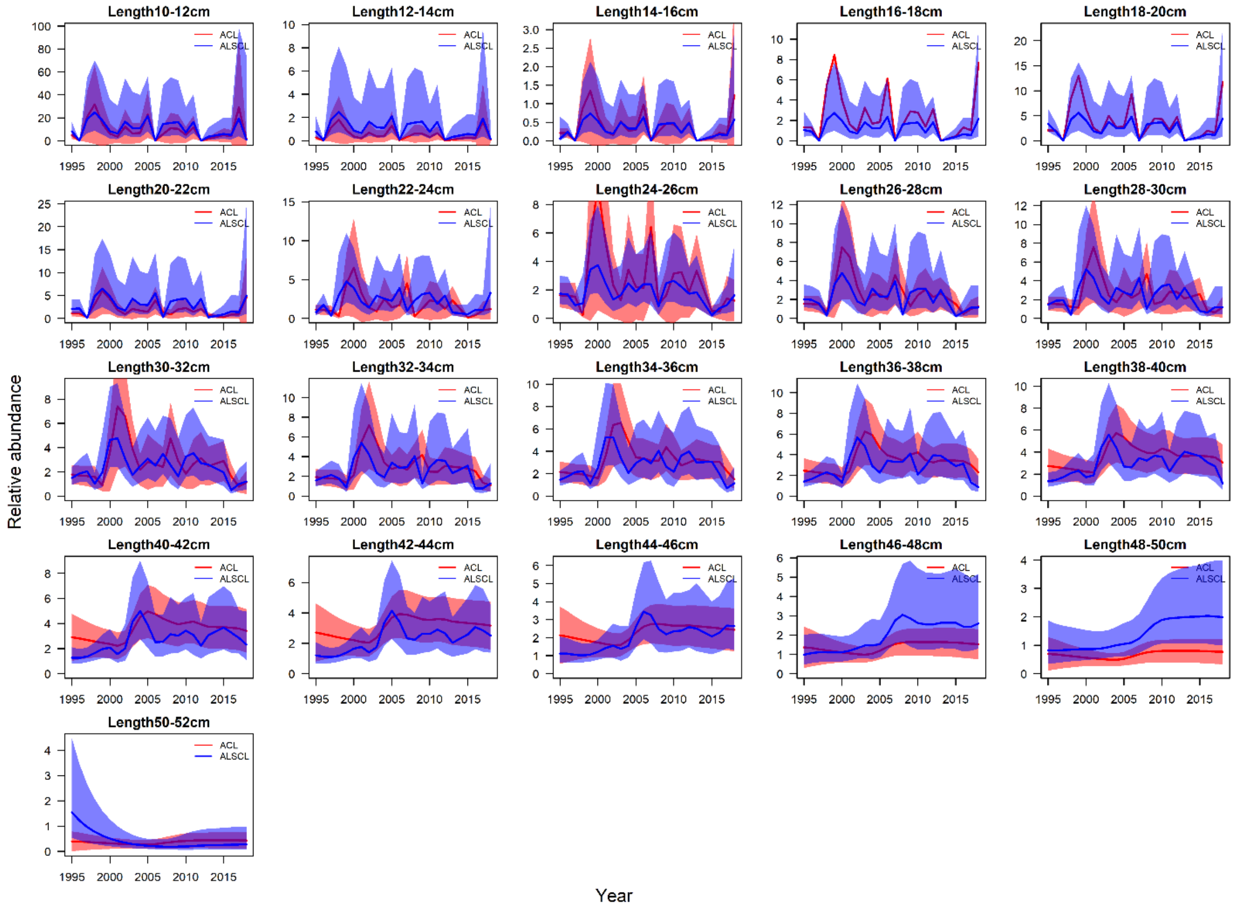

Figure 3.31 The estimated abundance-at-length (millions) for NAFO Div. 3NO witch flounder in ACL and ALSCL models with design-based indices. Red line is the estimates in ACL model and blue line is the estimates in ALSCL model. The covered areas by red and blue are 95% confidence intervals.

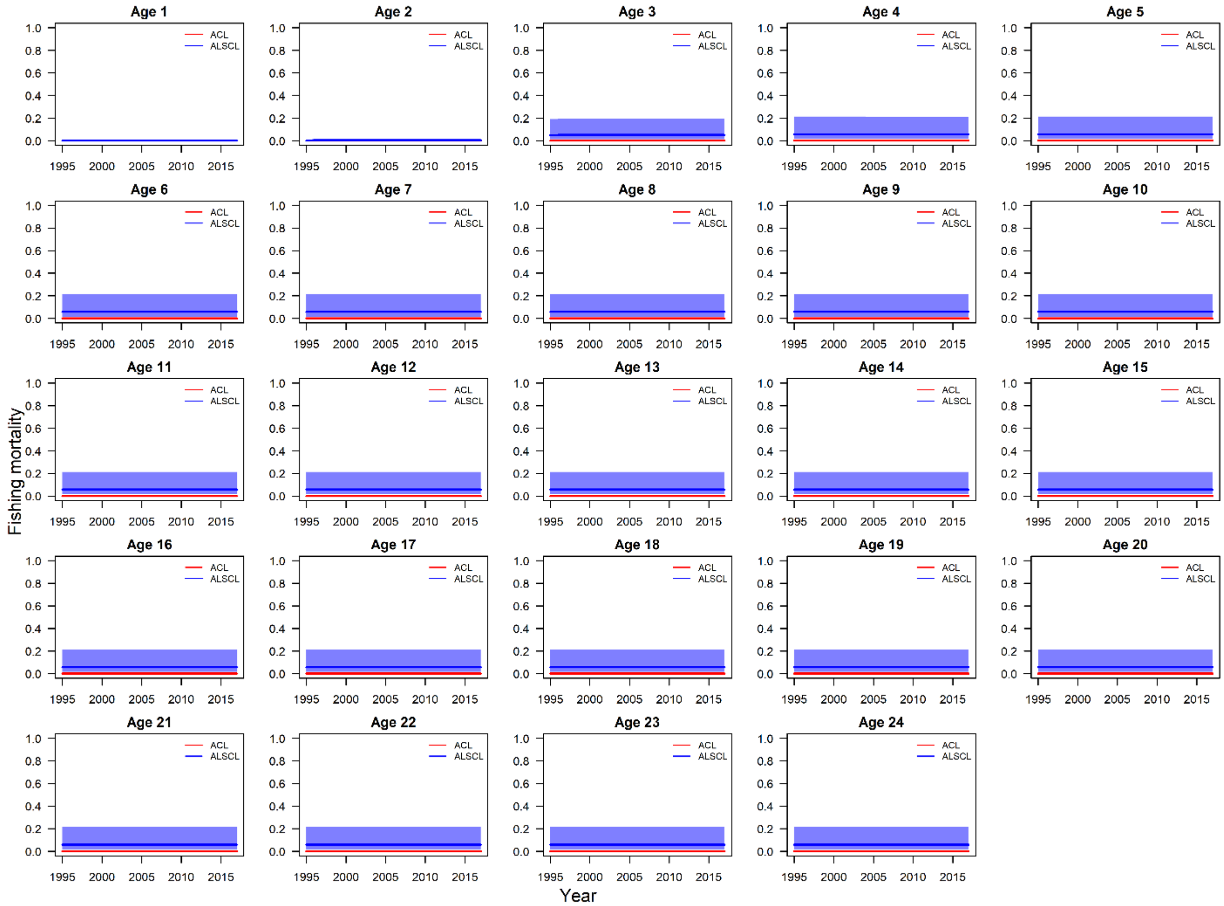

Figure 3.32 The estimated fishing mortality at age for NAFO Div. 3NO witch flounder in ACL and ALSCL models with design-based indices. Red line is the estimates in ACL model and blue line is the estimates in ALSCL model. The covered areas by red and blue are 95% confidence intervals.

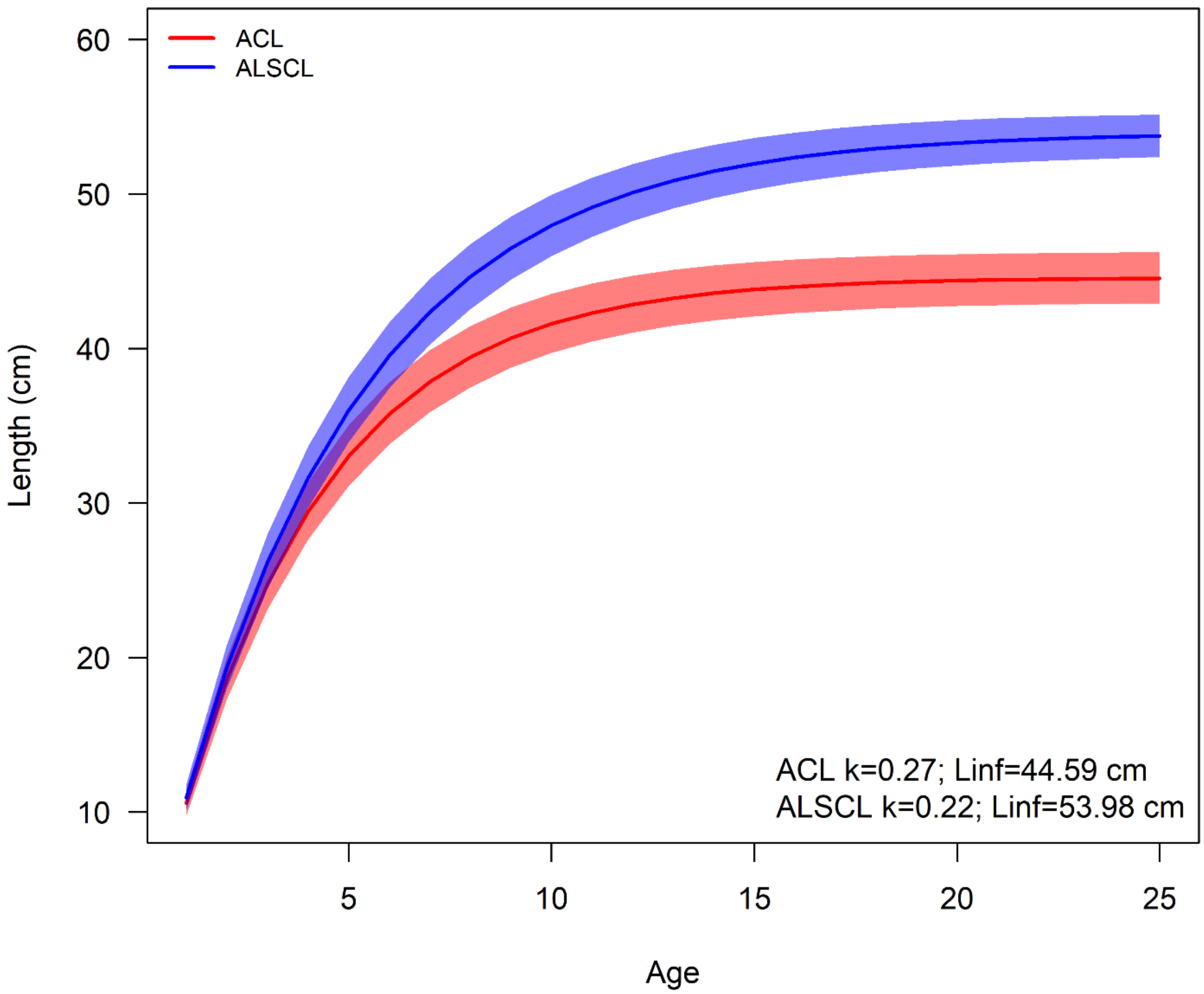

Figure 3.33 The estimated VonB growth curve of NAFO Div. 3NO witch flounder in ALSCL and ACL models with design-based indices. Red line is the estimates in ACL model and blue line is the estimates in ALSCL model. The covered areas by red and blue are 95% confidence intervals.

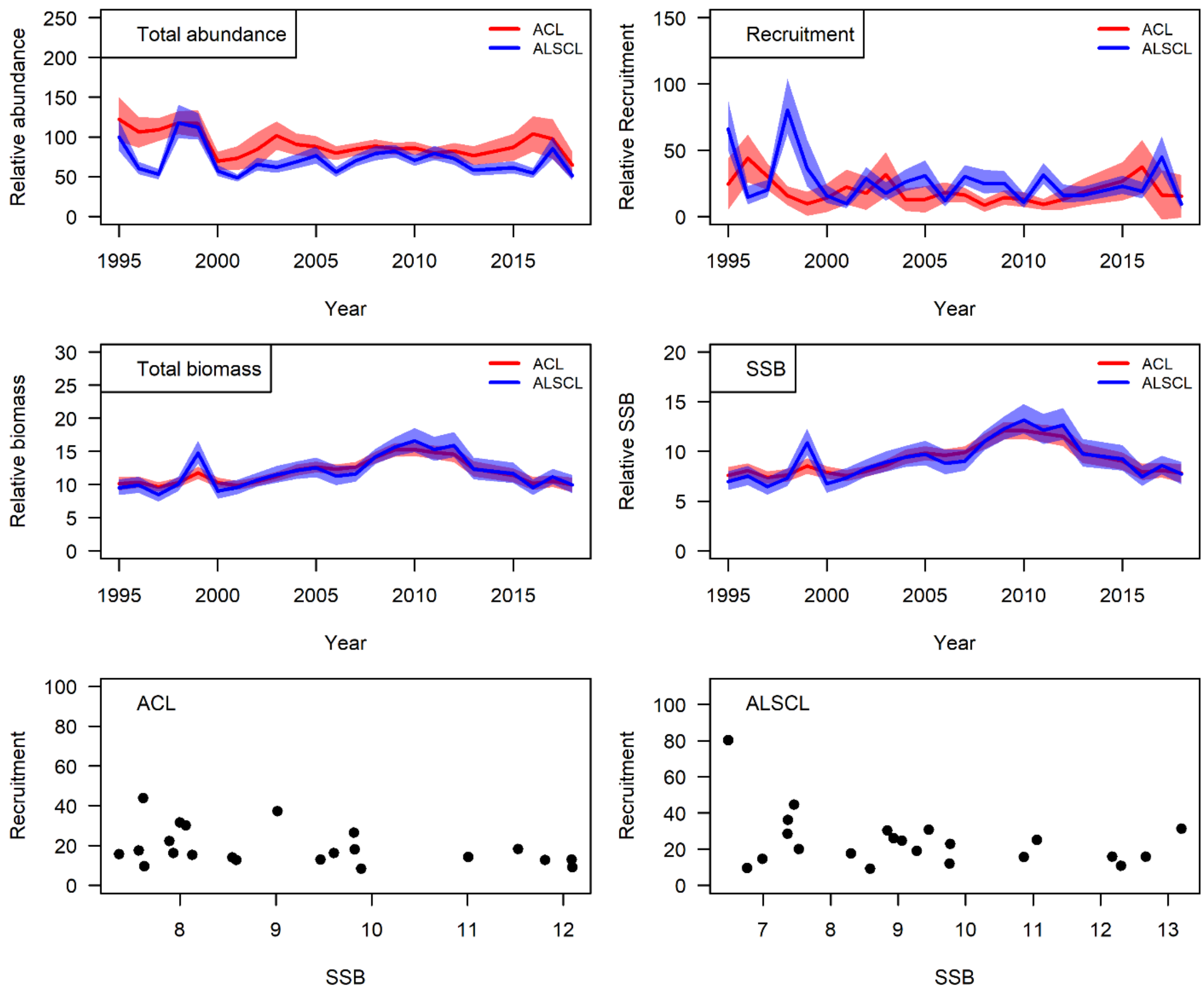

Figure 3.34 From top to bottom are the estimated total abundance and recruitment (millions), the estimated total biomass and spawning stock biomass (Kt), and the estimated stock-recruitment relationship for NAFO Div. 3NO witch flounder in ACL and ALSCL models with model-based indices. Red line is the estimates in ACL model and blue line is the estimates in ALSCL model. The covered areas by red and blue are 95% confidence intervals.

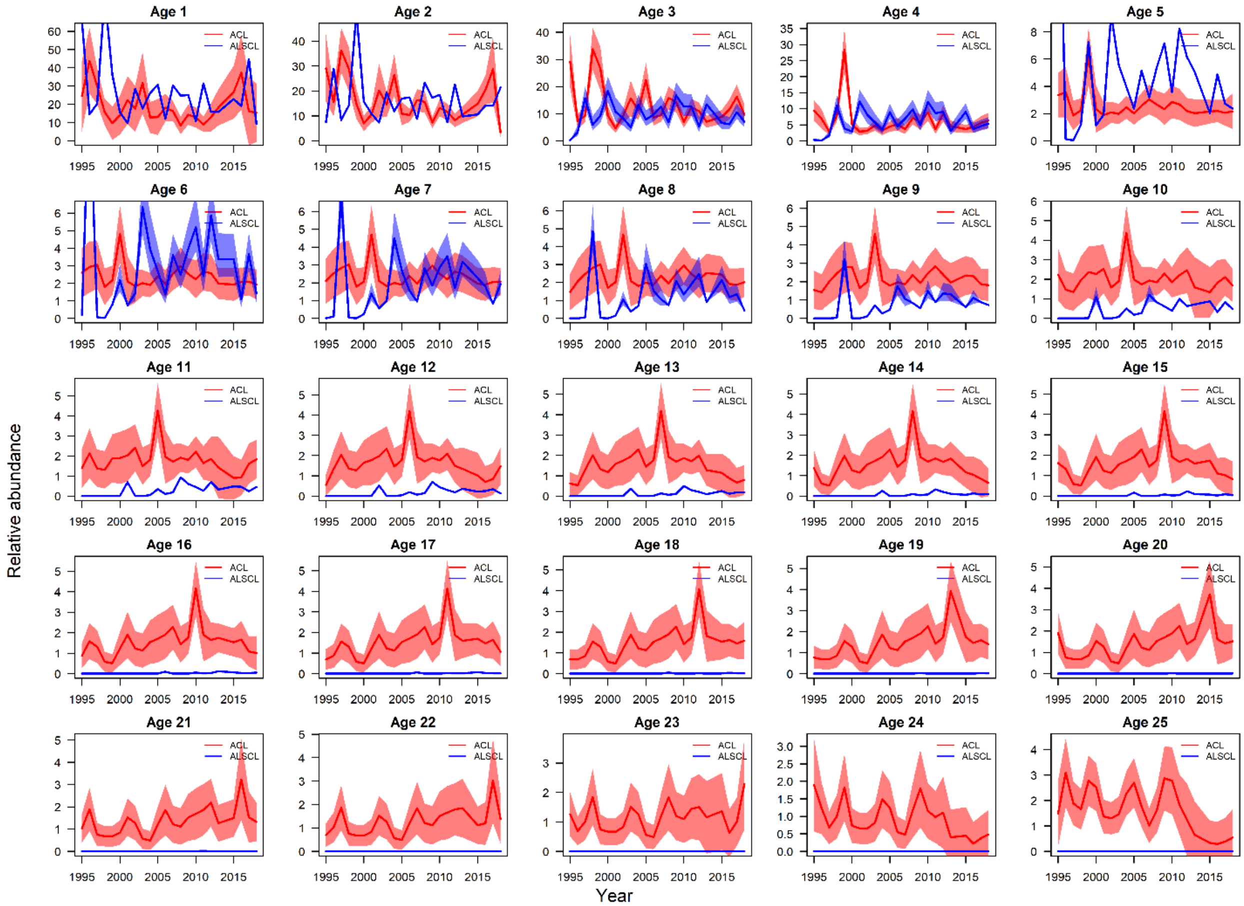

Figure 3.35 The estimated abundance-at-age (millions) for NAFO Div. 3NO witch flounder in ACL and ALSCL models with model-based indices. Red line is the estimates in ACL model and blue line is the estimates in ALSCL model. The covered areas by red and blue are 95% confidence intervals.

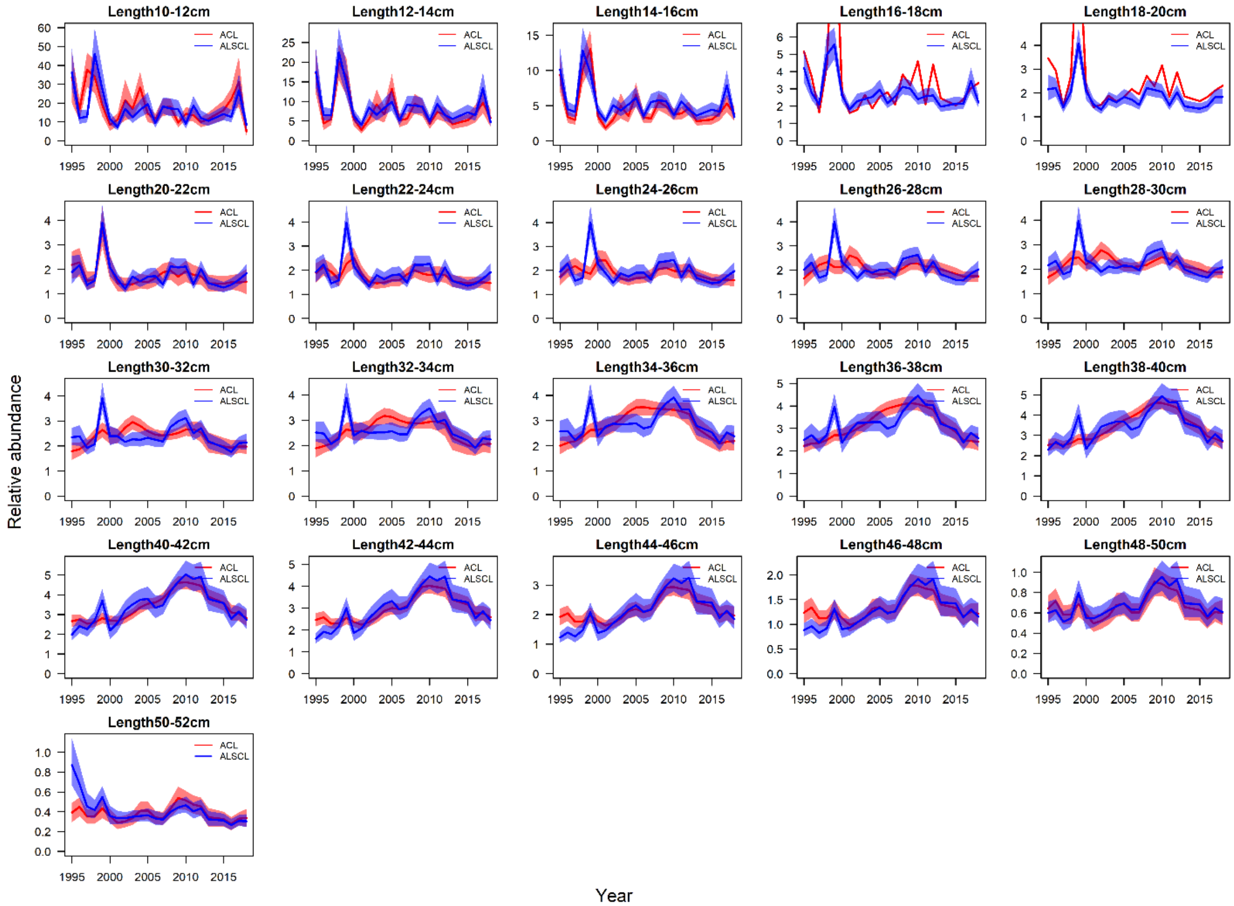

Figure 3.36 The estimated abundance-at-length (millions) for NAFO Div. 3NO witch flounder in ACL and ALSCL models with model-based indices. Red line is the estimates in ACL model and blue line is the estimates in ALSCL model. The covered areas by red and blue are 95% confidence intervals.

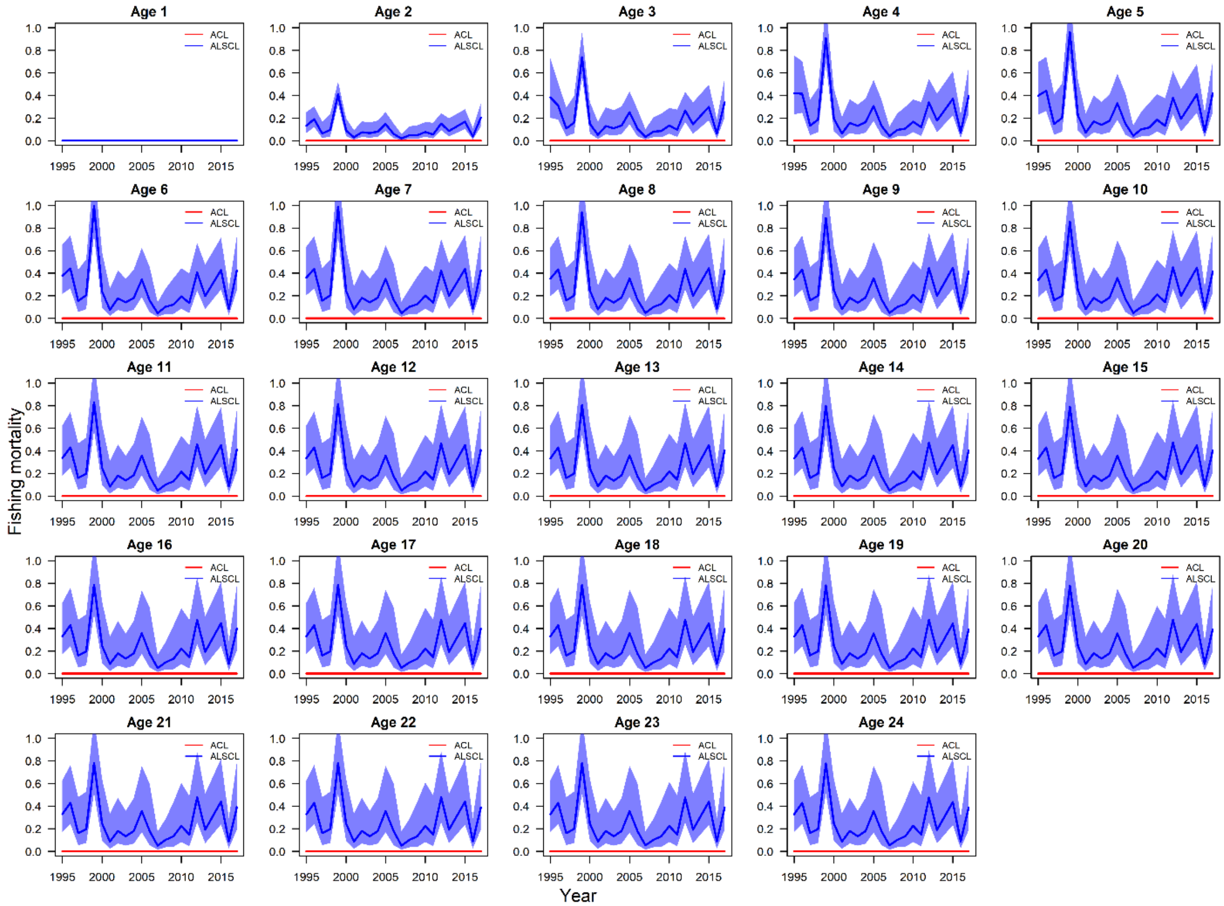

Figure 3.37 The estimated fishing mortality at age for NAFO Div. 3NO witch flounder in ACL and ALSCL models with model-based indices. Red line is the estimates in ACL model and blue line is the estimates in ALSCL model. The covered areas by red and blue are 95% confidence intervals.

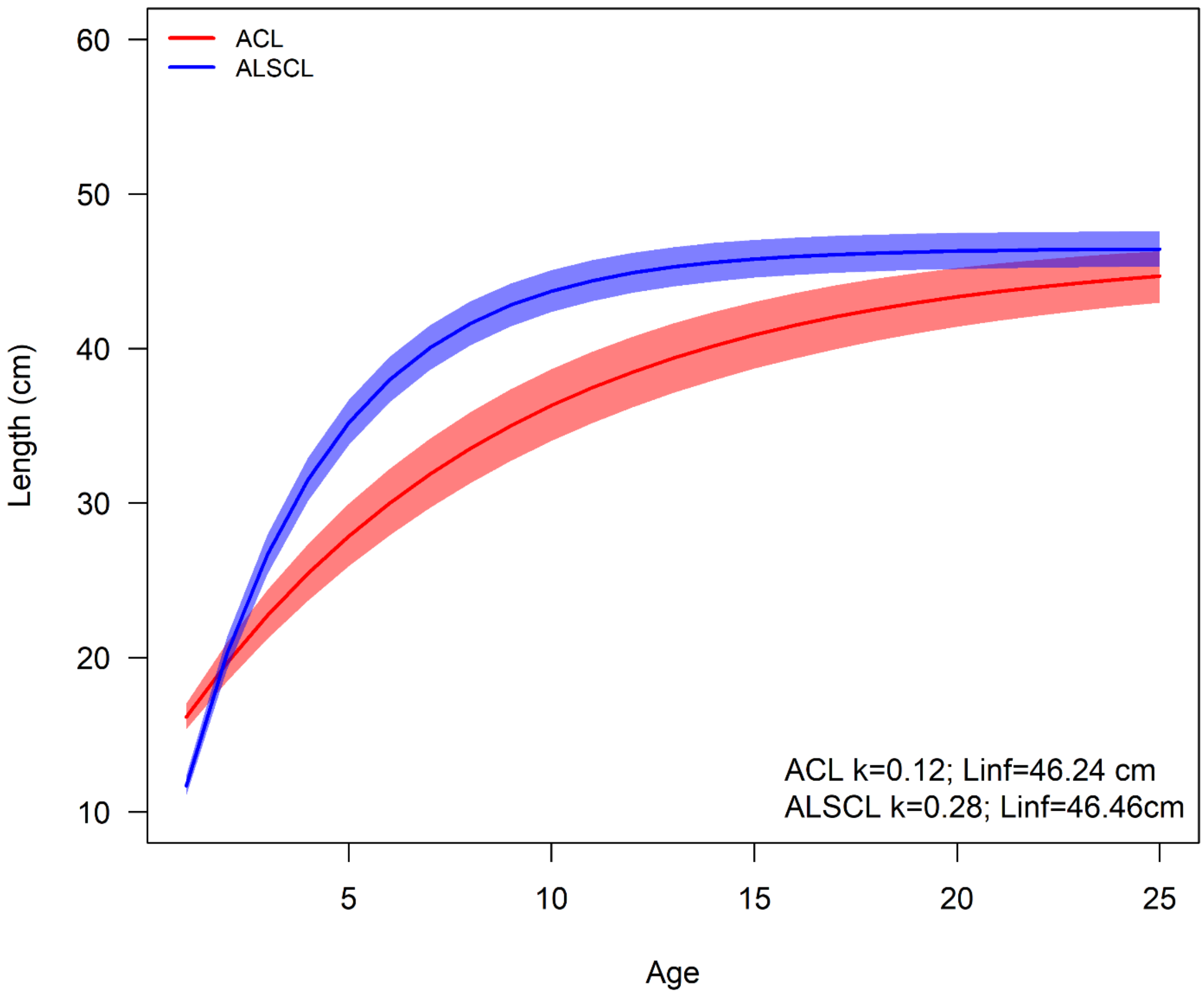

Figure 3.38 The estimated VonB growth curve of NAFO Div. 3NO witch flounder in ALSCL and ACL models with model-based indices. Red line is the estimates in ACL model and blue line is the estimates in ALSCL model. The covered areas by red and blue are 95% confidence intervals.

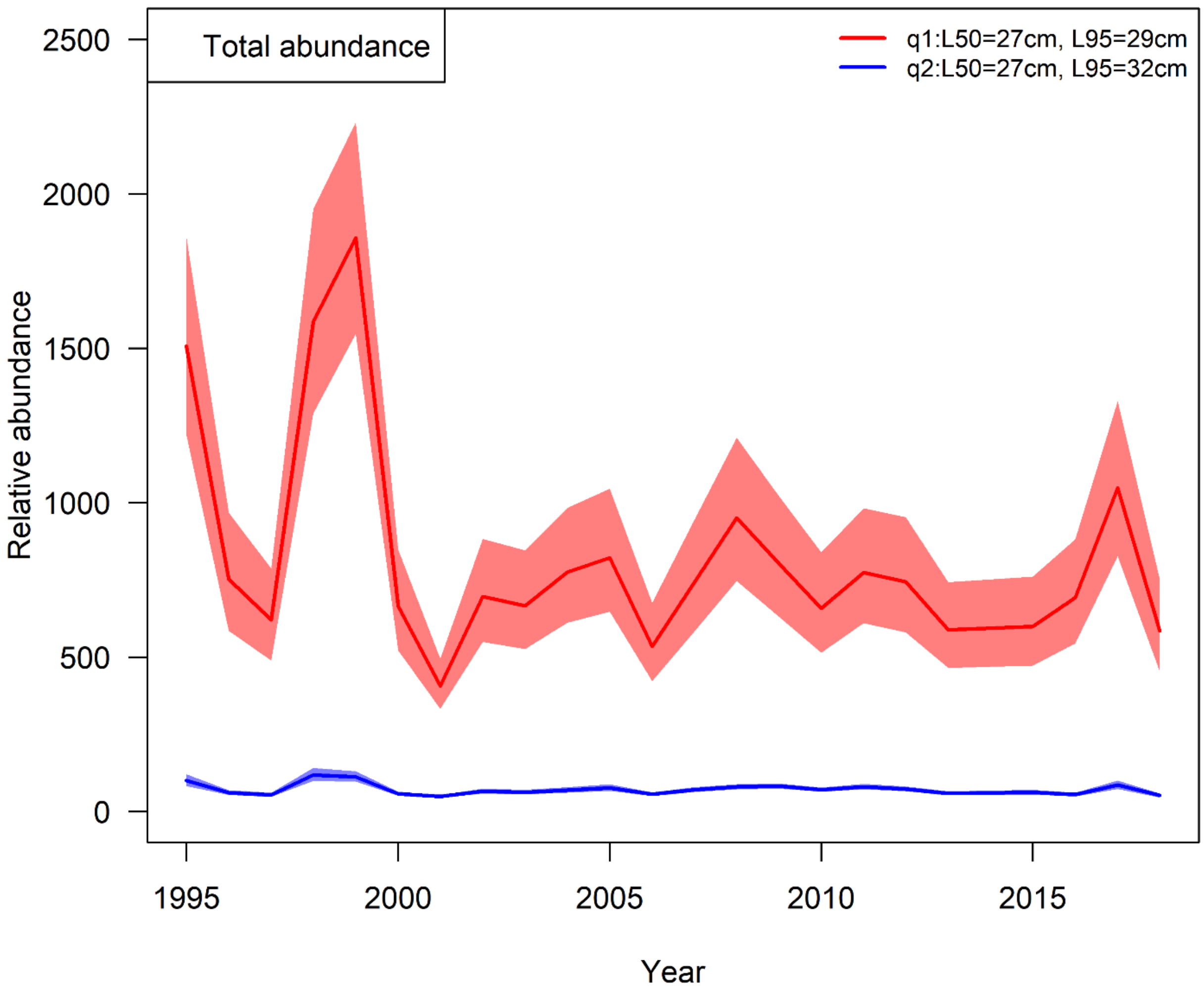

Figure 3.39 The estimated total abundance (millions) of NAFO Div. 3NO witch flounder in ALSCL with model-based indices from 1995 to 2018 (except 2014) for different survey catchabilities q1 and q2. Covered areas are 95% confidence intervals.

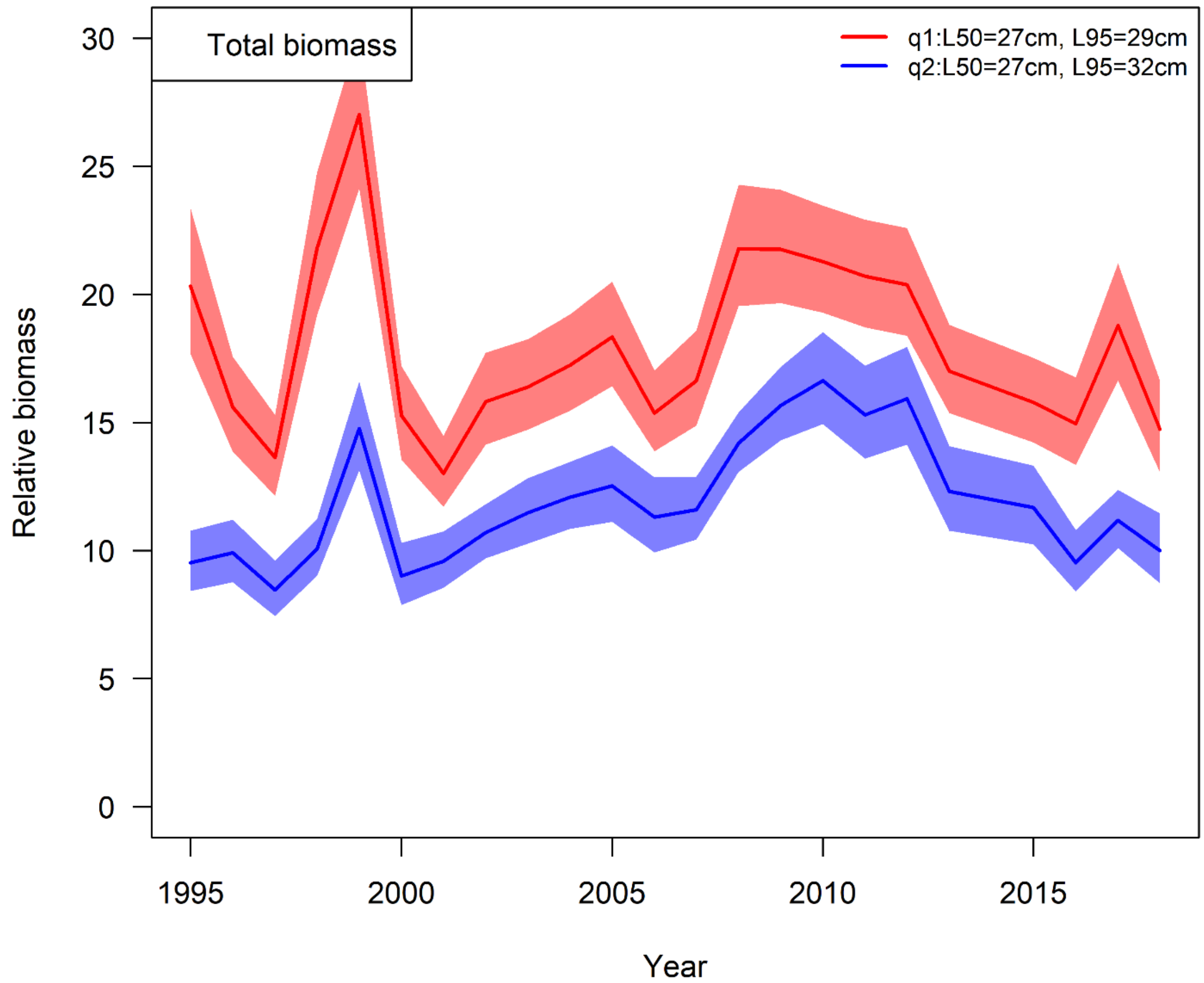

Figure 3.40 The estimated total biomass (Kt) of NAFO Div. 3NO witch flounder in ALSCL with model-based indices from 1995 to 2018 (except 2014) for different survey catchabilities q1 and q2. Covered areas are 95% confidence intervals.

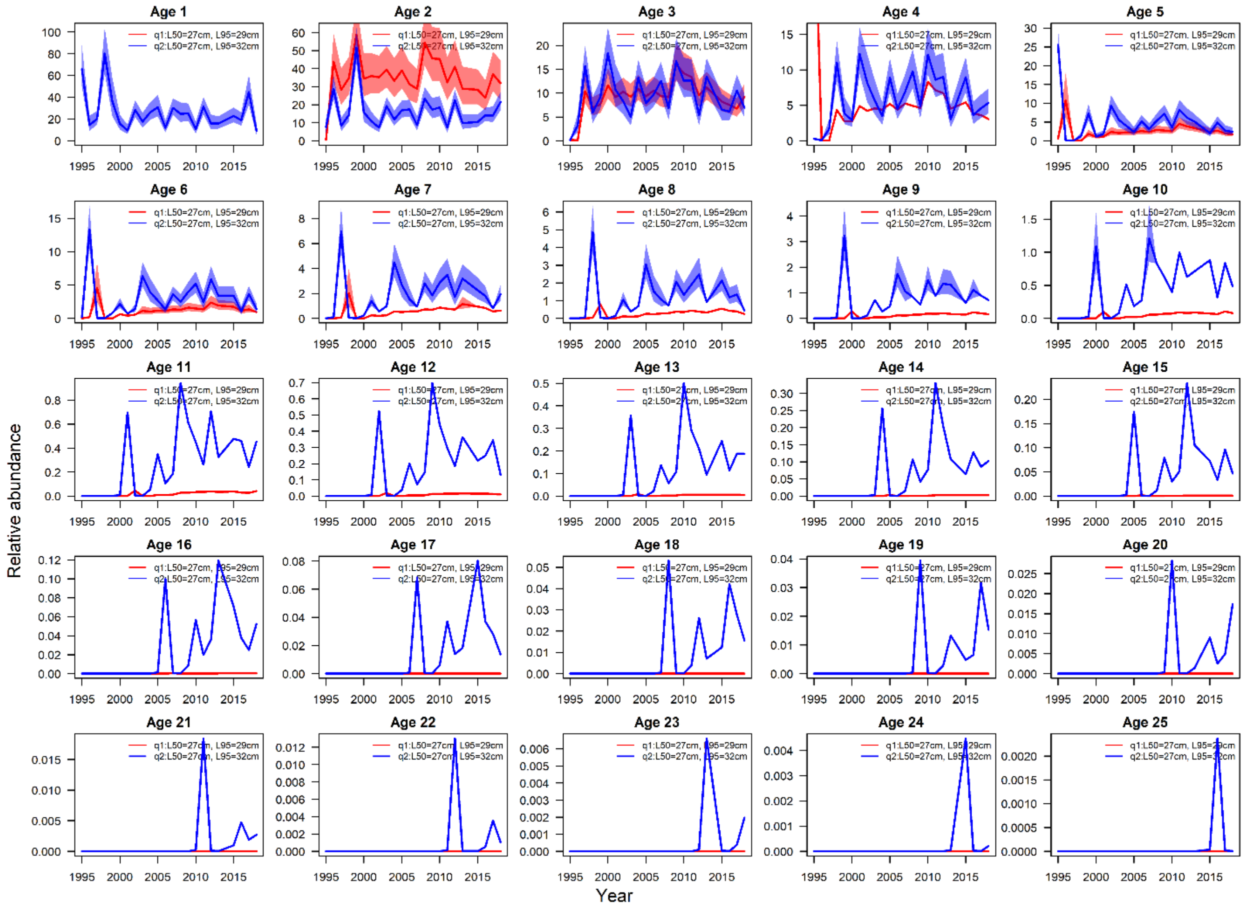

Figure 3.41 The estimated abundance at age (millions) of NAFO Div. 3NO witch flounder in ALSCL with model-based indices from 1995 to 2018 (except 2014) for different survey catchabilities q1 and q2. Covered areas are 95% confidence intervals.

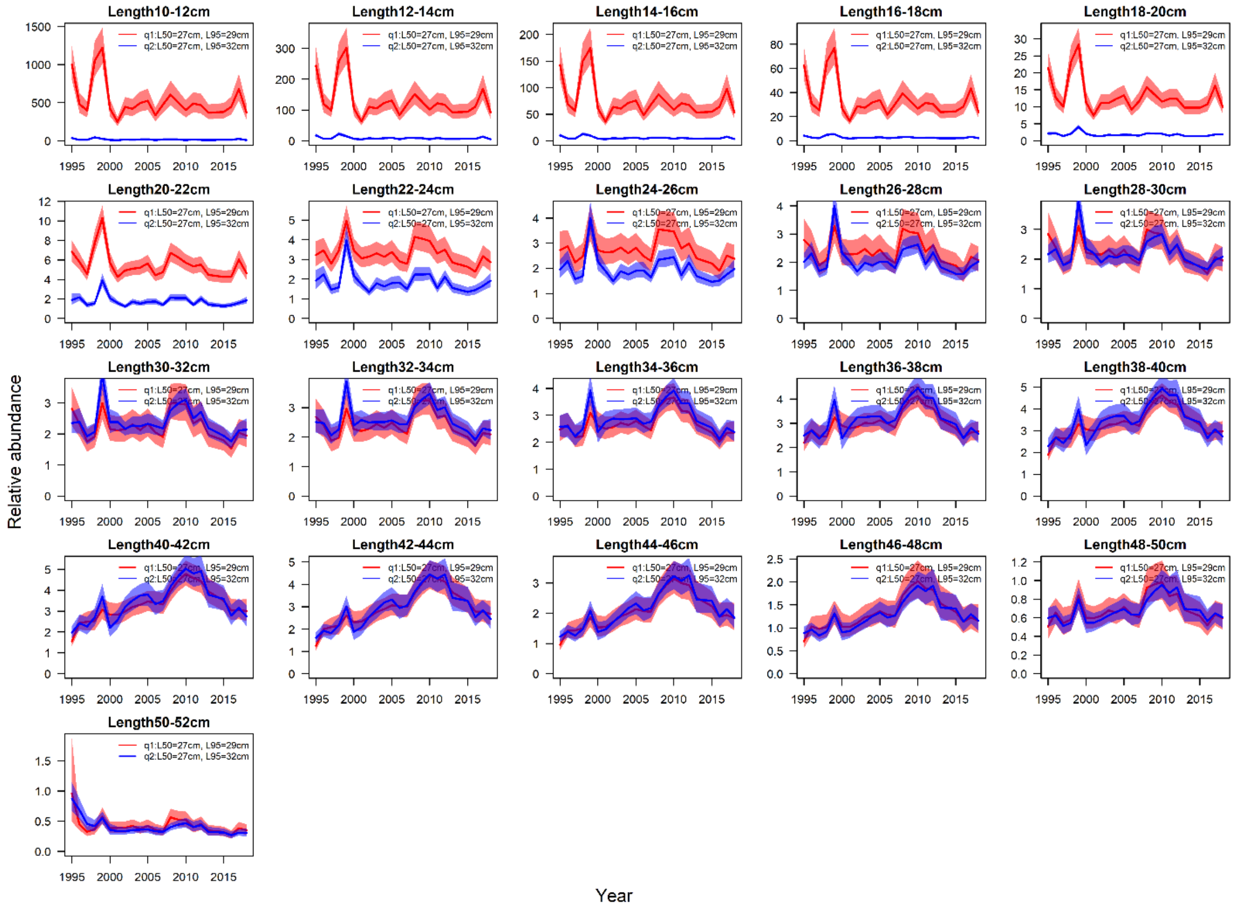

Figure 3.42 The estimated abundance at length (millions) of NAFO Div. 3NO witch flounder in ALSCL with model-based indices from 1995 to 2018 (except 2014) for different survey catchabilities q1 and q2. Covered areas are 95% confidence intervals.

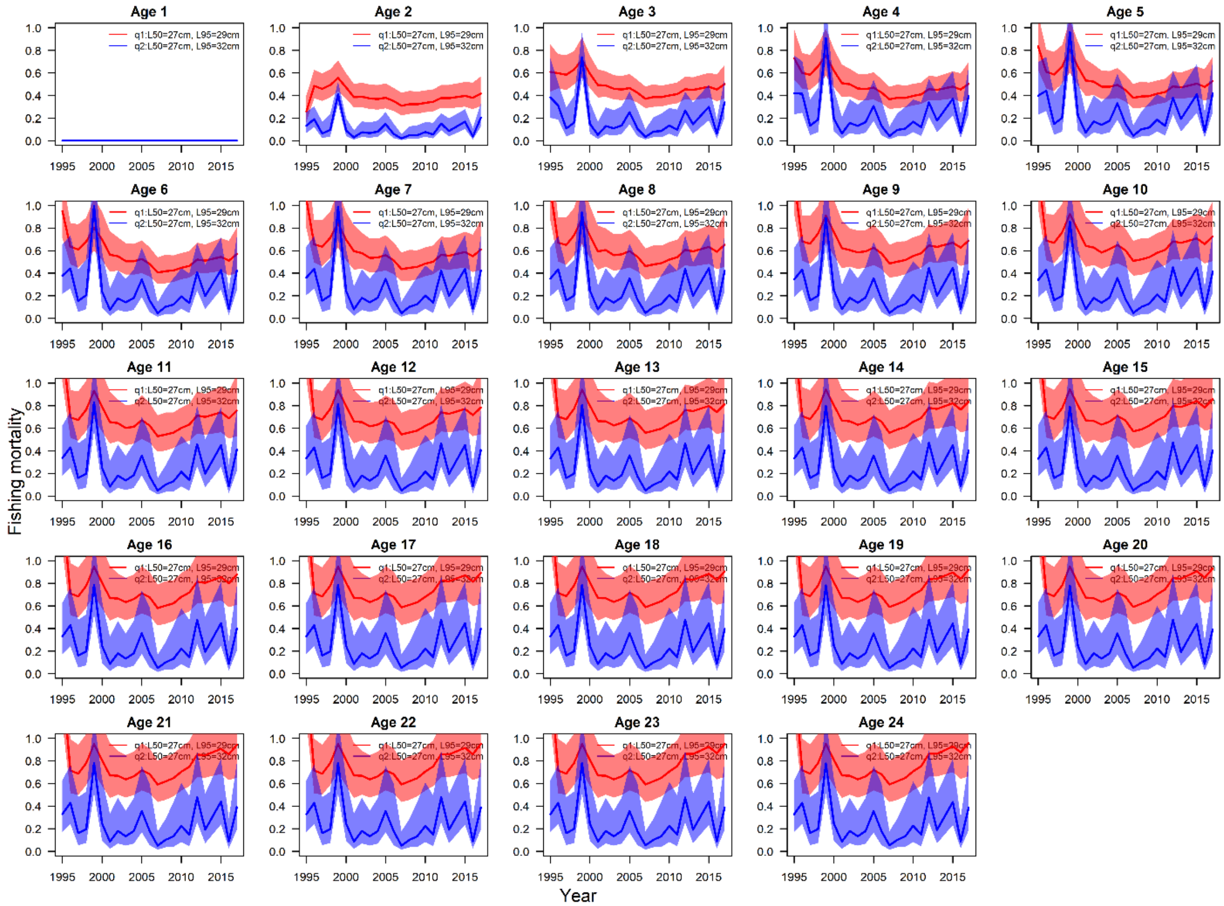

Figure 3.43 The estimated fishing mortality at age of NAFO Div. 3NO witch flounder in ALSCL with model-based indices from 1995 to 2018 (except 2014) for different survey catchabilities q1 and q2. Covered areas are 95% confidence intervals.

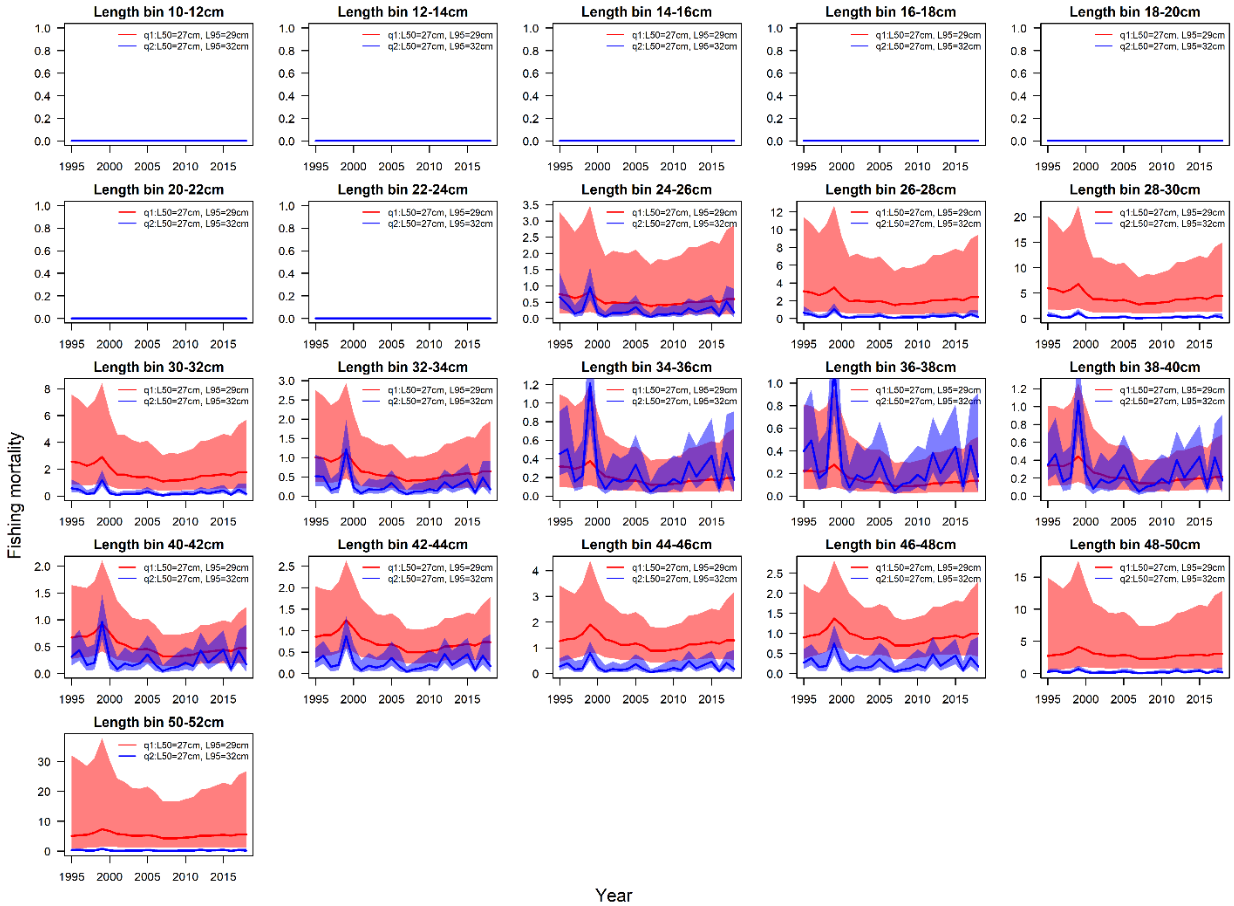

Figure 3.44 The estimated fishing mortality at length of NAFO Div. 3NO witch flounder in ALSCL with model-based indices from 1995 to 2018 (except 2014) for different survey catchabilities q1 and q2. Covered areas are 95% confidence intervals.

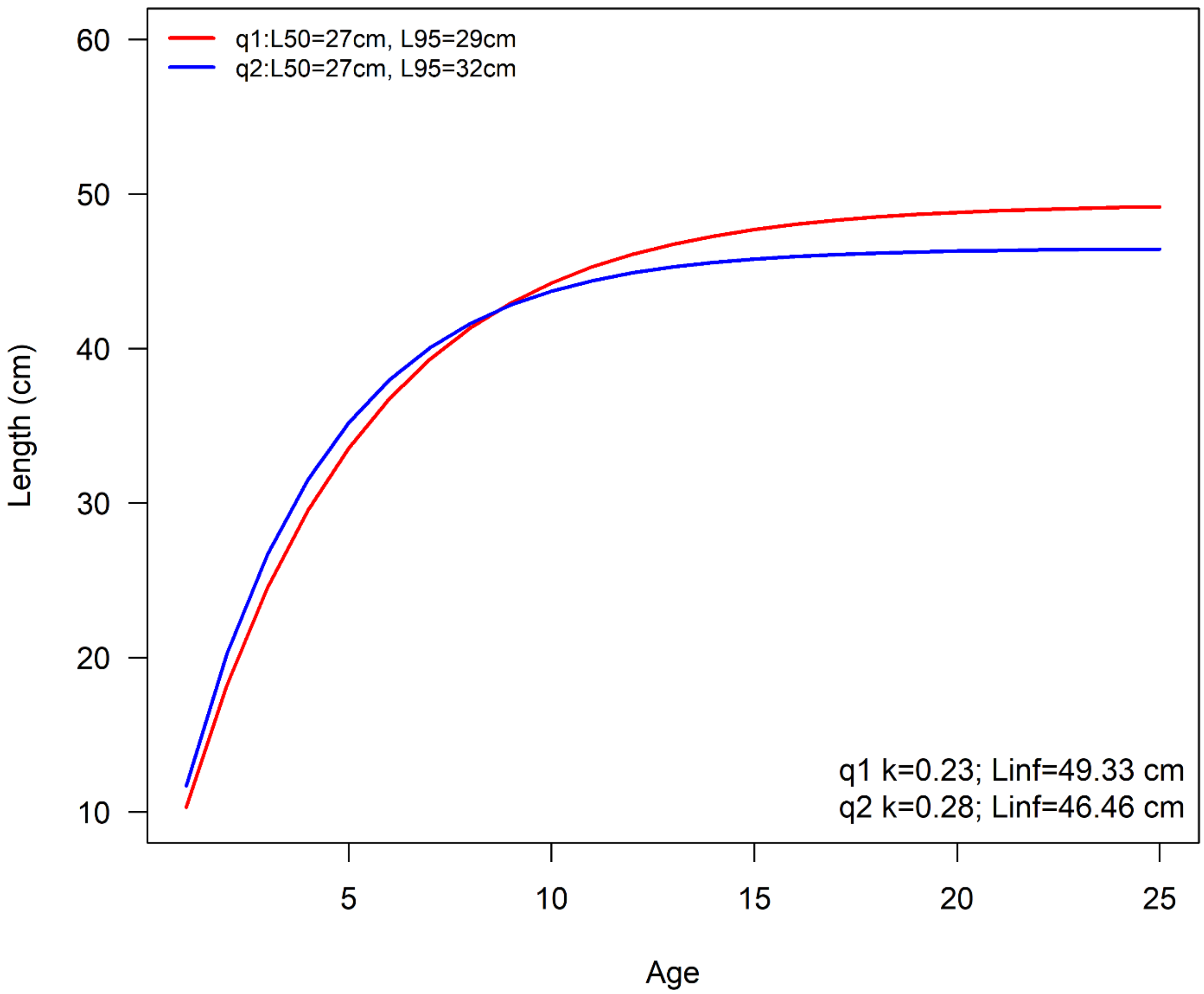

Figure 3.45 The estimated VonB growth curve of NAFO Div. 3NO witch flounder in ALSCL with model-based indices for different survey catchabilities q1 and q2.

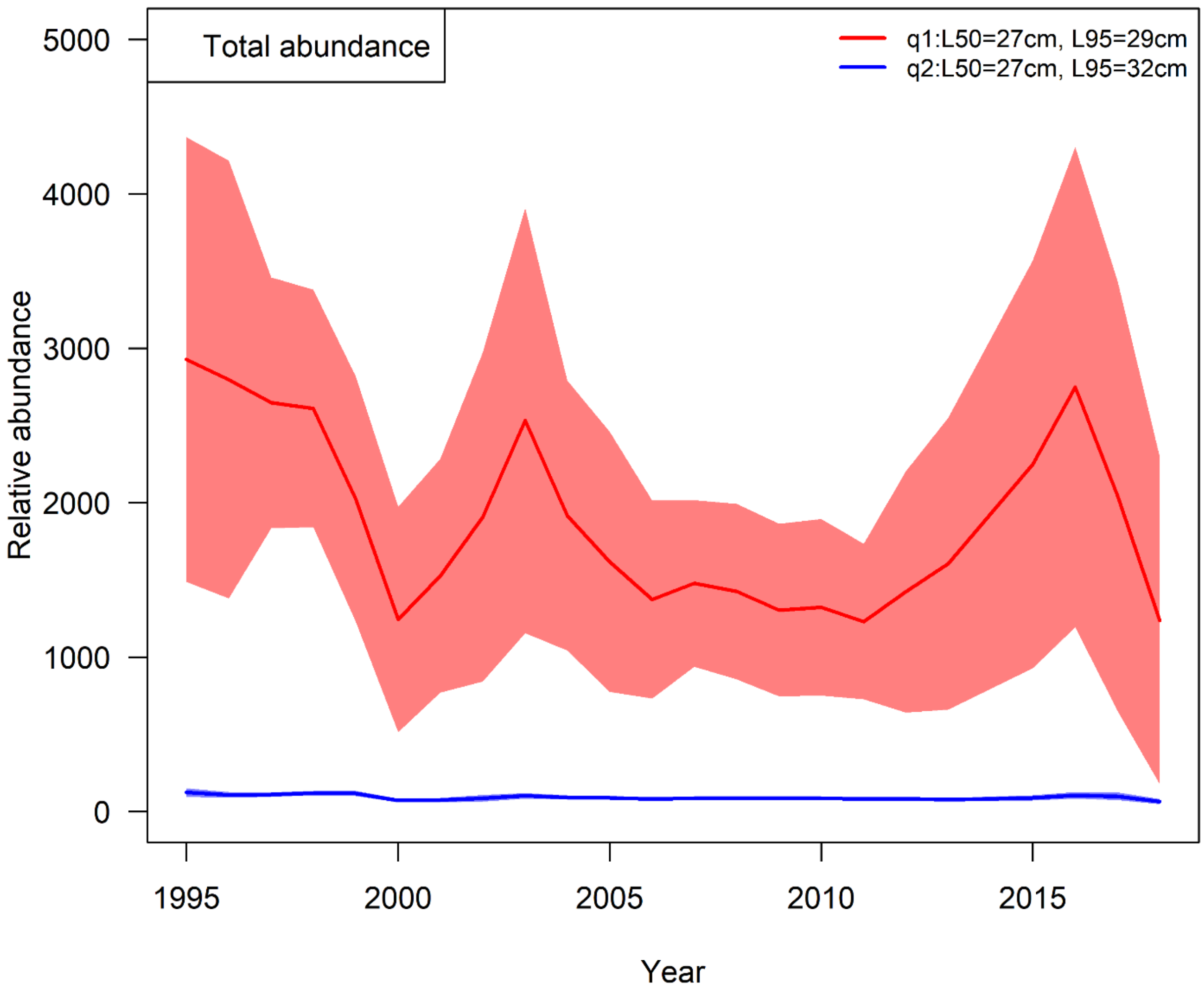

Figure 3.46 The estimated total abundance (millions) of NAFO Div. 3NO witch flounder in ACL with model-based indices from 1995 to 2018 (except 2014) for different survey catchabilities q1 and q2. Covered areas are 95% confidence intervals.

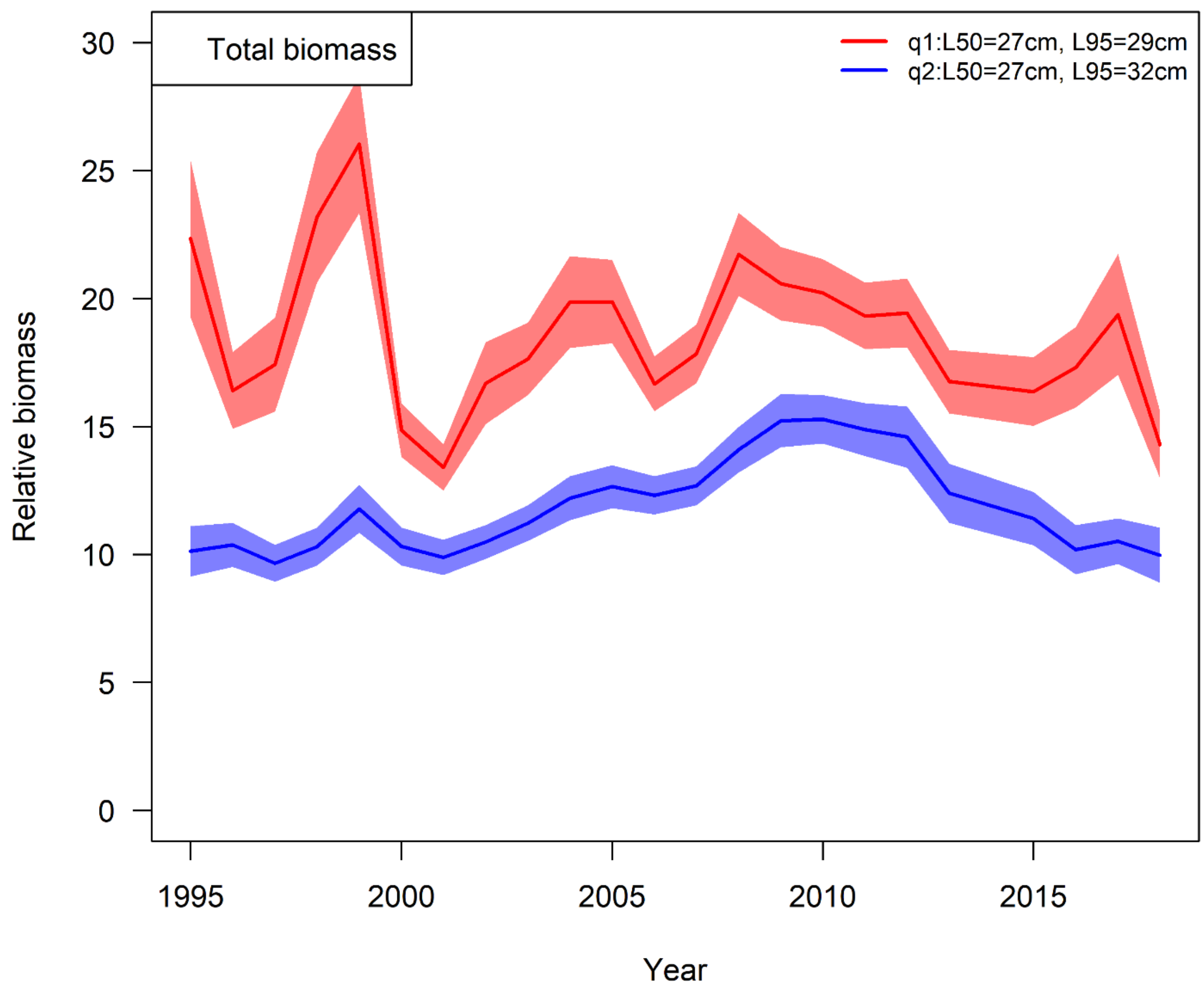

Figure 3.47 The estimated total biomass (Kt) of NAFO Div. 3NO witch flounder in ACL with model-based indices from 1995 to 2018 (except 2014) for different survey catchabilities q1 and q2. Covered areas are 95% confidence intervals.

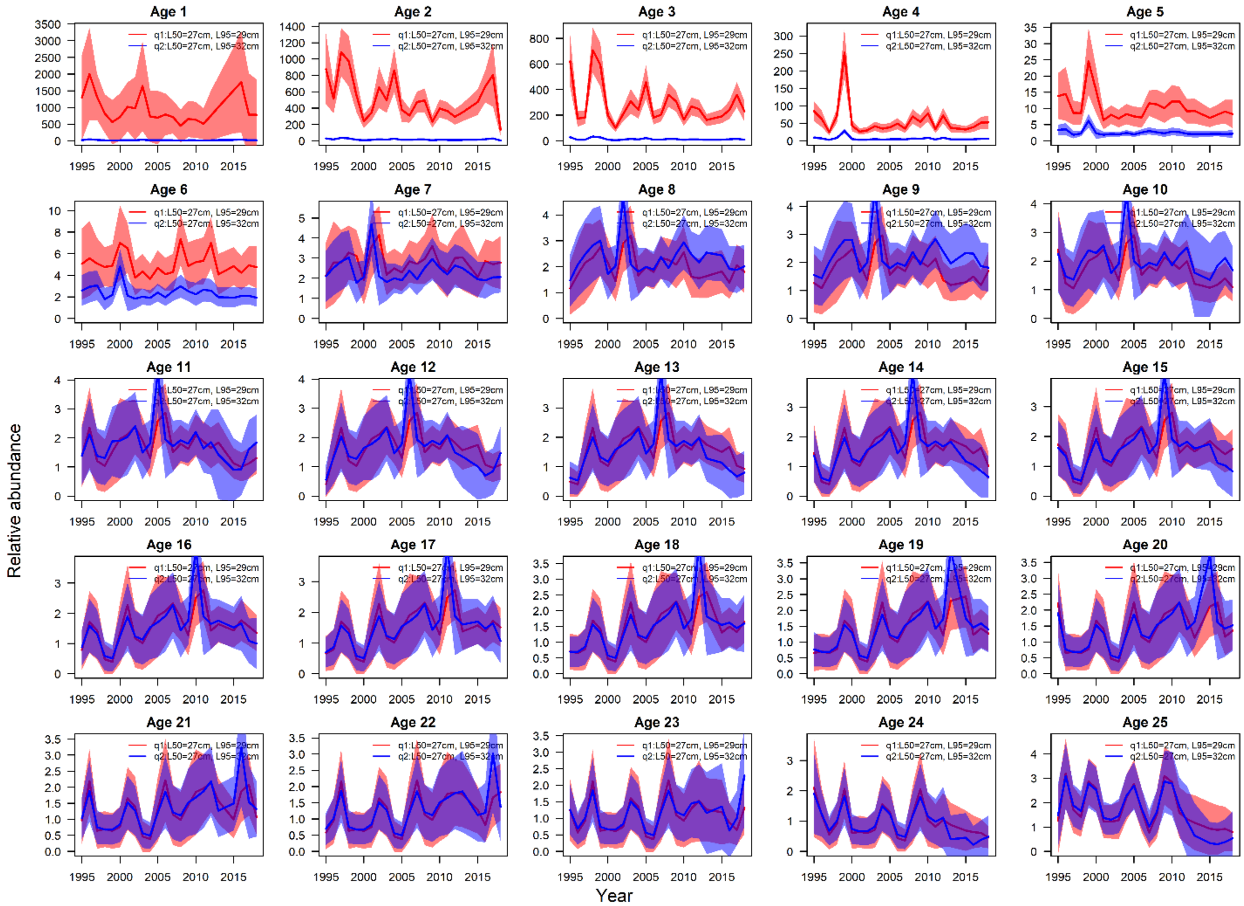

Figure 3.48 The estimated abundance at age (millions) of NAFO Div. 3NO witch flounder in ACL with model-based indices from 1995 to 2018 (except 2014) for different survey catchabilities q1 and q2. Covered areas are 95% confidence intervals.

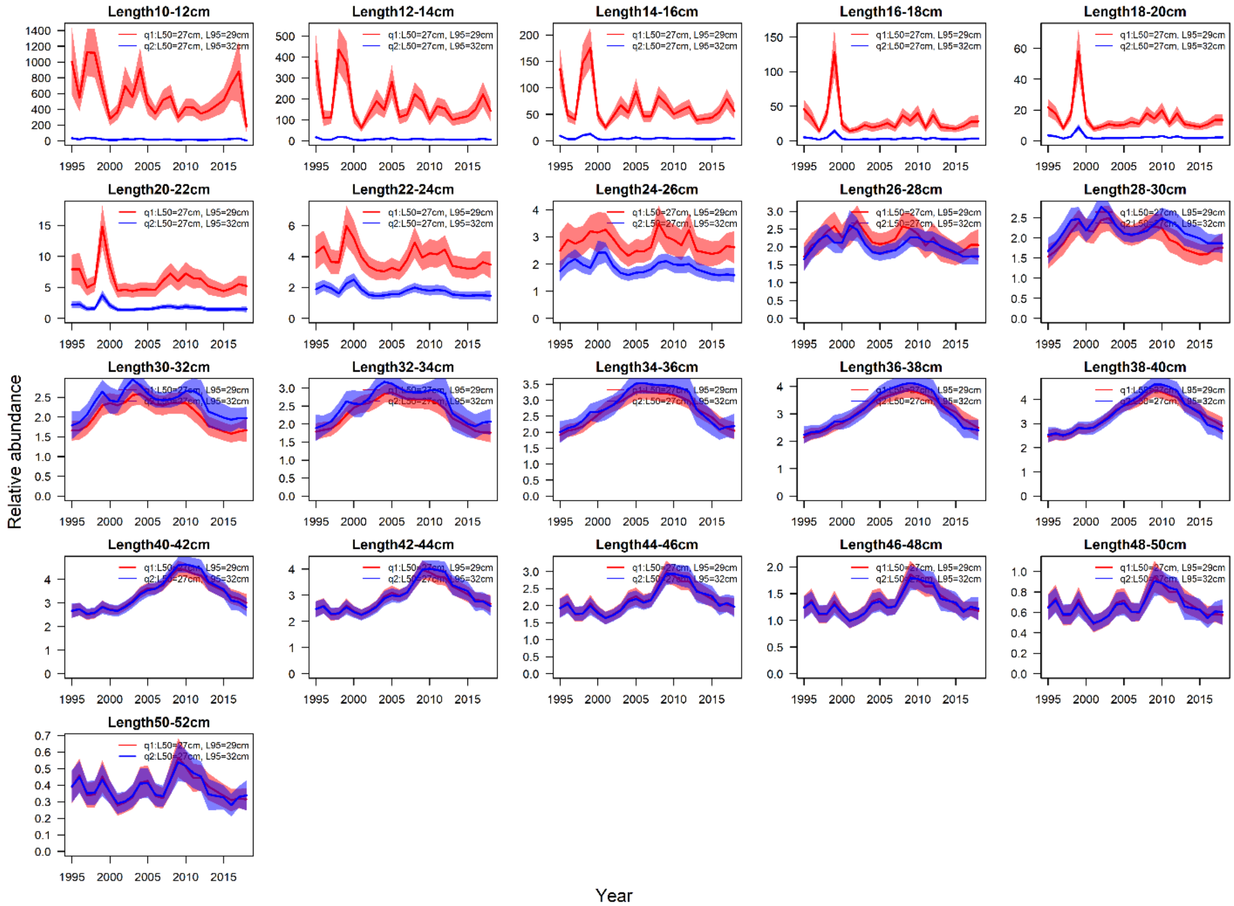

Figure 3.49 The estimated abundance at length (millions) of NAFO Div. 3NO witch flounder in ACL with model-based indices from 1995 to 2018 (except 2014) for different survey catchabilities q1 and q2. Covered areas are 95% confidence intervals.

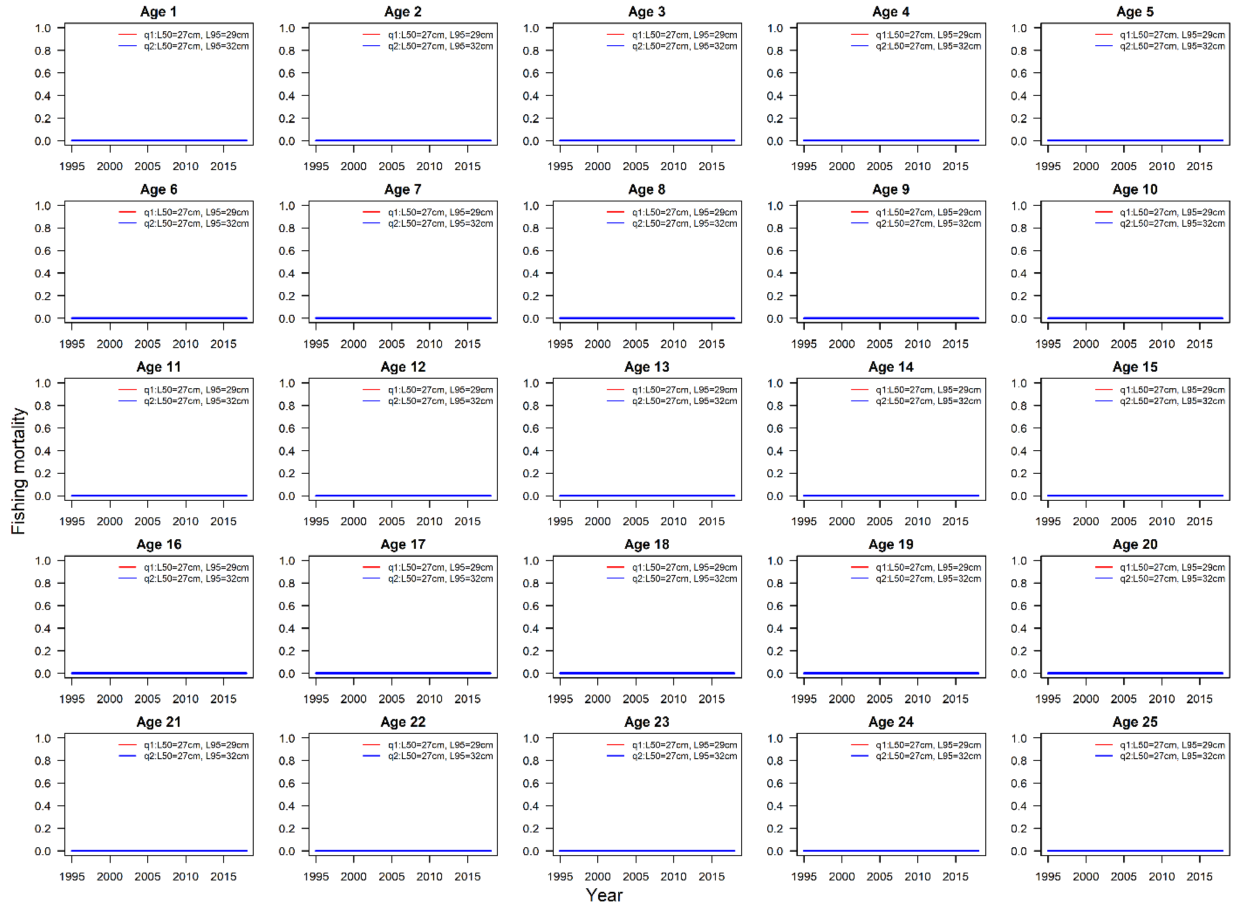

Figure 3.50 The estimated fishing mortality at age of NAFO Div. 3NO witch flounder in ACL with model-based indices from 1995 to 2018 (except 2014) for different survey catchabilities q1 and q2. Covered areas are 95% confidence intervals.

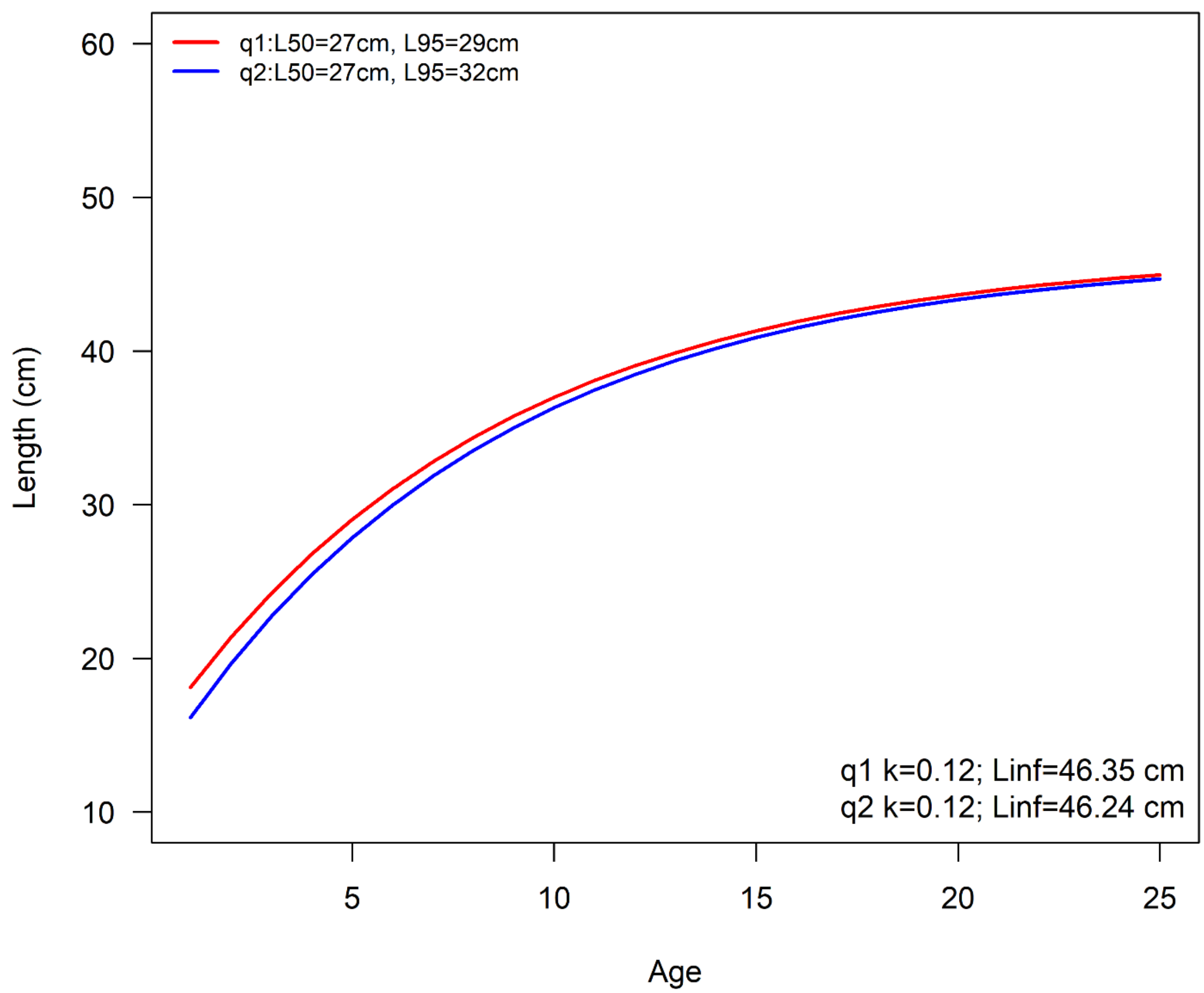

Figure 3.51 The estimated VonB growth curve of NAFO Div. 3NO witch flounder in ACL with model-based indices for different survey catchabilities q1 and q2.

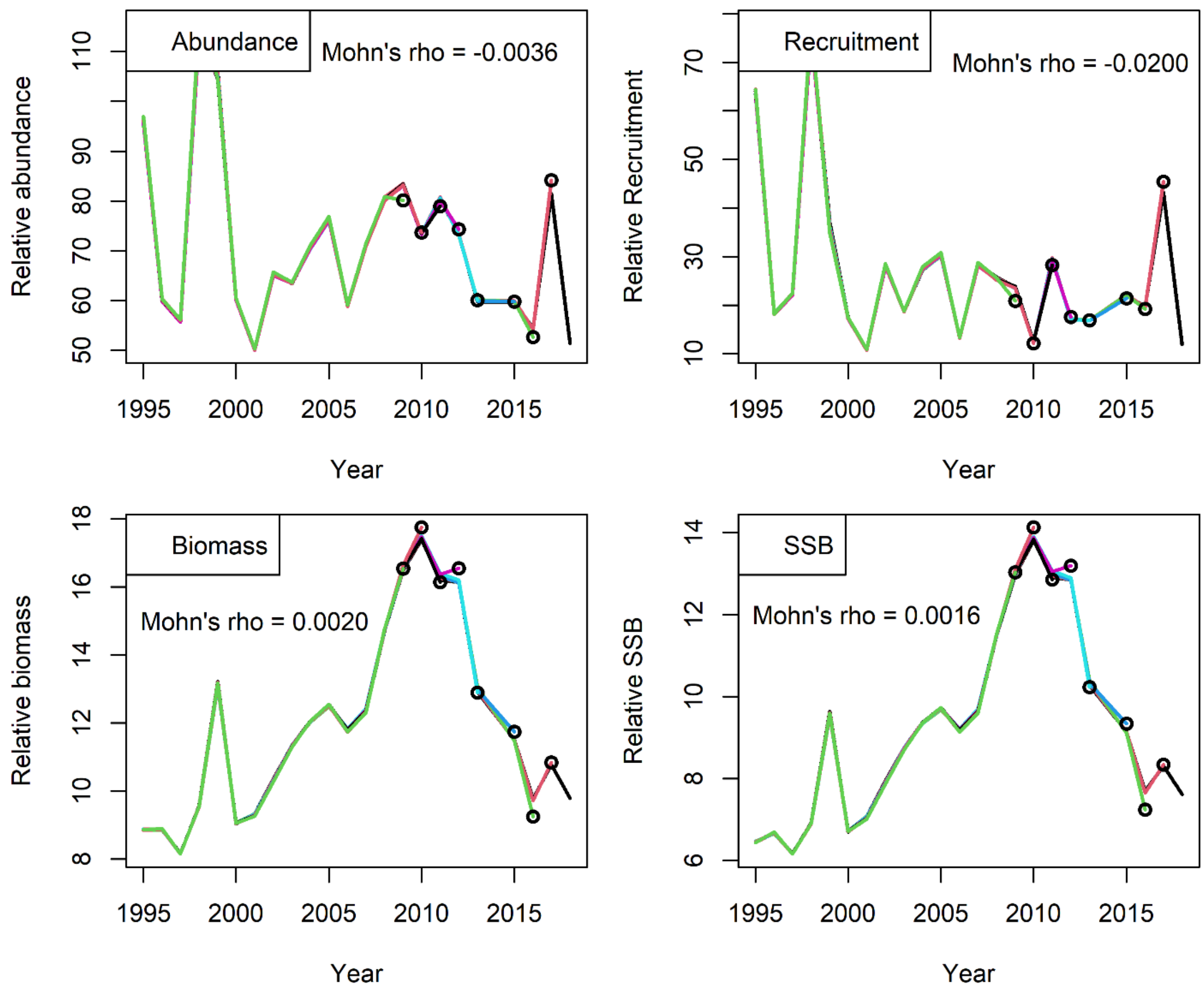

Figure 3.52 The retrospective analyses for NAFO Div. 3NO witch flounder in ALSCL with model-based indices from 1995 to 2018 (except 2014).

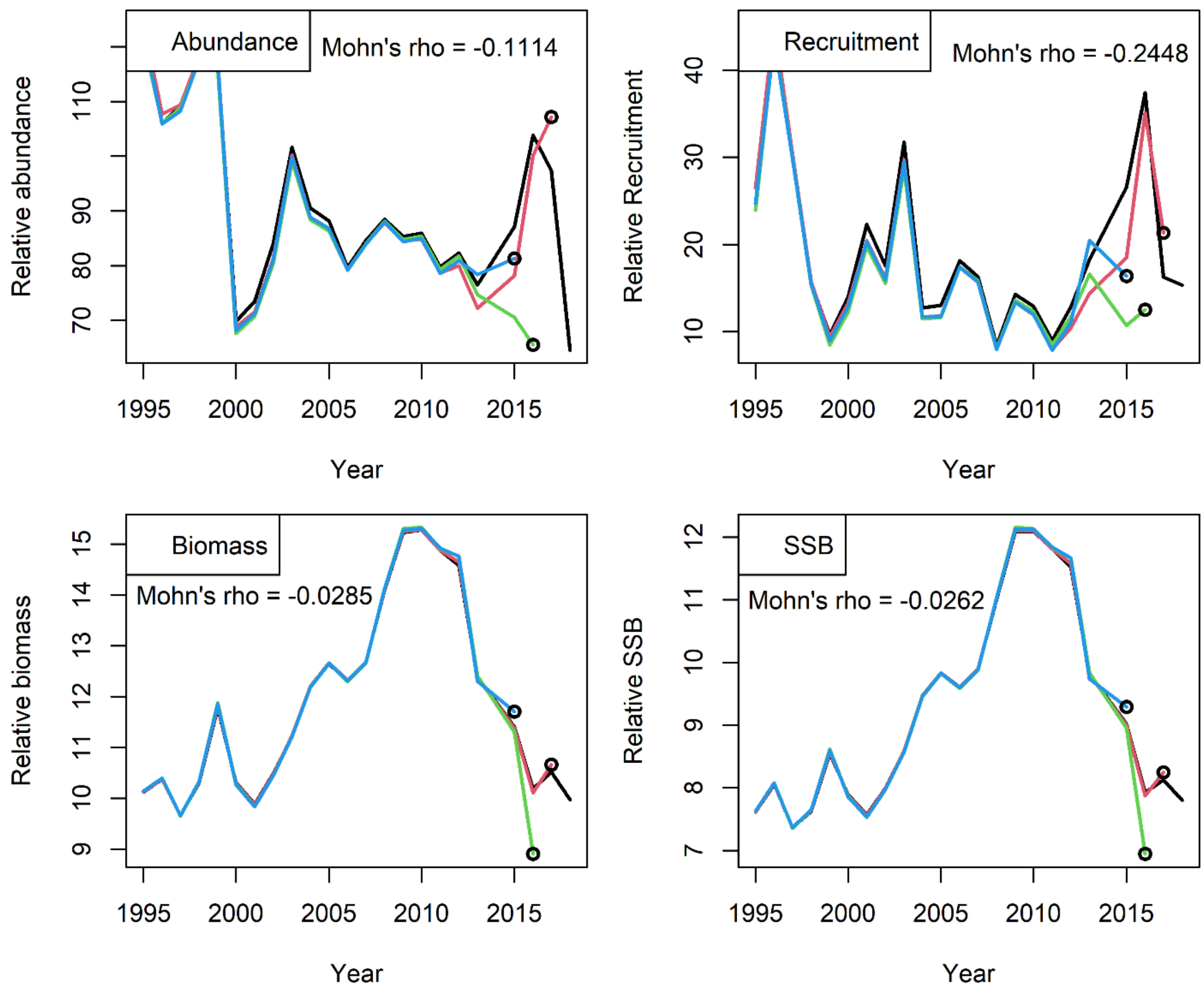

Figure 3.53 The retrospective analyses for NAFO Div. 3NO witch flounder in ACL with model-based indices from 1995 to 2018 (except 2014).

3.5 Bibliography

Akselrud, C. I. A., Punt, A. E., & Cronin-Fine, L. (2017). Exploring model structure uncertainty using a general stock assessment framework: The case of Pacific cod in the Eastern Bering Sea. *Fisheries Research*, *193*, 104–120.

Andersen, K. H. (2020). Size-based theory for fisheries advice. *ICES Journal of Marine Science*, *77*(7–8), 2445–2455.

Bowering, W. R. (1976). Distribution, Age and Growth, and Sexual Maturity of Witch Flounder (Glyptocephalus cynoglossus) in Newfoundland Waters. *Journal of the Fisheries Research Board of Canada*, *33*(7), 1574–1584. https://doi.org/10.1139/f76-198

Bowering, W. R. (1978). Fecundity of witch flounder (Glyptocephalus cynoglossus) from St. Pierre Bank and the Grand Bank of Newfoundland. *Journal of the Fisheries Board of Canada*, *35*(9), 1199–1206.

Burnett, J., Ross, M. R., & Clark, S. H. (1992). Several biological aspects of the witch flounder (Glyptocephalus cynoglossus (L.)) in the Gulf of Maine-Georges Bank region. *J. Northw. Atl. Fish. Sci*, *12*, 15–25.

Campana, S. E., & Thorrold, S. R. (2001). Otoliths, increments, and elements: Keys to a comprehensive understanding of fish populations? *Canadian Journal of Fisheries and Aquatic Sciences*, *58*(1), 30–38.

Chen, Y., Chen, L., & Stergiou, K. I. (2003). Impacts of data quantity on fisheries stock assessment. *Aquatic Sciences*, *65*(1), 92–98.

Cronin-Fine, L., & Punt, A. E. (2020). There is no best method for constructing size-transition matrices for size-structured stock assessments. *ICES Journal of Marine Science*, *77*(1), 136–147.

Durán, P., & Paz, X. (2000). Witch Flounder (Gyptocephalus cynoglossus) in the Spanish Deep-sea Fishery (NAFO Divisions 3LMNO), 1991–94. *Northwest Atl. Fish. Organ. Sci. Counc. Stud*, *33*, 117–127.

Fournier, D. A., Hampton, J., & Sibert, J. R. (1998). MULTIFAN-CL: a length-based, age-structured model for fisheries stock assessment, with application to South Pacific albacore, Thunnus alalunga. *Canadian Journal of Fisheries and Aquatic Sciences*, *55*(9), 2105–2116.

Fournier, D., & Archibald, C. P. (1982). A general theory for analyzing catch at age data. *Canadian Journal of Fisheries and Aquatic Sciences*, *39*(8), 1195–1207.

Hilborn, R., & Walters, C. J. (2013). *Quantitative fisheries stock assessment: Choice, dynamics and uncertainty*. Springer Science & Business Media.

Hurtado-Ferro, F., Szuwalski, C. S., Valero, J. L., Anderson, S. C., Cunningham, C. J., Johnson, K. F., Licandeo, R., McGilliard, C. R., Monnahan, C. C., & Muradian, M. L. (2015). Looking in the rear-view mirror: Bias and retrospective patterns in integrated, age-structured stock assessment models. *ICES Journal of Marine Science*, *72*(1), 99–110.

Kumar, R., Cadigan, N. G., Zheng, N., Varkey, D. A., & Morgan, M. J. (2020). A state-space spatial survey-based stock assessment (SSURBA) model to inform spatial variation in relative stock trends. *Canadian Journal of Fisheries and Aquatic Sciences*, *77*(10), 1638–1658.

Lorenzen, K. (2011). Age-and size-varying natural mortality rates: Biological causes and consequences for fisheries assessment. *Estimating Natural Mortality in Stock Assessment Applications*, 18–21.

Maddock Parsons, D., Rogers, B., & Rideout, R. (2020). An assessment of the witch flounder resource in NAFO Divisions 3NO. *NAFO SCR Doc*, *20*, 046.

Magnusson, A., & Hilborn, R. (2007). What makes fisheries data informative? *Fish and Fisheries*, *8*(4), 337–358.

Marriott, R. J., & Mapstone, B. D. (2006). Consequences of inappropriate criteria for accepting age estimates from otoliths, with a case study for a long-lived tropical reef fish. *Canadian Journal of Fisheries and Aquatic Sciences*, *63*(10), 2259–2274.

Maunder, M. N., & Wong, R. A. (2011). Approaches for estimating natural mortality: Application to summer flounder (Paralichthys dentatus) in the US mid-Atlantic. *Fisheries Research*, *111*(1–2), 92–99.

Methot Jr, R. D., & Wetzel, C. R. (2013). Stock synthesis: A biological and statistical framework for fish stock assessment and fishery management. *Fisheries Research*, *142*, 86–99.

Mohn, R. (1999). The retrospective problem in sequential population analysis: An investigation using cod fishery and simulated data. *ICES Journal of Marine Science*, *56*(4), 473–488.

Morgan, M. J., Hvingel, C., & Koen-Alonso, M. (2015). Surplus production models in a Bayesian framework applied to witch flounder in NAFO Div. 3NO. *NAFO SCR*, *15*, 37.

Morgan, M. J., & Lee, E. (2018). Surplus production model in a Bayesian framework applied to witch flounder in NAFO Div. 3NO. *NAFO SCR*, *18*, 53.

Ono, K., Licandeo, R., Muradian, M. L., Cunningham, C. J., Anderson, S. C., Hurtado-Ferro, F., Johnson, K. F., McGilliard, C. R., Monnahan, C. C., & Szuwalski, C. S. (2015). The importance of length and age composition data in statistical age-structured models for marine species. *ICES Journal of Marine Science*, *72*(1), 31–43.

Punt, A. E., Huang, T., & Maunder, M. N. (2013). Review of integrated size-structured models for stock assessment of hard-to-age crustacean and mollusc species. In *ICES Journal of Marine Science* (Vol. 70, Issue 1, pp. 16–33).

Quinn, T. J. (2003). Ruminations on the development and future of population dynamics models in fisheries. *Natural Resource Modeling*, *16*(4), 341–392.

Rogers, B., & Morgan, J. (2019). An assessment of the witch flounder resource in NAFO Divisions 3NO. *NAFO SCR Doc*, *19*, 034.

Swain, D. P., Savoie, L., Aubry, É., & du Golfe, R. (2012). *Assessment of witch flounder (Glyptocephalus cynoglossus) in the Gulf of St. Lawrence (NAFO Divisions 4RST), February 2012*.

Winker, H., Mourato, B., & Chang, Y. (2020). Unifying parameterizations between age-structured and surplus production models: An application to Atlantic white marlin (Kajika albida) with simulation testing. *Col. Vol. Sci. Pap. ICCAT*, *76*, 219–234.

Zhang, F., & Cadigan, N. G. (n.d.). An age-and length-structured statistical catch-at-length model for hard-to-age fisheries stocks. *Fish and Fisheries*.

Chapter 4 Summary and Future Research

The primary goal of my thesis was to standardize survey indices for NAFO Div. 3NO witch flounder and apply the age and length structured statistical catch-at-length (ALSCL) and the age-based catch-at-length model (ACL) models for this stock to estimate the age-based population dynamics. This thesis provides a case study for standardizing survey indices through a spatiotemporal model and assessing hard-to-age stock by the ALSCL and ACL models.

In Chapter 1, I provided an overview of the witch flounder fishery in NAFO Div. 3NO. I highlighted witch flounder life-history traits, catch history and stock management. I also described the Fisheries and Oceans Canada (DFO) research vessel survey indices and detail of this survey design. By doing so, I realized the survey indices derived from survey sampling only represent sample data from localized sample sites, which implies that these indices must be standardized precisely to represent the total stock. I attempt to this problem in Chapter 2.

In Chapter 2, I applied the design-based approach and the model-based approach (vector-autoregressive spatiotemporal, VAST) of standardizing fall RV survey size compositional data for NAFO Div. 3NO witch flounder. I found that the estimated abundance-at-length indices and the proportion-at-length indices from the model-based approach are smoother and show smaller CI than that from the design-based approach, and the estimated effective sample size in the model-based estimator is larger than that in the design-based estimator, which implies the model-based estimator provides more accurate estimations. I found general agreement in trends between design-based and model-based indices. However, from 2004 to 2013 (except 2007), design-based indices are considerably higher in 32 to 40 cm. This could be due to potential biases introduced by the model-based approach. Thorson and Haltuch (2019) demonstrated that VAST and design-based indices agree very well in a simulated dataset from bottom trawl surveys in the Eastern Bering Sea, which implies that future studies should quantify this potential bias by conducting a simulation experiment (Thorson & Haltuch, 2019).

The model-based approach I have presented only deals with poor sampling or occasional big sampling problems and didn't account for habitat covariates, catchability covariates and vessel effects. Ignoring these covariates will result in a biased estimate of the spatio-temporal variation of population density (Thorson, 2019). Future research should include habitat covariates (e.g. temperature), catchability covariates and vessel effects in the linear predictors of the model-based approach to improve the accuracy of model predictions.

In Chapter 3, I used ALSCL and ACL models with design-based and model-based indices to estimate the age-based population dynamics for NAFO Div. 3NO witch flounder. The ALSCL and ACL models were fit the fall survey standardized number-at-length indices, weight-at-length and maturity-at-length data to estimate the abundance, recruitment, biomass, spawning stock biomass and fishing mortality, and also to provide the growth curve for this stock. By doing model diagnostic and sensitivity analyses, I confirmed that the assessment results of NAFO Div. 3NO witch flounder are very sensitive to the choice of indices, and also sensitive to the choice of model based on the results in sensitivity and retrospective analyses. I also found that the ALSCL and ACL model fits are very sensitive to the choice of catchabilities, and the lower catchability values produce higher estimated abundance and biomass. The specification of survey catchability is a big challenge for ALSCL and ACL models. So future research should investigate potential changes in survey catchability i.e. integrating catch-at-length information in ALSCL.

Since no sex ratio information from the fall survey, the sex ratio was assumed to equal 1:1 in the ALSCL and ACL models. And I also assumed that the maturity-at-length is the same for males and females. However, the maturity of males and females witch flounder at the same body length is different, and the maximum body length that can be achieved is also different (Bowering, 1976). Assuming males and females have the same maturity may lead to bias in the estimated spawning stock biomass. Therefore, future research should apply different maturity for both sexes when sex ratio information and reliable estimates of maturity-at-length for males and females from ongoing research are available.

I assumed the natural mortality is constant and equal to 0.2 in ALSCL and ACL. But this value may smaller or larger for witch flounder and juvenile witch flounder experience higher natural mortality than mature adults (Brodziak et al., 2011), which can result in an inaccurate estimation of cohort dynamics. Future research should investigate factors that cause natural mortality for witch flounder to vary in time and space first and then try to apply the age- and size-varying natural mortality in the assessment model to evaluate the consequences.

4.1 Bibliography

Bowering, W. R. (1976). Distribution, Age and Growth, and Sexual Maturity of Witch Flounder (Glyptocephalus cynoglossus) in Newfoundland Waters. Journal of the Fisheries Research Board of Canada, 33(7), 1574–1584. https://doi.org/10.1139/f76-198

Brodziak, J. K. T., Ianelli, J. N., Lorenzen, K., & Methot, R. D. (2011). Estimating natural mortality in stock assessment applications. US Department of Commerce, National Oceanic and Atmospheric Administration ….

Thorson, J. T. (2019). Guidance for decisions using the Vector Autoregressive Spatio-Temporal (VAST) package in stock, ecosystem, habitat and climate assessments. Fisheries Research, 210, 143–161.

Thorson, J. T., & Haltuch, M. A. (2019). Spatiotemporal analysis of compositional data: Increased precision and improved workflow using model-based inputs to stock assessment. Canadian Journal of Fisheries and Aquatic Sciences, 76(3), 401–414.